DOCTORAT BRETAGNE LOIRE MATHSTIC

UNIVERSITÉ DE NANTES

THESE DE DOCTORAT DE

L'UNIVERSITE DE NANTES

ECOLE DOCTORALE N° 601
Mathématiques et Sciences et Technologies de l'Information et de la Communication
Spécialité : *Génie électrique*

Par **« Asma DABBABI »**

« Optimisation des architectures électriques des parcs éoliens offshore avec différents réseaux de distribution et de transmission AC et DC »

« Optimization of electrical architectures of offshore wind farms with different distribution and transmission networks AC and DC »

Thèse présentée et soutenue à « Saint-Nazaire », le « 23 octobre 2020 »

Unité de recherche : IREENA EA4642

Rapporteurs avant soutenance :

Bruno François — Professeur des Universités, L2EP, Ecole Centrale Lille, Lille
Marc Petit — Professeur des Universités, Geeps, CentraleSupélec, Paris

Membres du Jury :

Examinateurs :

Seddik Bacha — Professeur des Universités, G2ELab, Université Grenoble Alpes, Grenoble
Hamid Gualous — Professeur des Universités, LUSAC, Université de Caen Basse-Normandie, Caen

Dir. de thèse : Mohamed Machmoum — Professeur des universités, IREENA, Polytech Nantes, St-Nazaire
Encadrants : Salvy Bourguet — Maître de Conférences HDR, IREENA, Polytech Nantes, St-Nazaire
Rodica Loisel — Maître de Conférences, LEMNA, IAE Nantes, Nantes

Invité(s)

Philippe Baclet — Ingénieur, directeur de WEAMEC, Nantes

“If we knew what it was, we were doing, it would not be called research, would it?”
— **Albert Einstein**

Acknowledgements

Acronyms

HVAC	High Voltage Alternating Current
HVDC	High Voltage Direct Current
LV	Low Voltage
MV	Medium Voltage
HV	High Voltage
DP	Delivery Point
SCIG	Squirrel Cage Induction Generator
WRIG	Wound Rotor Induction Generator
MPPT	Maximum Power Point Tracking
DFIG	Double Fed Induction Generator
PMSG	Permanent Magnet Synchronous Generator
AEP	Annual Energy Production
SCFF	Self-Contained Fluid-Filled
HPGF	High-Pressure Gas Filled
HPFF	High Pressure Fluid-Filled
PILC	Paper-Insulated Lead-Covered
PPL	Paper Polypropylene Laminate
EPR	Ethylene Propylene Rubber
XLPE	Extruded cross-Linked Poly-Ethylene
INELFE	INterconnexion ELectrique France-Espagne
VSC	Voltage Source Converter
LCC	Line Commutated Converter
IGBT	Insulated Gate Bipolar Transistor
PWM	Pulse Width Modulation
PSO	Particle Swarm Optimization
GA	Genetic Algorithm
CAPEX	CApital EXpenditure
OPEX	OPerational EXpenditure
AED	Annual Energy Delivered
LCOE	Levelized Cost Of Energy
MMC	Multi-level Modular Converter
RD	Rotor Diameter

Content

General introduction

More than 80% of the world's energy consumption (transport, industry, heating) is based on fossil fuels (oil, coal, etc.) [1]. These percentage will continue to increase significantly in the coming years due to population growth and the gradual rise in living standards, particularly in developing countries. In fact, electricity represents 42% of the global energy consumption in France and this consumption is gradually increasing over time as the Réseau de Transport d'Electricité (RTE), the French public electricity grid operator, has recorded five huge consumption peaks over the last six years [2].

Furthermore, the combustion of fossil fuels presents a major problem for the future since it is the main cause of global warming. Besides, these energy sources are disappearing over the years. Indeed, according to the International Energy Agency (IEA), oil reserves will be exhausted in 2050, while gas reserves will be depleted in 2070 [3]. Therefore, it is imperative to find inexhaustible sources of energy in order to increase the production of electricity while ensuring the ecological conservation of the earth.

Among the renewable sources being considered and coveted is offshore wind power. Offshore wind farms have several advantages over onshore farms as long as the wind is stronger and regular at sea. An offshore wind turbine could reach its full power 40% of the time, compared to 25% for a good onshore wind turbine, so it could reach large powers above 5 MW, in addition, it has less impact on the terrestrial landscape. However, the installation of offshore wind turbine foundations at sea is more expensive than simple onshore installations.

This thesis work mainly focuses on the modeling and optimization of offshore wind farms with different distribution and transmission networks AC and DC. Indeed, the choice of the type of electrical connection is an important criterion in the search for the optimal architecture that offers the trade-off between minimal losses and minimal cost during the lifetime of an offshore wind park.

Problem statement

In France and in Europe more generally, the installation of large-power wind generators (greater than 8 MW) is strongly envisaged and the public authorities are asking companies to create a large-scale industrial and economic sector. In these developments, offshore wind power has tremendous potential, particularly in France, where several sites have been selected by

government calls for tenders for the installation of high-power offshore wind farms. In the near future, offshore wind farms will develop further offshore and the farm connection distances will be large enough (over 50 km) to seriously consider installations with direct current HVDC connections. It is therefore necessary today to plan and correctly size such high-power installations.

In the continuity of the work carried out in IREENA (Institut de recherche en Énergie Électrique de Nantes Atlantique) with Ouahid Dahmani's thesis work [22], that concerns the technical and economical optimization of full AC connected offshore wind farms, this thesis work must integrate DC systems either with AC/HVDC electrical architectures or with full DC connected wind farms. Hence, the goal is to analyze their performances and compare them with AC solutions.

Why DC?

In fact, the main problem of HVAC transport system is that the transmission capability of AC subsea cables is limited due to the presence of reactive power that evolves according to long transmission distances and high voltages.

On the other hand, since HVDC cables present only resistive losses so HVDC transmission system can overcome most of the HVAC transmission system flaws, but it includes higher cost related to converters. Nevertheless, distance-dependent costs are lower for HVDC than for HVAC system (high cost of HVAC cables for long distance with the additional cost of reactive compensation equipment). Consequently, this leads to a break-even distance where HVDC transmission system becomes most economical (see figure below). The break-even distance depends on many factors such as the total capacity power of the wind farm or the voltage level of different transmission systems. Determining the break-even distance is one of the principle goals of this thesis work, it will be useful for offshore wind operators to determine the best electrical architecture.

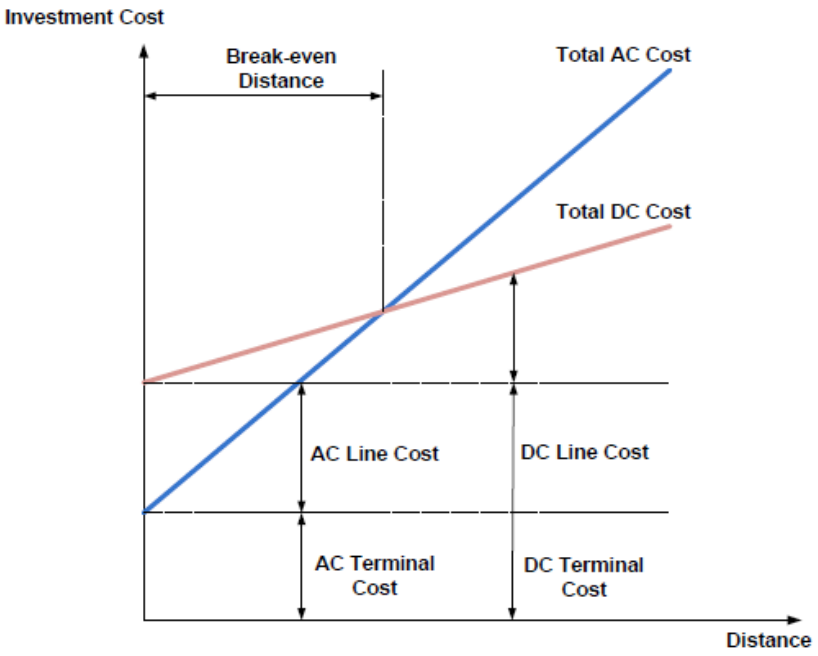

Break-even distance for HVAC and HVDC technologies [38]

Offshore wind farm modeling?

The architectures under study must respect the minimization of losses and costs. To reach this goal, the study must allow a review of different possible solutions (i.e. different electrical architectures) that are modelized differently. The modeling of an offshore wind farm architecture concerns the connections between the turbines, the overall structure of the turbines, the offshore sub-stations and their connection with the delivery point (terrestrial network). Since we have to integrate DC connection solutions for designing optimal offshore wind farms, we have to take into account the economic aspects related to new components cost, such as converters cost (AC/DC or DC/DC converters), DC sub-stations cost and DC subsea cables cost. Indeed, the cost and power losses of an offshore wind farm depends on various factors including the type of the transmission system chosen (HVAC or HVDC), the presence or not of additional power electronics structures guaranteeing a quality energy supply, the need or not to compensate reactive power, the transmission lengths and distances, the voltage levels, the capacity factor of the wind farm and the characteristics of the resource (without or with wake effect consideration).

Optimization framework?

The work will focus on creating a decision tool that allows the determination of the optimal electrical architecture depending in several conditions. In fact, this work consists of optimizing the electrical performance of the wind farm based on the selection of electrical equipment by choosing the appropriate voltage level and power rating. The positions of wind turbines are fixed but the substation positions and numbers are determined by the heuristic optimization algorithm, the inter array network is decided also by the optimization algorithm while minimizing the losses and cable costs. This approach is based on the idea of clustering turbines (string clustering, star clustering) so the algorithm decides the number of clusters and the number of turbines in each cluster. Indeed, the main criterion for performance comparison between architectures is the LCOE (Levelized Cost Of Energy) which links between the total investment and operational costs with the annual energy delivered to the final point that is concluded after the power losses calculation, during the lifetime of wind farm exploitation. For more realistic conditions, the wake effect between wind turbines is taken into account in the overall losses' calculation. Hence, the wake effect impact assessment is evaluated for each electrical architecture. For each iteration of the algorithm, electrical assessment of the wind farm architecture is made and then better topology is proposed taking into account optimization criteria (LCOE) until converging to the best one.

Thesis outline

The thesis main chapters are structured as follows:

- Chapter 1: The first chapter is a state of the art devoted to offshore wind energy in general. First, the market status of offshore wind installations in the world is exposed with more details for the European market and the main pioneer countries for offshore wind energy installation. Then, the main operating characteristics of an offshore wind turbine are presented. After that, the conceptual electrical architectures of offshore wind farm are shown with the comparison between HVAC and HVDC transmission networks regarding each one's economic extent. The last part focuses on the optimization framework for offshore wind farm design in order to show the state of the art of the different optimization approaches used until today for offshore wind farms. Besides, the optimization framework proposed in this PhD thesis is presented by showing the steps

of the wind farm electrical system evaluation and by identifying important criteria for the electrical network optimizing.

- Chapter 2: This chapter is dedicated to present the electrical and economical models of offshore wind farms as well as the methods for designing optimal offshore wind farm. In fact, electrical modeling consists in determining the electrical parameters that will be exploited for the load flow calculation, economical models aim to calculate the investment cost of each component that are then exploited to compute the LCOE. The load flows are evaluated for full AC and mixed AC/DC topologies with the library Mat AC/DC. However, for full DC topologies, a radial DC load flow is developed and then validated with an example. A calculation methodology for wake effect implementation is presented with the Katic Jensen model. Besides, a general wind farm topology modeling is exposed and then integrated in the optimization framework. The optimization algorithms used in this work are the genetic and Prim algorithms. Finally, the integration of load flow and wake effect calculations in the optimization algorithm is exposed.

- Chapter 3: The final chapter concerns the validation of the proposed optimization framework for offshore wind farms design. First of all, the optimization algorithm is applied for a real wind farm Borssele I and II in the aim to validate its effectiveness. Then, the wake effect calculation will be integrated in the different offshore electrical networks (Full AC, mixed AC/HVDC and full DC). Indeed, a study will be conducted to show the wake effect impact on these different architectures' performances for different transmission distances. Finally, a technical-economic analysis of the three different connection architectures will be detailed in order to determine the most suitable electrical technology for a given set of offshore wind farm characteristics. The LCOE and the losses of each technology are investigated according to transmission distance. Therefore, the strengths and weaknesses of each topology are exposed. Then, the break-even distance for the proposed technologies will be discussed.

Finally, we will present in the last part of this thesis work the general conclusions with some perspectives.

Contributions

Publications

1. A. Dabbabi, S. Bourguet, R. Loisel, M. Machmoum. ” Optimization of offshore wind farms with HVAC and HVDC transmission networks,” in Proc. of Electrimacs Conf., May, 2019.

2. A. Dabbabi, S. Bourguet, R. Loisel, M. Machmoum. ” Offshore wind farm layout optimization considering wake effects,” in Proc. of IEEE Conf., EPE, Nov, 2020.

Oral communication

3. Optimization of offshore wind farms with HVDC transmission network (COFMER’03), Marrakech-Maroc, 16 - 18 April 2019.

Chapter 1. *State of the art of offshore wind farms plants*

1 Introduction

The objective of this chapter is to present a general overview of offshore wind technology in order to explain the economic and technological context of electrical architecture concepts of offshore wind farms.

The market status of offshore wind installations in the world will be exposed. Thus, the current European status will be detailed. After that, main operating characteristics of an offshore wind turbine will be presented, before highlighting the different AC and DC electrical architectures by comparing the HVAC and HVDC transmission networks regarding each one's economic extent. The last part focuses on the optimization framework for offshore wind farm design in order to show the state of the art of the different optimization approaches used until today for offshore wind farms. Besides, we will present our optimization framework proposed in this PhD thesis by showing the steps of the wind farm electrical system evaluation and by identifying important criteria for the electrical network optimizing.

2 General context of offshore wind farm

2.1 Market status for offshore wind energy projects in the world

Compared to onshore wind farm, offshore wind farm has many advantages. It mainly focuses on a higher extracted wind speed with fewer fluctuations due to favorable wind conditions off the coast, a lower energy loss thanks to the possibility to extract maximum energy so as to improve the utilization of the installed wind energy capacity compared to onshore sites. Environmental influence is also under consideration since the offshore wind farms are less noisy and have less impact on the landscape.

Therefore, developing offshore wind farm is a promising trend to make the best exploitation of wind power. The year 2019 was the best year in history for the global offshore wind farms installation with 6.1 GW new capacity added. In fact, China achieved a new record in 2019 with the installation of 2.4 GW in a single year. The United Kingdom came in second place, with the contribution of 1.8 GW. Germany took the third-place tanks to 1.1 GW of new installations, followed by Denmark and Belgium [4].

Figure 1-1 shows that between 2015 and 2019, offshore wind installations have grown from 3.4 GW to 6.1 GW, the market share in global installations has increased from 5% to 10%.

Europe is the largest offshore market in 2019 with 75% of total global offshore wind installation. Nevertheless, Asia keeps growing their offshore wind installations with China contribution with 2.4 GW in 2019. Besides, Taiwan connected its first offshore wind farm, Vietnam, Japan, and South Korea are planning to install offshore wind projects soon. The United States does not contribute so much in the global offshore wind, it has only 30 MW but it aims to produce 9 GW by 2030 [5]. The top five offshore wind market in total offshore installations are: The UK, Germany, China, Denmark and Belgium.

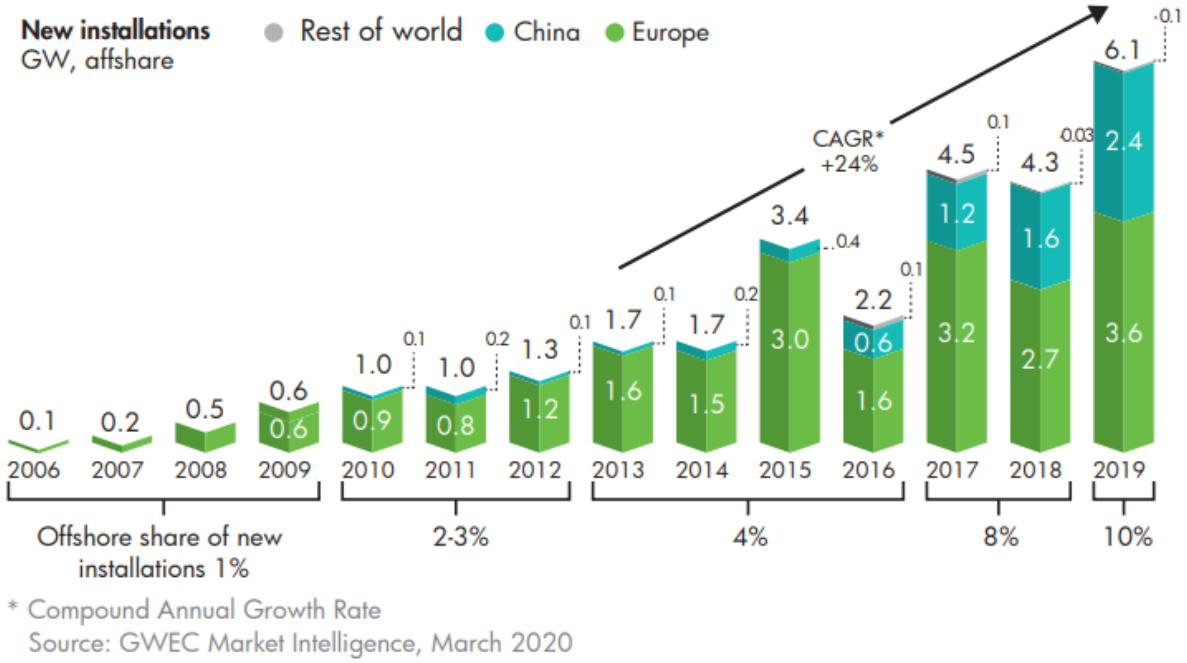

Figure 1-1 New installations of offshore wind projects in the world

2.2 Current European status for offshore wind energy projects

In this part, the current status of offshore wind technology in 2019 is presented. Europe is so far the first leader of offshore wind energy capacity with the installation of 502 new connected offshore wind turbines by the end of 2019 which added 3623 MW of net additional total capacity. Likewise, the total wind capacity installation in Europe is about 22072 MW gathered from 110 offshore wind farms in 12 countries with a total of 5047 grid connected wind turbines which represents more than 90% of the world's installed offshore wind capacity [6].

Figure 1-2 represents the annual offshore wind installations by country and cumulative installed capacity.

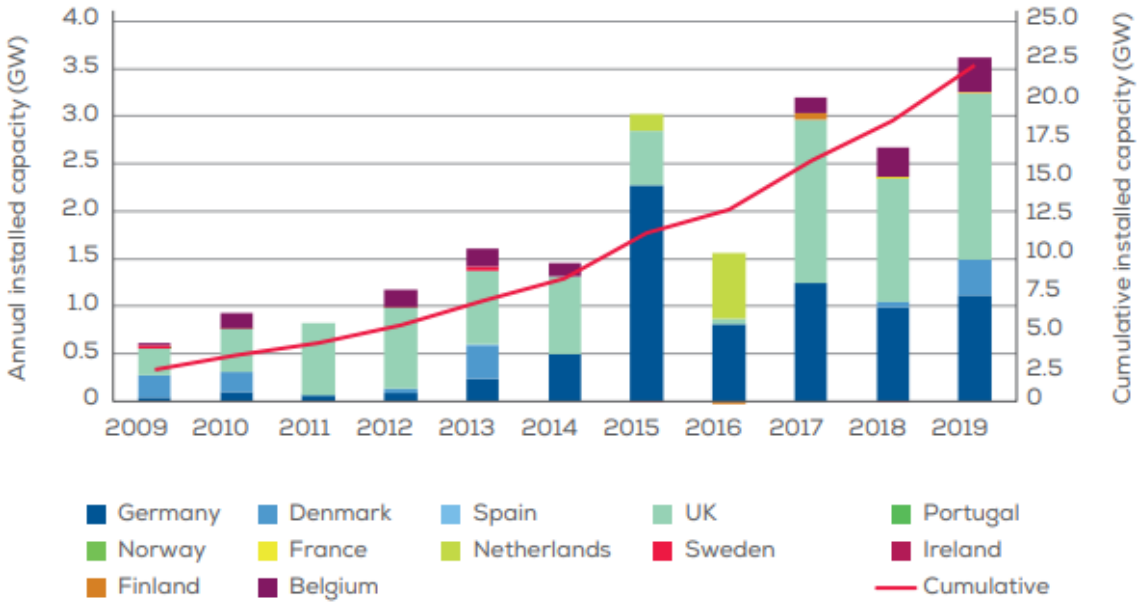

Figure 1-2 Additive offshore wind farm installations

Figure 1-3 detailed the gross installed capacity (MW) per country in 2019.

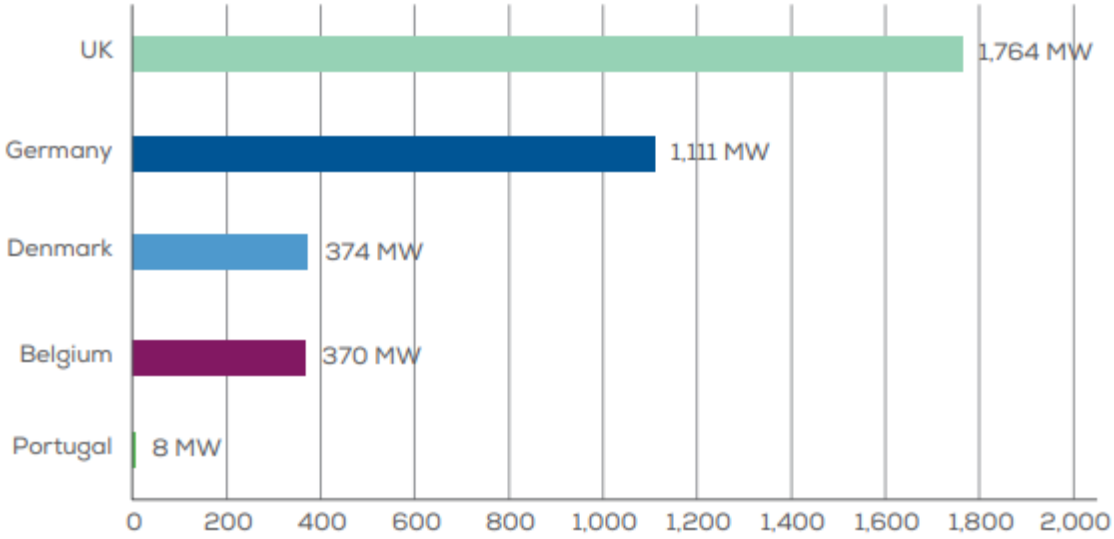

Figure 1-3 Additive offshore Gross installed capacity (MW)

The year 2019 is the best year for offshore installations' capacity. Focusing on this year, one may notice that the UK and Germany contribute mainly to the annual installed capacity in EU with respectively 1764 MW and 1111 MW. Thus, UK and Germany represented respectively 48.5% and 30.5% of Europe's gross capacity in 2019. Denmark contributed with 374 MW thanks to the installation of the largest wind farm in Denmark Horns Rev 3. Belgium connected 370 MW with the installation of biggest offshore wind farm in Belgium Norther. France does not contribute much with offshore installation compared to other European countries. In fact, it

has only 2 MW installed in 2018 that come from the connection of a floating wind turbine off the coast of Brittany (Floatgen project). The cumulative offshore installed capacity increases from one year to another especially between the years 2014 and 2019 and this proves that in the future, offshore wind power will invade the energy market because of its optimal energy yield compared to onshore wind farms [6]. The table below presents an overview of grids connected in offshore wind power projects at the end of year 2019 [6] [7] [8].

Table 1-1 Offshore connected grids for different countries in 2019

Country	No. of wind farms connected	Cumulative capacity (MW)	No. of turbines connected	Net capacity connected in 2019	No. of turbines connected in 2019
United Kingdom	40	9945	2225	1760	252
Germany	28	7445	1469	1111	160
Denmark	14	1703	559	374	45
Belgium	8	1556	318	370	44
Netherlands	6	1118	365	0	0
Sweden	5	192	80	0	0
Finland	3	70.7	19	0	0
Ireland	1	25.2	7	0	0
Spain	2	5	2	0	0
Portugal	1	8.4	1	8	1
France	1	2	1	0	0
Norway	1	2.3	1	0	0
Total (MW)	**110**	**22072**	**5047**	**3623**	**502**

The leader of turbine manufacturers in Europe is Siemens Gamesa with 68.1% of total installed capacity. In the second place, there is MHI Vestas offshore wind with 23.5%. The top 3 manufacturers (Siemens Gamesa, MHI Vestas and Senvion) represent 96% of all turbines connected in Europe in 2019.

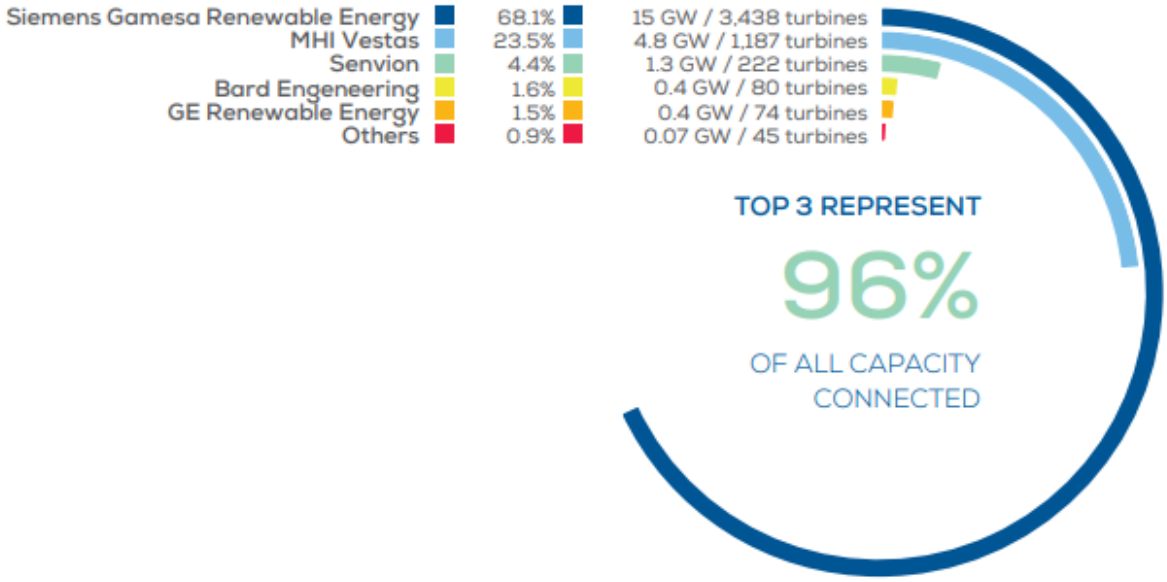

Figure 1-4 Wind turbine manufacturers [6]

2.3 Trends of offshore wind farms

2.3.1 Installed capacity

Current statistics reported in [6] [7] indicate that for new offshore wind farms projects the average wind turbine rated capacity has increased. So, between 1991 and 1999, the average rated turbine did not exceed 1 MW, this value was tripled between 2009 and 2010 and was raised to reach almost 8 MW in 2019.

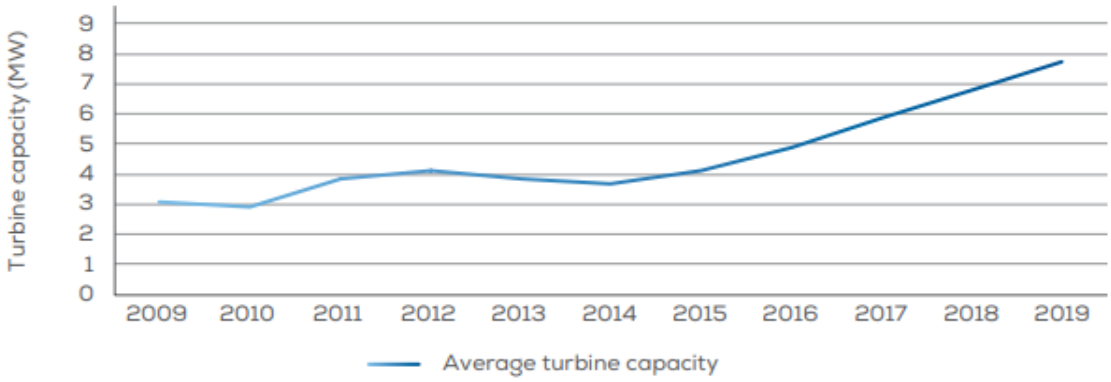

Figure 1-5 Installed offshore wind turbine rated capacity

The idea of raising turbines rated capacities throughout the years lies behind the concept of enlarging wind farms sizes without increasing the number of turbines. According to Figure 1-6, the average size of offshore wind farms is 621 MW in 2019 compared to only 313 MW in 2010.

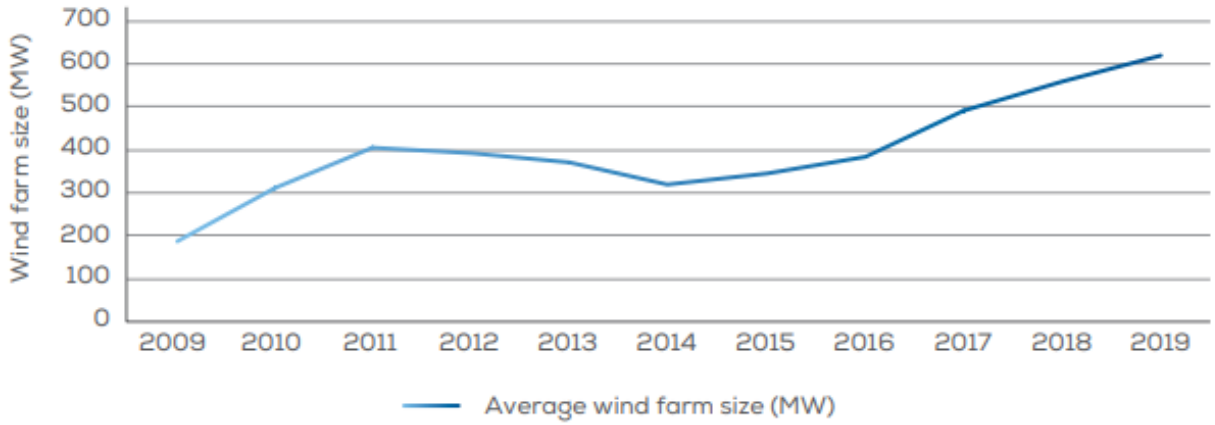

Figure 1-6 Average size of offshore wind farms

Figure 1-7 shows the turbine rated capacity and number of turbines of wind farms under construction in 2019 for different European countries. Most of the wind farms are using turbines of 7MW (the average rated power is 7.8 MW indicated with the red line). The trend towards larger projects will continue for the next decade [6].

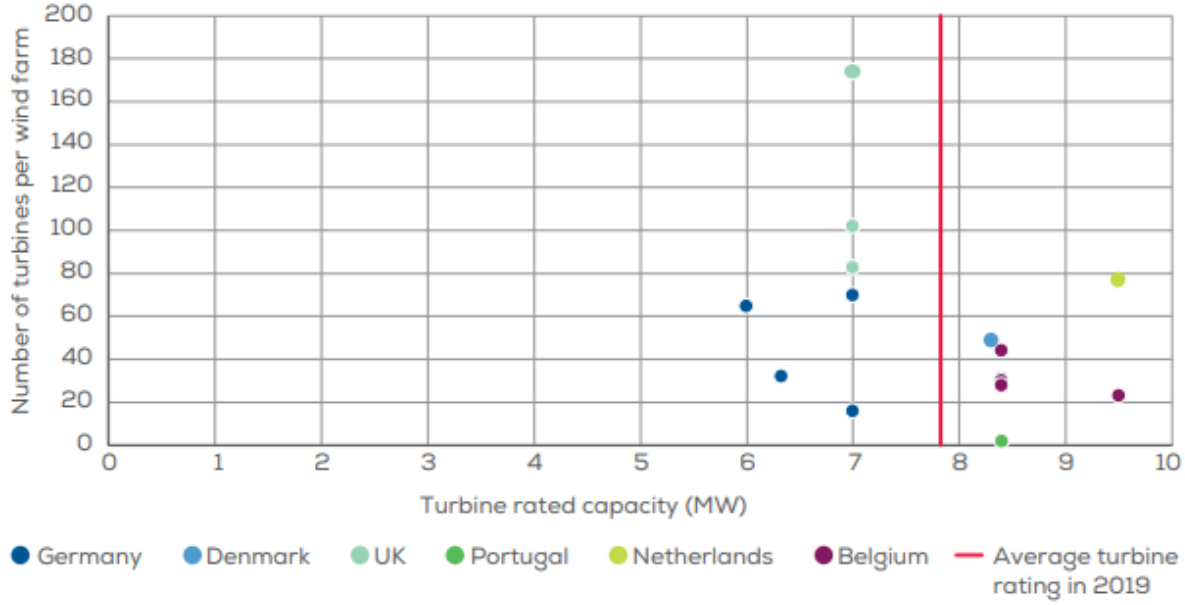

Figure 1-7 Turbine rated capacity and number of turbines of wind farms

2.3.2 Water depth and distance to shore

According to figure 1-8, until the end of 2019, the average water depth for constructed wind farms was 33 m and the average distance from the coast was 59 km. By analyzing projects under construction, these statistics are likely to increase considerably especially for floating parks where the average water depth can be twice deeper than the bottom fixed ones. The bubble size in figure 1-8 indicates the overall wind farm capacity [6] [7].

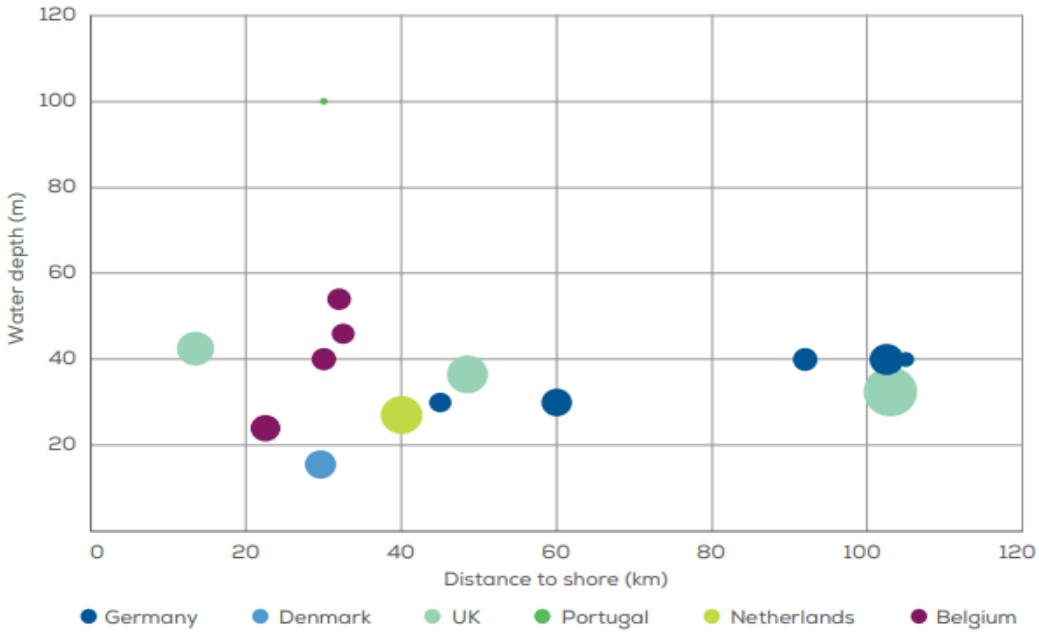

Figure 1-8 Average water depth and distance to shore of offshore wind farms

3 Operating characteristics of offshore wind technology

3.1 Principle of wind power extraction

Offshore wind turbines are classified according to the geometric arrangement of their shaft on which the propeller is mounted. There are two types of wind turbines: horizontal and vertical. Indeed, vertical axis wind turbines are the first forms used for the production of electrical energy. This type was developed but was not sufficiently industrialized, On the other hand, those with horizontal axis are currently more widely used because they are less expensive. The principal components of horizontal axis wind turbines are (figure 1-9): 1. blade 2. blade support 3. Pitch angle actuator 4. hub 5. spinner 6. main support 7. main shaft 8. aircraft warning lights 9. gearbox 10. mechanical brakes 11. hydraulic cooling devices 12. generator 13. power converter and electrical control 14. anemometers 15. transformer 16. nacelle 17. tower 18. yaw driving device.

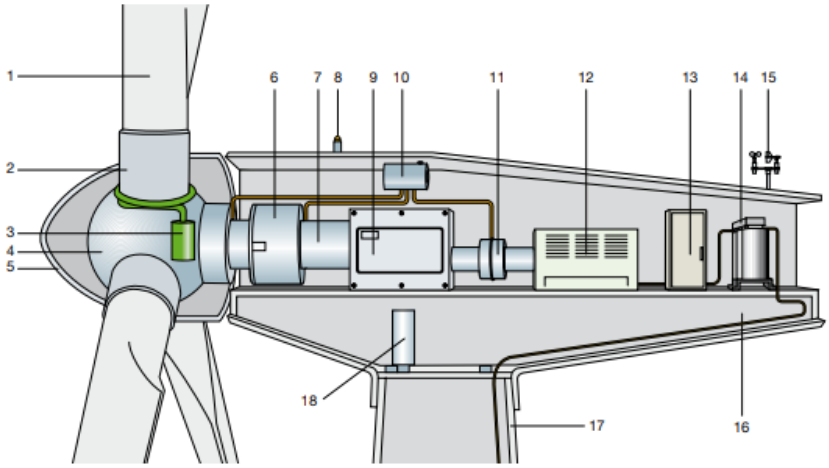

Figure 1-9 Offshore wind turbine constituents [9]

The tower: it allows to raise the wind turbine; it must be placed at a high altitude in order to capture the maximum kinetic energy of the wind for a better energy efficiency. In general, it consists of a steel tube that also allows the circulation of electrical cables.

The nacelle: it contains the mechanical elements that are used to couple the electric generator to the turbine shaft and to orient the turbine.

The gearbox: allows the speed of the wind turbine to be adapted to the generator speed since the rotation of the blades cannot directly drive the generator, hence the need to increase the speed with a gear system that constitutes the multiplier.

The generator: it is the component that allows the conversion of mechanical energy into electrical energy, it can be a synchronous, asynchronous cage or wound rotor machine.

The shaft: allows the hub to be connected to the gearbox, it consists of a mechanical brake that can be used in case of emergency (failure of the aerodynamic brake or maintenance of the wind turbine).

The pitch controller system: it is a system allowing the orientation of the wind turbine by regulating the power (aerodynamic adjustment).

A wind system is mainly used to convert the kinetic energy of the wind into electrical energy. This conversion is done in two main steps:

- Transformation into mechanical energy: in this step the kinetic energy of the wind is converted into mechanical energy at the turbine.

- Electric power generation: this is the step of converting mechanical energy into electrical energy at the generator level.

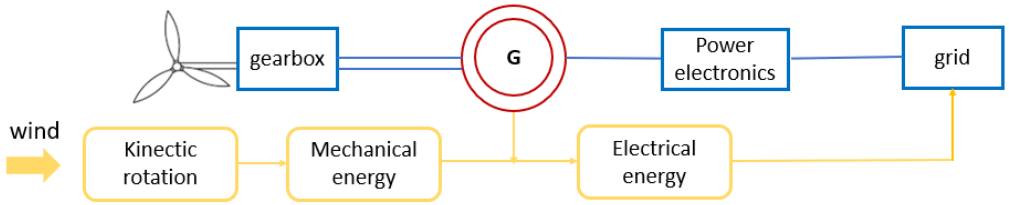

Figure 1-10 Energy conversion chain

To produce power at the wind turbine, the wind speed must be at least equal to 4 m/s (14.5 km/h), so the operating area could go up to a nominal speed around 12 m/s (43 km/h) and beyond this, the power produced stabilizes at the nominal power of the machine until the wind reaches the safety speed of about 25 m/s (90 km/h).

The mechanical power extracted from the wind can be expressed with the following relationship [10] [11]:

$$P_{mec}=\frac{1}{2}\ \rho\ \pi\ R_t^2\ C_p(\lambda,\beta)\ \ v^3 \tag{1-1}$$

Where ρ is the air density 1.225 kg/m^3, R_t is the radius of the turbine (m), v is the wind speed (m/s) and C_p is the power coefficient. This is the aerodynamic efficiency of the turbine. It is a non-linear function of the parameters λ and β which are respectively: the specific speed "tip ratio" and the pitch angle of blades. This coefficient has a theoretical limit (Betz limit) equal to 16/27. Ω_t is the turbine mechanical speed (rad/s).

$$\lambda=\frac{R_t\Omega_t}{v} \tag{1-2}$$

The variation of the power coefficient as a function of the blade pitch angle β and tip ratio λ is illustrated in the figure below:

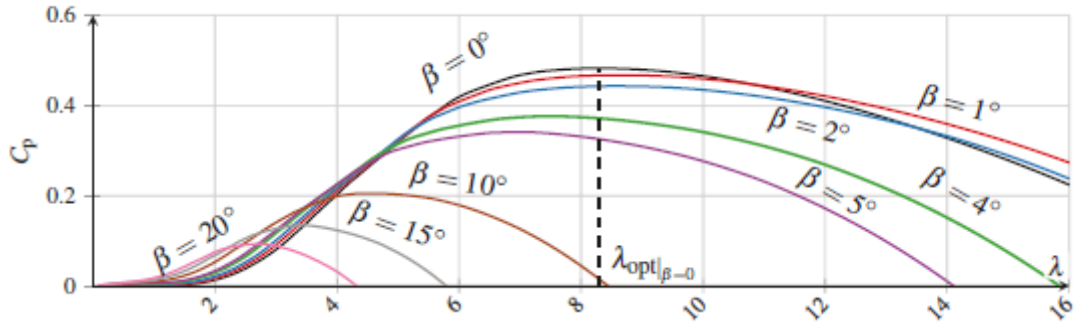

Figure 1-11 Variation of the power coefficient as a function of the pitch angle and the speed ratio using approximated data of a Vestas V90 wind turbine [12]

As shown in figure 1-11, the larger the pitch angle, the less the turbine will capture the kinetic energy of the wind. In fact, at low wind speeds, the blades are oriented downwind in order to extract maximum power, and once the nominal wind speed V_n is reached, they tilt to reach the "flag" position at maximum wind speed. The mechanical-electrical conversion is controlled by the pitch angle β, in fact, depending on the variation of β from 0° to 20° or 30°, it is possible to reduce or increase the power captured by the turbine. On the other hand, wind turbines can be controlled by other technologies such as active stall, which is based on small variations in the angle of setting (3° to 5°) or passive stall, which is mainly used with fixed speed wind turbines [13] [14].

3.2 Principle of electromechanical conversion

There are two principal types of generators for a wind turbine: either fixed speed or variable speed. The difference is mainly related to the arrangement and type of the different components such as the generator, converter and multiplier, it is also in the way the speed is controlled. Thus, there are 4 different types of turbine configurations:

- Type 1: Fixed speed wind turbine
- Type 2: Partial variable speed wind turbine
- Type 3: Variable speed wind turbine with partial rate converter
- Type 4: Variable speed wind turbine with full rate converter

3.2.1 Fixed speed wind turbines

These wind turbines generally consist of a turbine, a Gear box and a generator. This generator is mainly a Squirrel Cage Induction Generator (SCIG) directly coupled to the grid through an LV/MV transformer. The speed is maintained constant by the mechanical blade orientation

system (pitch control) [15] [16]. A capacitor bank and a soft starter are required to compensate the reactive power used to magnetize the asynchronous cage machine. The advantages of type 1 wind turbine are its robustness and its low cost thanks to the absence of power electronics since it is related to the use of standard machines. However, this turbine configuration presents some main drawbacks. In fact, it requires a reactive energy consuming device necessary for the magnetization of the asynchronous machine and it generates frequent variations in mechanical torque due to the movement of the blades to keep a constant speed, resulting current rapid variations in the system. Furthermore, the fact that there is no reactive energy control leads to no voltage and frequency provided to support the grid. Moreover, the extracted power by this turbine configuration is not optimized since it operates at a constant speed, so, maximum power generation cannot be always achieved for different wind speed.

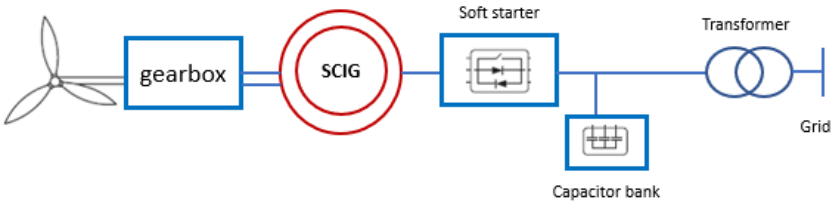

Figure 1-12 Squirrel cage induction generator (SCIG)

3.2.2 Partial variable speed wind turbines

This type includes a Wound Rotor Induction Generator (WRIG) connected to an external rotor resistance (R_{ext}) by means of power converter. Like Type 1, the stator is connected directly to the grid and there is a bank capacitor and a soft starter for reactive power compensation. In fact, by changing the external rotor resistance, this turbine regulates a slip range of 0 to 10 % above synchronous speed so the power extraction efficiency is partially improved. Nevertheless, it has mainly the same disadvantages as the fixed speed turbine.

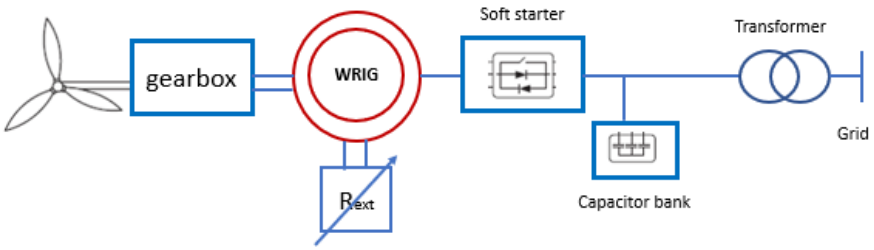

Figure 1-13 Wound Rotor Induction Generator (WRIG)

3.2.3 Variable speed wind turbines

Variable speed generators are connected to power converters before being connected to the grid, the installation of power electronics allows the control of these generators [17]. Figure 1-14 shows the mechanical power characteristics of a wind turbine as a function of the generator rotation speed for different wind speeds. Therefore, to optimize the operating point of wind turbines, it is advisable to adjust the rotational speed of the generator shaft according to wind speed to reach the maximum power points (Maximum Power Point Tracking, MPPT). Currently, most wind turbines adopt this speed variation technique because it has several advantages such as:

- The increase in the operating range as long as the maximum power can even be reached at low wind speeds.
- The reduction of mechanical stresses through the adaptation of the turbine speed to wind variations, thus reducing the impact of wind gusts on the power generated.
- Simplification of the blade orientation system thanks to the possibility of controlling the generator speed by the electromagnetic torque, which in turn allows the limitation of the turbine speed and the power generated at high wind speeds.
- A better integration of the wind turbine into the grid thanks to voltage and frequency support provided by converter control.
- Noise reduction during low power operation as the speed becomes low.

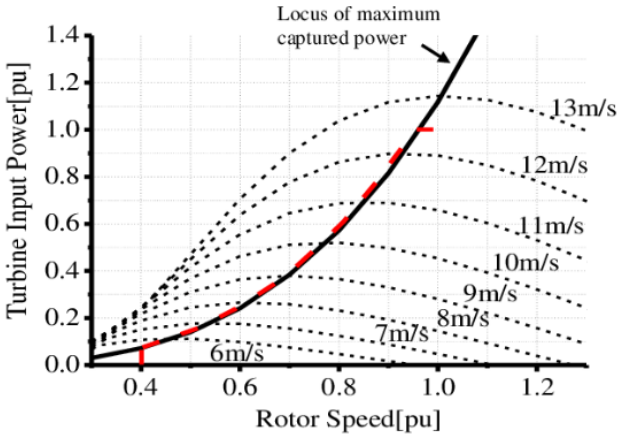

Figure 1-14 Speed control characteristic (MPPT) of a wind turbine

There are two types of variable speed generators:

- Double Fed Induction Generator (DFIG) [18][19][20].
- Permanent Magnet Synchronous Generator (PMSG) [21].

Table 1-2 presents the advantages and disadvantages of each generator topology.

Table 1-2 Advantages and disadvantages of 2 different types of variable speed generators

Turbine type	Descriptive Diagram / Avantages / Drawbacks
DFIG	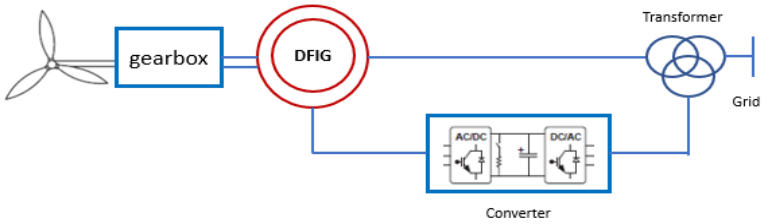 <u>Avantages</u> - Optimized extracted power - Managed magnetization of the machine in the case of a grid fault - Wider speed range (Power electronics dimensioned for 30% of the generator nominal power) - Simple generator connection <u>Drawbacks</u> - Higher cost - Possibility of machine operation failures due to the use of slip rings - Complex command control - Maintenance of the gearbox
PMSG	 <u>Avantages</u> - Variable speed operation over the entire speed range - Optimized extracted power because the maximum power extraction is achieved regardless of the wind speed by the means of full power converter control - Possibility of no gearbox - Simple generator connection <u>Drawbacks</u> - Higher cost - Specific machine - Power electronics dimensioned for the generator nominal power

Table 1-3 summarizes some offshore wind turbine topologies made by different manufacturers. According to the table, the trend is mainly the use of PMSG topology because of its benefits compared to DFIG generator. Therefore, in this work, the choice is made for PMSG wind turbine topologies.

Table 1-3 Overview of offshore wind turbine topologies [source: manufacturers websites]

Manufacturer	Siemens	GE	Vestas	Senvion
Type	SWT-8.0-154	Haliade 150	V 164-8.0	6.2M152
Hub height	Site-specific	100 m	Site-specific	97-124 m
Rotor diameter	154 m	150 m	164 m	152 m
Rated power	8 MW	6 MW	8 MW	6.15 MW
Generator	PMSG	PMSG	PMSG	DFIG
Shaft	direct drive	direct drive	gearbox	gearbox

3.3 Wind Energy producibility

3.3.1 Wind resource modeling

Wind turbines are energy sources depending on wind speed so for their model an analytical model based on the power curve depending on wind velocity is used [22]. In this work, the MPPT operating mode is applied for each turbine for each wind speed. A typical power curve for the Haliade wind turbine (6MW) is shown in figure 1-15. This curve can be divided into 3 phases:

- Phase 1: the power generated by the turbine is zero for low wind speeds. This phase is specified by the cut-in speed which is the minimum wind speed at which the turbine starts to rotate (from 0 m/s to 3.5 m/s).
- Phase 2: is the middle phase where for each wind speed, a power is assigned (from 3.5 m/s to 14 m/s).
- Phase 3: it represents the steady state of the turbine, the power achieved the nominal value and keep it until the cut-out speed at which the turbine blades stop to turn in order to avoid damage from high winds (from 14 m/s to 25 m/s).

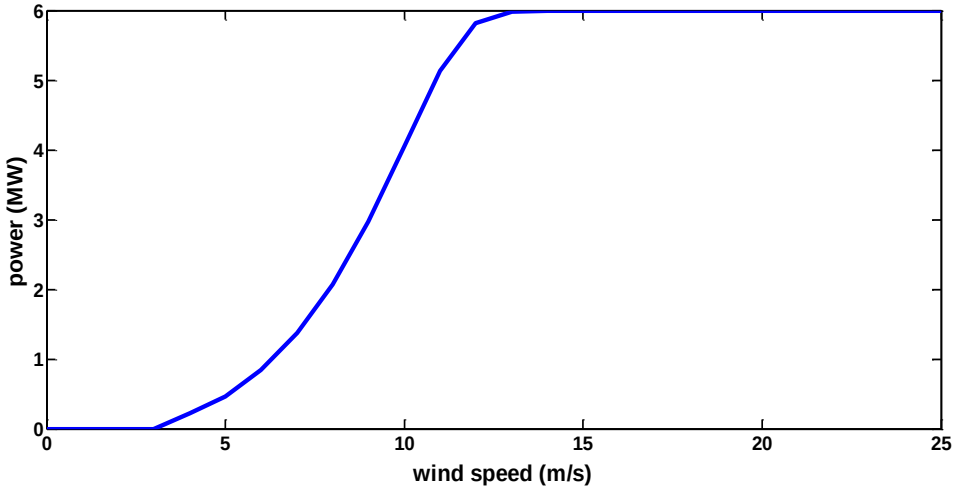

Figure 1-15 Power curve of the Haliade 6MW wind turbine

Knowing the mean speed of the wind at a particular site is not sufficient to determine the energy producibility of a wind turbine so it is necessary to have wind velocity data for certain period time (one year). Therefore, the wind is measured with an anemometer and the average wind speed is recorded every 10 minutes. These data can be classified into wind speed classes of 1 m/s each so the wind resource can be modeled with a probabilistic model which provides information on the occurrence probability of each wind speed. Generally, the Weibull distribution is a good approximation of the wind speed distribution, it is expressed by the following equation:

$$f_w(v)=\left(\frac{k}{c}\right)\left(\frac{v}{c}\right)^{k-1}\exp\left(-\left(\frac{v}{c}\right)^{k}\right) \quad (1\text{-}3)$$

With:

$$c=2\,v_{mean}/\sqrt{\Pi} \quad (1\text{-}4)$$

k is the Weibull parameter which takes a value between 1 and 3. In the case of marine wind, k is set at 2. Figure 1-16 shows the Weibull distribution for k=2.

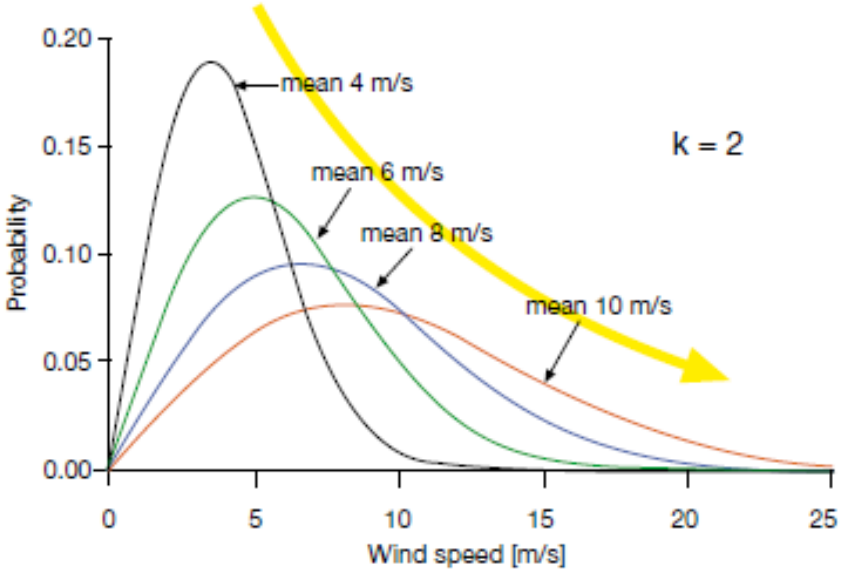

Figure 1-16 Weibull distribution (k=2)

Another information detail can be associated with wind resource which is the wind direction. In fact, for a specific location one can associate to each wind direction a probability of occurrence of the wind speed which can be modelized by the wind rose. The wind rose in the figure below shows wind conditions data for 16 different directions and 9 speed classes.

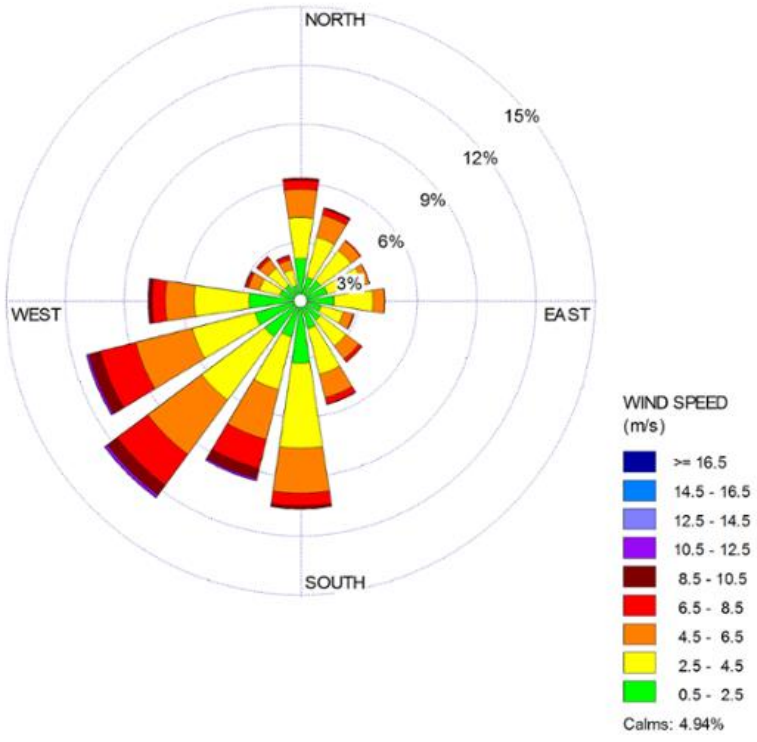

Figure 1-17 Wind rose [23]

3.3.2 Assessment of energy producibility

The annual energy production AEP (kWh) can be expressed as the product of the power curve of the turbine and the Weibull distribution during one year.

$$AEP = 8760 \int_0^{\infty} P(v)\, f_w(v)\, dv \tag{1-5}$$

Where: 8760 is the number of hours of wind farm operation per year and P(v) is the output power of the turbine (extracted from the power curve).

The total energy of a wind farm is obtained by multiplying the annual production energy with the total number of turbines. This value can be affected by losses produced by the aerodynamic interference between the turbines which called wake effects. In fact, the upstream wind turbine incurs the wind speed deficit on the downstream wind turbine so the total energy production will be reduced. The calculation of wake effect losses and its impact on the global chain of offshore wind energy production are studied in this work.

The evaluation of energy yield depends on different forms of connection between wind turbines as well as on the electrical architectures of transmission network. Thereby, a detailed state of the art of different electrical topologies for offshore wind farms is presented in the following section.

4 Electrical network architectures of offshore wind power plants

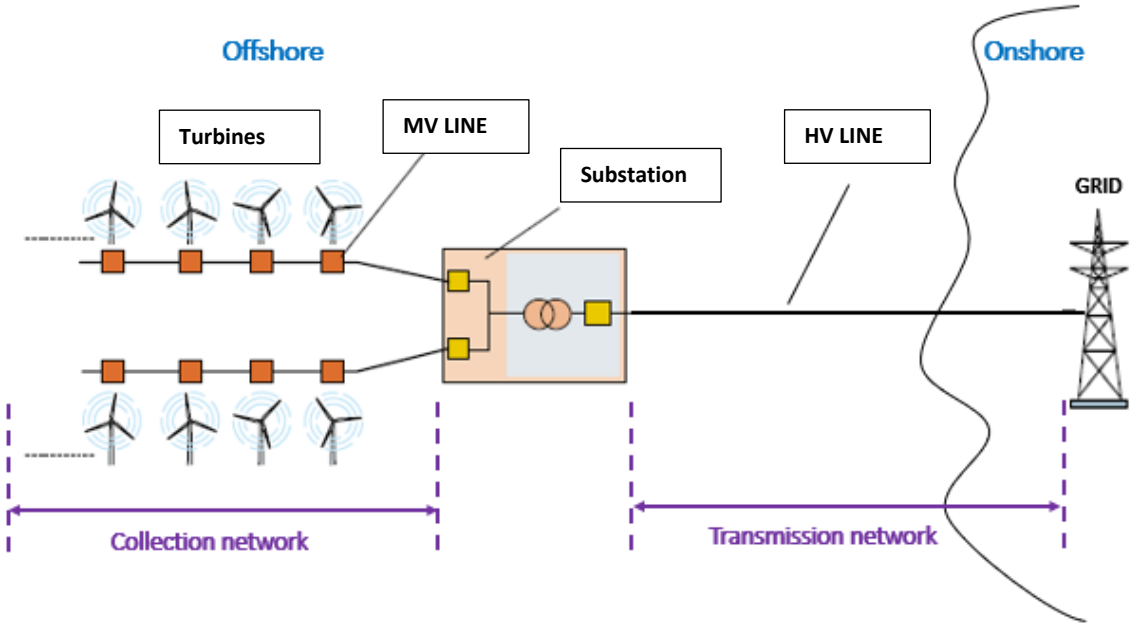

Figure 1-18 General topology of an offshore wind farm

Figure 1-18 shows the typical electrical architecture of an offshore wind farm, which consists of three main parts. The first is an energy production system where there are several wind turbines located offshore to harness wind energy to produce electricity. The second part is the internal **MV collection** grid (inter-array grid) in which there is the connection between wind turbines and the connection between turbines and offshore substations, this network operates at a medium voltage. Finally, the third part is the **HV transmission** network, thanks to offshore electrical substations, the voltage is increased and then transported in HVAC or HVDC transmission lines to the onshore point called delivery point (DP). A brief description of the main components of an offshore wind farm is presented below.

Submarine cables

There are two forms of cables: AC cables and DC cables. In fact, AC cables are "three phases" cables, and can be either single core or three core cables. For DC cables, their configuration depends on the DC system topology: monopolar or bipolar. It is mainly composed of two conductors laid separately or bundled in a co-axial arrangement. Cables are composed of different parts assembled concentrically. Indeed, there is a conductor in the center allowing the transport of electricity, which will then be covered with a layer of electrical insulation to prevent the flow of current to the ground, then everything is wound with a metal sheath to confine the electric field inside the cable and finally there is an external protection ensuring the mechanical properties and protection against external phenomena.

Three main technological families of submarine cables can be distinguished [24]:

1. Self-contained fluid-filled cables: SCFF (self-contained fluid-filled), HPGF (high-pressure gas filled) and HPFF (high pressure fluid-filled).
2. Paper insulated (lapped insulated) cables: PILC (paper-insulated lead-covered, high-viscosity insulating compound) and PPL (paper polypropylene laminate).
3. Extruded cables (figure 1-19): EPR (ethylene propylene rubber), PE (polyethylene) and XLPE (cross-linked polyethylene).

The most used submarine cables are XPLE ones because they are the most suited for high temperatures thanks to their polymeric molecular structure. Likewise, they can handle high voltages up to 300 kV and can be related to Voltage Source Converters (VSC) which are bidirectional (reversing power flow without reversing the polarity).

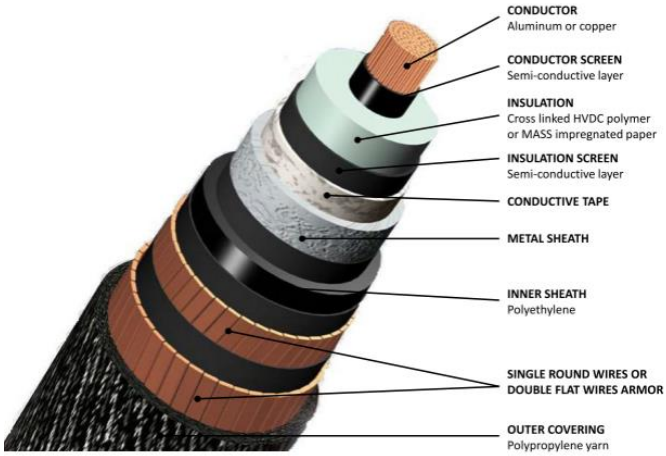

Figure 1-19 Single core (XLPE) for both AC and DC cable [25]

Offshore substations

The total produced electrical power in the MV grid is collected in offshore substations in order to be transported after that. These platforms are the intermediate between the collection and the transmission networks where the electrical losses are reduced by increasing the voltage from MV to HV. There are two different topologies of offshore substations based on the type of transmission lines: HVAC or HVDC.

HVAC platforms are mainly composed of transformers to step up the voltage from the MVAC collection network (33 kV, 66 kV) to the HVAC transmission network (132 kV, 220 kV). They can contain one or several parallel transformers. In fact, the use of one transformer can reduce the substation total cost but parallel transformers ensure the integration of redundancies, which improves the availability of platforms during their operating period. So, redundant paths increase the system reliability by reducing the energy not supplied in failure cases [26].

For HVDC platforms, the main component is converters, either AC/DC converter in the case of MVAC collection network or DC/DC converter in the case of inter array connected turbines with MVDC. Substations generally contain J-tubes to connect the collection grid cables to the platforms, switchgears to protect and isolate electrical components, diesel generators, and other different safety equipment.

Figure 1-20 First offshore substation at Race Bank wind farm

4.1 MV collection network

Offshore wind farms can take several configurations depending on the layout of the wind turbines and the connection between them, for example:

4.1.1 Radial connection

The radial collection network is composed of several feeders of wind turbines connected in string configuration to a common cable according to the current load capacity. Subsequently, many wind turbine radials are then connected to a substation that collects the power of the entire farm. It presents the cheapest collection configuration but it does not ensure a good reliability since in case of failure of one cable the lost power is important because it affects all the feeder. [27][28][29].

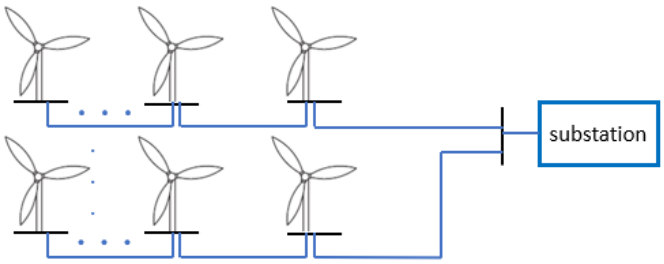

Figure 1-21 Radial collection system

4.1.2 Ring connection

Figure 1-22 shows a ring collection system. This configuration has greater reliability than the simple radial system. Since the ring connection can be reconfigured in fault cases, the energy produced is not lost thanks to redundant paths. It is more costly compared to radial

configuration, ring connections can be either single sided where the turbines are connected in one feeder or double sided where turbines are connected in two feeders. The system may require a more complex control system depending on the location and number of reconfiguration switches.

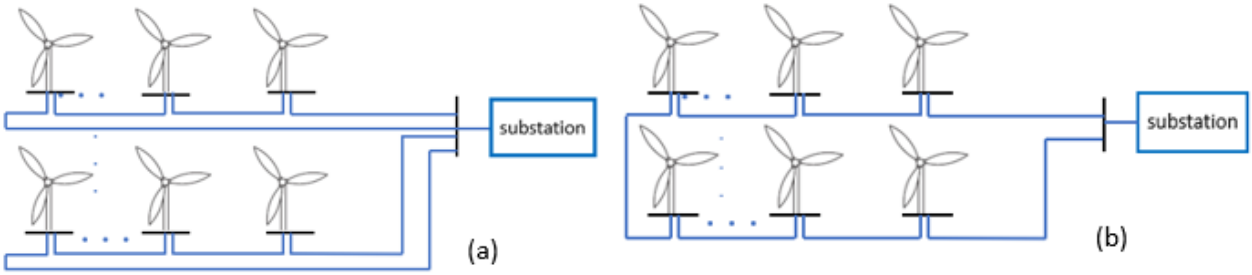

Figure 1-22 Ring collection system, (a): single sided ring, (b): double sided ring

4.1.3 Star connection

Figure 1-23 shows the topology of a star-connected wind farm. In this topology, each turbine is connected to an interconnection point (star/cluster point) by its own cable. Several of these turbines are connected to the star point according to the current load capacity of the main cable at the inter array system. With this configuration, a good system reliability is guaranteed since in the case of cable failure, the energy is lost only in one turbine [30][31][32][33][34].

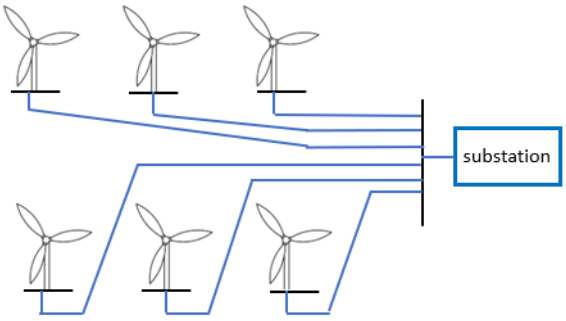

Figure 1-23 Star collection system

4.2 HV transmission network

Currently, available options for the High Voltage transmission networks of offshore wind farms are HVAC (High Voltage Alternating Current) and HVDC (High Voltage Direct Current) technologies. Indeed, a traditional AC transmission is carried out by AC submarine cables connecting the offshore substations to the delivery point. On each side of the HVAC line there

are equipment for compensation of reactive power. HVAC technology has been largely employed for the past century, thanks to the simple use of transformers for increasing voltages which are a high efficiency and low-priced components, but in front of the challenge of transmitting energy over long distances, this technology become limited due to the reactive power surplus of AC cables.

Throughout the years, due to the development of power electronics efficiency, HVDC technology has become a good alternative of energy transmission with 800 MW maximum power rating and voltage levels that can reach ±320 kV subsequently leading to lower cables losses (i.e. no dielectric losses and no reactive power, etc.). Some HVDC projects are shown in table 1-4.

4.2.1 Overview of HVDC transmission system

Over the years, HVDC projects worldwide are increasing since they offer economical and technical benefits. Among the biggest and the recent projects, one can mention INELFE (**IN**terconnexion **EL**ectrique **F**rance-**E**spagne) which is a HVDC line that connects the Baixas substation in France to the Santa Liogaia in Spain using two parallel electrical cables with a voltage of ±320 kV, approximately 65 km long. The total power transported is about 2GW. Table 1-4 sums up the different HVDC lines in the world.

Table 1-4 HVDC projects worldwide

Project	Country	Technology	Power (MW)	Voltage (kV)	Distance (km)	Year
Gotland HVDC light	Sweden	IGBT (First commercial installation with IGBT)	50	±60	100 (Submarine cable)	1999
Yunnan - Guangdong	China	Thyristor	5000	±800	1400	2010
Xiangjiaba - Shanghai	China	Thyristor	6400	±800	1980	2010
Jinping - Sunan	China	Thyristor	7200	±800	2090	2013
Rio Madeira	Brazil	Thyristor	3150	±600	2350	2014
INELFE	France-Spain	IGBT	2*1000	±320	65 (Submarine cable)	2015

The application of HVDC for bulk power transmission to the shore is preferred over HVAC for such situations:

- Asynchronous connection of AC power grids

Connection between two asynchronous AC networks or two grids with different frequency (50 Hz NE Japan and 60 Hz SW Japan, Nordel, Baltso, etc.) by the possibility of power flow control within VSC HVDC (back-to-back converter) so that improves the stability of an AC system.

- Long submarine cable connection

For long distances, HVDC provides a cost-effective way for power transmission compared to HVAC. In fact, AC cables have a capacitive charging current that causes the decrease of the available capacity for active power transfer because of reactive power generation. Subsequently, reactive power compensation is required so that affects in turn cable cost.

- Long distance power transmission

Transmission of large amount of energy within large distance where HVAC would be uneconomical. Indeed, HVDC converter losses are important but the DC cables losses are lower than AC cables. There is a break-even distance where HVDC losses become lower than HVAC losses.

Like mentioned in table 1-4, HVDC transmission network is ensured by the insertion of converters that can be based either on thyristors or IGBTs. Thus, the two main technologies of converters are presented in the section below. Furthermore, the different configurations of HVDC system are presented in Appendix 1.

4.2.2 HVDC converter stations

HVDC converters can be classified in two main categories: the classical **L**ine **C**ommutated **C**onverter (**LCC**) which consists of self-commutated thyristor valves and **V**oltage **S**ource **C**onverter (**VSC**) based on semiconductors operating at high voltage levels which are IGBTs (e.g. Insulated Gate Bipolar Transistors – IGBT). Both topologies are presented respectively in figures 1-24 and 1-25 [35].

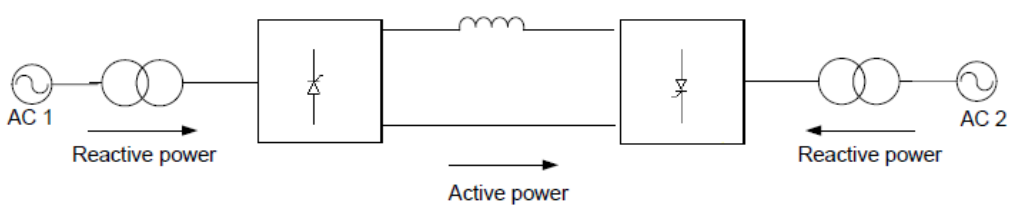

Figure 1-24 LCC-HVDC topology

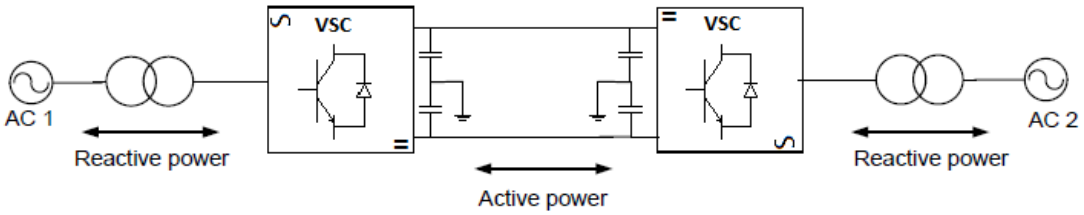

Figure 1-25 VSC-HVDC topology

The high switching frequencies of IGBTs (in the kHz range) compared to those of thyristors (50 Hz) prevent the use of filters for VSC converter so it has a smaller footprint compared to LCC converter. Furthermore, pulse width modulation (PWM) technique is used to set the output AC waveform so the AC voltage can be set at any desired value between the positive and the negative pole.

The operation principle of LCC converter is based on controlling the ignition delay angle α of the thyristors. Indeed, if α is between 0 degree and 90 degrees the converter operates in rectifier mode where it consumes reactive power and if α is up to 90 degrees, it is the inverter mode that is required. LCC converter technology has the ability to operate for high power applications due to higher power handling capacities of thyristors over IGBTs.

Table 1-5 presents a comparison between the two types of converters stations. For LCC system, the power inversion is made by the polarity inversion on the HVDC cable, while it is done by the current inversion for a VSC system: it is therefore easier to make multi-terminal links with VSCs. VSC HVDC has the possibility to control independently the active and reactive powers. The main weak point of VSC HVDC compared to LCC HVDC is its high losses especially switching losses. In fact, VSC losses can reach between 1.6% and 1.7% of the rated transmission power per converter at rated load against only 0.7% for LCC losses [36][37].

Table 1-5 Comparison between LCC and VSC converters

Converter type	Advantages	Drawbacks
LCC-HVDC converter	- low losses - high transmission capacity - high efficiency	- large space occupied (filters, transformers, compensation equipements, etc.) - no black capability (short-circuit capacity is required) - polarity inversion for flow inversion - only active power control
VSC-HVDC converter	- small footprint and environmental impact - automatically power reverse (due the current reverse) - independent control of active and reactive power - black start capability (i.e. ability to start without external additional power) - more flexible	- limited power - high losses

The VSC HVDC technology is more suitable for offshore installations due to their benefits compared to LCC HVDC converters. Therefore, in this work an emphasis is put on VSC HVDC topologies. The comparison between HVAC and HVDC transmission systems is crucial in order to see the performances and the efficiency of each technology.

4.2.3 HVAC vs HVDC

Bulk power is transmitted through high voltages in order to reduce line losses by reducing currents. The losses depend on the cross section of the cable, the conductor type as well as on the type of current AC or DC. HVDC transmission eliminates the skin effect because the DC current flows through the whole cross section of the DC cable whereas the AC current flows

only towards its surface which causes current density accumulation within the conductor that consequently boosts the skin effect and then increases the effective resistance and power losses.

For the same transmitted power, HVDC cables use less material than HVAC cables since they include all the power within only one line although AC link needs three power lines. Besides, DC cable insulation is simpler since AC line insulation has to take into account the peak voltage compared to the RMS voltage with a factor of $\sqrt{2}$ between the two. Therefore, for the same insulation requirements, DC line can carry more power per conductor.

Like mentioned before, HVDC lines are more beneficial concerning long-distance power transmission with important power capacities since there is no reactive power compensation equipment. Thus, investment costs for HVDC transmission system are reduced for long distance but high costs of converters can promote HVAC technology for small distances. For that, a break-even distance is necessary to show the distance from which HVDC becomes economically better than HVAC (figure 1-26). HVDC transmission system becomes more economical over HVAC when converter costs can be compensated by the low cost of DC cables and the cost of reactive power compensation equipment.

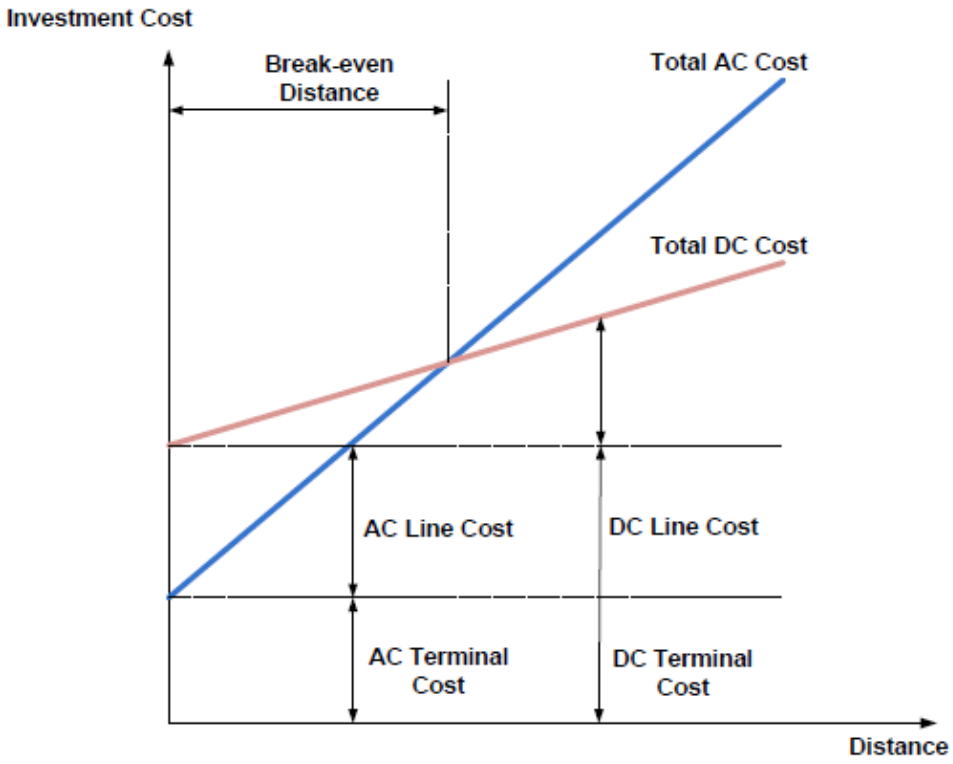

Figure 1-26 Break-even distance for HVAC and HVDC technologies [38]

4.3 Different electrical architectures of offshore wind farms: state of the art

Different electrical architectures can exist to connect an offshore wind farm that mainly depend on the connection between the wind turbines (inter-array layout), the distance from the coast, the number of turbines, the total capacity installed of the farm, the different voltage levels and the transmission configuration with the appropriate connection network AC or DC.

Several studies have sought to optimize the topologies of offshore wind farms with the aim of finding the best topology which offers less losses with a good economic compromise. In this section, a state of the art of different electrical architectures found in the literature is shown.

Wind farm architecture concepts can be either fully AC connected topologies, hybrid topologies with mixed AC and DC networks or finally fully DC connected topologies.

4.3.1 Full AC topologies

For total AC wind farm architecture, the wind turbine adapts its output power in AC, for that, the power electronic conversion inside the turbine goes through a double converter connected by the same DC bus. The first one is a rectifier (AC/DC converter) that controls the machine by managing the electromagnetic torque regulation and the second is an inverter (DC/AC converter) that maintains the DC bus voltage between the two converters and manages as well as the reactive power supplied to the collection network. The converters are followed by a transformer that increases the voltage to a level suitable for the collection network to reduce losses and also provides galvanic isolation.

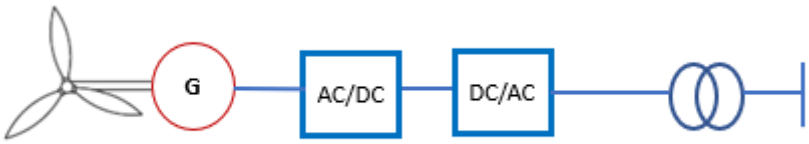

Figure 1-27 Internal topology of a wind turbine for AC network connection

According to the literature, it can be noticed that all the AC wind farms can be classified into two different AC systems referred to as small and large AC wind farms. In fact, small ones are made with the MVAC network for both collection and transmission systems. On the other hand, for larger wind farms, the HVAC technology is used for transmission with long distances. This internal topology is applied for all wind turbines shown in figures 1-28, 1-29, 1-30.

4.3.1.1 MVAC collection and transmission networks

According to this configuration, the wind power plants will be placed in a network totally in MVAC for the collection and the transmission systems up to the terrestrial grid. This electrical architecture concept adapts to small AC wind farms as proposed by Lundberg [39] (not exceeding 60 MW) with short transmission distance from the coast. In this case, the wind turbines are connected to each other with MVAC cables forming the inter-array system. The final point of each wind turbines cluster is related to the grid interface (delivery point) with an MVAC line. This means that there are several cables for transmitting the power to the grid and it involves the increase of cables costs with its installation hence the suitability of this configuration for small farms. The voltage levels can be either 33 kV or 66 kV, it is medium voltage adequate to avoid important loss lines for short transmission distance.

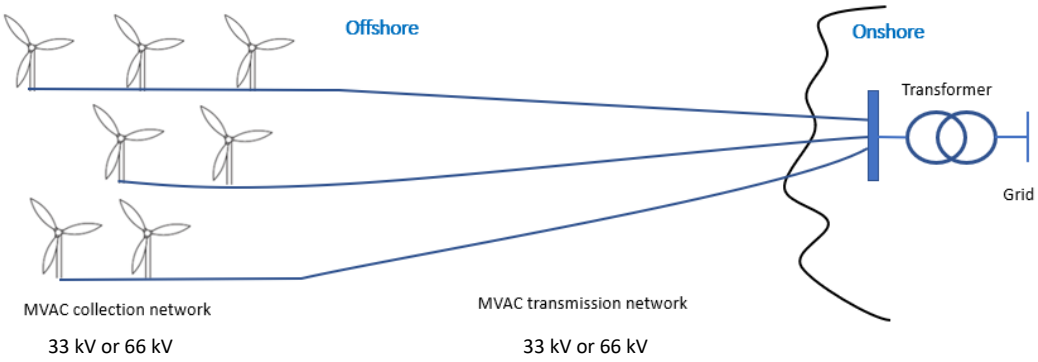

Figure 1-28 AC architecture with MVAC collection and transmission networks

4.3.1.2 MVAC collection and HVAC transmission networks

The full AC topology is a traditional configuration based on the general system in figure 1-29. This system has a set of wind turbines connecting with MVAC network (33 kV or 66 kV). After that, a transformer is required to ensure HVAC transmission (above 66 kV e.g. 132 kV or 220 kV). Therefore, an offshore platform is necessarily installed to encompass the transformer, switching equipment and shunt reactors for reactive power compensation injected by the inter-array system. Besides, the shunt reactors are installed as well as in the final extremity of the transmission line it means in the grid to compensate the reactive power injected by the HVAC cables. For transmission, by the means of the use of only one HV cable that can handle the total power produced by the cluster of wind turbines, the total cost of cables decreases so the investment cost of the wind farm is optimized [40].

The Horns Rev is an example of an offshore wind farm with 160 MW installed capacity, located at 14 km from the west coast of Denmark, is built according to this principle.

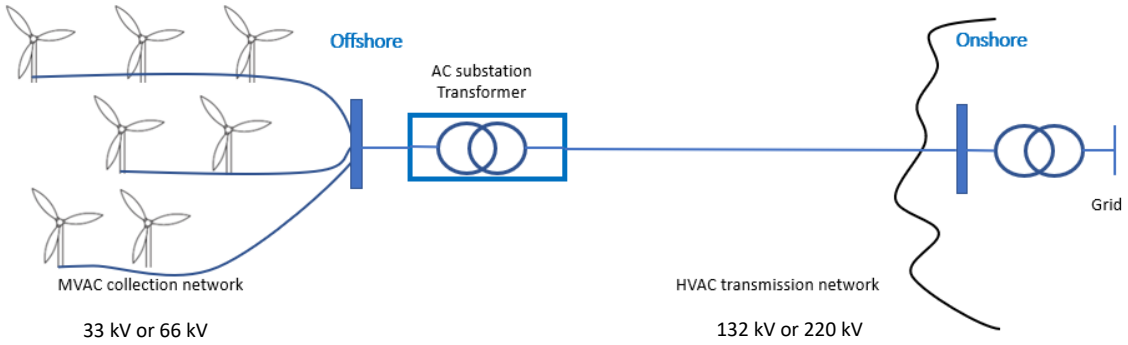

Figure 1-29 AC architecture with MVAC collection and HVAC transmission networks

4.3.2 Mixed AC and DC topologies

Referring to previous comparison between HVAC and HVDC technologies, one can conclude that when the distance from the shore gets more and more important with large wind farms HVDC transmission solution becomes advantageous. Indeed, two different mixed AC and DC topologies are presented in the following.

4.3.2.1 MVAC collection and HVDC transmission networks (rectifier / inverter for each turbine):

Wind turbines internal architecture for this topology are presented in figure 1-30. It is the standard configuration that is composed of a rectifier followed by an inverter and a transformer.

For this topology, wind turbines are connected with an AC collection network and the total power produced is transmitted in HVDC with a voltage around ±150 kV or ±320 kV so the necessity to implement AC/DC conversion by the means of a rectifier that is placed in an offshore substation, the latter allows the controllability of both voltage and frequency of the AC collection system so the electrical efficiency of each turbine is improved thanks to the MPPT process. The HVDC cables encompass the energy flow to the delivery point where an inverter is used to adjust the suitable voltage and frequency of the grid. Like HVAC transmission, the HVDC one is made also by one cable resulting the decrease of the cable costs noting that HVDC cable costs are lower than HVAC ones but the total investment cost can be raised by offshore converter station costs [41].

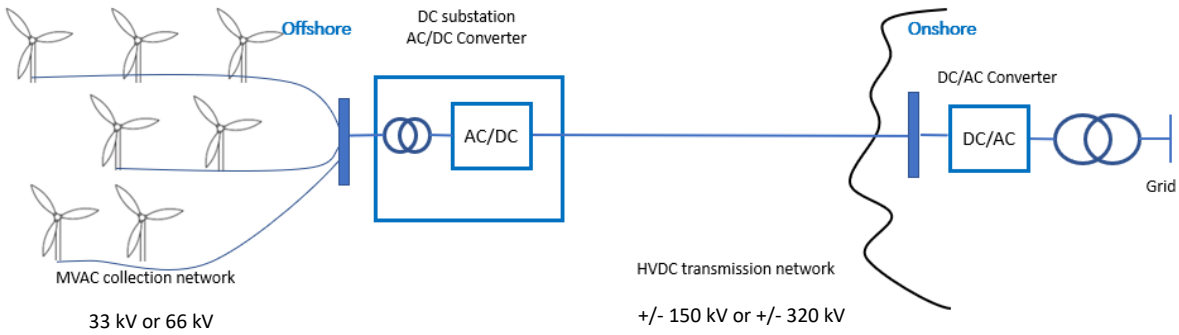

Figure 1-30 Mixed MVAC and HVDC standard topology

4.3.2.2 MVAC collection and HVDC transmission networks (controlled by a common AC/DC converter)

The internal configuration of the wind turbine can be used to optimize the total structure of the offshore park. For example, Mikel de Prada in his research [42] presents a new method for hybrid topologies. In fact, the approach consists in grouping the wind turbines into clusters and controlling each group by a single AC/DC converter installed jointly at the collection network then the power will be transmitted in HVDC after passing through an offshore platform containing a DC/DC converter. As a result, there are no more rectifiers and inverters connected to the output of each turbine, only the transformer is connected directly to the turbine.

As mentioned below, this structure aims to optimizing the electrical architecture of the offshore wind farm by taking into account the optimization of the number of AC/DC converters and the links between wind turbines via submarine cables (optimization of cable lengths). The purpose of removing the converters (rectifiers and inverters) connected to each turbine is to reduce the cost of components and maintenance. This concept can be applied to synchronous and asynchronous machines. The operating principle is to have a common converter for each wind turbine cluster operating at the optimal electrical frequency, i.e. wind turbines that are connected to the same AC/DC converter operate at the same frequency f* as shown in figure 1-31. Therefore, it is no longer a traditional control of wind turbines, because wind turbines linked to the same converter operate at the optimal frequency of the entire group and not at the optimal frequency of each turbine, which will subsequently degrade the performance of each turbine since the MPPT technique is no longer applied. This topology does not exist today considering the complexity of the practical control of wind turbines but it is under research study.

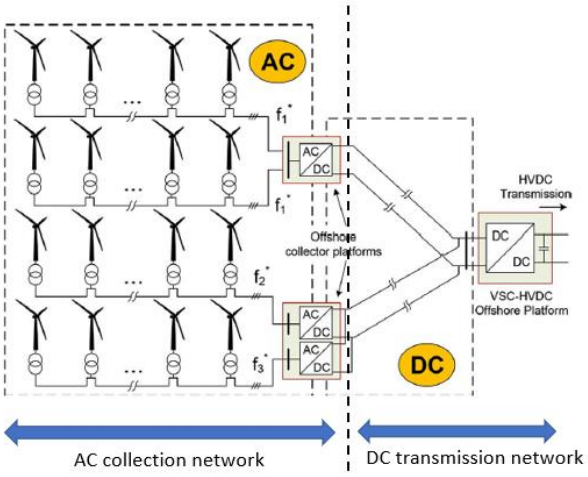

Figure 1-31 Mixed MVAC and HVDC innovant topology [42]

4.3.3 Full DC topologies

For full DC topologies, wind turbines must adapt its output to be in DC. In fact, the internal architecture of wind turbine for DC network connection is composed of a rectifier that controls the electrical torque followed by a DC/DC converter that replaces the transformer for AC wind turbine configuration.

Figure 1-32 Internal topology of a wind turbine for DC network connection

4.3.3.1 MVDC collection and transmission networks

Like for small AC wind farms (section 4.3.1.1), DC wind turbines are connected with MVDC collection network and then the power is directly transmitted to the grid by the means of MVDC cables. In the terrestrial network, there is an inverter for DC/AC conversion after that the power is injected to the grid. This topology has the advantage of reducing the additional cost of DC/DC converters, so it seeks to eliminate the offshore substations by directly connecting the collection network to the terrestrial network. This electrical configuration is suitable for small DC wind farms with short transmission distance. In general, total MVDC wind farms (MVDC collection and transmission systems) are more economical than total MVAC parks thanks to cost minimization of DC cables compared to AC ones. The voltage level of the MVDC network

may vary from ±40 kV up to ±80 kV. The internal topology of wind turbines in the figure below is presented in figure 1-32.

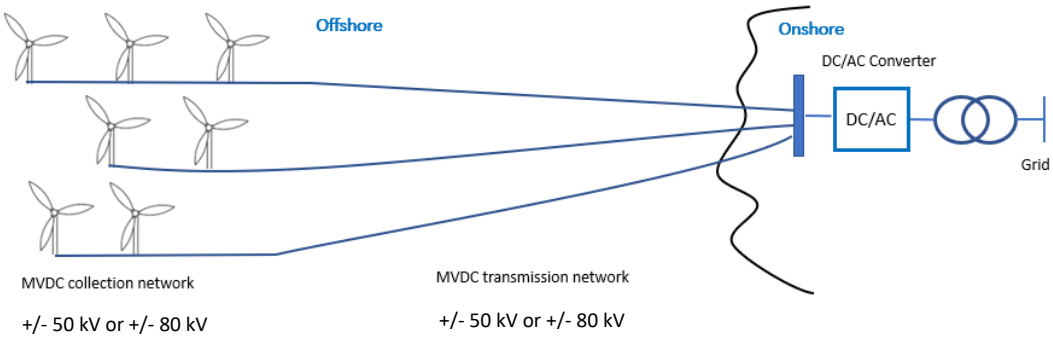

Figure 1-33 DC architecture with MVDC collection and transmission networks

4.3.3.2 MVDC collection and HVDC transmission networks

If the output voltage of the wind turbine rectifier is not high enough (5kV), a DC/DC converter is then required for voltage elevation (figure 1-32), that is called the first step DC transformation. After that and for HVDC transmission, all the wind turbines are grouped together and connected once again with another DC/DC converter which is placed in an offshore substation (figure 1-34). This second step transformation raises the voltage and then allows a high voltage transmission.

The addition of offshore substations increases the total cost of the wind farm and since each wind turbine is assigned a DC/DC converter, this topology may be very expensive. In other hand, the increase of voltage level for HVDC power transmission reduces the total energetic losses. In the aim of cut down the total cost, another topology is proposed by Meanjean [43] with a LVDC collection and a HVDC transmission networks. This solution consists in eliminating the DC/DC converters in the internal architecture of the wind turbine in order to keep only one DC transformation step with a huge DC/DC converter placed in the offshore platform (figure 1-35). The advantage of this solution is the reduced number of components due to the elimination of DC/DC converters for each wind turbine. On the other hand, low voltage in the collection system causes losses as long as the currents are high and therefore the cable cross-section will be large (additional cost).

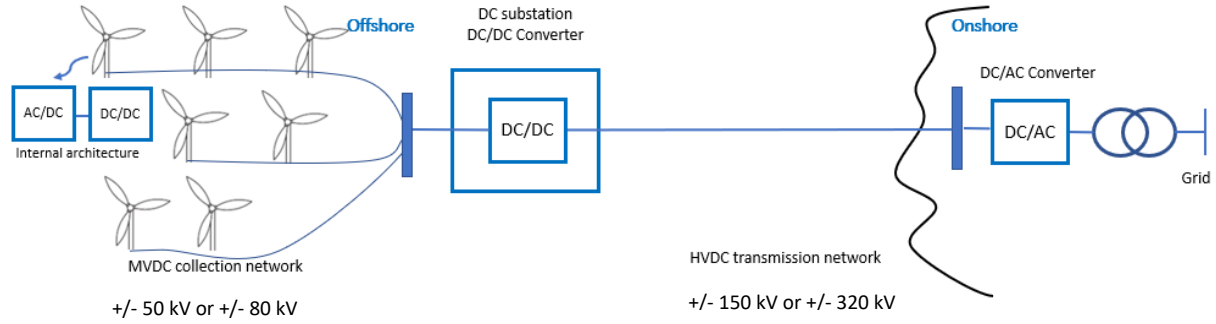

Figure 1-34 DC architecture with MVDC collection and HVDC transmission networks

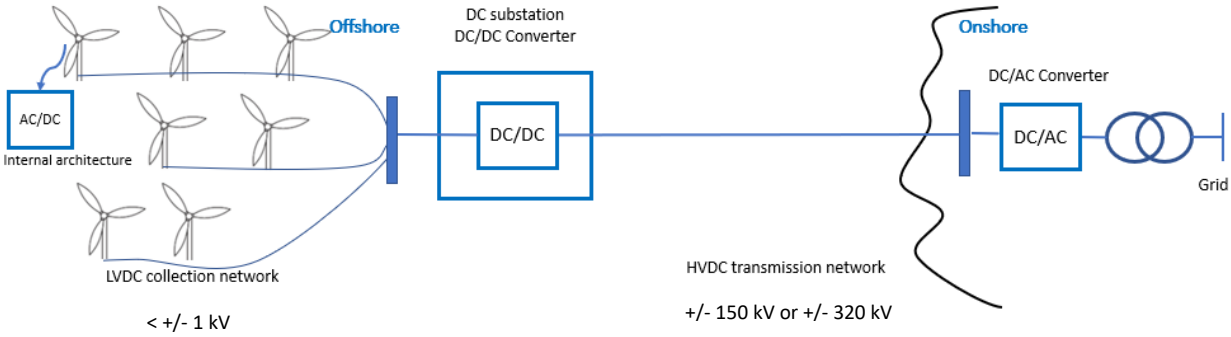

Figure 1-35 DC architecture with LVDC collection and HVDC transmission networks

4.3.3.3 DC topology with series connected wind turbines

For this topology, the wind turbines are connected in series and are connected in parallel with the terrestrial network. Each wind turbine is connected to its rectifier followed by a DC/DC converter to increase the DC voltage which will then be transmitted by DC cables without going through an offshore station so the voltage level is kept either MVDC or HVDC for the whole architecture. The series connected wind turbines allow the voltage boost. Therefore, this structure has the advantage of having a lower cost compared to other structures (no offshore platform) but it presents a problem for maintenance and reliability because the fault of one wind turbine can cause the loss power of the whole line. In addition, the serial connection of wind turbines presents a technical problem of their control due to the difficulty of voltage balancing between the wind turbines and the insulation during faults can be as well as difficult.

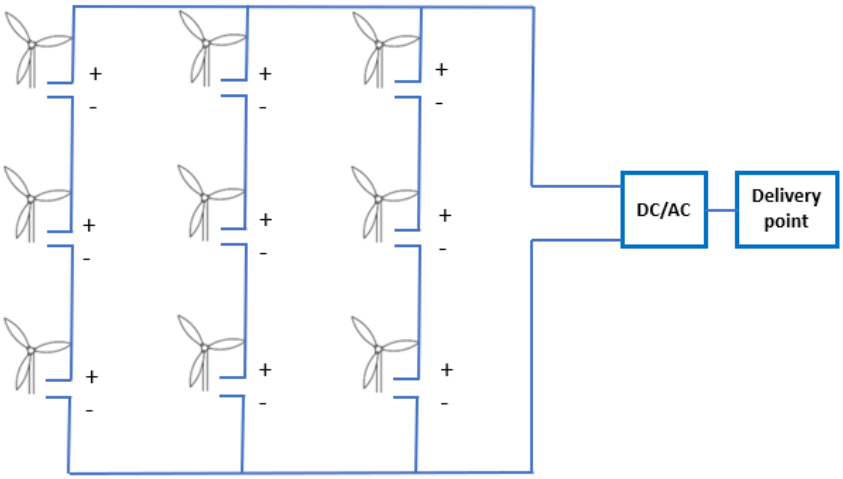

Figure 1-36 DC architecture with series connected wind turbines [39]

In the full DC offshore wind farms topologies already mentioned, there is always the presence of one or more DC/DC converters for voltage rise and turbine isolation on the transmission side. Therefore, DC/DC converters are key components in an all DC wind farm. Figure 1-37 shows an overview of the main components of a DC/DC converter.

Figure 1-37 DC/DC converter components

According to the diagram, the DC/DC converter consists of an inverter, a transformer and a rectifier. Indeed, the inverter (DC/AC) provides a single-phase alternating voltage that will be applied to the transformer. On the secondary side of the transformer, the AC voltage is rectified to a DC voltage. The waveform of the AC voltage depends on the topology of the converter. In addition, filters at the input and output of the DC/DC converter are required.

High power DC/DC converters are still under study and development [44] and are described in more detail in chapter 4. When designing converters, the choice of topology is important to achieve the lowest losses and ensure good dynamic performance of the wind farm.

After a detailed state of the art and towards this thesis work, only three electrical network architectures concepts are selected to be deeply studied in next chapters (figure 1-38). Indeed,

a comparison between the topologies will be presented taking into account the technological limits of each topology (site conditions, economic assessment, transmission distance, etc.).

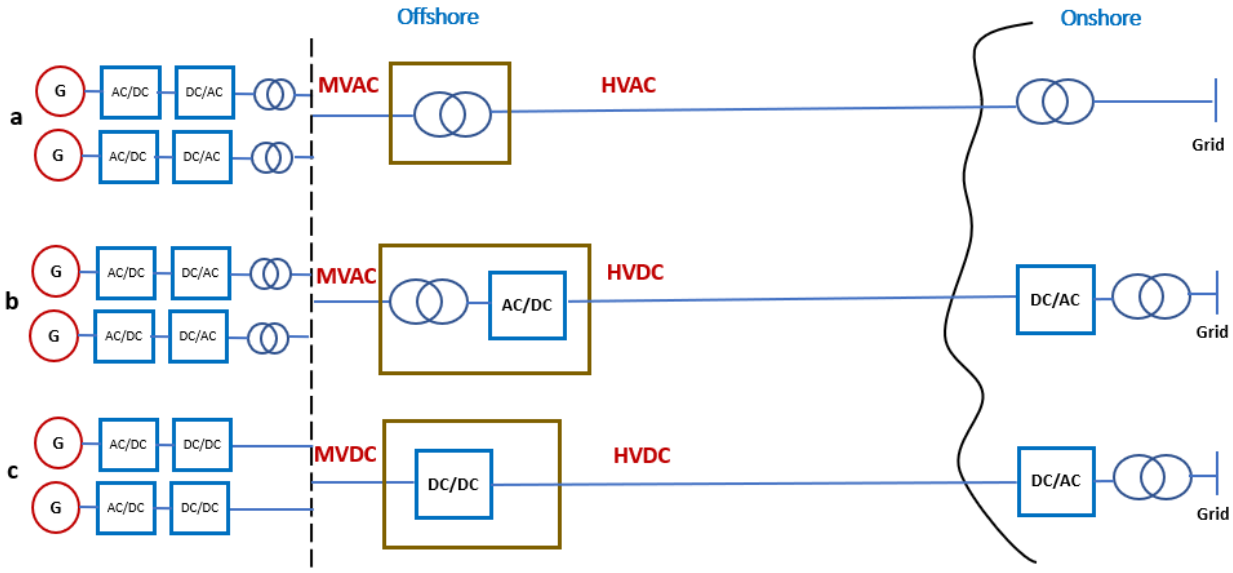

Figure 1-38 Simplified diagram of selected topologies

5 Electrical system optimization framework for offshore wind farms

In this section, the optimization framework for the design of offshore wind farms is discussed. Indeed, an optimal structure of a wind farm is a structure that verifies certain constraints such as minimizing the cost of energy transmitted to the grid and minimizing power losses of the offshore wind configuration. This is what constitutes an optimization problem framework that will have to be solved through optimization approaches.

In general terms, there are two basic categories of optimization algorithms: deterministic and probabilistic [45]. The first category will look for all possible solutions and choose the optimum, while the second is an iterative method that evaluates only a small number of solutions for each iteration, reaching a maximum or minimum over time. Deterministic algorithms are used when the number of variables is small and, therefore, the entire search space can be effectively explored. On the other hand, if the number of variables increases, deterministic algorithms do not solve this kind of problem because it will be difficult to find all the possible solutions and that is where probabilistic algorithms appear. Although they take much less time to arrive at the solution, probabilistic algorithms have a disadvantage, they always find a local maximum/minimum, but not necessarily the global maximum/minimum.

To overcome this problem, scientists and researchers have proposed a different optimization philosophy, which are algorithms that introduce an element of chance for example: Genetic Algorithm, PSO: Particle swarm optimization, etc.

5.1 State of the art for offshore wind farms optimization approaches

In this section, a state of the art for different optimization approaches used to date for the design of offshore wind farms is presented. In 2003, S. Lundberg [39] with his master thesis presented a comparative study of different electrical topology systems of wind farms. AC and DC architectures were compared and studied according to power losses, cost and reliability [46]. This work concerns the finding of the best electrical topology with no optimization method, it is only an economical and technical assessment. After that, several techniques for optimizing electrical architectures are used in the literature and they are based mainly on evolutionary algorithms (EA). In fact, in 1994, Mosetti et al. [47] and later, in 2005, Grady et al. [48] optimized the placement of wind turbines using the genetic algorithm. These studies were carried out on offshore wind farms where the number of turbines and the total power of the farm are unknown. The main objective of this study was to minimize the total cost of the wind farm by maximizing the energy produced.

Since 2005, many studies on the best positioning of wind turbines have been carried out [49] [50], but more recently, in 2009, Sisbot et al. [51] implemented a multi-objective genetic algorithm to optimize the placement of wind turbines by maximizing energy production capacity while limiting the turbine installation budget. In 2010, Wan et al. [46] proposed a particle swarm optimization algorithm (PSO) based on the Gaussian Mutation algorithm. The algorithm proved to be more accurate than the standard PSO and with a considerably reduced calculation time. It has been considered as a standard PSO but, if the algorithm does not improve for a predefined number of iterations, each particle undergoes a mutation that improves its position. The results of the method are more reliable once they have a lower standard deviation than the traditional PSO.

With the development of offshore wind energy, other aspects of optimization of offshore wind farms are observed. In addition to the optimization of turbine positions [52][53], the researchers studied both the collection and the transmission systems [52] [54] [55] because they are relevant to installation costs and electrical losses. Zhao et al. [54] use the genetic algorithm taking into account several variables such as the cross-sections of the different cables, the nominal power of the offshore substation and the voltages levels of the different systems to optimize the wind

farm with lower cost and higher reliability. On the other hand, Gonzalez et al. [56] focus their study on optimizing collection network using a modified genetic algorithm. The study showed that if the proposed method is applied, a reduction of approximately 11% in the total length of the cables can be achieved.

More recently, Wu et al. [52] and Hou et al. [53] respectively in 2014 and 2015, considered wake effects in the optimization of offshore wind farms, thus allowing the evaluation of energy loss in the system that promotes the optimization of offshore wind farms under more realistic conditions. Hou et al. [53] used a standard PSO with an inertial weight and assumed a dispersed topology of wind turbines (non-regular wind farm) with a constant distance between turbines of different rows. Wu et al. [52] applied two optimization algorithms. Indeed, the genetic algorithm was used to find the optimal positions of the turbines, then the ant colony algorithm (AC) was applied to optimize the connection of the MV collection network. The main problem with the proposed AC is that the optimization of the internal network is established by taking into account the distances between the turbines/substations without eliminating the possibility of having cable crossings.

In 2016, Hou et al. [56] brought back further studies by proposing a new way of positioning wind turbines for a regularly shaped wind farm, taking into account the optimization of the direction of placement of the wind farm and the spacing between the turbines, as well as the impact of the variation of the pitch angle assigned to each turbine on the energy yields of the entire structure.

Floating wind turbines appeared with the need to go further from the coast to capture higher wind speeds. Although the concept is in its primary stage, some characteristics of floating turbines are already considered advantages, such as the fact that a floating turbine should not always remain in the same position. Rodriguez et al. [57] proposed an optimization technique based on "Covariance Matrix Adaptation" where the turbines move in the optimal wind direction to minimize the wake effect. Moreover, Rodriguez [58] developed an optimization framework for the comparison between the different electrical architectures concepts of wind farms resulting on finding that the HVDC is more efficient than the HVAC from a certain transmission distance.

In 2014, Dahmani in his thesis [22] combined two approaches to optimizing offshore wind farms such as the genetic algorithm and the Prim algorithm. Indeed, the GA provides the first topologies of connections such as the connection between wind turbines and the connection of offshore substations as well as their positions. Then, the Prim algorithm is used to complete the

connection between each group of wind turbines and the nearest substation (search for the shortest path).

This PhD project is the continuity of Dahmani's research work, it consists of optimizing the electrical performance of the wind farm based on the selection of electrical equipment by choosing the appropriate voltage level and power rating. The positions of wind turbines are fixed but the substation positions and numbers are determined by the heuristic optimization (GA), the inter array network is decided also by the optimization algorithm while minimizing the losses and cable costs. This approach is based on the idea of clustering turbines (string clustering, star clustering) so the algorithm decides the number of clusters and the number of turbines in each cluster. For each iteration of the algorithm, electrical assessment of the wind farm architecture is made and then better topology is proposed taking into account optimization criteria until converging to the best one.

Dahmani's work concerns the optimization of full AC connected offshore wind farms. Power losses in the AC electrical system are mainly due to submarine cables. These cables have capacitive and inductive effects that produce reactive power. This reactive power presents a problem on power transmission capability, especially for important distances since HVAC losses line are very high. Thus, the integration of DC systems is the solution to transmit more power throughout long distances. In fact, DC systems do not present any sort of reactive power because the signals frequency is null (i.e. constant current and voltage). Therefore, DC systems are only limited by ohmic losses, as inductive and capacitive effects are not present. Consequently, there is no need to integrate reactive power compensation equipment which can increase the system investment cost.

Moreover, there is no dielectric losses for DC cables knowing also that the AC resistance line is higher than the DC one. That's why the DC resistive losses are lower. Besides, DC system allows the connection between asynchronous AC grids. So, it can guarantee system stability and prevent faults or overloads from spreading [59].

This thesis work aims at developing HVDC optimized architectures with either full DC or mixed AC/DC topologies and analyze their performances in order to compare them with full AC topologies.

5.2 Design concept of an optimal offshore wind farm

Each electrical topology of an offshore wind farm is characterized by a number of turbines and substations, wind turbine connections in the collection network and HV transmission grid

configurations. The number of turbines shows the installed capacity power of the park, the number of substations is the number of DC/DC converters for DC topologies and the number of transformers for AC topologies (not to mention reactive power compensation equipment).

On the one hand, the MV network is characterized by the following parameters:

- The number of wind turbine clusters,

- The number of wind turbines per cluster,

- The cross-sections of MV cables,

- The connection between substations.

On the other hand, the HV network is defined by:

- The number of parallel cables in each HV link

- HV cable cross-sections,

- Connections between offshore substations and the terrestrial network.

Finally, the optimization problem will involve all these parameters to evaluate the performance of offshore wind farm architectures.

5.2.1 Technical and economical objectives for optimization

Generally, and in most of the research done on the optimization of offshore wind farm topologies, four main criteria are identified that characterize each topology: the investment cost CAPEX (CApital EXpenditure), the maintenance costs OPEX (OPerational EXpenditure) and the power losses of the system. In fact, the CAPEX takes into account the turbines and foundation costs, the cable costs including its installation costs, the substation costs that include switchgear costs, reactive power compensation equipment cost, DC/DC converter costs, AC/DC converter costs and transformer costs and the onshore equipment like DC/AC converters and onshore transformers.

For each optimization problem, objective functions are defined to characterize the criteria to be minimized. For this work, two types of optimization are studied:

- Mono-objective optimization

It is a technique that optimizes a given criterion and the optimum found presents a unique optimal solution.

- Multi-objective optimization

It is an optimization context where we are faced with a problem of evaluating solutions in relation to a set of criteria considered. So, there is not a single global optimum that optimizes all criteria at once. It is characterized by the notion of the Pareto front [22].

In practice, a main common criterion is considered as a reference to assess electrical performance for offshore wind farms which is the Levelized Cost Of Energy (LCOE).

$$LCOE = \frac{\frac{CAPEX}{a} + OPEX}{AED} \quad (1\text{-}6)$$

Where:

a: the annuity factor, $\frac{1-(1+r)^{-N}}{r}$

CAPEX: the annual capital expenditure,

OPEX: the annual operational expenditure,

AED: the annual energy delivered= AEP – the total losses of the architecture,

r: the discount rate,

N: number of years of the wind farm exploitation.

The number of operation years can vary between 20 and 30 years and the discount rate can be between 4% and 10% depending on the inflation. These two parameters can affect the optimization.

5.2.2 Electrical network assessment

After having fixed the topology, the evaluation of power losses is done with the "load flow calculator" that calculates the modules and phases of nodal voltages from the electrical parameters of the topology under study. Power losses will generally be quantified in terms of cost. In this work, an optimization framework for design offshore wind farms is proposed with an emphasis on the assessment of electrical architectures to obtain the best topology. The framework is built with different modules that are linked to each other and that form the optimization problem. The offshore wind farm optimization framework can be modeled as

depicted in figure 1-39. The description of the optimization framework can be defined as follows:

The inputs block where three modules are specified. The first one is the wind resource database where wind rose data is identified with different occurrence of wind speeds. The second one is a general inputs database in which we put the number of the installed turbines then the total installed power is deducted, the coordinates of each turbine and the delivery point are defined. Besides, the different voltage levels of both collection and transmission networks must be clarified. The last database is dedicated to components models, it contains the economic models which is represented as a cost database since it collects the cost of the main electrical system equipment constructing a wind farm (turbines and its foundations, cables, substations). Therefore, the CAPEX of the whole wind farm is retrieved. However, the OPEX is calculated as a percentage of the CAPEX. Likewise, the electrical models of components like the power curve of turbines and the different parameters of cables (resistance, capacitance and inductance) are presented in this database.

Before the optimization, it is necessary to calculate the wake effects and the load flow. Indeed, the wake effect estimation block has as inputs the wind resource database and the general inputs module, its output is the power loss caused by the wake effects between turbines. The load flow block collects the output of wake effect estimator, the general inputs and the electrical parameters modeling of the components and calculates the power in each node in the global network. Therefore, the whole losses of the topology under study is deducted. So, from these two blocks, the power losses and the AEP are calculated. After that, the wind farm optimization block acquires the losses, the AEP, the CAPEX and OPEX and activates the iterative optimization algorithm to minimize the LCOE (objective function) for a given electrical architecture. The optimization algorithm generates in each iteration an electrical system design for a wind farm (a proposed topology) where a cable connection layout is proposed, the electrical components type is selected and the number and the positions of substations are fixed. The algorithm continues to run until it reaches an optimal LCOE value.

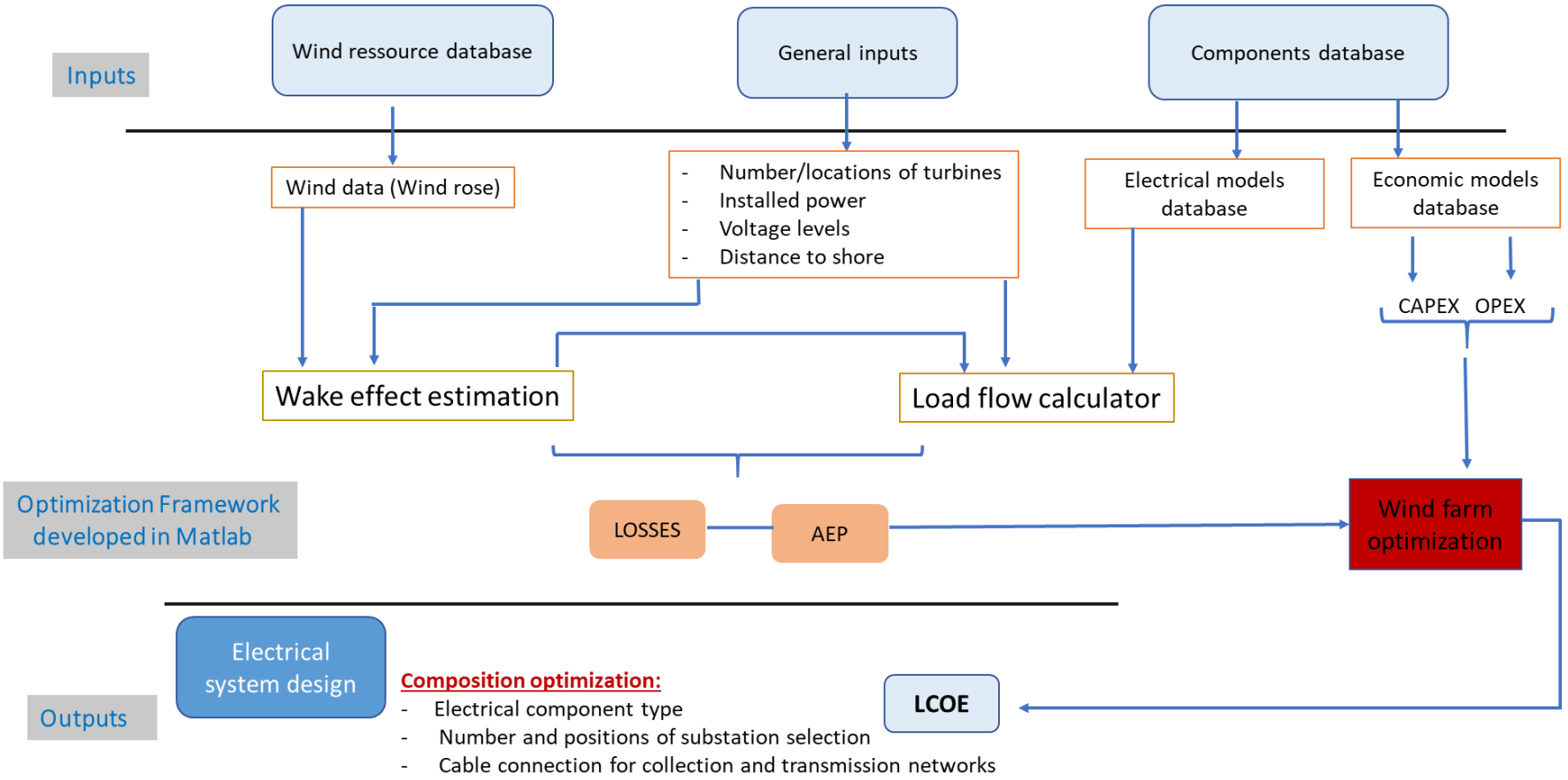

Figure 1-39 Diagram of proposed optimization framework

6 Conclusion

In this chapter, a state of the art of offshore wind farms was successfully completed on several aspects relative to the current trends of global and especially European market of developing offshore wind farms. Indeed, we analyzed the different existing offshore wind topologies in DC, AC and mixed AC/DC, which allowed us to make a preliminary comparison of the structures and to see the difference between HVDC and HVAC. Therefore, the curve of break-even distance for HVAC and HVDC technologies is presented. In chapter 3, a detailed comparison between the two transmission networks will be studied for a case study of a real existing park.

We also presented a state of the art of optimization approaches which allowed us to make a comparison between the optimization approaches of offshore wind farms and then put the choice to build our own optimization framework. This latter is based on the optimization of the LCOE which is a reference criterion used in the industrial field to assess the electrical performance of a given architecture concept. In this thesis, the study methodology of designing an optimal offshore wind farm includes modeling of different components that constitute a wind farm and simulation of the electrical performance taking into account realistic conditions like the calculation of wake effects between turbines. Next chapter will be dedicated to show the models and methods for wind farm optimization.

Bibliography

[1] IEA, International Energy Agency, ‘’Key world energy statistics’’, 2018.

[2] RTE, ‘’Electrical report 2018’’, 2018.

[3] O. Dumont, ‘’Rapport de la Banque Mondiale sur le Climat: Synthèse’’, 2012.

[4] J. Lee, F. Zhao ‘’Global offshore wind report 2020’’, august 2020.

[5] IRENA, ‘’FUTURE OF WIND**,** Deployment, investment, technology, grid integration and socio-economic aspects’’, october 2019.

[6] WindEurope, ‘’Offshore wind in Europe – key trends and statistics 2019’’, february 2020.

[7] WindEurope, trends and statistics, ‘’ Wind energy in Europe’’, 2019.

[8] ‘’Financing and investment trends’’, The European wind industry in 2018.

[9] ABB Online, Available: www.abb.com

[10] J. COURAULT, ‘’ Energy Collection on Offshore Wind Farm’’, GIRCEP, march 2002.

[11] B. Robyns, A. Davigny, C. Saudemont, A. Ansel, V. Courtecuisse, B. François, S. Plumel, J. Deuse, ‘’Impact de l’éolien sur le réseau de transport et la qualité de l’énergie‘’, Club Days EEA, 2006.

[12] A. Arjen A. van der Meer, ‘’ Offshore VSC-HVDC Networks’’, Delft University of Technology, Thesis in Electrical Engineering, 2017.

[13] A. Davigny, ‘’Participation aux services système de fermes d’éoliennes à vitesse variable intégrant du stockage inertiel d’énergie’’, University of Science and Technology of Lille, PhD in Electrical Engineering, 2007.

[14] T. Ghennam, ‘’Supervision d’une ferme éolienne pour son intégration dans la gestion d’un réseau électrique, Apports des convertisseurs multi niveaux au réglage des éoliennes à base de machine asynchrone à double alimentation’’, Ecole Militaire Polytechnique d'Alger and Ecole Centrale de Lille, Thesis in Electrical Engineering, 2011.

[15] L. Ludovic, ‘’ Apport du stockage inertiel associé à des éoliennes dans un réseau électrique en vue d’assurer des services systèmes’’, University of Science and Technology of Lille, PhD in Electrical Engineering, 2004.

[16] F. Poitiers, ‘’ Etude et commande de génératrices asynchrones pour l’utilisation de l’énergie éolienne’’, Nantes University, Thesis in Electrical Engineering, 2003.

[17] H. Polinder, S. W. H de Haan, M. R. Dubois, J. G. Slootweg, ‘’Basic Operation Principles and Electrical Conversion Systems of Wind Turbines’’, EPE Journal, Vol 15, no 4, pp. 43- 50, 2005.

[18] H. Camblong, ‘’Minimisation de l’impact des perturbations d’origine éolienne dans la génération d’électricité par des aérogénérateurs à vitesse variable’’, Ecole Nationale Supérieure d’Arts et Métiers, Bordeaux, PhD in automatic, 2003.

[19] S. El Aimani, Salma, ‘’Modélisation de différentes technologies d’éoliennes intégrées dans un réseau de moyenne tension’’, Ecole Centrale de Lille, Thesis in Electrical Engineering, 2004.

[20] I. Serban, ‘’Contributions to the control of variable speed generators for renewable energy’’, University Poilithenica of Timisoara, Thesis in Electrical Engineering, 2005.

[21] M. El Mokadem, ‘’ Modélisation et simulation d’un système hybride pour un site isolé, Problématique liée aux fluctuations et variations d’énergie au point de couplage’’, Havre university, Thesis in Electrical Engineering, 2006

[22] O. Dahmani, ‘’Modélisation, optimisation et analyse de fiabilité de topologies électriques AC de parcs éoliens offshore’’, University of Nantes, PhD thesis in Electrical Engineering, 2014.

[23] Online Data : https://www.smhi.se/en/services/professional-services/data-and-statistics/wind-roses-for-analysis-of-local-wind-conditions-1.124512

[24] M. Ardelean, Phi. Minnebo, ‘’HVDC submarine power cables in the world’’, JRC technical reports, 2015.

[25] European Network of Transmission System Operators for Electricity, ‘’Offshore transmission technology‘’, 2012.

[26] O. Dahmani, S.Bourguet, M. Machmoum, ‘’Optimization and Reliability Evaluation of an Offshore Wind Farm Architecture’’, IEEE Transactions on Sustainable Energy (Volume: 8 , Issue: 2) , April 2017.

[27] S. J. Shao and V. G. Agelidis, ‘’ Review of DC system technologies for large scale integration of wind energy systems with electricity grids’’, Energies, 3, pp 1303-1319, 2010.

[28] S. Lundberg, ‘’ Evaluation of wind farm layouts”, NORPIE 04, pp 1-8, 2008.

[29] P. Bauer, S. De Haan, C. Meyl, J. Pierik, ‘’Evaluation of electrical systems for offshore windfarms”, Industry Applications Conference, Conference Record of the 2000 IEEE, Italy, 2000.

[30] M. Alexander Parker and O. Anaya-Lara. ‘’Cost and losses associated with oshore wind farm collection networks which centralise the turbine power electronic converters‘’, IET Renewable Power Generation, 390-400, 2013.

[31] P. K. Steimer, O. Apeldoorn, L. Dalessandro, R. Grinberg, and S. Ebner.’’Efficient medium voltage power collection windparks’’. European Wind Energy Conference & Exhibition (EWEC), Copenhagen, Denmark, April 2012.

[32] T. Haugsten Hansen. ‘’Offshore Wind Farm Layouts. Performance Comparison or a 540 MW offshore Wind Farm’’. Master's thesis, Norwegian University of Science and Technology. Department of Electric Power Engineering, July 2009.

[33] A. Sannino, H. Breder, and E. K. Nielsen. ‘’Reliability of collection grids for large offshore wind parks’’. In 9th International Conference on Probabilistic Methods Applied to Power Systems, KTH, Stockholm, Sweden, 2006.

[34] J. T. G. Pierik, M. E. C. Damen, P. Bauer, and S. W. H. de Haan. ‘’ Steady state electrical design, power performance and economic modeling of offshore wind farms’’. EPE Journal, 2006

[35] N. Florentzou, '' VSC-Based HVDC Power Transmission Systems: An Overview'', IEEE Transactions on Power Electronics, 2009.

[36] ABB, '' HVDC Classic® transmission losses''. Available: www.abb.com

[37] ABB, '' HVDC Light® transmission losses ''. Available: www.abb.com

[38] ABB, '' HVDC transmission for lower investment cost''. Available: www.abb.com

[39] S. Lundberg, ''Wind Farm Configuration and Energy Efficiency Studies - Series DC versus AC Layouts '', Chalmers University of technology, PhD in Electrical Engineering, Sweden 2006.

[40] M. Dicorato, G. Forte, M. Pisani, M. Trovato, '' Guidelines for assessment of investment cost for offshore wind generation'', Renewable Energy 36, 2011.

[41] J. Rebled ''Power transmission system for offshore wind farms: Technical economic analysis'', ETSEIB, bachelor thesis, 2015.

[42] M. Gil, L. Igualada, C. Corchero, O. Gomis-Bellmunt, A. Sumper,''Hybrid AC-DC Offshore Wind Power Plant Topology: Optimal Design'', IEEE Transactions on Power Systems (Vol: 30, Issue:4), 2015

[43] P. Monjean, ''Optimisation de l'architecture et des flux énergétiques de centrales à énergies renouvelables offshore et onshore équipées de liaisons en continu '', National School of Arts and Crafts, PhD thesis in Electrical Engineering, 2012.

[44] C.Meyer, R.W. De Doncker, '' Design of a three-phase series resonant converter for offshore DC grids'', in Proc. the 42th IEEE Industry Application Society Annual Meeting (IAS), vol. 2, pp. 216 -223, USA, 2007.

[45] P. S. Valverde, A. Sarmento, M. Alves, ''Offshore Wind farm layout optimization - State of the art'', In the Twenty-third International Offshore and Polar Engineering Conference, Journal of Ocean and Wind Energy, Vol. 1, No. 1, pp. 23–29, February 2014.

[46] H. J. Bahirat, B. A. Mork, H. K. Hoidalen, ''Comparison of wind farm topologies for offshore applications'', IEEE Power and Energy Society General Meeting, pp. 1-8, 2012.

[47] G. Mosetti, C. Poloni, B. Diviacco, ''Optimization of wind turbine positioning in large windfarms by means of a genetic algorithm'', Journal of Wind Engineering and Industrial Aerodynamics, Vol 51, Issue 1, pp 105-116, January 1994.

[48] S.A. Grady, M.Y. Hussaini, M. Abdullah, ''Placement of wind turbines using genetic algorithms", Renewable Energy, Vol 30, Issue 2, pp 259- 270, February 2005.

[49] J.C. Mora, J.M. Calero Baron, J. R. Santos, M. B. Payan, ''An evolutive algorithm for wind farm optimal design'', Neurocomputing, Vol 70, Issues 16–18, pp 2651–2658, on the 3rd International Work-Conference on Artificial Neural Networks (IWANN), october 2007.

[50] A. Kusiak and Z. Song, ''Design of wind farm layout for maximum wind energy capture'', Renewable Energy, Vol 35, Issue 3, pp 685–694, march 2010.

[51] S. Sisbot, O. Turgut, M. Tunc, U. amdali, ''Optimal positioning of wind turbines on Gokçeada using multi-objective genetic algorithm'', Wind Energy, Vol 13, Issue 4, pp 297–306, may 2010.

[52] Y. K. Wu, C. Y. Lee, C. R. Chen, K. W. Hsu, H. T. Tseng, ''Optimization of the Wind Turbine Layout and Transmission System Planning for a Large-Scale Offshore WindFarm by AI technology'', Industry Applications Society Annual Meeting (IAS), Industry Applications Society Annual Meeting (IAS), USA, 2012.

[53] P. Hou, W. Hu, M. Soltani, Z. Chen ''Optimized Placement of Wind Turbines in Large-Scale Offshore Wind Farm Using Particle Swarm Optimization Algorithm'', IEEE Transactions on Sustainable Energy, Vol 6, Issue 4, 2015.

[54] M. Zhao, Z. Chen, F. Blaabjerg ''Optimisation of electrical system for offshore wind farms via genetic algorithm'', IET Renewable Power Generation, Vol 3, Issue 2, pp 205- 216, june 2009.

[55] F. G. Longatt, P. Wall, P. Regulski, V. Terzija, ''Optimal Electric Network Design for a Large Offshore Wind Farm Based on a Modified Genetic Algorithm Approach'', IEEE Systems Journal, Vol 6, Issue 1, pp 164 - 172, march 2012.

[56] M. S. P. Hou, W. Hu, ''Offshore Wind Farm Layout Design Considering Optimized Power Dispatch Strategy'', IEEE Transactions on Sustainable Energy, Vol 8, Issue 2, pp 638 - 647, april 2017.

[57] S.F. Rodrigues, R. T. Pinto, M. Soleimanzadeh, P. A.N. Bosman, P. Bauer, ''Wake losses optimization of offshore wind farms with moveable floating wind turbines'', Energy Conversion and Management, Vol 89, pp 933- 941, january 2015.

[58] S. Fragoso Rodrigues, ''A Multi-Objective Optimization Framework for the Design of Offshore Wind Farms'', Delft university of technology, PhD thesis in Electrical Engineering, 2016.

[59] R. Teixeira Pinto, ''MULTI-TERMINAL DC NETWORKS - System Integration, Dynamics and Control,'' Electrical Engineering, Mathematics and Computer Science, University of Sao Paulo, PhD thesis, 2014.

Chapter 2. *Modeling of components and general optimization framework for offshore wind farms*

1 Introduction

The present chapter aims at developing the different tools to make up the optimization framework. The first section is dedicated to electrical and economical models of offshore wind farms. In fact, electrical modeling consists in determining the electrical parameters that will be exploited for the load flow calculation, economical models aim to calculate the investment cost of each component that are then exploited to compute the LCOE.

The second part is dedicated to load flow calculations. The AC/DC Mat library is used to evaluate the load flow only for fully AC or mixed AC/DC electrical architectures. The steps to set up the input data in the library are presented. For full DC topologies, a radial DC load flow is developed. The algorithm validation is exposed. A calculation methodology for wake effect implementation is presented with the Katic Jensen model. In section 5, the optimization framework is detailed with the definition of different objective functions, the mathematical formulation of the optimal design problem is shown. The optimization algorithms used in this work are the genetic and Prim algorithms. Finally, in the last sections, the integration of load flow and wake effect calculations in the optimization framework is exposed.

2 Electrical and economical modeling of an offshore wind farm

2.1 Electrical models

The electrical modeling of an offshore wind farm is the modeling of the different components constituting the wind farm. The study of the energy losses is carried out over an estimated total lifetime between 20 and 30 years. As the analysis is made on the long term, the modelling of the different components is carried out for a balanced, permanent and sinusoidal operating regime. In this work, the load flow calculation is done with the Matlab library Mat AC/DC [1]. For that, the electrical models of Mat AC/DC are exploited.

In Mat AC/DC, an electrical connection between two buses is modelled as presented in figure 2-1. This branch model is applied to model both cables and transformers. The model parameters r_s, b_c and x_s are normalized with the base impedance which is calculated by the following equation where the base power is the power of the entire system under study (rated power produced by all the turbines).

$$\text{base impedance} = \frac{\text{base voltage}^2}{\text{base power}} \tag{2-1}$$

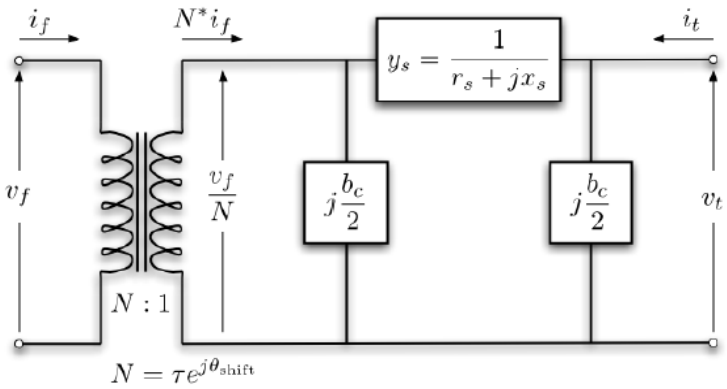

Figure 2-1 Branch model in MatAC/DC [1]

2.1.1 AC submarine cable model with Mat AC/DC

For cable modeling with Mat AC/DC, the AC cable electrical parameters L (the linear inductance and the mutual between phases in [mH/km]), C (the shunt capacity in [µF/km]) and R_{ac} (the resistance in [Ω/km]) must be exploited to calculate the branch parameters r_s, b_c and x_s. Here, the following equations show the transformation from the basic parameters L, C and R_{ac} to rs, b_c and x_s (in per unit). The main objective of using per unit system is to facilitate the load flow calculation.

$$x_s = \frac{2.\pi.f.d.L}{\text{base impedance}} \tag{2-2}$$

$$b_c = 2.\pi.f.d.C.\ \text{base impedance} \tag{2-3}$$

$$r_s = \frac{R_{ac}.d}{\text{base impedance}} \tag{2-4}$$

where d is the length of the cable in km.

The modeling of a DC cable is simpler since the link can be modeled just by equivalent resistance (no capacitance and no inductance). The properties of AC and DC cables according to voltage level and cable cross section are presented in Appendix 2.

2.1.2 Transformer model with Mat AC/DC

The transformer is the main component of offshore AC power substations. It is the component that makes the link between the AC collection network (33 kV or 66 kV) and the HVAC transmission network (132 kV or 220 kV). The equivalent electrical model of a transformer in

p.u. between two nodes i and j is shown in figure 2-2. O. Dahmani [2] has detailed the equations showing the equivalence between this simplified model and the real model of a transformer with its transformation ratio.

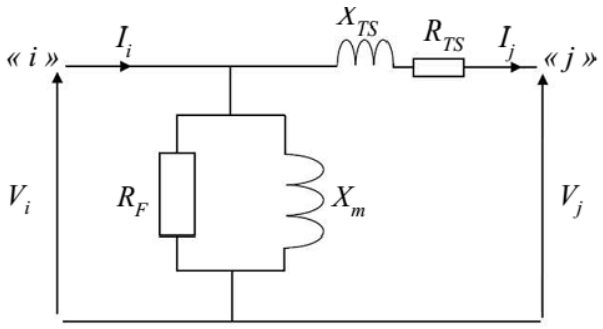

Figure 2-2 Equivalent model in per unit of a transformer

It is a T-model where the series impedance Z_{ij} and the shunt admittance Y_{ij} are presented by the equations below:

$$Z_{ij} = R_{TS} + j.X_{TS} \tag{2-5}$$

$$Y_{ij} = \frac{1}{R_F} - j.\frac{1}{X_m} \tag{2-6}$$

The parameter values are given by Dahmani are R_{TS} = 0.007 p. u, X_{TS} = 0.1 p. u, $R_F = \infty$ and X_m = 50 p.u [3] [4] [5].

The same branch model presented in figure 2-1 is used for transformer modeling in Mat AC/DC, the parameters R_{TS}, X_{TS} and X_m are used for the calculation of parameters r_s, b_c and x_s. Otherwise, the base power of the load flow must correspond to the transformer power, so a change for the calculation of the parameters r_s, b_c and x_s must be made (equations (2-7), (2-8) and (2-9)). S_T is the apparent power of the transformer.

$$r_s = R_{TS}\frac{(\text{base voltage})^2}{\text{base impedance}.\ S_T} \tag{2-7}$$

$$x_s = X_{TS}\frac{(\text{base voltage})^2}{\text{base impedance}.\ S_T} \tag{2-8}$$

$$b_c = \frac{-1}{X_m}\frac{\text{base impedance}.\ S_T}{(\text{base voltage})^2} \tag{2-9}$$

2.1.3 VSC HVDC converter model with Mat AC/DC

The VSC HVDC converter modeling with Mat AC/DC showing the different components with their different impedances are shown in the figure 2-3. S_s is the apparent power of the AC side,

Sc is the apparent power of the converter which is represented as a controllable voltage source $\underline{U_c}$, P_{dc} is the DC power flowing through the dc cable, $\underline{Z_{tf}}$ is the transformer impedance, $\underline{Z_c}$ is the phase reactor impedance and B_f is the susceptance of the filter.

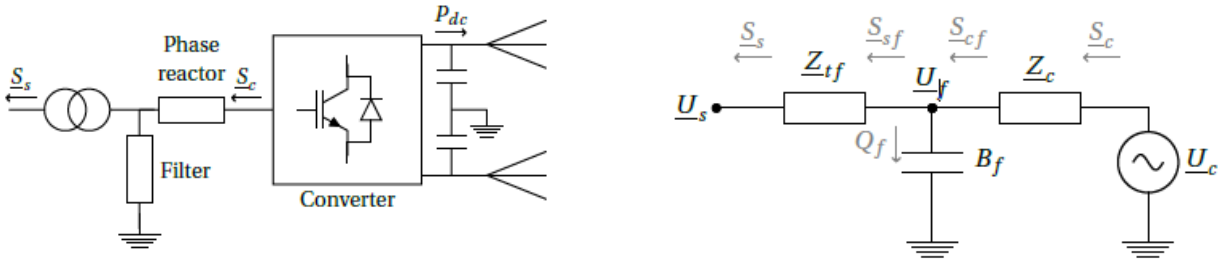

Figure 2-3 HVDC VSC converter equivalent model in MatAC/DC [1]

The different components that compose the VSC HVDC converter are the converter transformer, the AC filters, the phase reactor and the converter. In fact, for MMC converters, the waveform of the AC voltage is obtained thanks to the multi-level converter so that reduces the harmonics and that's why in this case there is no need to add AC filters. Indeed, the converter model shown is figure 2-3 can be simplified with an equivalent model system without filters which is presented by figure 2-4.

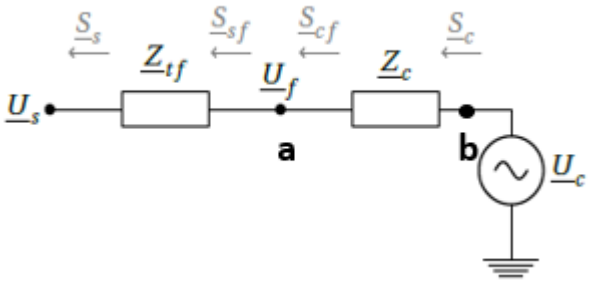

Figure 2-4 MMC equivalent model [1]

The active and reactive powers between points a and b are given by the equations below.

$$P = \frac{U_f U_C}{Z_C} \sin\delta \qquad (2\text{-}10)$$

$$Q = \frac{U_f (U_f - U_C . \cos\delta)}{Z_C} \qquad (2\text{-}11)$$

where δ is the phase angle difference between voltages U_f and U_c.

The active power control in the VSC HVDC converter is made by changing the phase angle difference δ whereas the reactive power control is done by changing the voltage amplitude difference between voltages U_f and U_c. In fact, the voltage and amplitude of the converter can be modified with the PWM control. Thus, the VSC HVDC offers the possibility to control independently the active and the reactive powers. For reactive power control, there are two methods, the first one is when the converter inject a predefined amount of reactive power to the AC grid, the second one is realized by holding a constant voltage AC (AC voltage control) and for that the converter vary its reactive power to keep the AC voltage constant. Indeed, to vary the reactive power, the converter voltage must be varied between the upper and the lower converter voltage limit. Thus, there is an operating area of the converter that must be checked with the capability chart.

The capability chart of VSC HVDC is a PQ diagram that presents the converter current and voltage limits. The figure below presents the capability chart of VSC HVDC.

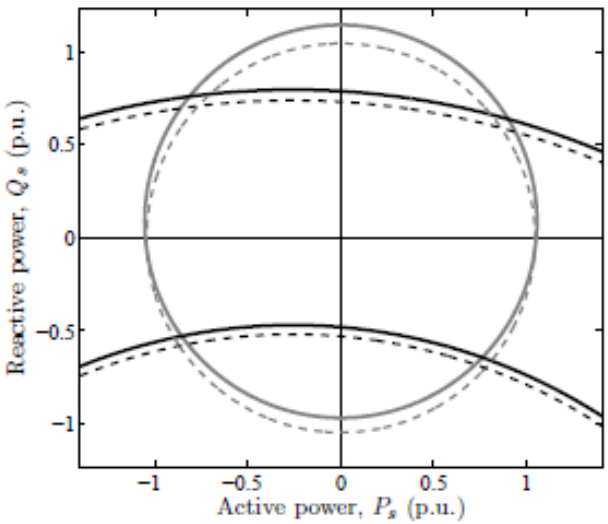

Figure 2-5 VSC HVDC capability chart [1]

To ensure an overall safe operation of the converter station, the steady state working point must be situated within the capability chart of the converter. The full lines are for converters with filters, the dotted lines neglect the filters. The full circle informs us about the converter current limit. The arcs present the upper and lower converter voltage limits.

In this work, a generalized loss model of VSC HVDC station is used for losses calculation. It's a model from ABB Corporate Research Sweden, based on data from the HVDC Light link from

Södra Länken, evaluated with 600 MW and ± 300 kV [6]. The loss model takes into account all the components of a VSC HVDC conversion station.

The converter losses can be expressed as a function of the converter current I_c determined by the active and reactive power exchanged with the AC system. The overall losses of the converter P_{MMC} can be calculated with the quadratic equation presented below.

$$P_{MMC}=a+ b\, I_c+ c\, I_c^2 \tag{2-12}$$

With

$$I_c=\frac{\sqrt{P_c^{\,2}+Q_c^{\,2}}}{\sqrt{3}\,U_c} \tag{2-13}$$

a presents the no load losses, b presents the linear losses and c presents the quadratic losses.

The losses of the rectifier of the Södra Länken project in function of phase reactor current are shown in figure 2-6. After interpolation of the curve, the equation (2-12) is validated and the values of the constants a, b and c are shown in the table 2-1.

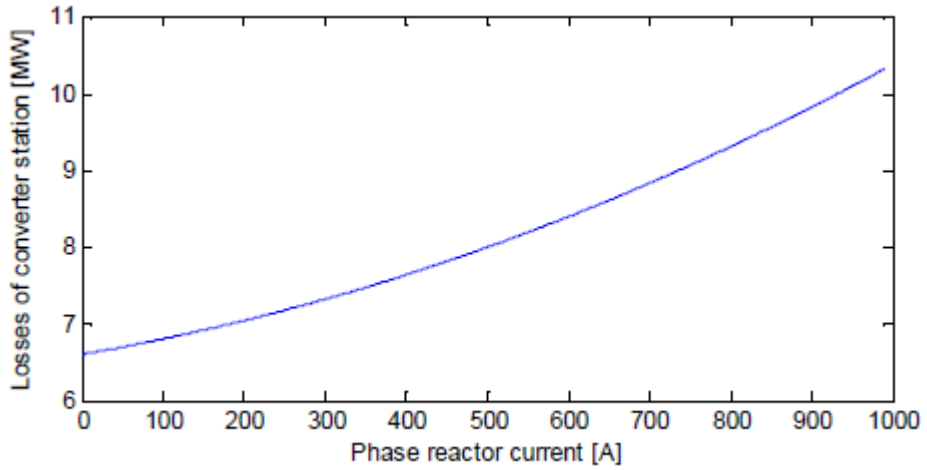

Figure 2-6 Losses of the rectifier in function of the phase reactor current

Table 2-1 Values of constants a, b and c for the generalized model of the converter

VSC	a (MW)	b (kV)	c (Ω)
rectifier	6.62	1.8	1.98
inverter	6.62	1.8	3

The equation (2-12) presents the generalized loss model for a VSC converter substation that takes into account the losses in all components. The table 2-2 shows the detailed losses of the Södra Länken HVDC Light® link [7].

Table 2-2 Detailed losses of the Södra Länken HVDC Light® converter

Constant losses	**Losses in MW**	**Losses as a percentage of the nominal power**
Incl. filter, excl. transformer	5 MW	0.83%
Transformer load losses	1.26 MW	0.21%
Transformer no load losses	0.36 MW	0.06%
a (MW)	6.62 MW	
Current dependent losses		**Nominal condition**
Linear	3 x 600 V x I_c	0.30% (rect) 0.28% (inv)
Square (rectifier)	3 x 0.66 Ω x I_c^2	0.32%
Square (inverter)	3 x 1 Ω x I_c^2	0.43%
Total losses (rectifier)	**10.34 MW**	**1.72%**
Total losses (inverter)	**10.86 MW**	**1.81%**

Note that the losses of the inverter are higher than those of the rectifier because it uses IGBTs more often, while the rectifier uses diodes more frequently. The result of 10.34 MW (rectifier) and 10.86 MW (inverter) are respectively 1.72% and 1.81% of the nominal power of the VSC HVDC link, which are reasonable results according to the literature [8] [9] where the percentage of losses varies between 1% and 3% of the converter rated power.

The values a, b and c depend on the rated power of the converter and its voltage level. Therefore, for different power and voltage values other than those of Södra Länken's model, a calculation of a, b and c must be performed [10]. For more details concerning MMC modeling, consult Appendix 3.

2.2 Economical models

The main objective of this section part is to present the investment costs modelling to calculate the CAPEX of different components for the different electrical network architectures. The CAPEX is a primordial factor to determine the LCOE in the aim to identify in the final way the

best electrical topology. The economic models are extracted from available data in the bibliography.

2.2.1 Turbines cost

For turbines producing between 0.5 MW and 2.5 MW, an estimation cost is given in [11]. In this work, the minimum rated power capacity used is 4 MW. Considering that, and for turbine rated power more than 2 MW, the turbine cost expressed in k€ derived from actual projects is presented in [12] and is evaluated using the following expression:

$$C_{turbine}=2.95\ 10^{3}\ \ln(P_{turbine})\ -375.2 \qquad (2\text{-}14)$$

With $P_{turbine}$ is the rated power capacity [MW] of a wind turbine. The formulation corresponds to the actual costs for wind farms such as Arklow Bank (930 M€/MW) and Barrow (1110 M€/MW) [13].

2.2.2 Foundations cost

The most commonly used structure for turbine foundations is the monopile structure. The cost of a monopile structure including the transport and installation costs is expressed by the following equation (M €) [14]:

$$C_{foundations}=0.54\ P_{turbine}(1+0.02\ (w_d-8))(1+0.8\ 10^{-6}(h.(\frac{RD}{2})^{2}-10^{5}) \qquad (2\text{-}15)$$

With:

$P_{turbine}$: rated power of a wind turbine [MW],

w_d: water depth [m],

h: turbine hub height [m],

RD: rotor diameter [m].

2.2.3 Cables cost

2.2.3.1 AC cables cost

In the literature, the most common model of the AC cables cost S. Lundberg's model [11] since it is more detailed due to the fact that there is more information on the cost in function of the cross-section and nominal cable voltage. Several research works used this model. The equation below illustrates the AC cable's cost model:

$$Cost_{AC}=A_{AC}+B_{AC}\exp\left(\frac{C_{AC}S_n}{10^8}\right) \quad (2\text{-}16)$$

$$S_n=\sqrt{3}\,U_nI_n$$

With:

$Cost_{AC}$: AC cable cost in [SEK/km],

U_n: rated cable voltage, pole to pole [V],

I_n: rated current of the cable [A],

S_n: rated apparent power in [VA],

A_{AC}, B_{AC}, C_{AC}: Constants.

As shown by equation (2-16), the AC cables cost increases exponentially with the cable rated power. The following table shows the values of the constants A_{AC}, B_{AC} and C_{AC} for different voltage levels.

Table 2-3 Values of the constants A_{AC}, B_{AC} and C_{AC} for different AC cable voltages [11]

Rated voltage [kV]	A_{AC} [10^6]	B_{AC} [10^6]	C_{AC}
22	0.284	0.583	6.15
33	0.411	0.596	4.1
45	0.516	0.612	3
66	0.688	0.625	2.05
132	1.971	0.209	1.66
220	3.181	0.11	1.16

2.2.3.2 DC cables cost

In the same way as for AC cables, the cost model for DC cables is based on its power rating. In the equation (2-17), the S. Lundberg's cost model [11] is presented as a linear model instead of the exponential model used for AC cables.

$$Cost_{DC}=A_{DC}+B_{DC}P_n \quad (2\text{-}17)$$

$$P_n=U_n.I_n$$

With

$Cost_{DC}$: DC cables cost [SEK / km],

U_n: rated cable voltage, pole to pole [V],

I_n: rated current of the cable [A],

P_n: rated power of the cable [W]

A_{DC}, B_{DC}: constants.

The table below shows the values of the constants used for the DC cable cost model, for different nominal voltages. As shown by equation (2-17) and table 2-4, the cost of DC cables increases linearly with the its rated power.

Table 2-4 Values of the constants A_{DC} and B_{DC} for different DC cable voltages [11]

Rated voltage [kV]	A_{DC} [10^6]	B_{DC}
5	-0.346	0.408
40	-0.314	0.0618
160	-0.1	0.0164
230	0.079	0.0120
300	0.286	0.00969

The S. Lundberg's model dated from 2003 [11] [15] is one among several methods for estimating cables cost, other approaches were revealed either the authors assume a fixed cost [16] [17] or they consider a cost function. However, DC cable technology (extruded XLPE) has made considerable progress since 2003 [18], so that S. Lundberg's cost function may be outdated. Therefore, a new cost function has been planned for HVDC cables. Equation (2-18) presents the DC cable cost per pair [19].

$$Cost_{\text{HVDC cable pair}} = 0.652 + 0.00098\ P_{n,\ \text{cable pair}} - 0.002363\ U_{HVDC} \qquad (2\text{-}18)$$

With

$Cost_{\text{HVDC cable pair}}$: cost per cable pair [M€/km],

$P_{n,\text{cable pair}}$: rated power per cable pair [MW],

U_{HVDC}: HVDC voltage [kV].

For MVDC cables cost, the equation (2-17) is used due to lack of information.

2.2.4 Offshore Substations cost

2.2.4.1 AC substation cost

In the literature, there are several cost models for AC platforms, among them we choose three different models which their characteristics cost/power are presented in figure 2-7.

The first model is presented by the following equation [20]:

$$Cost1_{platAC}=2.534+0.0887\ P_{ss} \quad (2\text{-}19)$$

Where P_{ss} is the sum of the nominal power of the turbines connected to the platform (MW) and $Cost_{platAC}$ is the AC platform cost (M€).

The second model is a model that O. Dahmani used in his research, it is based on the model of M. Zubiaga [21] and it is presented by the following equation.

$$Cost1_{platAC}=2.14+0.0747\ P_{ss} \quad (2\text{-}20)$$

The last model is used by S. Rodriguez in his thesis work [22], it is expressed by the equation below.

$$Cost1_{platAC}=2.8286+0.099\ P_{ss} \quad (2\text{-}21)$$

The following figure shows the cost of an AC platform in function of power for the three models already mentioned. The three costs evolve linearly with the power.

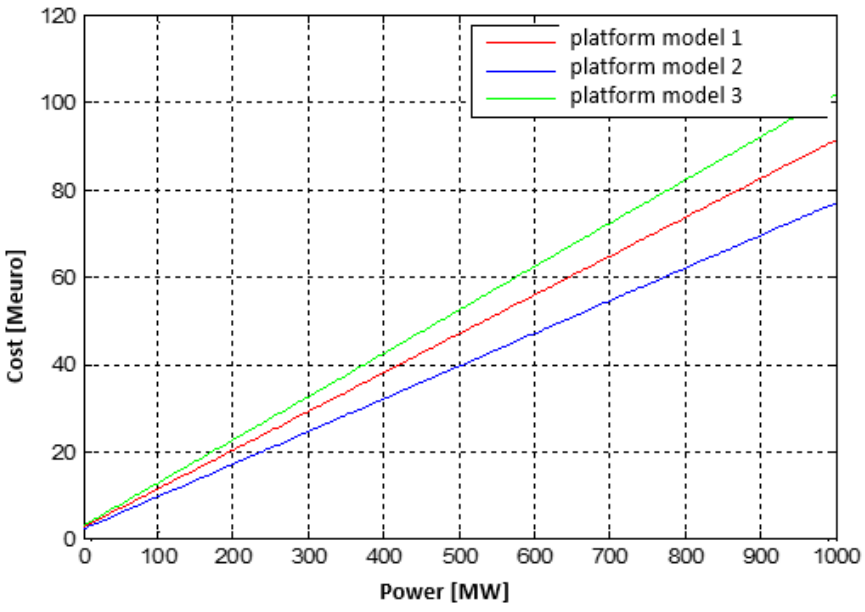

Figure 2-7 AC substation's cost for three models in function of the power

In this work, the model 1 is chosen for the AC substation's cost because it presents almost the average between the two other models so having too optimistic or too pessimistic scenarios is eliminated.

2.2.4.2 DC substation cost

It is known that an offshore VSC-HVDC platform needs to be larger than an AC platform. Therefore, its costs will be higher. Based on the data in [19], it can be estimated that the costs of VSC platforms are 57.9% to 115.4% higher than those of an HVAC platform for the same power rating. In addition, it is reported that a VSC platform is 85% larger than an AC platform [16]. Since 85% is in the middle of the range of cost increase, this is a conservative value to consider. Therefore, the cost of a DC substation is modelled as follows in M€.

$$Cost_{platDC}=1.85(2.534+0.0887\ P_{ss}) \quad (2\text{-}22)$$

2.2.5 Converters cost

In the literature, Lancheros [17] estimates that the cost of a 1000MW converter (2013) is 120M€, while Lazaridis [15] and Lundberg [11] agree on a cost of 0.11M€/MW (2005 and 2003). Schoenmakers [23] proposes a cost of 0.085M€/MW for a ±150 kV converter and 0.093M€/MW for a ±300 kV converter (2008).

These cost proposals give rise to analytical cost models proportional to the converter rated power. Three different models are presented for comparison.

The first MMC cost model is expressed in M€ is presented by the equation (2-23) [20].

$$Cost1_{MMC}=54.985+0.0589\ P_{MMC} \quad (2\text{-}23)$$

P_{MMC} is the rated power of the converter [MW].

The second economic model is presented by the equation (2-24) [24].

$$Cost2_{MMC}=42+(\frac{27}{300})\ P_{MMC} \quad (2\text{-}24)$$

And the latest cost model is presented by the equation below [25]:

$$Cost3_{MMC}=61.377+0.0657\ P_{MMC} \quad (2\text{-}25)$$

The following figure shows the costs of the three models in function of converter power. In this work, the model used is the first since it is the least expensive compared to the others.

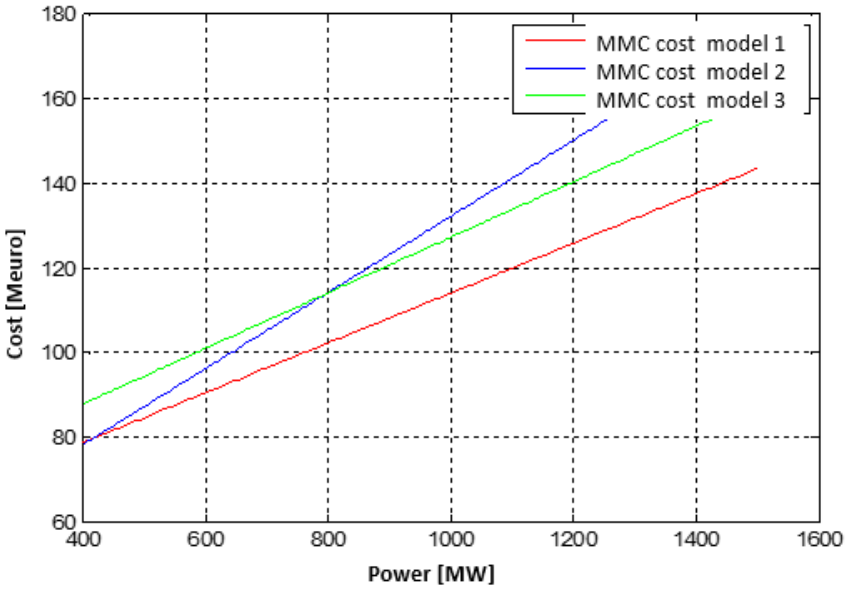

Figure 2-8 MMC cost for three models in function of the power

2.2.6 Transformers cost

O. Dahmani [2] compared the cost models of a transformer. This research resulted in the use of the simplest model which is the model of P.L. Lazaridis [25] and M. Zubiaga [21] presented by the following equation.

$$Cost_{transfo}=0.03327\ P_n^{0.7513} \quad (2\text{-}26)$$

With:

$Cost_{transfo}$: transformer cost [M€];

P_n: transformer rated power [VA].

2.2.7 Compensation equipment's cost

O. Dahmani [2] undertook a complete analysis and compares various models in the literature and its various sources have given consistent results. Indeed, the cost of reactive power compensation is the sum of the cost of the compensation equipment C_{ec} (€) and the increased cost of the platform $C_{increment}$ (€).

$$C_{comp}=C_{ec}+C_{increment} \quad (2\text{-}27)$$

The cost of the compensation equipment C_{ec} is proportional to the total reactive power of the network Q_{comp} (consumed or produced).

$$C_{ec}=\alpha_{ec}+\beta_{ec}Q_{comp}^{\gamma_{ec}} \quad (2\text{-}28)$$

$C_{increment}$ is proportional to the reactive power installed on each offshore substation $Q_{comp,\,sub}$.

$$C_{increment}=608.\ Q_{comp,sub}^{0.765} \quad (2\text{-}29)$$

G. Guidi's model is used to estimate the parameters α_{ec}, β_{ec}, γ_{ec} and $C_{increment}$ [2].

2.2.8 Switchgears cost

Switchgears are very important components for the protection of the system. For both architectures' AC and DC, switchgears are installed at both ends of the HV transmission cable.

The cost of AC switchgear is presented by equation (2-30) [26]. However, it is estimated that the equivalent price of the DC breaker is double the price of AC one [26].

$$C_{SG}=A+B\ U_{SG\ rated} \quad (2\text{-}30)$$

Where

C_{SG}: cost of cubical in SEK;

$U_{SG\ rated}$: rated line to line voltage of switchgear in V;

$A= 320.\ 10^3$ offset constant;

B=6 slope constant

3 Load flow calculation

The load flow calculations methods are developed in Mat AC/DC which is a Matlab library [1] developed by Jef Beerten in K.U. Leuven university in Belgium. Mat AC/DC is a developed version of Matpower [27] that can calculate the mixed AC/DC load flow by integrating the converters modeling and taking into account their control modes. This library is an open source software, the parameters for AC and DC part are separated and the input code is easy to manipulate, it uses matrices to define buses, generators, converters and branches. However, a

total DC electrical network cannot be modelled with this library so the need to develop a DC load flow algorithm. All load flow calculations are made in the system steady state.

3.1 AC load flow

3.1.1 Methodology implementation

The load flow calculation method in Mat AC/DC is based on the Newton-Raphson approach [28] which is characterized by its rapid convergence efficiency compared to other methods (Gauss Seidel method). The detailed equations for Newton Raphson approach are detailed in Appendix 4.

For AC load flow calculation, Mat AC/DC uses a file where the wind farm electrical connection topology is modelled. In fact, three matrices are used:

- ***Bus data*:** contains all the buses (nodes) of the electrical configuration under study.

Generally, the different nodes of an electrical network can be classified into three families: PV nodes where the active power and the voltage are known but the reactive power and the load angle δ will be determined after the convergence of the power flow calculations, PQ nodes are characterized by their active and reactive powers so the voltage and the load angle are the variables to be calculated and slack nodes are defined by the voltage and the load angle (δ=0), this type of node is used to balance the active power P and the reactive power Q in a system while performing load flow calculations that's why it is called also the reference node. After solving the load flow problem, the active and reactive powers of the slack bus are determined.

The turbines are considered to be PQ nodes in the *bus data* matrix, the active power of each turbine is set to the values obtained after the estimation of wake effect losses. The turbine is assumed not to produce reactive power (Q=0) i.e. the power factor is equal to 1. The reactive power value is not easy to define since it depends on the control strategy of the turbine. Likewise, each transformer block is modeled by two PQ nodes that are at the transformer's input and output. There is no injection of active or reactive power in these nodes, they represent virtual PQ nodes that facilitates transformer's modelling. Between the two nodes, the transformer will be modelized in *Branch data* with its appropriate parameters. PV nodes are present at each offshore sub-station and at the final end of the transmission line. By supposing that no active power flows in these nodes, the total reactive power compensation is determined.

- ***Generator data*:** contains the buses that are defined as generators, in general case for load flow calculation of a wind farm topology, there are no generators nodes unless the slack nodes that must be present in both matrices' *bus data* and *generator data.*

- ***Branch data*:** contains the electrical connection between two buses by inserting the values of the resistance r, the reactance x and the susceptance B expressed in per unit (seen in chapter 2).

3.1.2 Validation of the algorithm

Here for the algorithm validation, an example of a mini wind farm is chosen (figure 2-9), 5 wind turbines are under study connected in a collection network with a voltage 66 kV, each wind turbine produces 6 MW so the base power of pu system is 6x5= 30 MW. The substation encompasses a tranformer with a nominal power 40 MVA. There is only one HVAC cable with a voltage 220 kV and a cross section 500 mm^2 that carries the energy to the delivery point. The MVAC cable chosen has a cross section 240 mm^2, the characteristics of the cables in pu are presented in the table 2-6. Nodes 9 and 10 are the compensation nodes respectively at the sub-station and the DP. Figure 2-9 presents the AC load flow modeling of a wind farm with the type specification of different nodes.

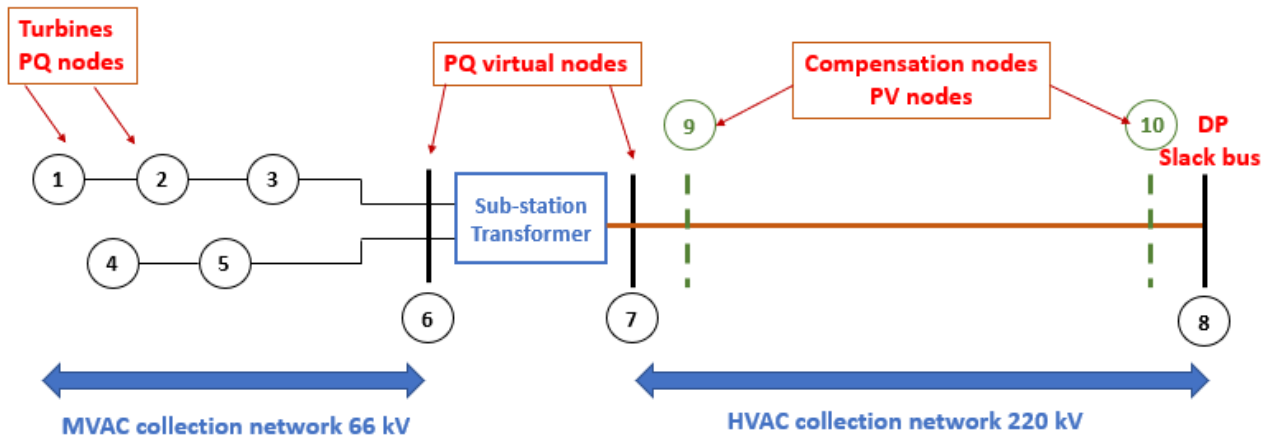

Figure 2-9 Example of validation for AC load flow

The table below presents the nodes of the system with its types.

Table 2-5 The example nodes and their types

Node	Type
1, 2, 3, 4, 5	PQ with P= -6 MW and Q=0 MVAR
6, 7	PQ with P= Q= 0 (virtual node for the transfo)
8	Slack bus
9, 10	PV

The characteristics of the MV cable are: R_MV= 85 10^{-3} (ohm/km), L_MV= 0.38 (mH/km) and C_MV= 220 10^{-3} (μF/km) and the characteristics of the HV cable are: R_ HV = 39.1 10^{-3} (ohm/km), L_ HV = 0.43 (mH/km) and C_ HV = 140 10^{-3} (μF/km).

Table 2-6 The branches and their characteristics

Branches	Distance (km)	Branch characteristics (pu/km)	Branch characteristics (pu)
1→2	2	MV cable r = 5.85 10^{-4}, x= 8.22 10^{-4}, b= 0.01	r=0.0012, x = 0.0016, b = 0.02
2→3	3	MV cable r = 5.85 10^{-4}, x= 8.22 10^{-4}, b= 0.01	r = 0.0018, x = 0.0025, b = 0.03
4→5	5	MV cable r = 5.85 10^{-4}, x= 8.22 10^{-4}, b= 0.01	r = 0.0029, x = 0.0041, b = 0.05
3→6	7	MV cable r = 5.85 10^{-4}, x= 8.22 10^{-4}, b= 0.01	r = 0.0041, x =0.0058, b = 0.07
5→6	8	MV cable r = 5.85 10^{-4}, x= 8.22 10^{-4}, b= 0.01	r = 0.0047, x = 0.0066, b = 0.08
6→7	--	Transfo	r = 0.0053, x= 0.0752, b= -0.0267
7→9	Insignificant distance 10^{-3}	HV cable r = 2.42 10^{-5}, x= 8.39 10^{-5} , b= 0.07	r = 2.42e-8, x = 8.39e-8, b= 7 e-5
9→10	Transmission distance 50	HV cable r = 2.42 10^{-5}, x= 8.39 10^{-5}, b= 0.07	r = 0.0012, x = 0.0042, b= 3.5
10→8	Insignificant distance 10^{-3}	HV cable r = 2.42 10^{-5}, x= 8.39 10^{-5}, b= 0.07	r = 2.42e-8, x = 8.39e-8, b= 7 e-5

The results of the AC load flow are presented in the table 2-7. The Newton's method power flow converged in 3 iterations.

The losses between the nodes 7-9 and 10-8 are zero since the distance between them is insignificant (about 10^{-3} km). Practically, the compensation nodes must be at the HV cable extremities so we can say that in real nodes 7 and 8 are respectively the same nodes 9 and 10.

The total active losses are 0.278 MW which are the sum of losses between each two nodes. The table 3-3 shows the detailed power flow at each node from node 1 to the slack bus. The validation of these results can be proved by the fact that the power of the slack bus (node 8/ 29.72 MW) is equal to the power produced by the whole farm (30 MW, 5 turbines where each produces 6 MW) minus the total losses (0.278 MW).

Table 2-7 The results of the AC load flow

Branches	From bus	To bus	From bus injection		To bus injection		Losses	
			P(MW)	Q(MVAR)	P(MW)	Q(MVAR)	P(MW)	Q(MVAR)
1	1	2	6	-0	-6	-0.63	0.001	0
2	2	3	12	0.63	-11.99	-1.56	0.008	0.01
3	4	5	6	-0	-6	-1.57	0.003	0
4	3	6	17.99	1.56	-17.95	-3.69	0.043	0.06
5	5	6	12	1.57	-11.97	-4.04	0.023	0.03
6	6	7	29.92	7.73	-29.76	-4.63	0.161	2.28
7	7	9	29.76	4.63	-29.76	-4.63	0	0
8	9	10	29.76	-60.93	-29.72	-43.94	0.038	0.13
9	10	8	29.72	-8.58	-29.72	8.56	0	0
TOTAL							0.278	2.53

3.2 Hybrid AC/DC load flow

Two main power flow calculating methods for hybrid AC/DC network are developed and widely used, which are sequential method and simultaneous method. The sequential method will be explained in details as it is the method applied in this work.

3.2.1 Nodes type

Like mentioned before for a classic AC power flow calculation, two of four parameters of each node are known previously: V, δ P, Q and the value of the two others can't be known before calculation. Therefore, all the nodes can be divided into PQ nodes, PV nodes and slack buses. PV bus includes nodes connected with generators or converters in the case of AC/DC load flow calculation which can provide sufficient reactive power to sustain the voltage constant. PQ bus usually represents node of constant active and reactive powers, such as load nodes (turbines). Slack bus is responsible for the power balance of whole grid, in addition, it sets a benchmark for voltage and load angle.

Hybrid AC/DC network involves more conditions for AC and DC connecting buses types, including converter node and DC transmission line ends. The type model of a converter has a relation to its controlling strategy, and the active power and reactive power control can be separated.

In fact, for the active power injection control which represents the converter control mode for the DC side, there are three control modes:

1) constant P: The converter controls the active power injected to the AC grid.
2) constant U_{dc}: The active power changes to keep DC bus voltage constant.
3) DC droop control: the active power changes linearly with its voltage.

And for the reactive power injection control which is represents the converter control mode for the AC side, there are two control modes:

1) Constant Q: The converter controls the reactive power injected to the AC grid.
2) Constant U_s: The reactive power adapts to keep AC bus voltage U_s constant.

The relation between the active power P and the voltage U_{dc} is shown in figure 2-10.

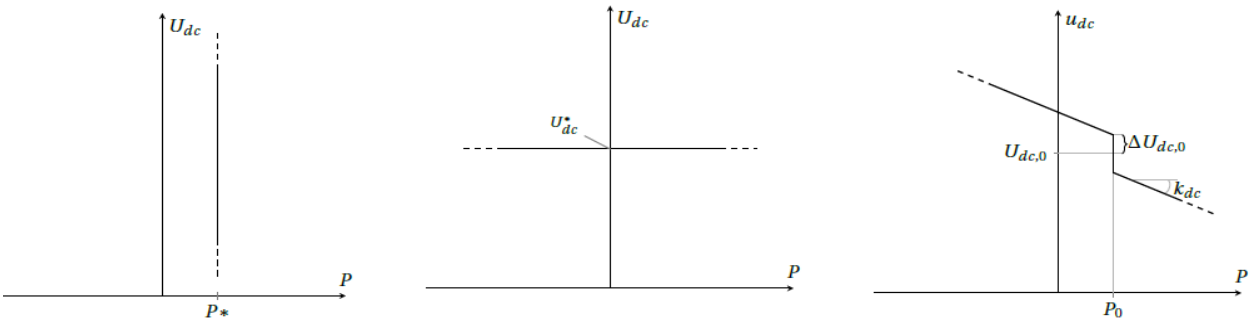

Figure 2-10 Converter steady-state control modes [29]

In general, for every HVDC transmission line, one converter must control the active power injection into AC grid (Constant P control) and the other converter must adjust its active power injection to control the DC bus voltage U_{dc}. In this way, this converter is treated as a "DC Slack converter". The active power injection value of this converter is obtained after the power flow because it depends on the losses in the DC transmission lines and the converter station. In this thesis work, the DC droop control is not taken into consideration.

Hybrid AC/DC load flow method is based on separating the AC zones from DC zones. In each AC zone, one bus should be chosen as the slack bus to keep the power balanced. The other nodes can be PV or PQ buses depending on its controlling strategy. Besides, each DC network must contain a DC slack bus like a reference node to facilitate the DC load flow calculations. A slack bus on either the DC or AC side must not correspond with a voltage control mode otherwise there will be a conflicting voltage control on the same bus and MatAC/DC generates an error.

3.2.2 Sequential method

Sequential method means calculating the state variables of AC and DC systems respectively in an independent way in each iteration, until all the state variables converged. During this process, AC and DC power flow equations are solved separately. To calculate the variables of AC system, the converter of DC system can be regarded as an equivalent PQ node connecting to an AC bus. Then to solve DC equations, AC system is regarded as a constant voltage of the bus bar of the converter. Thus, the output power of the converter is equal to the output power of the AC network minus the losses in the converter station. With this method we end up with the calculation of a simple energy balance.

Figure 2-11 The interface of AC and DC networks

To illustrate this algorithm clearly, the calculation procedure is shown in figure 2-12.

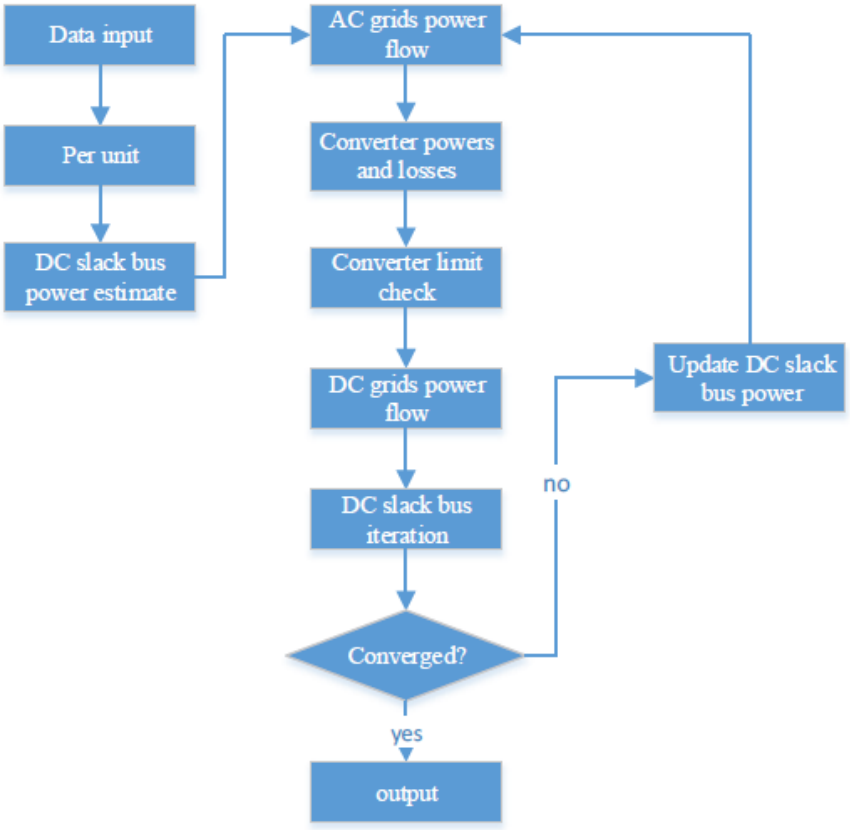

Figure 2-12 The flow chart of the sequential AC/DC power flow algorithm [10]

The converter equations, DC grid model with its equations, the modelling of the AC/DC networks power flow with the imposed control modes and the active and reactive powers flowing in each component for solving the sequential power flow problem are presented with details in Mat AC/DC manual [29].

For a mixed AC/DC power flow, AC parameters inputs are kept the same that were explained in section 3.1.1. For the DC inputs network, the system involves three matrices: *DC bus data*, *DC converters data*, and *DC branches data*.

- ***DC Bus data*:** contains the connection between DC nodes and AC nodes with specifying of the DC voltage level of each node.
- ***DC converters data:*** contains the DC nodes that are linked to converters with specifying of the different control modes of each converter for both sides AC and DC without forgetting to mention the active and reactive powers injected in the AC grid. The constants values for calculating converter losses are mentioned. It contains also the resistance and reactance of both the transformer and the phase reactor as well as the converter limits voltage magnitude.
- ***DC branches data:*** contains the connection between DC nodes, it is represented by the resistance $R_{dc\ i,j}$.

As all of the calculating steps are designed, standardized input data are required. Data matrices are used to store all the initial information of both AC and DC networks and their connection in Mat AC/DC. There is a big convenience on modifying target data. The detailed representation of matrices for both AC and DC networks is exposed in Appendix 5.

3.2.3 Validation of the sequential algorithm

The same example presented in section 3.1.2 is modified by inserting a HVDC transmission line. The figure 2-13 presents the graph of the example under study. The base power of pu system is 30 MW. The MVAC cable is kept the same and the HVDC cable has a voltage +/- 320 Kv with a resistance R_{dc}_HV= 75.4 10^{-3} (ohm/km) and a cross section of 240 mm^2. Like mentionned before, the sequential algorithm is based on separating the AC side from the DC side and posing a slack bus for each AC zone (nodes 6 for zone 1 and node 10 for zone 2). The rated power of the two converters is 100 MVA, the loss constants are calculated according to the converter power and voltage. Nodes 7 and 8 are DC nodes, the transmission distance between these nodes is 50 km. The length of HVAC cable in the onshore part (zone 2) is 2 km, the cable has the same characteristics used before in the first example.

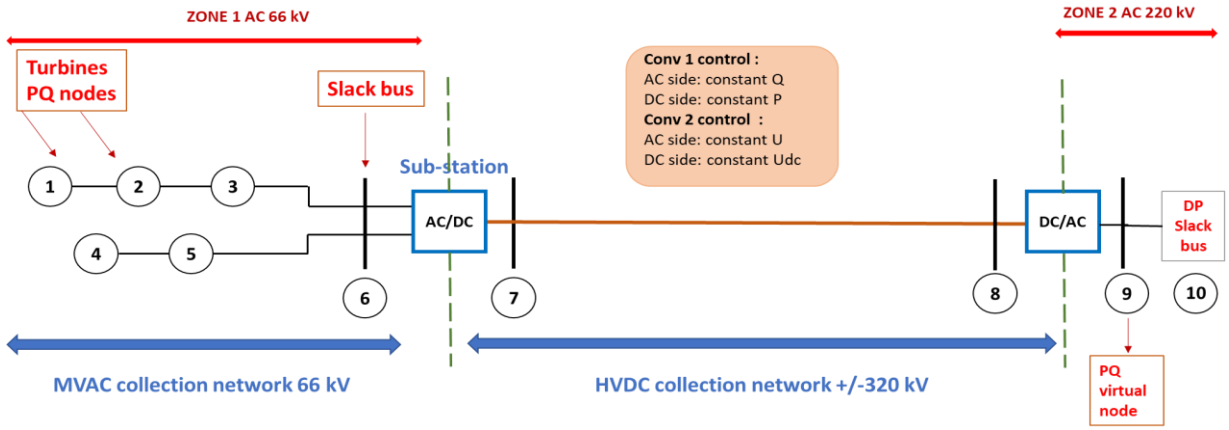

Figure 2-13 Example of validation for AC/DC load flow

The sequential solution method converged in 4 iterations (0.12 seconds). Here, we present the results values for losses between AC branches in the both zones 1 and 2 in table 3-4. The table 2-9 presents the results of the DC bus data where the DC power injected in the AC grid is determined (the power in node 6 which is the slack bus in AC zone 1 is determined in branch data and then it is injected in the AC grid because the first converter is controlled by active and reactive power injection), the active and reactive power in node 6 are respectively -29.92 MW and -7.42 MVAR. The table 2-10 presents the VSC converter data where the converter losses are calculated and the losses in the different components of the converter are shown (phase reactor and transformer). The final table shows the losses in the DC branch.

Table 2-8 The branch data for AC load flow in zone 1 and 2

Branches	From bus	To bus	From bus injection		To bus injection		Losses	
			P(MW)	Q(MVAR)	P(MW)	Q(MVAR)	P(MW)	Q(MVAR)
1	1	2	6	-0	-6	-0.60	0.001	0
2	2	3	12	0.60	-11.99	-1.50	0.009	0.01
3	4	5	6	-0	-6	-1.50	0.004	0
4	3	6	17.99	1.50	-17.95	-3.54	0.045	0.06
5	5	6	12	1.50	-11.97	-3.88	0.024	0.03
6	9	10	25.59	-9.48	-25.59	5.28	0	0
TOTAL							0.083	0.12

Table 2-9 The DC bus data

Bus	Bus	Voltage	Power
DC	AC	Mag (pu)	P(MW)
7	6	1	-26.94
8	9	1	26.92

Table 2-10 The VSC converter data

Bus	Bus injection		Converter voltage		Total losses
DC	P(MW)	Q(MVAR)	Mag(pu)	Ang (deg)	P(MW)
7	-29.92	-7.42	0.970	-16.486	2.98
8	25.59	-9.48	0.944	14.499	1.34
Total					4.32

Here the total losses in the VSC substation are 4.32 MW. The detailed losses in the different components are:

- Transformer losses: P(MW) = 0.08 and Q(MVAR)= 6.33
- Reactor losses: P(MW) = 0.01 and Q(MVAR)= 9.28
- Converter losses: P (conv 1, MW) = 2.93 and P (conv 2, MW) = 1.30 ➔ the total converter losses are 4.23 MW

Table 2-11 The DC branch losses

Branch	From		To		loss
	Bus	Bus	P (MW)	P (MW)	P (MW)
1	7	8	26.94	-26.93	0.01
Total					0.01

The total losses in the DC branches is 0.01 MW.

The validation of these results is done based on the principle of power conservation. In fact, the slack bus power in node 10 (25.59 MW) is equal to the total power transmitted to the DC substation (node 6 = 29.92 MW) minus the converter losses (4.32 MW) and the DC line losses (0.01 MW).

3.3 DC load flow

3.3.1 DC power flow algorithm methodology

This section describes the development of the DC power flow algorithm. In the literature [30], the DC power flow calculation is based on the AC power flow method by linearization of the AC system. For an AC system with n nodes, the power flow problem has 2n non-linear equations which have to be solved iteratively. With the simplification of this problem, a linear non-iterative DC power flow algorithm is obtained through three assumptions:

• DC cable resistances are neglected i.e. R << X, this means that the grid active losses are zero.

• Voltage angle differences are supposed to be small i.e. the linearization of sin and cos terms, $\sin(\Theta) = \Theta$ and $\cos(\Theta) = 1$.

• The voltage magnitude of all nodes is set to 1.0 per unit (flat voltage profile).

These "crude" assumptions pushed Purchala [31][32] to study the correctness of the DC power flow method. In fact, with a test network of 30 nodes, the result gives that the average error is about 5 % for a R/X ratio equal or below to 0.5 and decreases to 2 % for 0.2 ratios. Knowing that the ratio is getting smaller with higher voltages level so the first simplification is more accurate with high transmission network. However, for MVDC collection network with at most a +/- 80 kV voltage level, the assumption can affect the results. Furthermore, the fact of considering a flat voltage profile can accent the DC power flow errors by not taking account a realistic set with the voltage's fluctuations. By way of indication, a small voltage deviation (0.01 pu) causes a 5 % error.

For all these reasons, this DC load flow calculation approach is eliminated and another algorithm inspired by the Backward/Forward Sweep load flow method is used [33]. This method is accurate for simple connected networks like radial ones. It is a cumulative method that calculates the load flow in each node in the power flow direction. In the special case of radial connection topologies, the active power transmitted through the DC network branches (no reactive power) can be evaluated by knowing the production of each wind turbine and the voltage level in the inter-array network using a tree-path method from the wind turbines to the onshore point.

The inputs of the algorithm are:

- M_topology: it's a square matrix of dimension (n) where n is the number of nodes including the slack bus. M_topology (i, j) =1 if there is a connection in the downstream direction between nodes i and j.
- M_resistance: it's a diagonal matrix of dimension n that contains the resistances of the DC branches. Thus, the column vector R of dimension (nx1) can be defined, it contains the resistances of the DC branches.
- P_nodes: it's a column vector of dimension (nx1) that contains the power injected in each node.
- V_Init: it's a column vector of dimension (nx1) that contains the initial voltage magnitude of each node.

And the outputs are:

- Branches_power: it's a column vector of dimension (nx1) that contains the power in each node in the downstream direction.
- Branches_losses: it's a column vector of dimension (nx1) that contains the losses in branches.
- V: it's a column vector of dimension (nx1) that contains the voltages in each branch.
- I: it's a column vector of dimension (nx1) that contains the currents in each branch.

The flow chart of the DC load flow algorithm is presented in the figure below. the convergence criterion is based on voltage convergence.

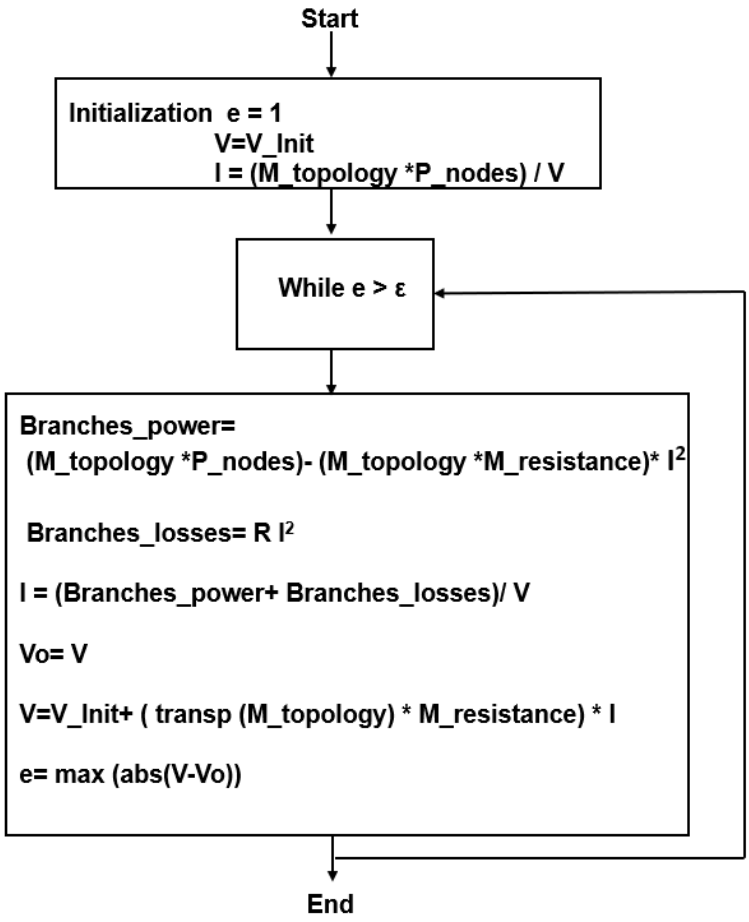

Figure 2-14 The flow chart of radial DC power flow algorithm

3.3.2 DC power flow algorithm validation

The DC network example for the validation of the algorithm is presented in figure 2-15. It consists of 5 nodes and a slack bus.

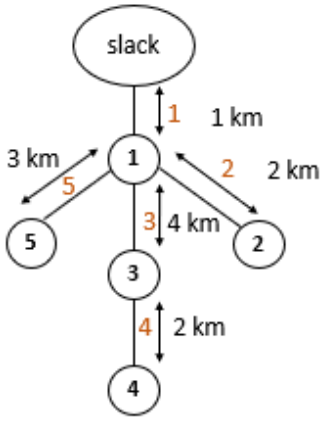

Figure 2-15 DC network representation

The DC cable chosen has a cross section 500 mm^2 with a resistance at 20°C equal to 0.0366 ohm/km, its voltage is 80 kV which is considered as the base voltage of the system. The power output for each node is 6 MW which is considered as the base power. Thus, the base impedance is 1066 ohm. The distance between the nodes is marked on the graph. The branch resistance must be in per unit. All the values of V_Init are equal to 1 pu. The M_topology is expressed as follow :

$$M\_topology=\begin{bmatrix}1 & 1 & 1 & 1 & 1\\ 0 & 1 & 0 & 0 & 0\\ 0 & 0 & 1 & 1 & 0\\ 0 & 0 & 0 & 1 & 0\\ 0 & 0 & 0 & 0 & 1\end{bmatrix} \quad (3\text{-}31)$$

Results of the DC load flow calculation are presented in the table below.

Table 2-12 The DC load flow results

node	Branches_power	Branches_losses 1.e-03 *	V	I
1	4.9983	0.8572	1.0002	4.9983
2	0.9999	0.0686	1.0002	0.9998
3	1.9994	0.5480	1.0004	1.9990
4	0.9999	0.0686	1.0005	0.9995
5	0.9999	0.1300	1.0003	0.9997

The DC load flow algorithm can be validated by the power and the current conservation. In fact, the power injected in each node is its initial power minus the losses. One can conclude that the node 1 is equal to the total power cumulated in the slack bus minus the sum of the total power losses. ε is fixed to 10^{-3} and the program converge after 3 iterations.

In this approach, the slack bus comes upstream of the DC substation. Then, for the load flow calculation of the whole network a power balance is applied. In fact, first of all the converters losses are evaluated by the quadratic equation presented in section 2.1.3. The DC/DC converter is composed of an inverter followed by a rectifier where each converter has its appropriate quadratic equation for losses calculation. Then, the power in the final onshore point is obtained from the power of the slack bus minus the converter's losses (DC/DC and DC/AC converters) and the HVDC lines losses.

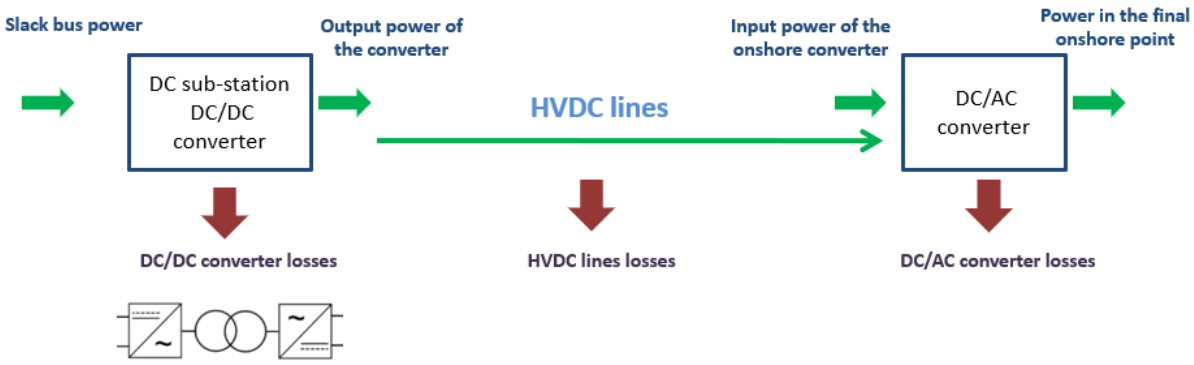

Figure 2-16 Power balance diagram for a DC network

4 Wake effect calculation

4.1.1 State of the art of the existing wake effect models

In order to get closer to the realistic framework for calculating losses on a wind farm. It is necessary to integrate the wake effects losses due to the turbine's placement. There is a variety of models that calculate the wake effects with different accuracy levels. In the literature, the wake models can be divided into two different families, the first one is the Kinematic models like Larsen, Frandsen and Jensen's wake model [34] [35] and the second one is the models that integrate the turbulence models by solving the Reynolds-averaged Navier–Stokes equations. Eddy viscosity belongs to this class [36]. In general, four analytical wake effect models can be considered: Lissaman's wake model, Larsen's wake model, Jensen's wake model and Ainslie's wake model, these models can be called low fidelity engineering models because it describes the wake losses with a simple mathematical way with a rapid computation time and an accurate way to estimate the velocity deficit even for far wake zones. Other models are more accurate such as the Dynamic Wake Meandering model [37] and the Computational Fluid Dynamics [38] but they evaluate the wake effect calculation during several weeks.

The most common model used is the Jensen model because it offers a rapid computation time to calculate multiple wake effects, it's a model that can estimate the partial or the multiple wake effect. Mikel de Prada in his research [39], studies the impact of the wake effect on overall losses using the Jensen's wake model, the proposed idea was trying to operate the turbines at their non-optimum points in the aim to reduce their wake effects. In fact, the results show that there is an increase from 1.86% up to almost 6.5% in the annual energy captured by the whole wind farm if the upstream turbines operate a little bit away from their optimum point reducing thereafter the

wake losses. Peng Hou et al [40] integrate the Jensen's wake effect model in the optimization of the wind farm layout design. In fact, an evolutionary algorithm (PSO) was applied for a regular shaped wind farm to determine the optimal direction placement of the wind farm with the optimal spacing between the wind turbines. The control strategy's impact on the total losses was discussed by optimizing the pitch angle for each wind turbine. Seim et al [41] validates three wake models using the Windsim software for eight single wake cases. The results show the Larsen's model overestimated the width of a wake and the Jensen's wake model is simpler and requires a very short time of calculations. Jeon et al [42] made also a brief comparison between the different analytical wake effect models and they conclude that Jensen's wake model out performed comparing to other wake models.

4.1.2 Katic Jensen model

In this thesis work, the Katic Jensen model [43][44] is used to calculate the wake effect between turbines. This model was developed by Jensen in 1983 and further improved by Katic et al in 1986. The calculation of the wake effect is not based on an optimization algorithm aiming at positioning the turbines in the optimal location. The calculation approach has as input the fixed positions of the turbines and after that the calculation of the wake effect is estimated by the Katic Jensen analytical model to determine the output power of each turbine taking into account the occurrence of different wind speeds (wind rose).

Considering two turbines j and k mounted next to each other in figure 2-17, the wind speed seen by the turbine j is given by:

$$U_j = U_0(1\text{-deficit}) \tag{2-32}$$

Where: U_0 is the ambient wind speed, it represents the wind speed seen by the turbine k and the deficit is the speed decrease caused by wake effects which is expressed by the following equation.

$$\text{deficit} = \sqrt{\sum_{k=1}^{n} U_{kj}^2} \text{ with } U_{kj} = \frac{1-\sqrt{1-C_{Tk}}}{\left(1+\frac{\alpha d_{kj}}{R_j}\right)^2} \frac{A_{kj}}{A_j} \tag{2-33}$$

Where: C_{Tk} is the thrust coefficient of the turbine k at a given wind speed, A_j is the rotor area for turbine j and A_{kj} is the rotor area for the turbine j influenced by the turbine k.

The A_{kj} can be expressed differently depending on the type of wake effect:

- $A_{kj=} \pi R_j^2$ when the turbine j is totally affected by the turbine k.

- $A_{kj=}$ 0 when there is no wake effect
- $A_{kj=} \frac{1}{2} \left(R_{kw}^2 \left(2 \arccos \left(\frac{R_{kw+}^2 C_{kj-}^2 R_j^2}{2R_{kw}C_{kj}} \right) - \sin\left(2\arccos\left(\frac{R_{kw+}^2 C_{kj-}^2 R_j^2}{2R_{kw}C_{kj}}\right)\right)\right)\right) +$

  $\frac{1}{2} \left(R_j^2 \left(2 \arccos \left(\frac{-R_{kw+}^2 C_{kj+}^2 R_j^2}{2R_jC_{kj}} \right) - \sin\left(2 \arccos\left(\frac{-R_{kw+}^2 C_{kj+}^2 R_j^2}{2R_jC_{kj}}\right)\right)\right)\right)$ when the turbine j is partially affected by the turbine k.

The wake expansion is expressed by:

$$R_{kw}=R_{k+}\alpha d_{kj} \tag{2-34}$$

Where: R_k is the turbine rotor radius and α is the wake decay coefficient that can be calculated by the following expression

$$\alpha=\frac{0.5}{\log\left(\frac{T_{HUB}}{0.0005}\right)} \tag{2-35}$$

Where, the T_{HUB} is the turbine hub height.

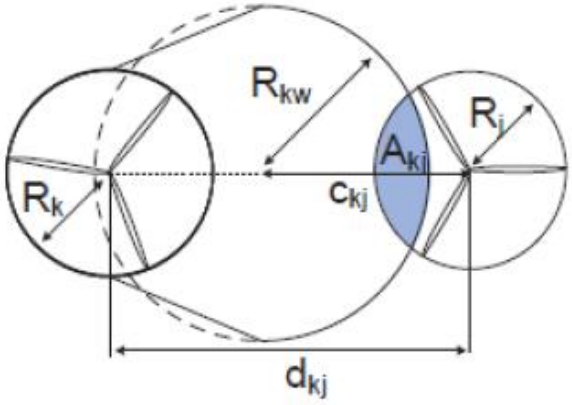

Figure 2-17 The partial wake effect caused by the turbine k on the turbine j [22]

4.1.3 Calculation methodology

In our case, a calculation tool is developed to determine the wake effect between the turbines in a wind farm with a regular or irregular shape. The calculation steps are as follows:

Step 1: choose the wind direction,

Step 2: change of the reference mark related to turbines positions according to the axis of rotation which is the wind direction,

Step 3: determination of the turbines affected by the wake effect: creation of an influence matrix M which is a square matrix of N dimension where N is the number of turbines. In fact, $M_{ij} = 1$ if there is a wake effect between turbine i and turbine j and $M_{ij} = 0$ if there is no wake effect,

Step 4: exploitation of the matrix M to know each turbine is affected by how many turbines (multiple wake effect),

Step 5: calculate the wake effect for each turbine with the Katic Jensen model.

5 Overall problem of optimization

5.1 Optimization goals

As mentioned in chapter 1, the LCOE criterion is a reference to assess electrical performance for offshore wind farms. The minimization of the LCOE is the main objective in the optimization framework. This economic function is expressed by the following equation:

$$LCOE = \frac{\frac{CAPEX}{a} + OPEX}{AED} \quad (2\text{-}36)$$

Where:

a: the annuity factor, $\frac{1-(1+r)^{-N}}{r}$

CAPEX: the annual capital expenditure,

OPEX: the annual operational expenditure,

AED: the annual energy delivered= AEP – the total losses of the architecture,

r: the discount rate,

N: number of years of the wind farm exploitation.

The LCOE is an indicator that links both the investment and maintenance costs to the annual energy delivered. It represents the average minimum price at which electricity must be sold to achieve profitability during the wind farm lifetime. The discount rate r can change throughout the lifetime exploitation so the LCOE may not be the best indicator but it remains a tool to help researchers guide decision-making in favor of particular energy production systems.

The LCOE function can be dissected to have other economic functions such as the total investment cost which is expressed by this equation:

$$\text{INVEST} = \frac{\text{CAPEX N}}{\text{a}} \tag{2-37}$$

As it is reported in chapter 1, two types of optimization are studied in this work. The first one is the mono-objective optimization where only one economic function is fixed for the optimization. The economic functions studied in the context of mono objective optimization are the total investment cost INVEST, the AED and the LCOE. The second type is the multi objective optimization where two functions are coupled to form the Pareto Front. We can consider for example the couple (INVEST, AED) or (LCOE, AED).

5.2 Designing of the optimization framework

Designing an optimal connection architecture for an offshore wind farm is the need sought by the designers. Generally, in the planning phase, offshore wind farms are set up based on feedback from other wind farms by comparing them and then choosing the most suitable architecture after having made some technical restrictions related to the site conditions such as environmental constraints (fishing area or birdlife zone), water depth which has an impact on the investment cost of components, the existing sub-sea cabling area that must be exploited as well as the location with a suitable wind resource. After that, the criteria (LCOE, INVEST, AED) are calculated for the selected architecture so this process leads us to not have an optimal topology according to a fixed economic criterion. However, the designers should not do the designs themselves beforehand, they should explore all the designs by studying several economic functions and then select the most suitable design. That is the main objective of the optimization which is developing a decision support tool to help designers and researchers to choose the "optimal" electrical architecture.

Within the general framework of optimization, some assumptions must be made to simplify the formulation of the optimization problem:

- The number and positions of the wind turbines are fixed: turbine positions and number are input data and are not included in the optimization,
- Turbines do not produce any reactive power; their power factor is equal to 1 (simplification of power flow calculations),
- The MVDC collection network is made by a radial or a star connection (no meshed networks in DC topologies because it is not straightforward to control the active and reactive powers in converters),

- The AC topologies can be meshed,
- Losses in the wind turbine internal architecture (generators, convertors and transformers) are neglected. The wind turbines are assumed to be sources of energy production,
- Redundancy for cables is not studied,
- If the power transmitted surpasses the nominal power of the transformer and the HV cable, there is the possibility to put transformers and HV cables in parallel. However, in the collection network, only one cable can connect two nodes,
- No loss power in the reactive compensation devices.

Within the framework of optimization, the electrical topology is built up by blocks: the first step is the construction of the MV collection network where the turbines are connected. In fact, this phase is based on the clustering concept and that's means gathering the turbines into groups, the optimization heuristic algorithm proposes at each iteration the turbine's clustering until the optimal collection network is defined. The output data to be retrieved once the MV network layout is set are: the number of clusters connected to each sub-station, the number of turbines in each cluster and the definition of the MV cables cross section. The second block, like presented in the figure below, is the placement of offshores sub-stations. In our case and for every topology AC or DC, the maximum possible number of sub-stations that can be installed is 4, the number and location of sub-stations are important aspects that impact the increase of the CAPEX and the total length and dimension of the collection network. Furthermore, the type of the sub-station has also a significant impact in the CAPEX as long as the DC substations that include the converters are much more expensive. The last block presents the construction of the HV transmission network, where the number of HV connections is fixed with the definition of the number of the HV cables installed in parallel as well as their cross section. The design of the HV network layout includes also the connection between substations.

In this work, three different ways of sizing the cross sections of MV cables are proposed:

1. Variable cross sections: each MV cable has a cross section according to the apparent power that can flow in this cable,
2. Fixed cross sections per cluster: the MV cables in the same cluster have the same cross sections, so the largest cross section of the cluster is chosen,
3. Fixed cross sections: all MV cables have identical cross sections. The largest cross section is fixed for all cables.

In fact, the cables with different cross sections is used for the purpose of optimization, as long as it reduces the investment costs related to the cables with their installation costs. Designing the optimal electrical architecture according to a specific economic function requests to make the sizing of power components. The power rating of the transformers, the converters and the cables are determined depending on the amount of the power transmitted. In this phase, the constraints relative to cable ampacities and the power rating of transformers and converters are verified. Thus, the choice of the cables cross section and the determination of the number of transformers installed in parallel as well as the number of HV parallel cables are done.

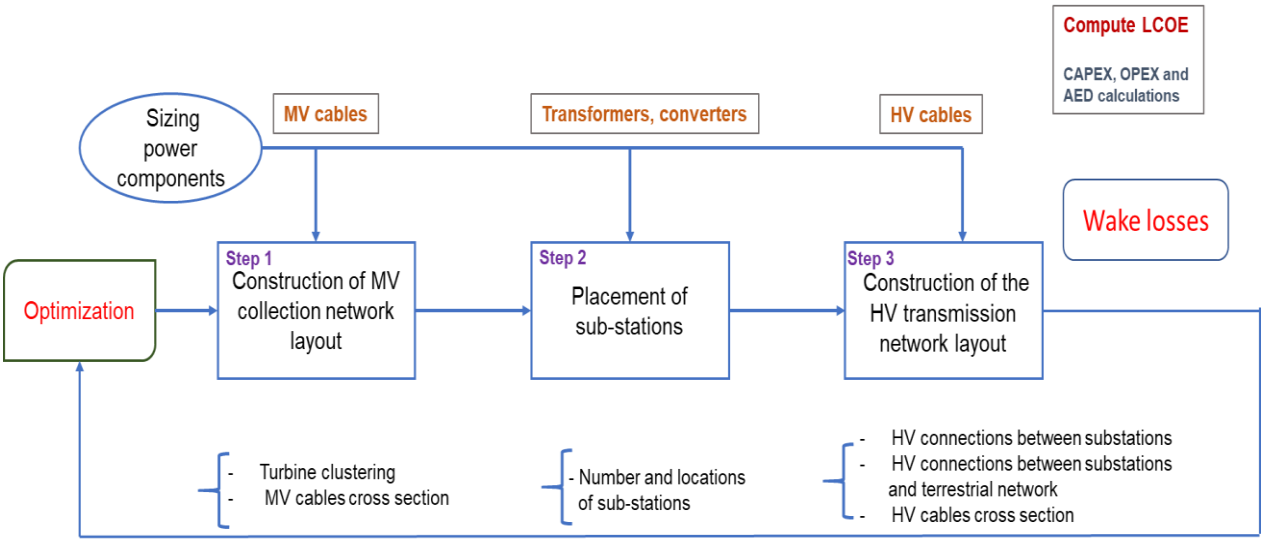

Figure 2-18 The steps for designing the optimal electrical architecture

Once the 3 steps are done with the right dimensioning of the components, the evaluation of the electrical architecture is done by the LCOE calculation. The optimization algorithm repeats the three steps until the determination of the optimal topology. The formulation of the optimization problem of a wind farm design can be presented by constraints that must be checked:

$$P_{i,j} \leq P_{n\text{-cable}} \tag{2-38}$$

Where: $i, j \in [1, N]$, $N = n_{WTs} + n_{substations} + n_{DP}$

n_{WTs} : the number of wind turbines, $n_{substations}$ is the number of offshores substations, n_{DP} is the number of delivery point which is fixed to 1 and N is the total number of nodes.

The power transmitted $P_{i,j}$ carried in each link must be less than the nominal power of the cable $P_{n\text{-cable}}$ which depends on its cross section. The table of the different cables cross section used in this work is presented in Appendix 2.

$$D_{eol\text{-}substation} \geq d_{min} \tag{2-39}$$

The distance between the turbine and the substation must be greater than a minimum distance fixed by the user. This distance requires the placement of substations outside the wind turbines. However, for minimization of the collection system length the substations can be placed inside the wind farm.

$$n_{substations} \leq n^{max}_{substations} \tag{2-40}$$

The number of installed substations must not exceed the maximum possible number of installed sub-stations $n^{max}_{substations}$ which is equal to 4.

$$\{X_{substation}, Y_{substation}\} \in [X, Y_{min\text{-}substation}, X, Y_{max\text{-}substation}] \tag{2-41}$$

The coordinates of the sub-stations must be limited by an interval, which limits the search space of their positions.

$$P_{substation} \leq P_{n\text{-}transformer} \tag{2-42}$$

$$P_{substation} \leq P_{n\text{-}converter}$$

The power encompassed in the substation must be less than the rated power of the transformer $P_{n\text{-}transformer}$ in the case of an AC substation. Same constraint is applied for the rated power in the converter in the case of a DC substation. Nominal power values for transformers and converters are respectively the following P-transformers (MVA) = [50, 100, 125, 150, 180, 200, 250, 300, 400, 630, 722, 800] and P-converters (MVA) = [100, 200, 300, 400, 500, 600, 700, 800].

$$V_{MVAC\_network} \in \{33\ kV, 66\ kV\} \tag{2-43}$$

$$V_{MVDC\_network} \in \{+/-50\ kV, +/-80\ kV\}$$

MVAC network voltages should be set at the industry standard levels 33 kV or 66 kV, the same for MVDC network voltages +/- 50 kV or +/- 80 kV.

$$V_{HVAC\_network} \in \{132\ kV, 220\ kV\} \tag{2-44}$$

$$V_{HVDC\_network} \in \{+/-150\ kV, +/-320\ kV\}$$

The same constraint is applied for HV networks.

5.3 Problem statement

5.3.1 Wind farm topology modeling

In this part, the electrical connection topology of a wind farm is explained and modeled by a binary adjacency matrix AM. This approach of modeling is proposed by O. Dahmani [2] in his PhD thesis work. We adopt the same approach in our work. Modeling the wind farm topology allows to define the optimization variables which are the binary variables of the architecture connection layout and the number and positions of substations.

According to Dahmani's research, a connection topology is represented by a graph G with a set of nodes that represent the turbines, the substations and the delivery point and a set of lines connecting them. The proposed nodes numbering is as follow:

- The delivery point DP represents the first node,
- The substations can be numbered from 2 to 5 because the maximum number of substations is 4,
- The turbines are numbered from $n_{DP} + n_{substations}+1$ to $n_{DP} + n_{substations}+ n_{WTs}$.

A topology layout of a numbered wind farm is shown in the figure below. In this example, a topology is presented with 1 substation and 8 wind turbines.

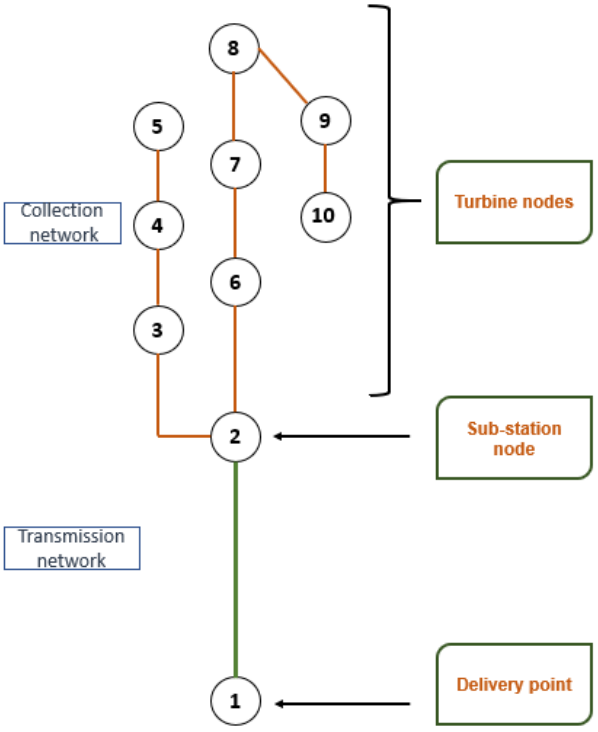

Figure 2-19 Numbered wind farm representation

From the numbered graph, two input matrices M_MV and M_HV are defined to represent the disposition of the turbines and substations. In fact, these matrices represent inputs for the optimization algorithm that allow to minimize the connection possibilities of each node of the network according to its location in relation to its neighbors. We assume that each node M_MV/HV (i, j) can only be linked to its eight direct neighbors.

M_MV/HV (i-1, j- 1)	M_MV/HV (i-1, j)	M_MV/HV (i-1, j +1)
M_MV/HV (i, j-1)	M_MV/HV (i, j)	M_MV/HV (i, j +1)
M_MV/HV (i +1, j-1)	M_MV/HV (i +1, j)	M_MV/HV (i +1, j +1)

For the example presented in figure 2-19, the matrices M_MV and M_HV are expressed by equation (2-45).

$$M\_MV=\begin{bmatrix}3 & 4 & 5\\ 6 & 7 & 8\\ 0 & 9 & 10\end{bmatrix} \quad M\_HV=\begin{bmatrix}2 & 0\\ 0 & 0\end{bmatrix} \tag{2-45}$$

The size of M_HV is 2x2 because the maximum number of the substations is set to 4.

With the input matrices, the optimization algorithm determines the binary variables of the topology's connections and the number and positions of the offshore substations that will be represented by the adjacency matrix AM. It's a square matrix of dimension $N=n_{WTs}+n_{substations}+n_{DP}$. In order to simplify the filling of this matrix, only the upper triangular part is taken, since if a connection is defined between two nodes i and j, AM (i, j) = AM (j, i) = 1. The construction of the adjacency matrix AM depends on the numbering sequence of the network nodes and it is divided into four sub-matrices defined below [2]:

- AM_{WTs}: submatrix of connection between the turbine nodes,
- $AM_{substations}$: submatrix of connection between substation nodes,
- $AM_{DP\text{-}substations}$: submatrix of connection between the delivery point node and the nodes of substations,
- $AM_{substations\text{-}WTs}$: submatrix of connection between the substations and the wind turbines.

	$n_{DP}=1$	$n_{DP}+n_{substations}$	N
$n_{DP}=1$	1	$AM_{DP\text{-}substations}$.	. . .
.		1	
.		1	. . .
.		.	
.		.	
$n_{DP}+n_{substations}$		$AM_{substations}$ 1	$AM_{substations\text{-}WTs}$.
.			1 . .
.			1
.			.
.			. .
.			AM_{WTs}
.			1
N			

(2-46)

The adjacency matrix AM of the example of the figure 2-19 is:

$$AM=\begin{bmatrix}1&1&0&0&0&0&0&0&0&0\\0&1&1&0&0&1&0&0&0&0\\0&0&1&1&0&0&0&0&0&0\\0&0&0&1&1&0&0&0&0&0\\0&0&0&0&1&0&0&0&0&0\\0&0&0&0&0&1&1&0&0&0\\0&0&0&0&0&0&1&1&0&0\\0&0&0&0&0&0&0&1&1&0\\0&0&0&0&0&0&0&0&1&1\\0&0&0&0&0&0&0&0&0&1\end{bmatrix} \quad (2\text{-}47)$$

5.3.2 Optimization algorithms

The two main algorithms used for the optimization are: Genetic and Prim algorithms. The genetic algorithm provides the first topologies of connections such as the connection between the wind turbines and the connection between offshore substations. Next, the Prim's algorithm is used to complete the connection between each group of wind turbines and the nearest substation as well as between the DP to the nearest substation (search for the shortest path) [2]. The optimization algorithm flowchart is depicted in figure 2-20.

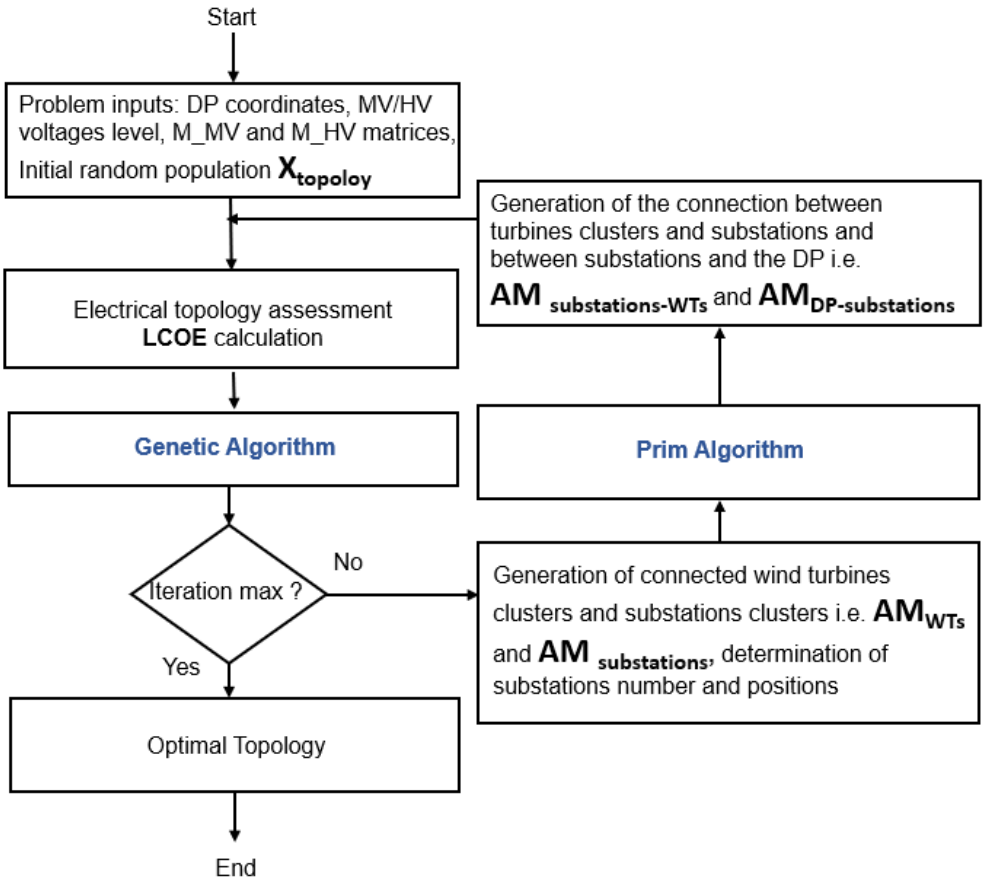

Figure 2-20 The optimization algorithm flowchart

First of all, the problem inputs are defined and a random generation of a population $X_{topology}$ is fixed. In fact, the initial population $X_{topology}$ is a matrix where its rows are the chromosomes $X^i_{topology}$ that contains the binary variables of the connection of wind turbines and substations, it includes also the binary coding of sub-station positions (further presented in this section). For each $X^i_{topology}$ the electrical topology assessment is done by the LCOE calculation, the genetic algorithm applies its properties the selection, the crossover and the mutation to get the diversity between the different chromosomes in the aim to converge to the optimal topology. If the maximum number of iterations is not achieved, for each $X^i_{topology,}$ the matrices AM_{WTs} and $AM_{substations}$ are determined, the substations number and positions are identified. Finally, the matrices $AM_{DP\text{-}substations}$ and $AM_{substations\text{-}WTs}$ are determined by Prim's algorithm. The process is looped until the best topology with the minimum LCOE is obtained.

Figure 2-21, shows the chromosome's $X^i_{topology}$ representation. The chromosome consists of three parts:

- The matrix AM_{WTs} elements where each node of the electrical network has the possibility to connect to the 8 direct neighbors' nodes, the number of these elements is variable and depends on the configuration of the M_MV matrix,
- The matrix $AM_{substations}$ elements, they are 6 binary variables for the connection between the substations since the maximum number of substations is 4,
- The binary sequence of N_{pos} elements where the substations positions are coded. The coordinate $X_{substation}$ is a real number that can be decoded with the following equation:

$$X_{substation} = X_{min\text{-}substation} + \frac{X_{max\text{-}substation} - X_{min\text{-}substation}}{2^q - 1} \sum_{k=1}^{q} a_k \, 2^{q-k} \tag{2-48}$$

Where: $\{a_1, a_2, \ldots\ldots, a_q\}$ is a vector containing q bits for coding substation's position and $N_{pos} = 2\ q\ n_{substations}$.

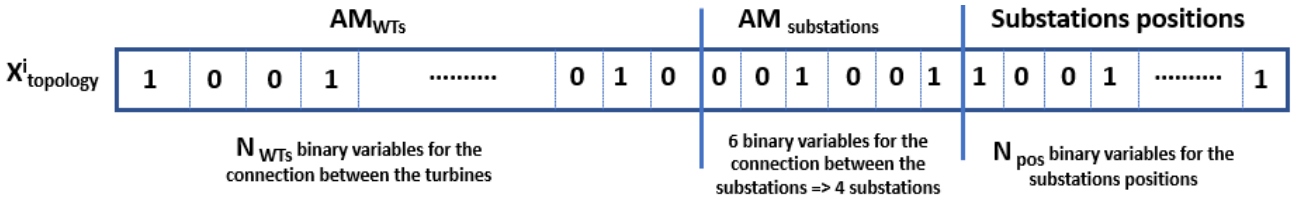

Figure 2-21 The chromosome's representation for the genetic algorithm

5.3.2.1 Genetic algorithm

The fundamentals of genetic algorithms were exposed by Holland [45] and their computer implementation was tested by Goldberg [46]. It is a global search technique that mimics natural genetic operators. Operators inspired by the mechanism of natural selection, the crossover and the mutation, are applied to a population of binary tables encoding the space of parameters.

An initial population is randomly selected, an individual corresponds to a possible solution to the problem posed. Genetic operators are applied to this population in order to create children from the parents. Thus, the new population is constituted by selecting the best individuals. At each generation, the algorithm explores different areas of the parameter space and then directs the search to regions where a high probability of finding a better performance exists.

5.3.2.2 Prim's algorithm

Prim's algorithm is an algorithm that is based on the graph theory that finds a minimum spanning tree of minimum weight "MST - Minimum Spanning Tree" in a related weighted and non-oriented graph which is the topology layout. This algorithm is used after the genetic algorithm to complete the optimization framework. In fact, after the generation of turbines clusters and substations cluster with the GA, the Prim's algorithm intervenes to complete the connection between the turbines clusters and the substations clusters, to ensure finding the optimal topology the searching of the shortest path is applied. Thus, the turbine belonging to a group must be connected to the nearest substation. Likewise, the DP must be connected to the nearest substation. Optimizing the length of the connection minimizes the investment cost of the cables, which in turn minimizes the LCOE.

Cable crossings in the MV collection network, i.e. between the wind turbines and in the HV connections between the substations are eliminated thanks to the application of the constraint that one node in the matrices M_MV and M_HV can linked only with their 8 direct neighbors. However, cable crossings between wind turbines and substations as well as between MV and HV cables are tolerated.

6 Coupling of the wake effect calculation with the load flow calculation

The integration of the wake model tool in the optimization framework requires first of all the coupling between the wake effect calculation and the load flow calculation. In fact, as depicted in figure 2-22, after setting the inputs data and for fixed wind speed V and wind direction, Katic Jensen wake model provides the different wind speed for each wind turbine (Vwt_1, Vwt_2,.., Vwt_nWTs). The power curve determines the power outputs for each wind turbine corresponding to wind speeds values already found with the wake model tool. The different power outputs are entered as data in the ***Bus data*** matrix which will be used later for the load flow calculation. The final outputs are the electrical parameters of the wind farm:

- The active and reactive powers in each node;
- The voltages in each node;
- The currents in each node;
- The losses between branches (cables, transformers or converters)

Practically, there are 26 points of wind speed varying between 0 m/s and 25 m/s and 12 directions (from 0 deg to 330 deg), with the wake effect estimated for all directions and wind speeds we can determine the AED = AEP – losses (including wake losses).

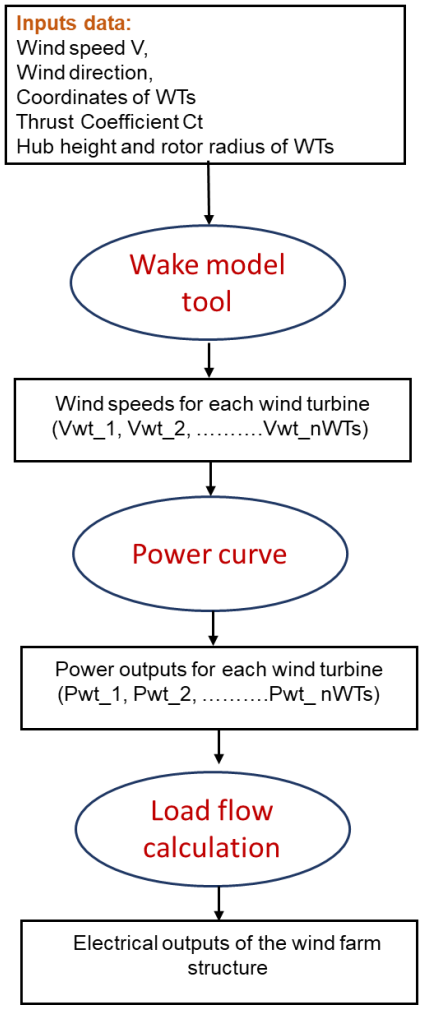

Figure 2-22 The program flowchart for the coupling between wake effect tool and load flow calculation

7 Coupling of the load flow calculation with the optimization

Like mentioned in section 3, the Mat AC/DC library uses matrix representation for input data for load flow calculation. During the optimization, and for each iteration the algorithm proposes different connection topologies that we have to calculate their load flow. The load flow depends on the transmission technology HVAC or HVDC, the number of wind turbine clusters, the number of wind turbines per cluster, the number of substations and their connections. Consequently, the matrices size can change for each iteration. Therefore, a program is developed to generate the matrices in a general way. For each iteration of the GA, the matrix AM is defined

and change its size and variables according to the proposed connection topology. From AM matrix, all the other matrices for building the load flow execution file can be determined. The program flowchart for the generalization of load flow calculations for any connection topology. The problem inputs are the AM matrix and the sizing components where the cable parameters, the transformer parameters and the converter loss constants are defined. In case of AC load flow, to construct the ***Bus data*** matrix we have to distinguish turbine nodes from substation nodes and assign each node its type with the appropriate voltage level, for ***Generator data*** matrix, the slack node and the compensation nodes are defined. Finally, for the ***Branch data*** matrix, we put the branch parameters r, x and B between nodes. Besides, for AC/DC load flow, the AC matrices can be modified by adding the possibility to have several slack buses so the definition of node zones is primordial. There are no compensation nodes in this case. The DC nodes, the control modes of converters and the converter loss constants must be defined in the matrices ***DC Bus data***, ***DC converter data*** and ***DC Branches data***. In the case of MVDC and HVDC networks, the matrix AM is also exploited for the construction of the M_topology matrix. After the sizing components phase, cable resistances are defined so the M_resistance matrix is set. Thus, the DC load flow algorithm is applied.

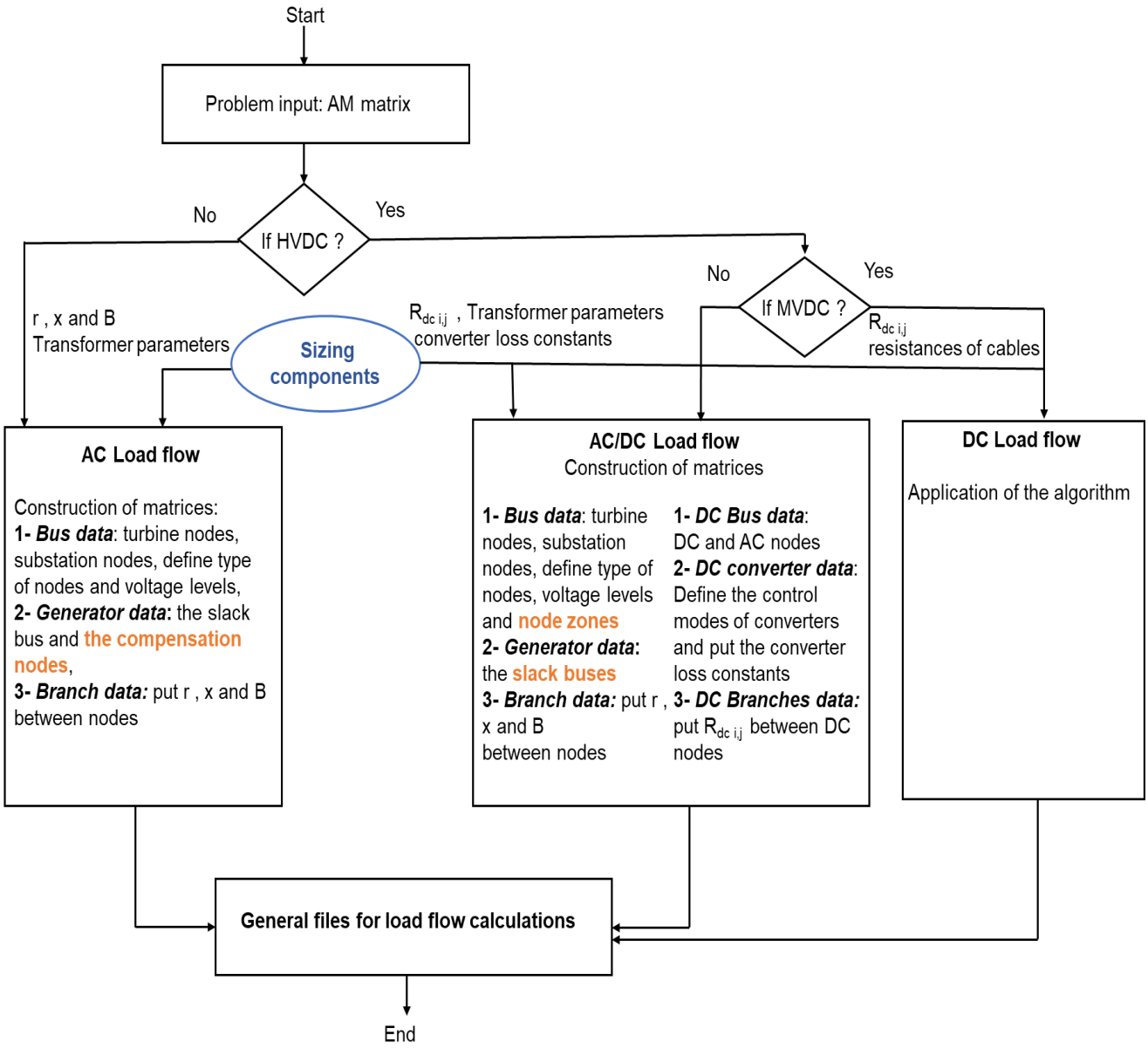

Figure 2-23 The program flowchart for a general load flow calculation

8 Conclusion

In this chapter, electrical and economical models of the different components of an offshore wind farm are presented, these models will be applied as variables for the optimization algorithm. In fact, electrical models are defined in order to evaluate the total losses of the electrical architecture under study. On the other hand, analytical models related to component costs are investigated from the literature in the aim to calculate the total investment cost CAPEX.

This chapter has highlighted the tools that are primordial for designing the general framework of optimization. The load flow calculations for different electrical architectures are shown with the mastery of the library MatAC/DC. A DC load flow algorithm is developed and validated. The state of the art presented allowed us to choose the Katic Jensen model for the wake effect calculation because it is the simplest and the fastest to implement and it gives a good accuracy in a first step/approach. The overall problem of optimization is presented with the definition of the inputs and the different variables to be optimized. The algorithms used to solve the optimization problem are GA and Prim, the two are complementary since the GA determines the turbine and the substations clusters and the prim's algorithm completes the connection between the turbines and the nearest substation as well as the connection between the DP and the nearest substation. Finally, the coupling of the load flow calculation taking into account wake effect with the optimization problem is exposed where the general load flow calculation case for any topology is shown by exploiting at each iteration the outputs of the optimization algorithm (the matrix of connection AM).

Bibliography

[1] J. Beerten, ‘’Modeling and control of DC grids‘’, ARENBERG Doctoral school, Dissertation presented in partial fulfillment of the requirements for the degree of Doctor in Engineering Science, 2013.

[2] O. Dahmani, ‘’Modélisation, optimisation et analyse de fiabilité de topologies électriques AC de parcs éoliens offshore’’, University of Nantes, PhD in Electrical engineering 2014.

[3] T.H. Hansen, “Offshore Wind Farm Layouts - Performance Comparison for a 540 MW Offshore Wind Farm,” M.S. Thesis, Energy and Environment, Norwegian University of Science and Technology (NTNU), Norway, 2009.

[4] J.L. LILIEN, “Transport et distribution de l’énergie électrique,” Practic work manual for the applied sciences course, University of Liège, 1999.

[5] T.V. CUTSEM, “Analyse et fonctionnement des systèmes d’énergie électrique,” course notes ELEC 0029, electronics and computer science, University of Liège, 1999.

[6] J. Beerten, S. Cole, R. Belmans ‘’A sequential AC/DC power flow algorithm for networks containing multi-terminal VSC HVDC systems’’, IEEE, General assembly of power and Energy Society, 2010.

[7] Eindwerk, Gilles daelemans, ‘’VSC HVDC in meshed networks’’, Master in electrical engineering, KU Leuven, 2008.

[8] Gnanarathna, Udana N, Gole, Aniruddha M.Chaudhary, K. Sanjay, ‘’Multilevel Modular Converter for VSC-HVDC Transmission Applications: Control and Operational Aspects’’, Published in: Proceedings of the 16th National Power Systems Conference, NPSC 2010.

[9] N. Serbia, ‘’Modular Multilevel Converters for HVDC power stations’’, Phd thesis in electrical engineering, Toulouse university, 2014.

[10] J. Beerten, S. Cole, R. Belmans ‘’Generalized steady state VSC MTDC model for sequential AC/DC power flow algorithms’’ , IEEE transactions on power systems, 2012.

[11] S. Lundberg ‘’Performance comparison of wind park configuration’’, rapport technique, Chalmers University of Technology, Göteborg, Sweden; 2003.

[12] DTI (Department of Trade and Industry), Study of the costs of offshore wind generation, URN number: 07/779, contractor ODE Limited, 2007.

[13] S. Bellone, D. Dale, ‘’Town of Babylon cost accounting e long island offshore wind project’’, report; 2006.

[14] M. Dicorato, G. Forte, M. Pisani, M. Trovato, ‘’Guidelines for assessment of investment cost for offshore wind generation’’, Renewable Energy 36, 2011.

[15] L. P. Lazaridis, ‘’Economic Comparison of HVAC and HVDC Solutions for Large Offshore Wind Farms under Special Consideration of Reliability’’, KTH electrical engineering, Master’s Thesis, Stockholm, 2005.

[16] B. Van Eeckhout, ‘’The economic value of VSC HVDC compared to HVAC for offshore wind farms’’, University of Leuven, Master’s Thesis, 2007-2008.

[17] C. Lancheros, ‘’Transmission systems for offshore wind farms: a technical, environmental and economical assesment’’, Hamburg University of Technology, Master, 2013.

[18] M. Sakamaki, K. Abe, Y. Inoue, S. Mashio, S. Kashiyama, O. Matsunaga, T. Igi, M. Watanabe, S. Asai and S. Katakai Y Murata, ‘’Development of High Voltage DC-XLPE Cable System’’, SEI TECHNICAL REVIEW, Number 76, april 2013.

[19] ENTSOE, ‘’Offshore transmission technology’’, November 2011.

[20] J. Lebled Liuch, ‘’Power transmission systems for offshore wind farms: Technical-economic analysis’’, ETSEIB, Phd thesis in electrical engineering, 2015.

[21] M. Zubiaga, G.Abad, J.A.Barrena, et al., “Evaluation and selection of AC transmission lay-outs for large offshore wind farms”, IEEE-13th European Conference on Power Electronics and Applications (EPE), Barcelona, Sep. 8-10, 2009.

[22] S. Fragoso Rodrigues, ‘’A Multi-Objective Optimization Framework for the Design of Offshore Wind Farms’’, Delft university of technology, PhD thesis in Electrical Engineering, 2016.

[23] D. Schoenmakers, ‘’Optimization of the coupled grid connection of offshore wind farms’’, Graduation project at Evelop Netherlands BV Technical University of Eindhoven, september 2008.

[24] H. Ergan, D.V.Hertem, and R. Belmans, ‘’Transmission system topology optimization for large-scale offshore wind integration,” Sustainable Energy, IEEE Transactions on, vol. 3, no. 4, pp. 908-917, october 2012.

[25] P.L. Lazaridis,’’Economic Comparison of HVAC and HVDC Solutions for Large Offshore Wind Farms under Special Consideration of Reliability”, M.S. Thesis, Electrical Engineering, Royal Institute of Technology, Sweden, 2005.

[26] G Stamatiou ‘’Techno-Economical Analysis of DC Collection Grid for Offshore Wind Parks’’, master of science thesis, september 2008.

[27] D. Zimmerman, E. Murillo-S´anchez, ‘’ Matpower manuel ‘’, Version 7.0, June 20, 2019.

[28] A. Pazderin, S, Yuferev , ‘’ Power flow calculation by combination of Newton-Raphson method and Newton's method in optimization’’, Published in: 2009 35th Annual Conference of IEEE Industrial Electronics, Porto, 2010.

[29] Jef Beerten, ‘’Mat AC/DC Manuel ‘’, University of Leuven (KU leuven), Dept. Electrical Engineering, Version 1.0, July 4, 2012.

[30] K Van den Bergh, E Delarue, W D'haeseleer, ‘’DC power flow in unit commitment models ‘’, TME Working Paper - Energy and Environment, 2014.

[31] K. Purchala, ‘’Modeling and Analysis of Techno-Economic Interactions in Meshed High Voltage Grids Exhibiting Congestion ‘’, Ph.D. Thesis, University of Leuven (KU Leuven), December 2005.

[32] K. Purchala, L. Meeus, D. Van Dommelen, and R. Belmans, ‘’Usefulness of DC Power Flow for Active Power Flow Analysis ‘’, IEEE Power Engineering Society General Meeting, 2005.

[33] G. Chang, S. Chu, and H. Wang, ‘’An improved backward/forward sweep load flow algorithm for radial distribution systems ‘’, Power Systems, IEEE Transactions, 2007.

[34] S. Frandsen et al., “Analytical modelling of wind speed deficit in large offshore wind farms,” Wind Energy, vol. 9, no. 1–2, pp. 39–53, 2006.

[35] L. G. C., “A simple stationary semi-analytical wake model,” Riso National Laboratory, Roskilde, Tech. Rep. Riso-R-1713(EN), 2009.

[36] F. F. Ainslie, “Calculating the flowfield in the wake of wind turbines,” Journal of Wind Engineering and Industrial Aerodynamics, 1988.

[37] G C. Larsen, H. Aa. Madsen, F. Bingol, J. Mann, “Dynamic wake meandering modeling,”, Riso National Laboratory, Roskilde, Tech. Rep. Riso-R- 1607(EN), 2007.

[38] B. Sanderse, “Aerodynamics of wind turbine wakes - literature review,” Energy Research Centre of the Netherlands (ECN), Petten, The Netherlands, Tech. Rep., 2009.

[39] M. Gil, L. Igualada, C. Corchero, O. Gomis-Bellmunt, A. Sumper,’’Hybrid AC-DC Offshore Wind Power Plant Topology: Optimal Design’, IEEE Transactions on Power Systems (Vol: 30, Issue:4), 2015

[40] P Hou, W Hu and Z Chen, ‘’Offshore wind farm layout design considering optimized power dispatch strategy’’, IEEE Transactions on Sustainable Energy, september 2016.

[41] F Seim, A R. Gravdahl , M S. Adaramola, ‘’Validation of kinematic wind turbine wake models in complex terrain using actual wind farm production data’’, Energy Journal, 2017.

[42] J Hong Jeon, G Hun Kim, I Keun Yu, ‘’Modelling and simulation of the wake effect in a wind farm ‘’ , Journal of International Council on Electrical Engineering, 5:1, 74-77, 2015.

[43] N. Jensen, “A note on wind generator interaction,” Riso National Laboratory, Roskilde, Denmark, Tech. Rep. Riso-M-2411, 1983.

[44] I. Katic, J. Hojstrup, and N. Jensen, “A simple model for cluster efficiency,” in EWEC’86. Proceedings.Vol. 1, 1986, pp. 407–410.

[45] J H Holland, ‘’Adaptation in natural and artificial systems‘’, Book, Ann Arbor, University of Michigan Press, 1975.

[46] D E Goldberg, ‘’Genetic algorithms in search, optimization and machine learning’’, Book, Addison Wesley, 1989.

Chapter 3. *Optimization of an offshore wind farm with wake effect consideration: analysis of a case study*

1 Introduction

The final chapter is dedicated for the validation of the proposed optimization framework for offshore wind farms design. First of all, the optimization algorithm is applied for a real wind farm Borssele I and II in the aim to validate its effectiveness. Then, the wake effect calculation will be integrated in the different offshore electrical networks (Full AC, mixed AC/HVDC and full DC). Indeed, a study will be conducted to show the wake effect impact on these different architectures' performances for different transmission distances. Thus, the percentage of wake effect influence on energy yield and losses will be relieved to exploit it afterwards in the further results. Finally, a technical-economic analysis of the three different connection architectures will be detailed in order to determine the most suitable electrical technology for a given set of offshore wind farm characteristics. The LCOE and the losses of each technology are investigated according to transmission distance. Therefore, the strengths and weaknesses of each topology are exposed. Then, the break-even distance for the proposed technologies will be discussed.

2 Optimization framework considering wake effects (case study: Borssele I and II)

The development of the optimization framework with its different steps and its objective function, the calculation of wake effect and its integration in the calculation of overall losses were introduced in the previous chapter. Now, the proposed framework is applied to a case study which is Borssele I and II wind farm. The goal is to demonstrate the effectiveness of the optimization tool for designing offshore wind farms.

2.1 Real topology

2.1.1 Wind farm data

The Borssele wind farm project is part of the Netherlands Energy Agreement plan developed by the Dutch government. The ultimate goal is to achieve 4.5GW of offshore wind capacity by 2024 through the Borssele, Holland Coast (South) and Holland Coast (North) offshore zones. In 2018, project follow-ups announced that an additional 7GW of offshore wind capacity could be achieved by 2030 [1].

Like mentioned in figure 3.1, the Borssele wind farm is divided into four sites with a total installed power equal to 1400 MW, therefore, there are two 700 MW offshore substations where each one connects two sites to the onshore grid. The offshore park is situated 0.5 km away from the Belgian economic zone with a total area of 344 km^2 [2].

In this thesis work, the first two zones of Borssele wind farm are considered for the case study.

The Borssele wind farm I and II data are the following:

- MVAC for the distribution network and HVAC for the transport network,
- 116 wind turbines where each one produces 6 MW, so the total installed power is 696 MW,
- Wind turbine clusters of 10 to 13 wind turbines per cluster,
- 66 kV voltage level for MVAC network and 220 kV voltage level for HVAC network,
- 2 cable cross-sections used to connect the distribution network: 630 mm^2 and 240 mm^2,
- The transmission distance is equal to 50 km.

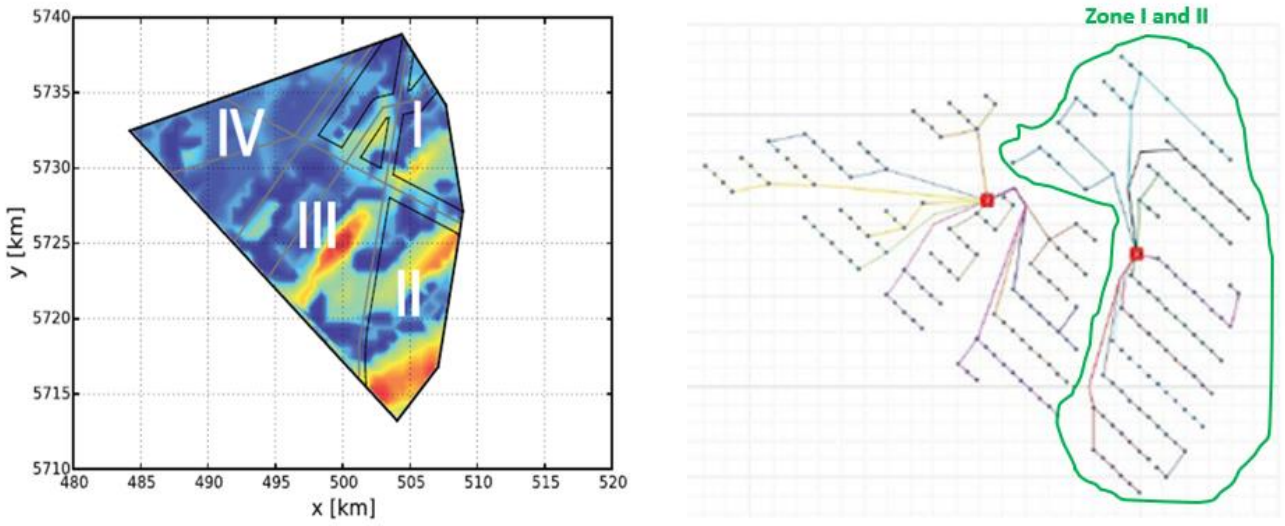

Figure 3-1 Borssele offshore wind farm

The wind resource data is presented by the wind rose that shows the probability of occurrence of wind speeds for each wind direction. The wind rose in the figure below shows wind conditions data of Borssele Park I and II at an altitude of 100 m. The wind rose presents wind data of 7 different wind speed classes and for 12 different directions.

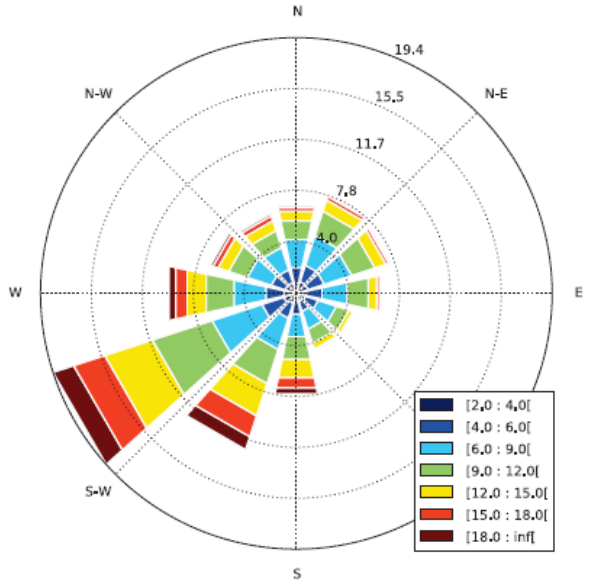

Figure 3-2 Borssele wind rose at height of 100 m [3]

The wind rose data are exploited to determine a matrix Prob_wind (26x12) that contains the probability occurrence of 26 points of wind speeds from 0 m/s to 25 m/s for 12 wind directions. The mean wind speed of the whole wind farm for all directions is 9.03 m/s. The wind rose measurements can be interpolated with the Weibull distribution function for the mean wind speed 9.03 m/s. The figure 3-3 validates the interpolation between the Weibull distribution and the wind rose data.

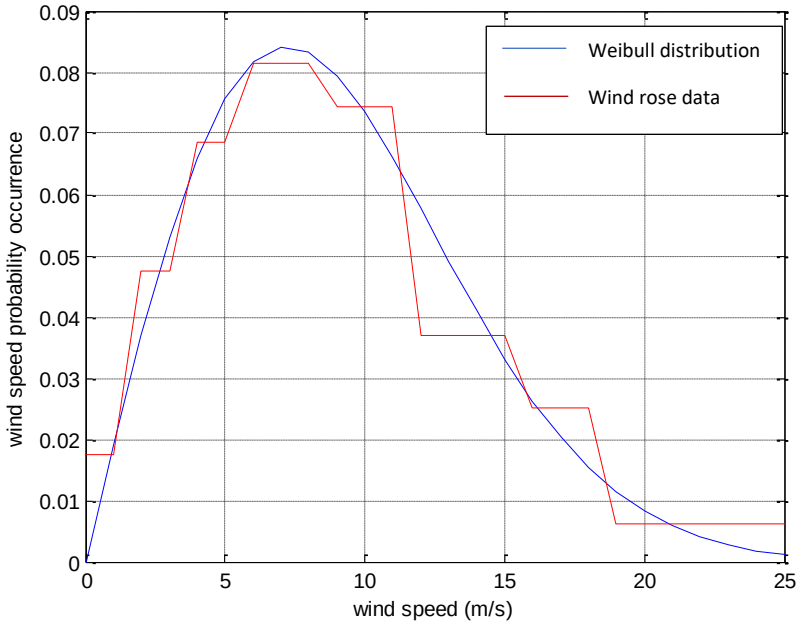

Figure 3-3 Wind speed probability occurrence, blue: Weibull distribution for 9.03 m/s, red: wind rose data curve

In this work, the turbines used for this study are General Electric Haliade with a rotor diameter (RD) of 150 m and a hub height of 100 m [4]. Each turbine is modelled by an active power generation curve as a function of wind speed. Besides, the thrust C_t changes in function of wind speeds. The typical production curve and the thrust curve of the Haliade wind turbine is shown in figure 3-4.

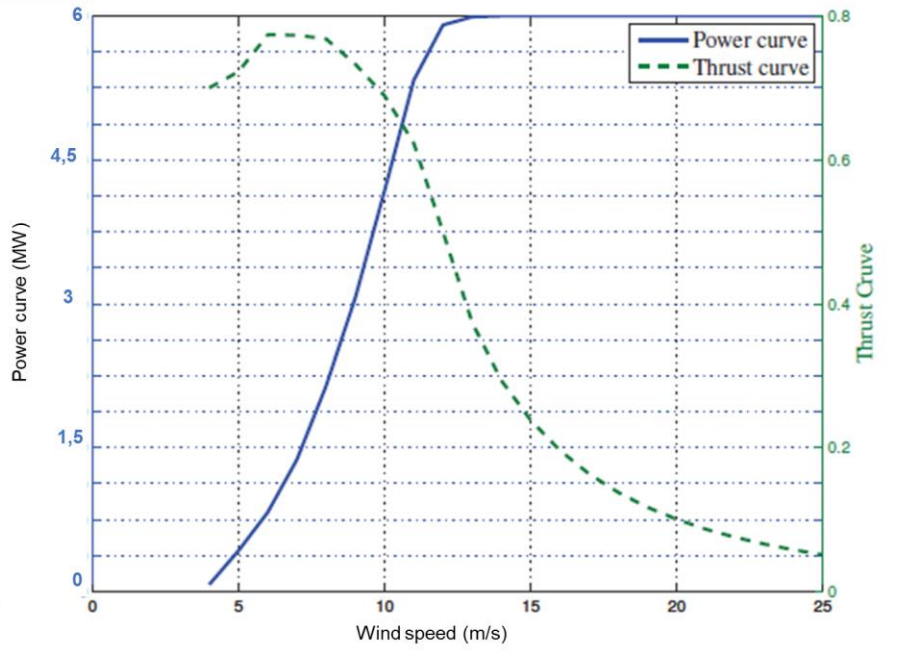

Figure 3-4 Power and thrust curves of the Haliade 6 MW wind turbine

2.1.2 Wake effect impact

This section is dedicated to study the wake effect impact on the real Borssele I and II topology. A comparison between park performances with and without wake effect calculation will be discussed. Then, the percentage of wake effect impact on the energy yield will be revealed.

2.1.2.1 Borssele I and II without wake effect

For the case study of this wind farm, the lifetime exploitation of the park is fixed to 20 years, the discount rate is fixed to 8% and the OPEX is set to 50 k€/MW [5]. The real Borssele park has a collection network with a voltage level 66 kV, this is made with 97 cables with a cross-section 240 mm^2 and 19 cables with a cross section 630 mm^2. The transmission network is ensured by three HVAC cables of 500 mm^2 cross section under a voltage 220 kV. Like presented in figure 3-5, the topology contains 10 feeders where the number of turbines per cluster varies between

Nmin=10 and Nmax=13. The length of MVAC cables is 128.08 km and the length of HVAC cables is 149.73 km.

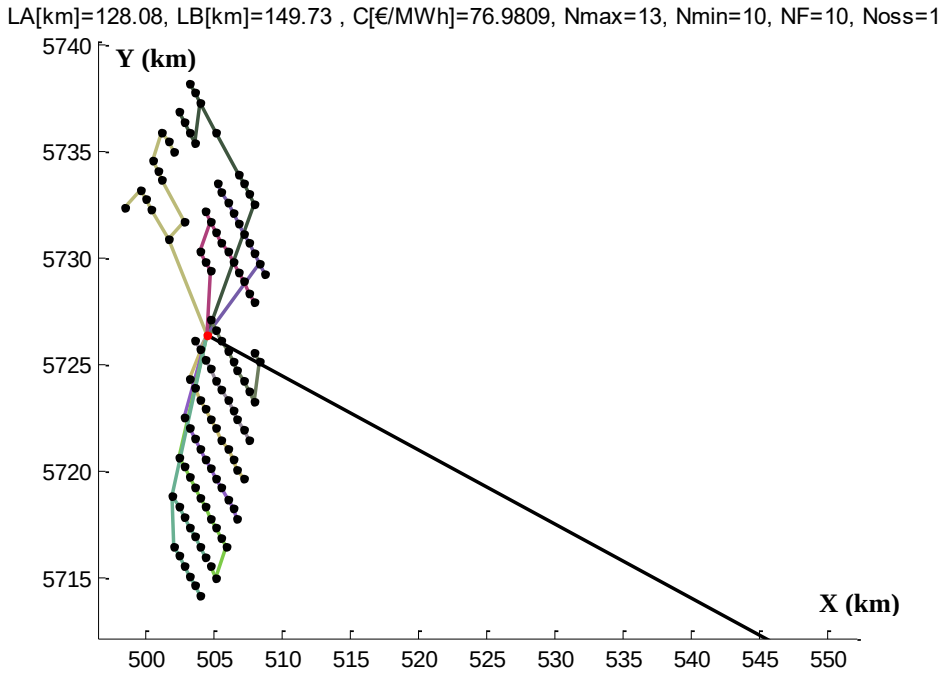

Figure 3-5 The real topology of Borssele I and II

The table 3-1 exposes the components cost for real Borssele I and II without wake effect calculation. The LCOE evaluated is equal to **76.98** €/MWh. The total investment cost (CAPEX) is assessed to **1807.21** M€, it includes the foundations and the turbines costs, the MVAC and HVAC switchgears cost, the AC offshore substation cost, the transformers cost and MVAC and HVAC cables costs.

Table 3-1 Components cost without wake effect for real Borssele I and II

	Components	Cost (Meuros)
	MV cables	207.64
	HV cables	197.39
	Transformers	9.34
	AC substation	66.57
	MV switchgears	0.67
	HV switchgears	0.92
	Compensation equipment	13.58
	Turbines	569.61
	Foundations	741.45
Total cost= CAPEX	**1807.21 M€**	
LCOE	**76.98 €/MWh**	

2.1.2.2 Borssele I and II with wake effect

For the case without the wake effect calculation (section 2.1.2.1), the annual energy produced AEP of the wind farm is obtained by the calculation of the mean power produced by one turbine and then multiplied by the total number of turbines. In fact, the mean power is obtained by the sum of 26 points calculated with the multiplication between the wind speed probability occurrence and their corresponding power outputs. For this part, the wake effect is considered in the calculation of the total losses so the AEP is calculated with the exploitation of the wind rose data, in other words, with wind speeds probability occurrence presented in matrix Prob_wind (26x12). Therefore, the power and the thrust curves in function of wind speeds are exploited to calculate the power produced by each turbine thanks to Katic Jensen model equations. Then, the AEP of the whole wind farm for 12 directions and 26 wind speeds is the sum of the different annual energy produced by each turbine. The complete calculation of the wake effect requires 12 iterations for each wind speed. Consequently, we need 12x26= 312 operations to obtain the complete calculation. This approach requires an important computational time.

Here, the wake effect calculation is applied to the same topology connection as section 2.1.2.1 (real topology) so many parameters remained the same such as the cables length, the number of clusters and the number of turbines per cluster. Therefore, almost all the costs are also the same, unless the cost of the compensation equipment that evolves from 13.58 M€ to 17.32 M€. This price increase is explained by the increase of the reactive power Q_{comp} with the integration of the wake effect. In other words, the wake effect modifies the power produced by each turbine so the total losses and the reactive power to compensate are also changed. Then, the CAPEX evaluated is **1810.96** M€ with a LCOE equal to **95.81** €/MWh. Further detailed performances comparison between the two cases (without and with wake effect) is presented in section 2.1.2.3.

Figure 3-6 exposes the wind speed attenuation for the direction 30° for all turbines for a fixed wind speed 14 m/s. In fact, the turbines that are marked with 100, catch the actual real wind speed (14 m/s) because there are no upstream turbines that can cause wake effect. If a turbine undergoes the wake effect (partial or total or both), the wind speed captured by this turbine decreases which allows the reduction of the power produced. The minimum wind speed noted in this case is 86.17% since the turbine is affected by an important wake effect caused by many upstream turbines.

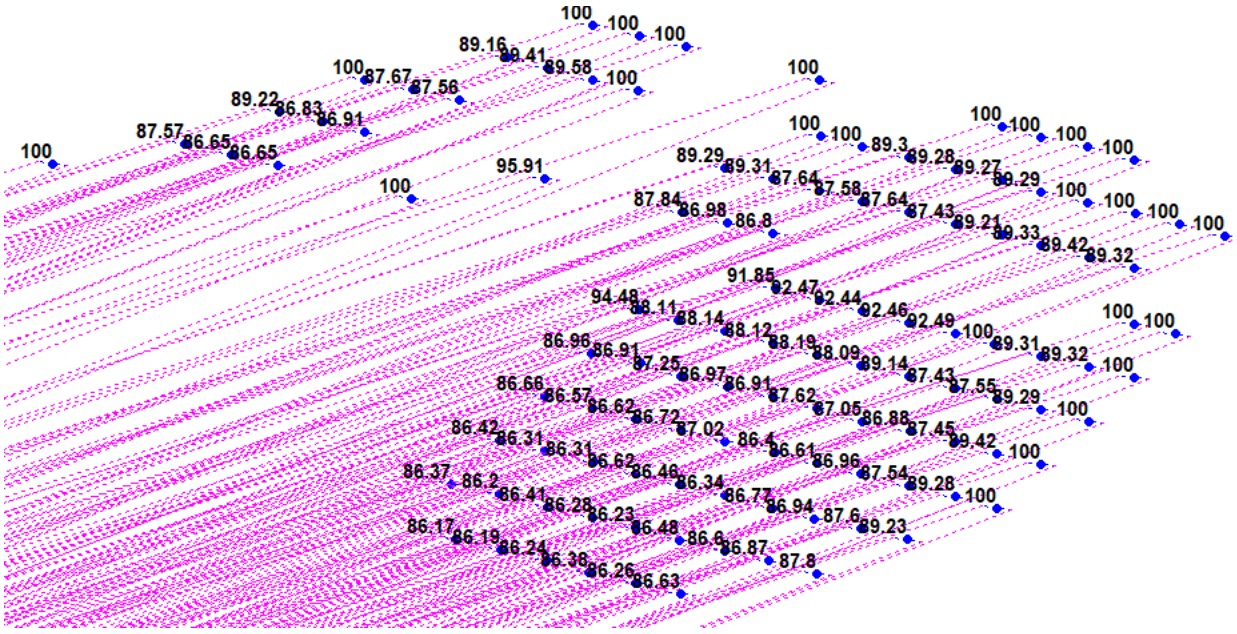

Figure 3-6 Wake effect visualization for the direction 30° for wind speed 14 m/s

Figures 3-7 and 3-8 present the wind attenuation for all turbines and 12 directions respectively for wind speeds 7 m/s and 14 m/s. The difference between these figures and figure 3-6 is that the wake effect is calculated for all the directions. The figures present a color grid that can be read as follows: horizontally we have 116 turbines and vertically we have 12 wind directions from 0 deg to 330 deg, the color variation for each turbine tells us about the wind attenuation, if the color changes to yellow to become white, the wind attenuation is at 100% (low wake effect), on the other hand, if the color becomes darker (red) the turbine picks up less wind speed (<80%).

In fact, for the direction 30°, the first 8 turbines are not impacted by the wake effect that's why they captured 100 % of the wind speed (white color) whereas the turbines number 9, 10 and 11 pick-ups less wind speed. With the wind speed 7 m/s, the wind attenuation varies between 54.15% (the minimum wind) and 100%, however, the wind variation interval is between 82.56% and 100% for the wind speed 14 m/s. This is explained by the fact that the turbine produces more power with 14 m/s than with 7 m/s (see power curve).

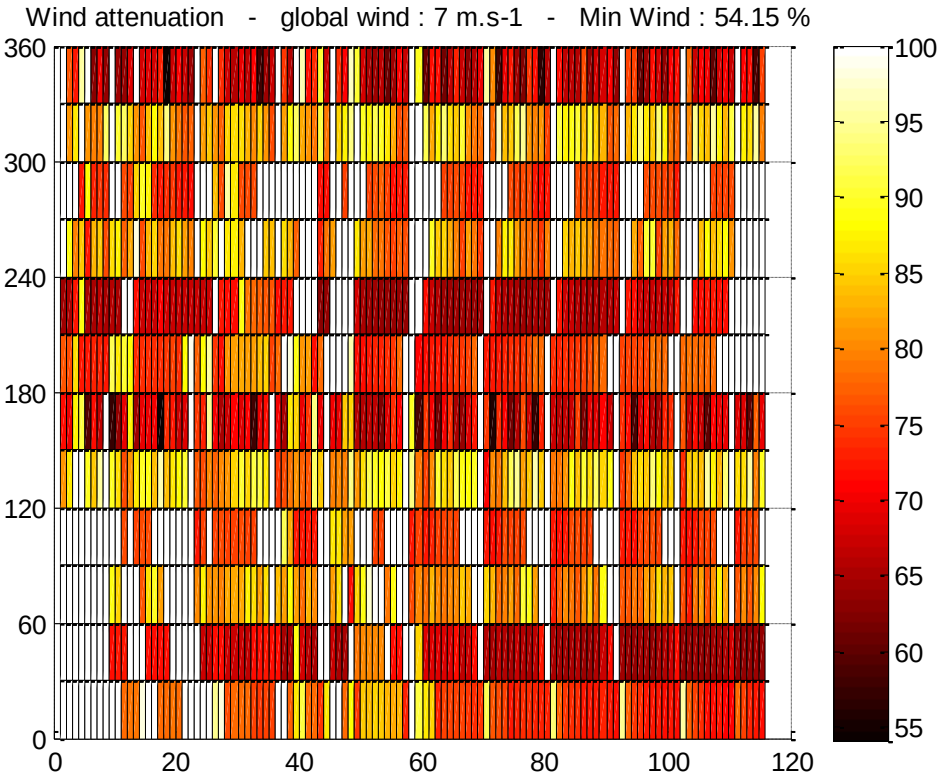

Figure 3-7 Wind attenuation for all turbines for all directions for wind speed 7 m/s

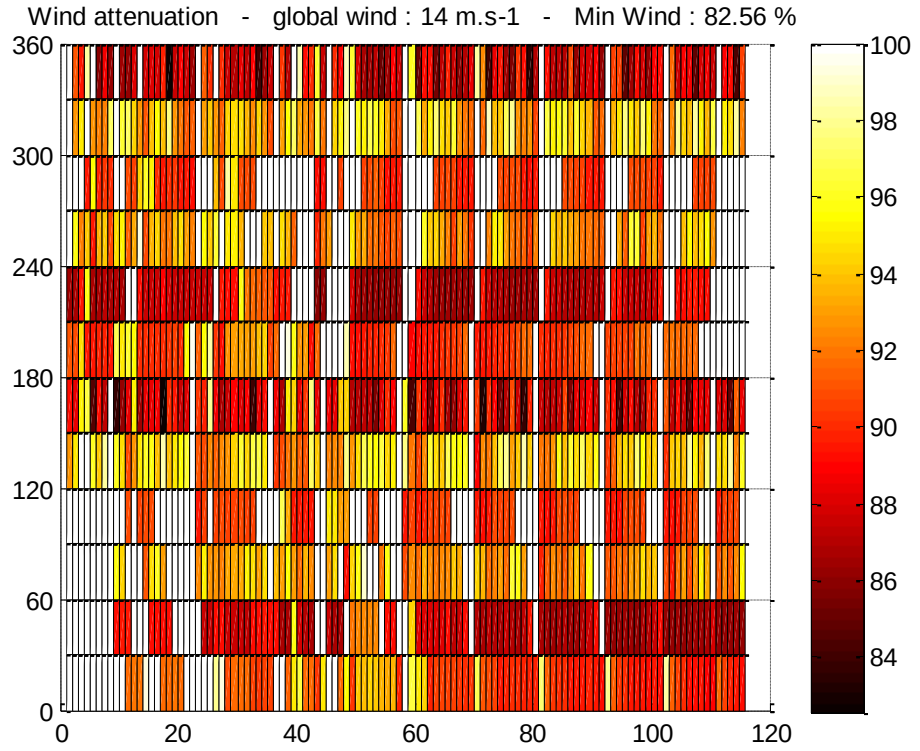

Figure 3-8 Wind attenuation for all turbines for all directions for wind speed 14 m/s

Figures 3-9 and 3-10 show the distribution of power attenuation for each wind turbine (116 turbines) according to all directions for two wind speeds 7 m/s and 14 m/s. Obviously, the power production for two wind speeds is different (more yellow color for figure 3-10), the minimum powers produced are 0 MW and 4.88 MW respectively for 7 m/s and 14 m/s. In fact, with a wind speed 14 m/s, the power of the first 11 turbines in the direction 0° can reach 5.98 MW (almost the nominal power 6 MW) but it is equal to 0.85 MW with a speed wind 7 m/s.

We have chosen to show just the results for two wind speeds 7 m/s and 14 m/s because for 7 m/s the turbine starts to produce a considerable power and for 14 m/s the turbine can reach almost its nominal power. These are two extreme examples to show the results variation.

From this graph, one can conclude that the four directions 30°, 150°, 210°, and 330° are the worst directions where the power is mostly lost (great wake effect) since several wind turbines don't really produce power (red black color). However, the directions 60°, 90°, 120°, 240°, 270° and 300° are the most favorable directions for power production.

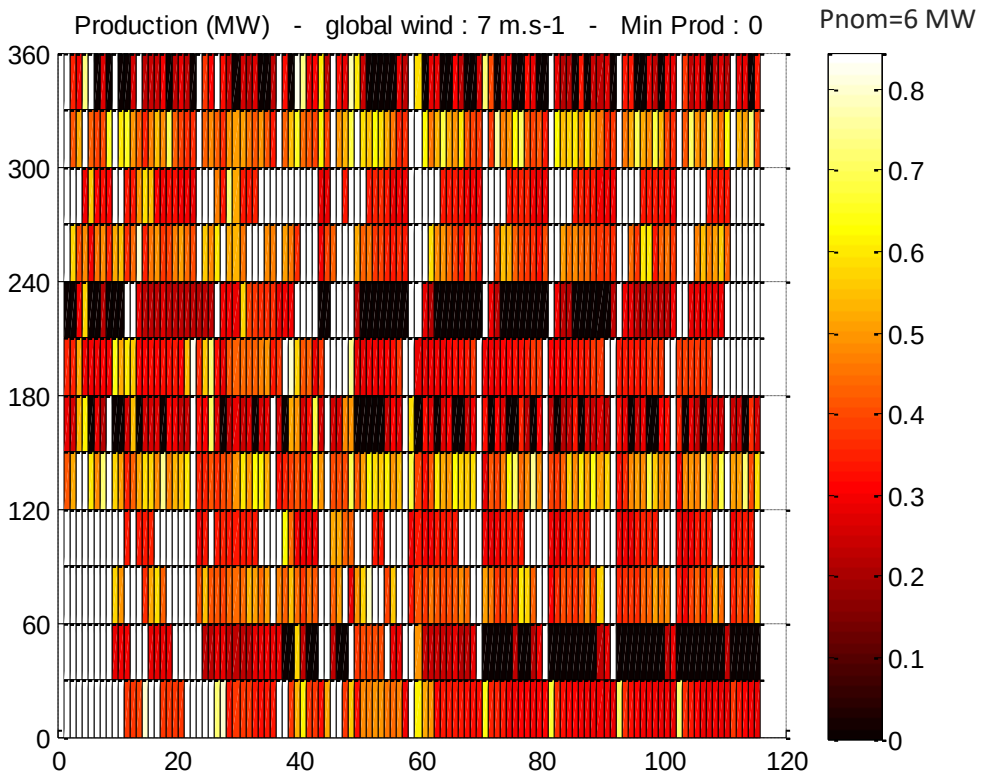

Figure 3-9 Power attenuation caused by wake effect for all turbines for all directions for wind speed 7 m/s

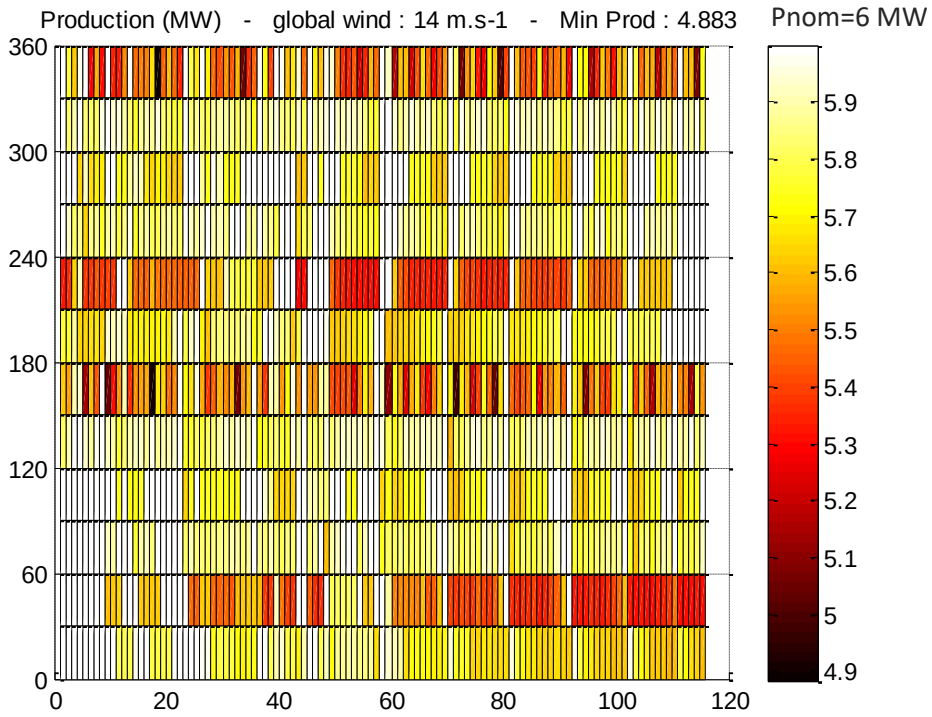

Figure 3-10 Power attenuation caused by wake effect for all turbines for all directions for wind speed 14 m/s

Figure 3-11 shows the mean power produced for one turbine for all directions and for different wind speeds 7 m/s and 14 m/s. Like mentioned before, with a wind speed 7 m/s the mean power per turbine cannot exceed 0.6 MW but can get close to the nominal power (5.98 MW) with a wind speed 14 m/s. This figure validates that the directions 60°, 90°, 120°, 240°, 270° and 300° are the best ones as long as the maximum power can be reached.

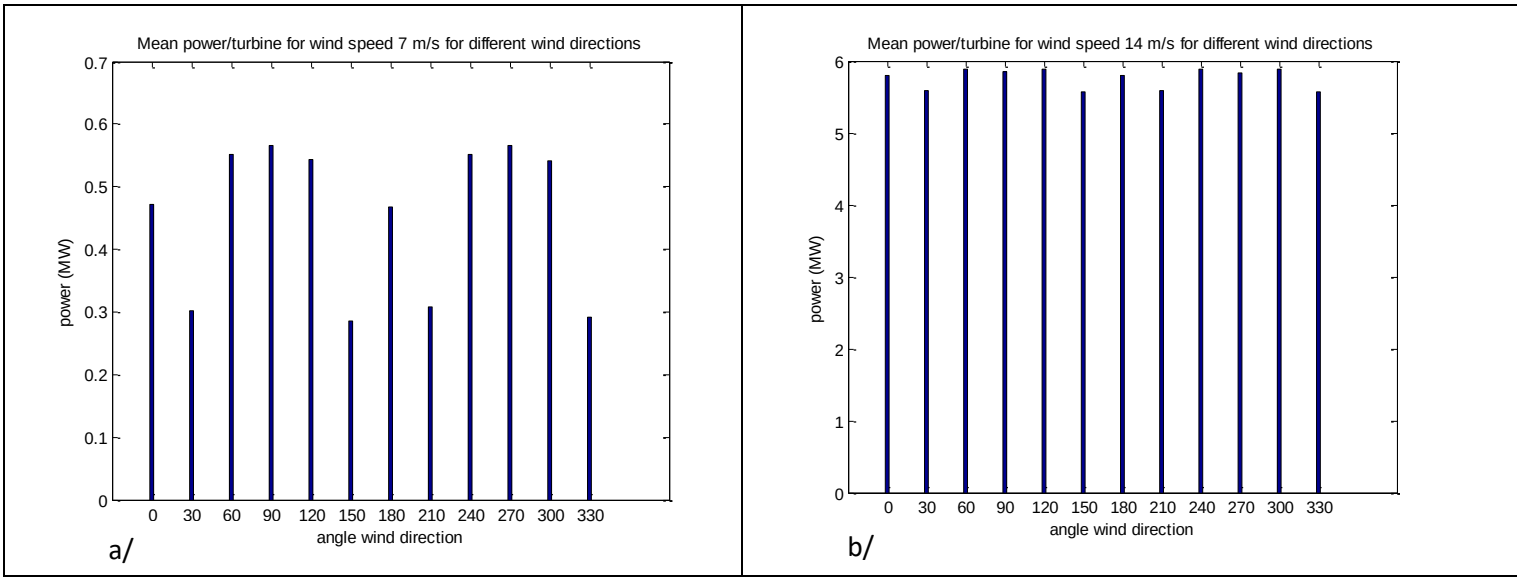

Figure 3-11 Mean power/ turbine for all directions, a/ wind speed 14 m/s, b/ wind speed 7 m/s

Figure 3-12 exposes the total efficiency for each turbine after wake effect calculation for all directions and all wind speeds, it represents the percentage value of the capacity factor for all turbines. This value tells us about the production capacity of each turbine, according to the figure, there are turbines that can produce more than others. This efficiency variation is due to the fact that the turbines are arranged in an irregular way and as a result there is a distance variation between turbines. In general, to reduce the wake effect, a minimum separation between two turbines of 3*RD (rotor diameter) must be respected [6]. Here, the minimum distance between the turbines is 0.53 km which is equal to 3.5*RD (RD= 150 m for Haliade wind turbine). The maximum capacity factor noted is 44.9 %, this value is explained by the fact that the corresponding wind turbine is placed in the middle of the wind park and it is much spaced from other neighbors so the wake effect impact is not very important. However, the lowest efficiency value is 36.2 % which is related to a turbine highly affected by the wake effect. The farm global capacity factor is equal to 39.5 %. By way of perspectives, the capacity factor for each turbine can be exploited to see which part of the park produces more power and therefore, it is preferable to make redundant paths between those turbines so the maximum of power will be exploited even when there is a failure (reliability study in perspectives part).

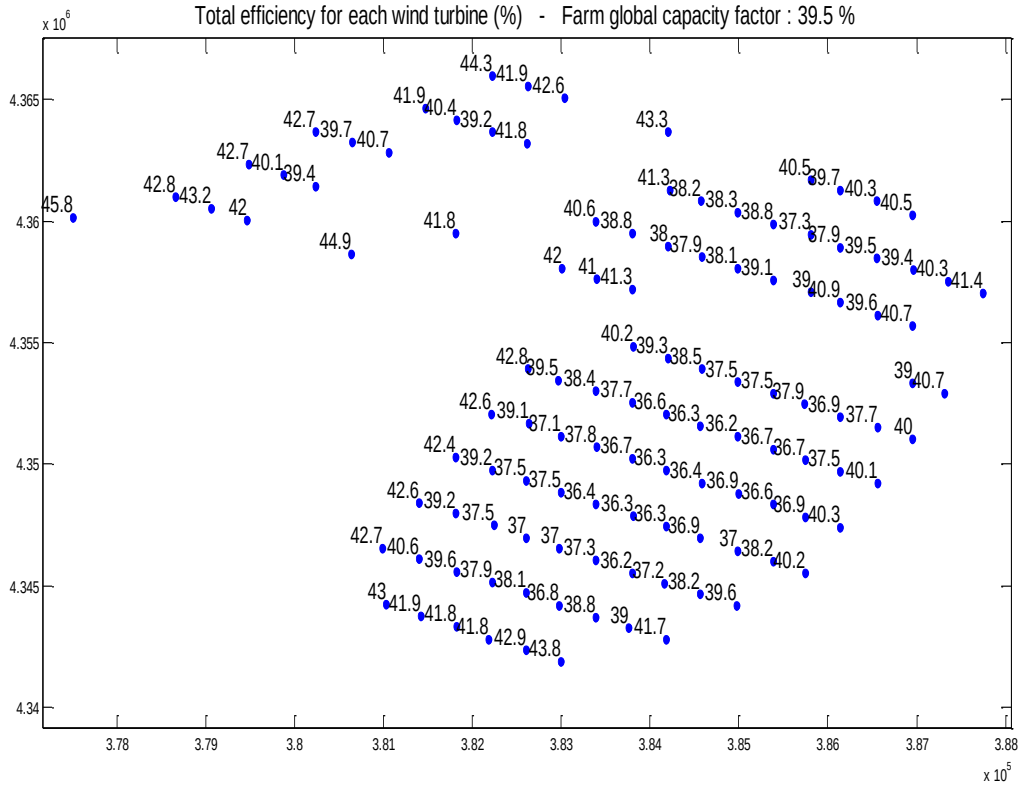

Figure 3-12 Total efficiency (%) for each wind turbine

2.1.2.3 Performances comparison between two cases (with and without wake effect)

For the same architecture (Borssele I and II connected in AC) and for the same transmission distance 50 km, the calculation results of the two cases with and without wake effect calculation are shown in table 3-2. It can be noticed that the percentage of wake effect for the energy yield AEP (annual energy produced) is significant and equals to **17.99** %. The losses are also impacted by the wake effect with a percentage **28.66** %. Consequently, the AED (annual energy delivered to the onshore grid), the capacity factor and the LCOE are modified.

Table 3-2 Parameters comparison between the two cases (with and without wake effect) for real Borssele topology

Parameters	Losses (MW)	AEP (MW)	AED (MW)	Capacity factor	LCOE (€/MWh)
Real topology without wake effect	10.64	335.20	324.56	0.46	76.98
Real topology with wake effect	13.69	274.90	261.21	0.395	95.81
Difference (%)	28.66 %	17.99 %	19.51 %	15.22 %	24.46 %

2.2 Optimized topology

In this part, the Borssele topology is taken under study for optimization in order to evaluate and validate the performance of the optimization approach presented, this algorithm studies only radial / star electrical connections with variable cross section cables (each cable has a cross section according to the apparent power that can flow into it). Meshed networks are not taken into consideration in this work.

For this purpose, the same simulation conditions are applied as for the real topology:

- N= 20 years,
- r=8%,
- OPEX= 50 k€/MW,
- Distance of transmission 50 km,

- 116 turbines each producing a nominal power 6 MW, hub high = 100 m and rotor diameter (RD) =150 m,
- MVAC network 66 kV, HVAC network 220 kV,
- Turbines positions are fixed (the same turbine positions as the real topology),
- Substations positions are variable and its number vary between 1 and 4.

The algorithm parameters are set as fellow:

- Maximum number of iterations =2500
- The crossing probability = 0.8, the selection probability = 0.9,
- the mutation probability = 0.01, replacement rate = 0.7
- The population size is fixed to 50 (generated randomly)

Figure 3-13 presents the electrical connection of the optimized Borssele topology without wake effect consideration. The optimal topology has only one offshore substation like the real topology. Its position is determined by the optimization algorithm which is almost the same as the real topology substation location. It is seen that the connection type between wind turbines found with the optimization algorithm is mainly the mixed radial / star electrical connection as opposed to the real topology which has only radial connections. From table 3-3, one can notice that these two electrical networks are similar in terms of MV and HV voltages levels (66 kV and 220 kV), the number of substations and the number and cross-sections of HV cables (3 parallel cables with a cross section 500 mm^2 and a total length 149.73 km). On the other hand, the two architectures are different in the connection topology of the MV collection network. In fact, for the optimized one, the number of feeders is 15 which is higher than the real topology that has only 10 feeders but it contains fewer turbines per clusters (from Nmin= 2 to Nmax= 9 turbines per cluster). When the number of feeders increases, the number max of turbines per cluster decreases so the power transported in the cable is also reduced and that's why only small cable cross-sections are needed. For the optimized topology, there are 116 cables with a cross section 240 mm^2 whereas the real topology is connected with 97 cables with a cross section 240 mm^2 and 19 cables with a cross section 630 mm^2. Since there are more feeders for the optimized topology so the length of MV cables is more important, 160.66 km compared to only 128.08 km for the real architecture. The obtained LCOE for the optimized topology is equal to **75.70** €/MWh which is less than the LCOE of the real topology (**76.98** €/MWh). In other words, the optimization algorithm is validated since it achieves a better LCOE than that of the real topology.

By exploiting figure 3-14, we can see that the algorithm converges to the final solution after about 500 generations. In the rest of the iterations, the best objective function varies very slightly. These small variations correspond to small improvements in the best individual in the population which do not significantly affect the LCOE.

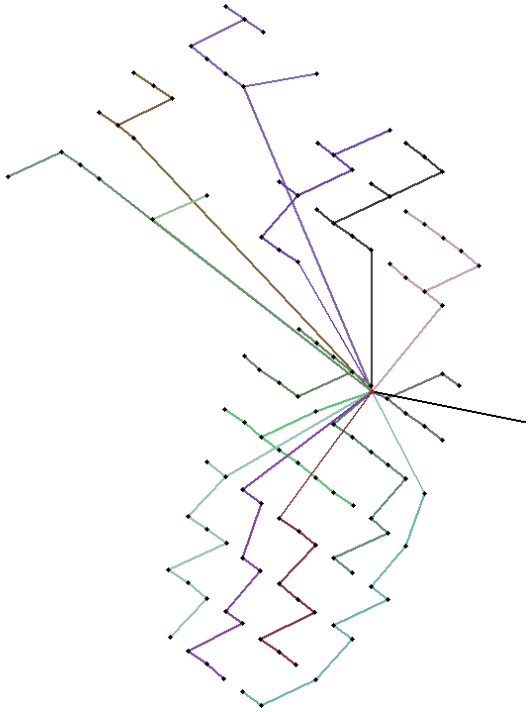

Figure 3-13 The optimized Borssele topology without wake losses calculation

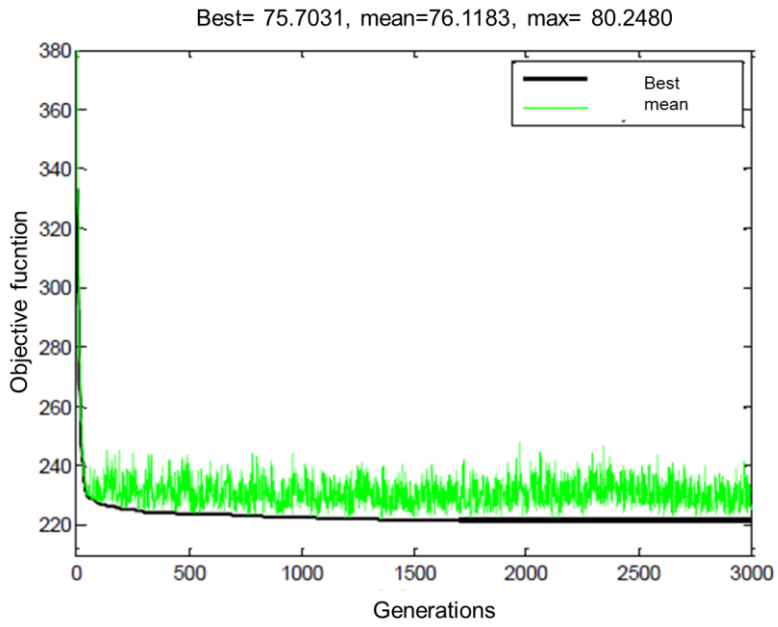

Figure 3-14 Evaluation of the objective function LCOE at each generation

Table 3-3 Comparison between real and optimized topologies for Borssele park

	Real topology		Optimized Topology
MV voltage level	66 kV		66 kV
HV voltage level	220 kV		220 kV
Number of feeders	10		15
Nmax (max turbine/ feeder)	13		9
Nmin (min turbine/ feeder)	10		2
Number of substations	1		1
Number of MV cables	97	19	116
Cross sections of MV cables	240 mm^2	630 mm^2	240 mm^2
Length of MV cables	128.08 km		160.66 km
Number of HV cables	3		3
Cross sections of HV cables	500 mm^2		500 mm^2
Length of HV cables	149.73 km		149.74 km
LCOE	**76.98 €/MWh**		**75.70 €/MWh**

2.2.1 Comparison between the real and the optimized topologies

Figure 3-15 exposes components cost for real and optimized topologies. The two topologies have almost the same costs, the only difference is related to the MV cables cost and MV switchgears cost. Indeed, we have 207.64 M€ of MV cables cost for the real topology compared to only 171.29 M€ for the optimized topology. This is due to the fact that the optimized topology has fewer turbines per clusters so the total power per cluster is smaller and can be transmitted with only one cross section cable 240 mm^2 (the optimized topology has only 116 MV cables with a cross section 240 mm^2). Otherwise, the 630 mm^2 cross section cables used for the real topology connection increase the total price of MV cables. Furthermore, since there are more feeders for the optimal topology so there are more MV switchgears and that's why the price increases by 0.33 M€. Besides, it's noted that the reactive compensation equipment cost is almost identical for the two topologies. This is due to the fact that the compensation is influenced by the lengths and cross-sections of MV and HV cables and the sizing of transformers which are the same for both topologies except the MV network connection.

The total investment cost CAPEX of the optimized topology is **1771.20** M€ compared to **1807.21** M€ for the real topology. One can conclude, that just with a different connection of the MV collection network, we can obtain a better architecture in terms of the total investment cost.

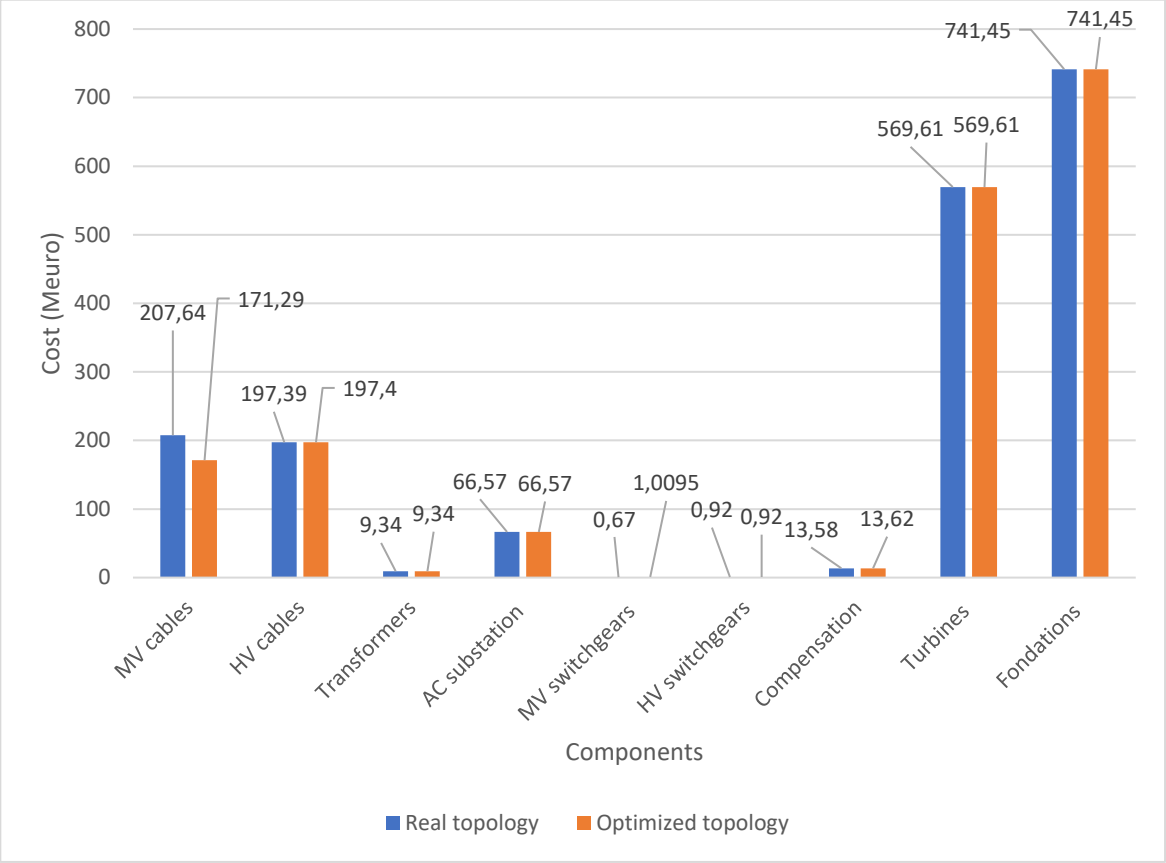

Figure 3-15 Components cost for both real and optimized topologies

The table below summarizes the parameters comparison between the real and the optimized topologies. Actually, there is no significant difference between both topologies. Although there is a difference in losses of 0.04 MW between the real and the optimized topologies, the difference in the CAPEX value leads to obtain a better LCOE value for the optimized one. Therefore, one can conclude that the optimization algorithm converges and gives optimal results.

Table 3-4 Parameters comparison between Borssele real and optimized topologies

Parameters	Losses (MW)	AEP (MW)	AED (MW)	Capacity factor	LCOE (€/MWh)
Borssele real topology	10.64	335.20	324.56	0.46	76.98
Borssele optimized topology	10.68	335.20	324.52	0.46	75.70
Difference (%)	0.37 %	0 %	0.012 %	0 %	1.66 %

2.2.2 Wake effect impact

Here, wake effect calculation is applied for the optimized topology, the table 3-5 shows the difference parameters values between the two cases: the optimized topology with and without wake effect integration. Like seen before in section 2.1.2.3, the wake effect consideration can change only the compensation equipment cost since Q_{comp} changes. So, for the same transmission distance (50 km) and the same technology connection (full AC), the AEP value does not change from section 2.1.2.3 since this parameter is only affected by the arrangement of the turbines and is not affected by the connection between them. Therefore, the percentage between with and without wake effect remains the same **17.99**%. Besides, the percentage difference in losses is **28.18**% compared to **28.66** % for the case of Borssele real topology with and without wake effect. One can conclude that for a fixed transmission distance and for the same technology architecture (full AC), the percentages of losses and AEP with and without wake effect are almost the same.

Table 3-5 Parameters comparison between the two cases (with and without wake effect) for Borssele optimized topology

Parameters	Losses (MW)	AEP (MW)	AED (MW)	Capacity factor	LCOE (€/MWh)
Optimized topology without wake effect	10.68	335.20	324.52	0.46	75.70
Optimized topology with wake effect	13.69	274.90	261.21	0.395	94.21
Difference (%)	28.18 %	17.99 %	19.50 %	15.22 %	24.45 %

3 The distance impact on the optimization of the different architectures of offshore wind farms

In this section, the optimization framework is performed on the wind farm Borssele I and II for the three different architectures: full AC, mixed AC/HVDC and full DC. The ultimate goal is to compare the topologies according to the transmission distance in order to have a decision support framework for offshore wind farm electrical networks. Indeed, the losses and the LCOE will be studied for each case to determine the break-even distance for different technologies. The optimization will take into account the wake effect losses. To do so, in section 3.1, the wake effect impact will be studied for different topologies and different transmission distances. The influence on the different parameters Losses, AEP and AED is discussed. The purpose of this

study is to find out whether the wake effect can be approximated by a simple coefficient or whether it is necessary to do the full calculation to take it into account. As an indication, the optimization of Borssele park (4000 iterations) with the complete calculation of wake effect takes 72 hours whereas the simple calculation taking just a percentage to integrate the wake effect takes only 3 hours.

3.1 Wake effect impact on different architectures performances for different transmission distances

The objective of this part is to show the influence of the wake effect integration on different electrical architectures according to different transmission distances on Borssele real topology.

3.1.1 Full AC topology

As set out in the table 3-6, the AEP value is not influenced by the transmission distance or the connection technology. Indeed, it is the same in tables 3-6, 3-7 and 3-8 with a percentage of 17.99 %. However, the losses value gets influenced and changed from 28.66 % for 50 km to 23.14 % for 200 km. The change for every additional 50 km varies between +2.3 % and +1.5%. The mean percentage between these four distances is about 25.7 %. So, for further studies, we fixed a value of **26 %** for the wake effect impact related to losses for **full AC** topology at any transmission distance. The change of AED value is less significant and varies between 19.51 % for 50 km and 22.41 % for 200 km (between +1.13 % and +0.86 % for every additional 50 km).

Table 3-6 Wake effect impact for full AC architecture according to transmission distance

	Full AC		
	Parameters without wake effect (MW)	Parameters with wake effect (MW)	Difference (%)
50 km	Losses = 10.64 AEP = 335.20 AED = 324.56	Losses = 13.69 AEP = 274.90 AED = 261.21	Diff losses 28.66 % Diff AEP 17.99 % Diff AED 19.51 %
100 km	Losses = 18.93 AEP = 335.20 AED = 316.27	Losses = 23.92 AEP = 274.90 AED = 250.98	Diff losses 26.36 % Diff AEP 17.99 % Diff AED 20.64 %
150 km	Losses = 25.85 AEP = 335.20 AED = 309.34	Losses = 32.22 AEP = 274.90 AED = 242.67	Diff losses 24.64 % Diff AEP 17.99 % Diff AED 21.55 %
200 km	Losses = 32.54 AEP = 335.20 AED = 302.66	Losses = 40.07 AEP = 274.90 AED = 234.83	Diff losses 23.14 % Diff AEP 17.99 % Diff AED 22.41 %

3.1.2 Mixed AC/DC topology

The following table exposes the wake effect impact for AC/HVDC topology for different distances. In fact, the overall losses are divided into MVAC losses, HVDC losses and converter losses. Both MVAC losses and converter losses don't change according distances so their percentages are respectively 30.60 % and 2.45 %, however, the HVDC losses evolve with transmission distances and the percentage varies between 30.55 % for 50 km and 30.84 % for 200 km. The HVDC losses variation leads to a total variation in overall losses with a percentage equal to 5.19 % for 50 km and 6.92 % for 200 km. The little variation of converter losses for both cases with and without wake effect is due to the fact that most of the converter losses come from constant losses (independent of the current) so the current variation caused by the wake effect does not have much impact on converter losses **Erreur ! Source du renvoi introuvable.**. Thereafter, the fixed percentage related to **AC/HVDC** topology for total losses is **6 %**. The AED varies between 19.92 % for 50 km and 20.26 % for 200 km.

Table 3-7 Wake effect impact for AC/HVDC architecture according to transmission distance

	Mixed AC/ HVDC		
	Parameters without wake effect (MW)	Parameters with wake effect (MW)	Difference (%)
50 km	Losses = 25.80 Losses MVAC= 1.83 Losses HVDC = 0.72 Converters losses =23.25 AEP = 335.20 AED = 309.40	Losses = 27.14 Losses MVAC= 2.39 Losses HVDC = 0.94 Converters losses= 23.81 AEP = 274.90 AED = 247.76	Diff losses 5.19 % Diff losses MVAC 30.60 % Diff losses HVDC 30.55 % Diff conv losses 2.45% Diff AEP 17.99 % Diff AED 19.92 %
100 km	Losses = 26.55 Losses MVAC= 1.83 Losses HVDC = 1.47 Converters losses = 23.25 AEP = 335.20 AED = 308.65	Losses = 28.13 Losses MVAC= 2.39 Losses HVDC = 1.93 Converters losses = 23.81 AEP = 274.90 AED = 246.77	Diff losses 5.84 % Diff losses MVAC 30.60 % Diff losses HVDC 31.29 % Diff conv losses 2.45% Diff AEP 17.99 % Diff AED 20.04 %
150 km	Losses = 27.22 Losses MVAC= 1.83 Losses HVDC = 2.14 Converters losses = 23.25 AEP = 335.20 AED =307.98	Losses = 29 Losses MVAC= 2.39 Losses HVDC = 2.80 Converters losses = 23.81 AEP = 274.90 AED = 245.90	Diff losses 6.43 % Diff losses MVAC 30.60 % Diff losses HVDC 30.84 % Diff conv losses 2.45% Diff AEP 17.99 % Diff AED 20.15 %
200 km	Losses = 27.89 Losses MVAC= 1.83 Losses HVDC = 2.81 Converters losses = 23.25 AEP = 335.20 AED =307.31	Losses = 29.86 Losses MVAC= 2.39 Losses HVDC = 3.66 Converters losses = 23.81 AEP = 274.90 AED = 245.04	Diff losses 6.92 % Diff losses MVAC 30.66 % Diff losses HVDC 30.24 % Diff conv losses 2.45% Diff AEP 17.99 % Diff AED 20.26 %

3.1.3 Full DC topology

For full DC topology, the DC/DC converter upgraded to offshore substation is composed of an inverter DC/AC and a rectifier AC/DC. Thus, the losses are the sum of the losses in the two converters where each losses part is calculated by the quadratic equation. Therefore, according to table 3-8, converter losses are the most important losses. Its percentage is equal to 2.24 % and it does not vary according to distance (like mentioned in section 3.1.2). The total losses percentage variation is between 3.04 % for 50 km and 4.72 % for 200 km. Thus, the total losses percentage of wake effect impact for **full DC** topology is fixed to **4 %**. The AED variation is between 20.48 % for 50 km and 20.88 % for 200 km.

Table 3-8 Wake effect impact for full DC architecture according to transmission distance

	Full DC		
	Parameters without wake effect (MW)	Parameters with wake effect (MW)	Difference (%)
50 km	Losses = 35.56 Losses MVDC= 0.44 Losses HVDC = 0.78 Converters losses = 34.34 AEP = 335.20 AED = 299.64	Losses = 36.64 Losses MVDC= 0.59 Losses HVDC = 1.03 Converters losses = 35.02 AEP = 274.90 AED = 238.26	Diff losses 3.04 % Diff losses MVDC 34 % Diff losses HVDC 32 % Diff conv losses 2.24 % Diff AEP 17.99 % Diff AED 20.48 %
100 km	Losses = 36.38 Losses MVDC= 0.44 Losses HVDC = 1.60 Converters losses = 34.34 AEP = 335.20 AED = 298.82	Losses = 37.71 Losses MVDC= 0.59 Losses HVDC = 2.1 Converters losses = 35.02 AEP = 274.90 AED = 237.19	Diff losses 3.65 % Diff losses MVDC 34 % Diff losses HVDC 31.25% Diff conv losses 2.24 % Diff AEP 17.99 % Diff AED 20.62 %
150 km	Losses = 37.12 Losses MVDC= 0.44 Losses HVDC = 2.34 Converters losses = 34.34 AEP = 335.20 AED =298.08	Losses = 38.68 Losses MVDC= 0.59 Losses HVDC = 3.07 Converters losses = 35.02 AEP = 274.90 AED = 236.22	Diff losses 4.20 % Diff losses MVDC 34 % Diff losses HVDC 31.19 % Diff conv losses 2.24 % Diff AEP 17.99 % Diff AED 20.75 %
200 km	Losses = 37.87 Losses MVDC= 0.44 Losses HVDC = 3.09 Converters losses = 34.34 AEP = 335.20 AED = 297.33	Losses = 39.66 Losses MVDC= 0.59 Losses HVDC = 4.05 Converters losses = 35.02 AEP = 274.90 AED = 235.24	Diff losses 4.72 % Diff losses MVDC 34 % Diff losses HVDC Diff conv losses 2.24 % Diff AEP 17.99 % Diff AED 20.88 %

After the wake effect impact study for different electrical topologies, one can conclude that mixed AC/HVDC and full DC architectures are less impacted by the wake effect calculation than the full AC electrical network. The impact of the wake effect for different transmission distance does

not change too much. So, in order to simplify calculations and to reduce the simulation time, these assumptions are set:

- 18 % as a percentage for AEP with and without wake effect,
- 26 % as a percentage for total losses for full AC topology,
- 6 % as a percentage for total losses for mixed AC/HVDC topology,
- 4 % as a percentage for total losses for full DC topology,
- 20 % as a percentage for AED, (this value is validated by the literature [5] [7] [9]).

These fixed percentages of wake effect impact are integrated in the optimization algorithm in the aim to avoid the important computation time for the complete case of wake effect integration.

3.2 Comparison of different architectures for different distances

In the present section, the proposed optimization design framework is applied for different electrical architectures. Once the connection technology is fixed, the algorithm proposes an electrical connection for each iteration. So, the electrical assessment is done. Accordingly, the economic models shown in chapter 2 are used to evaluate the CAPEX of each topology. Furthermore, the electrical models are integrated to MatAC/DC in order to compute the load flow. Then, the losses and the LCOE are obtained. These two parameters present the basis for comparison between the different topologies. The objective of this section is to highlight the competitiveness of the architecture concepts according to transmission distance.

The simulations are done with MATLAB R2014a, 64-bit DELL PC with Intel ® Core TM i7-6700 CPU @ 3.40 GHz and RAM 8 Giga-byte. One simulation for one topology lasts at least 2 hours without taking into account the calculation of the wake effect (it depends on the number of iterations and the size of the park). The simulation conditions are the same as shown in section 2.2.2, but here the transmission distance is variable.

The optimization algorithm is applied for four different distances (50km, 100km, 150km and 200 km). Thus, the optimized topologies with different technologies connection are shown for each distance, the aim here is to compare the electrical characteristics and to determine the distance impact on different connection technologies.

Tables 3-9 and 3-10 present respectively the detailed obtained parameters after optimization and the wind farm layouts for different electrical topologies for each transmission distance.

In fact, for all distances, the topologies full AC and mixed AC/DC have either 15 or 16 feeders where the maximum and minimum number of turbines per group are respectively 9 and 2. However, for full DC topologies the number of feeders is fixed to 12 which leads to have more turbines per group (Nmax= 13 turbines/group). The minimum number of turbines per group is remaining the same (Nmin=2). For all topologies and all distances, the collection network is connected with 116 MV cables with a cross section 240 mm^2 because the optimization algorithm is generated under the condition of having connections with variable cable cross-sections. Here, the HVAC transmission network is ensured by three parallel HVAC cables with a cross section 500 mm^2 whereas the HVDC transport is made with one bipolar HVDC cable with a cross section 630 mm^2. From there, we can say that the three HVAC cables in parallel can cost more than one HVDC cable especially when the transmission distance increases. All the optimized topologies have one single substation but its position barely changes from one topology to another, that's why we notice a little change related to the length of MV cables for each transmission distance.

For 50 km, the length of HVAC cables is about 150 km (3 x transmission distance 50 km), on the other hand, the length of the HVDC cable is 50 km since there is only one cable for the transport. For a distance 100 km, the MV and HV cables used for the connection of different topologies are the same as the cables used for 50 km. The only thing that changed is obviously the total length of HV cables since the transmission distance is doubled. For important distances like150 km and 200 km, the total HVAC cables length noted are respectively 461.01 km and 610.22 km compared to only 155 km and 204 km for HVDC cables length for both AC/HVDC and full DC architectures. These differences in length have an impact after on the total cost of the transmission architecture.

From figures shown in table 3-10, all the proposed connection layouts present no cable crossings in the MV collection network, i.e. between the wind turbines. However, there are crossings between the substation and wind turbines as well as between MV and HV cables since these connections are ensured by the Prim algorithm which is based on the connection with the shortest path concept. The developed optimization algorithm does not take into account the elimination of these intersections. Furthermore, we notice that the connection type is mainly the mixed radial/star which is efficient in the case of several turbines per cluster.

Table 3-9 Detailed parameters results for the three topologies for different distances

	50 km			**100 km**			**150 km**			**200 km**		
	Full AC	AC/HVDC	Full DC	Full AC	AC/HVDC	Full DC	Full AC	AC/HVDC	Full DC	Full AC	AC/HVDC	Full DC
MV voltage level (kV)	66	66	+/-80	66	66	+/-80	66	66	+/-80	66	66	+/-80
HV voltage level (kV)	220	+/-320	+/-320	220	+/-320	+/-320	220	+/-320	+/-320	220	+/-320	+/-320
Number of feeders	15	16	12	16	15	12	15	16	12	16	16	12
Nmax	9	9	13	9	9	13	9	9	13	9	9	13
Nmin	2	2	2	2	2	2	2	2	2	2	2	2
Number of substations	1 offshore substation											
Number of MV cables	116											
Cross sections of MV cables (mm^2)	240											
Length of MV cables (km)	160.66	161.54	140.41	159.57	157.65	144.62	158.53	160.37	136	161.56	161.72	140.24
Number of HV cables	3	1 bipolar	1 bipolar	3	1 bipolar	1 bipolar	3	1 bipolar	1 bipolar	3	1 bipolar	1 bipolar
Cross sections of HV cables (mm^2)	500	630	630	500	630	630	500	630	630	500	630	630
Length of HV cables (km)	149.74	50.46	50.73	313.88	104.95	105.54	461.01	155.73	155.26	610.22	204.85	204.38

Table 3-10 The three topologies (full AC, Mixed AC/DC and full DC) for different distances

50 km	Figures without zoom **1/ Full AC** 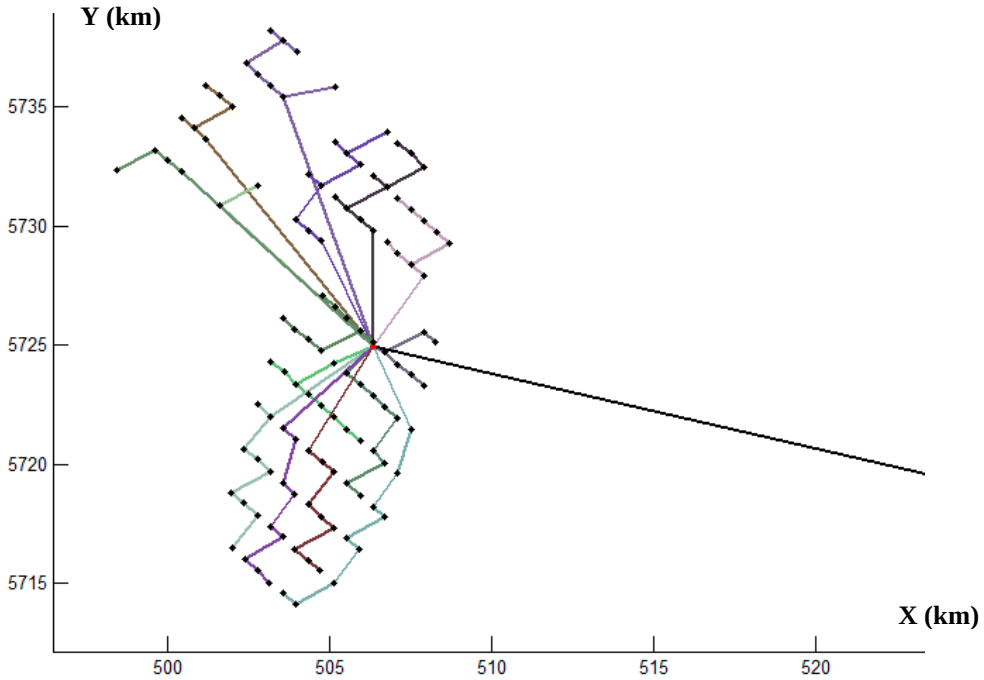	Figures with zoom **1/ Full AC** 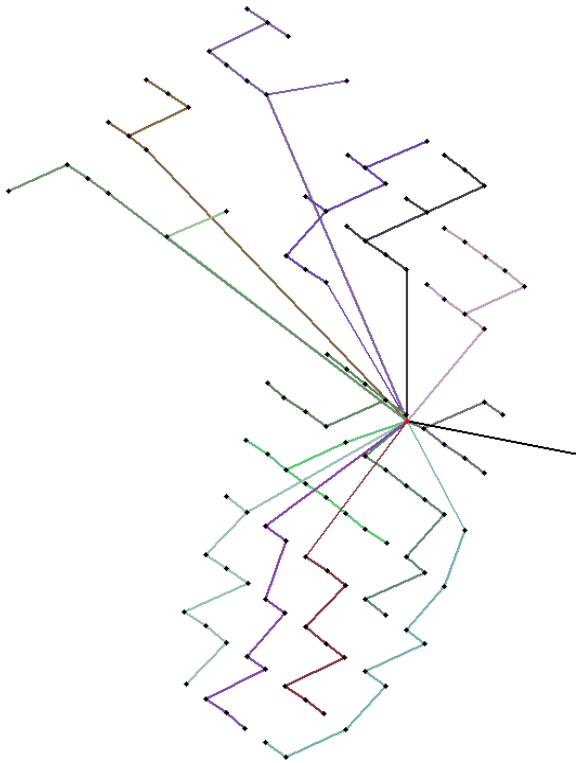

2/ AC/HVDC

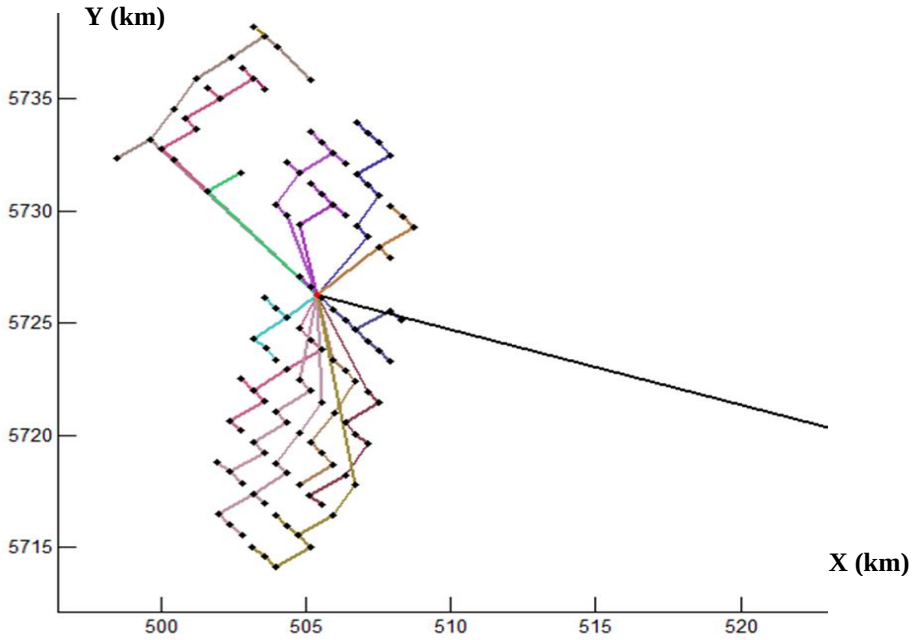

2/ AC/HVDC

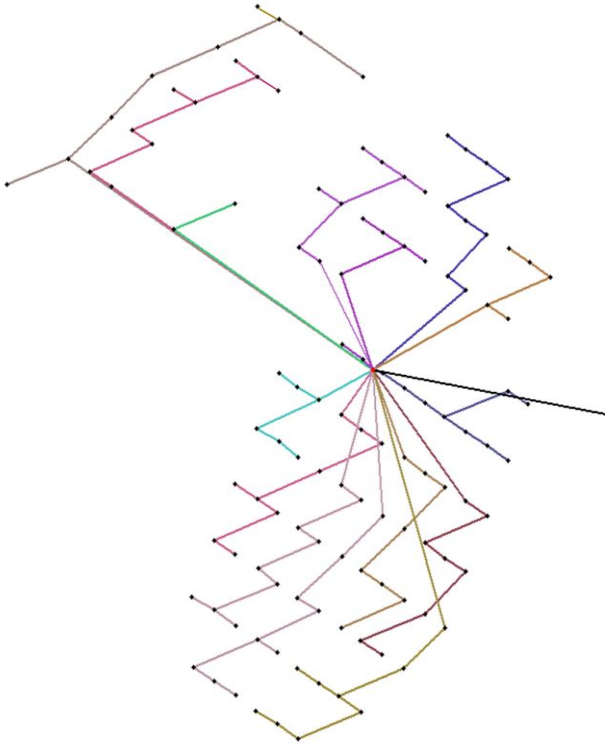

3/ Full DC

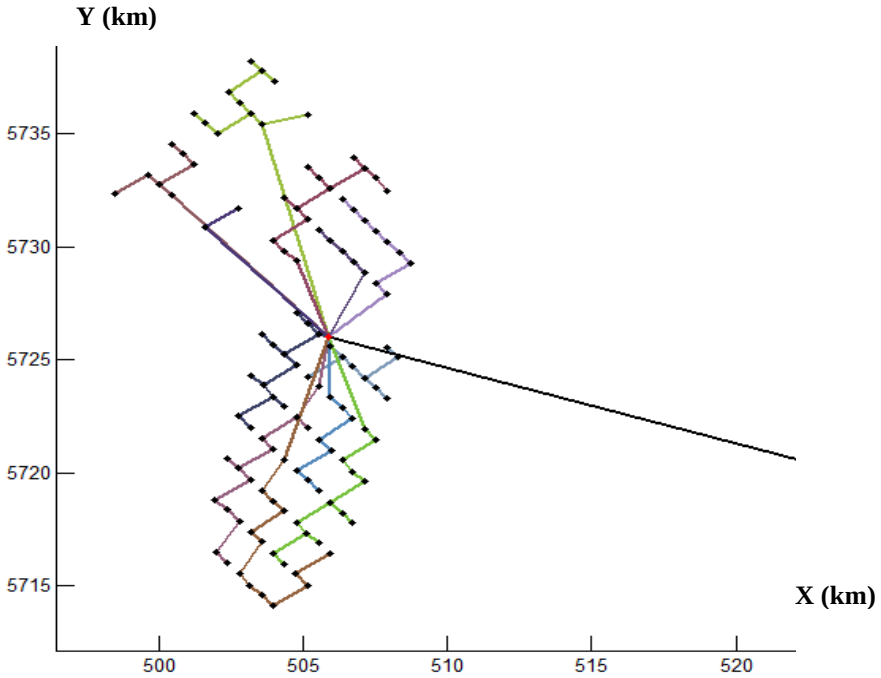

3/ Full DC

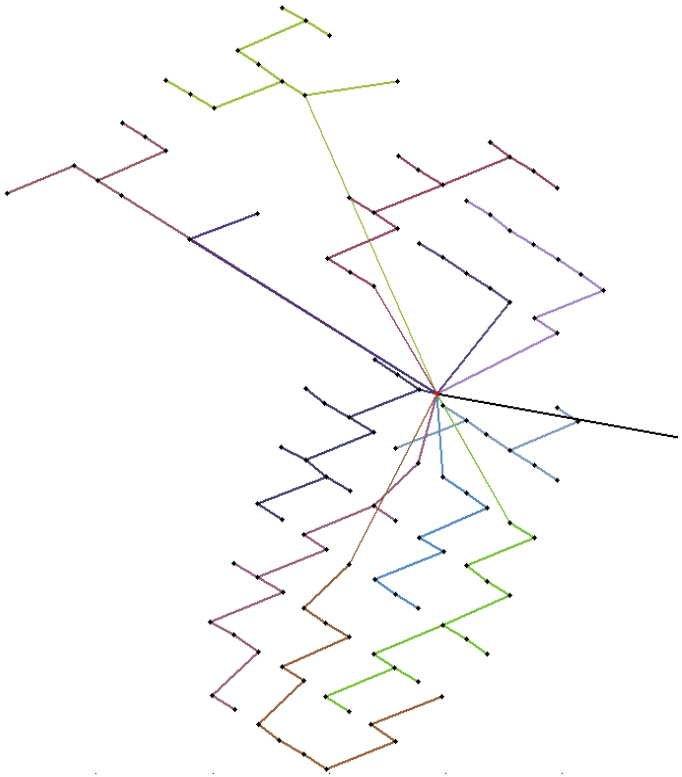

100 km	**1/ Full AC** 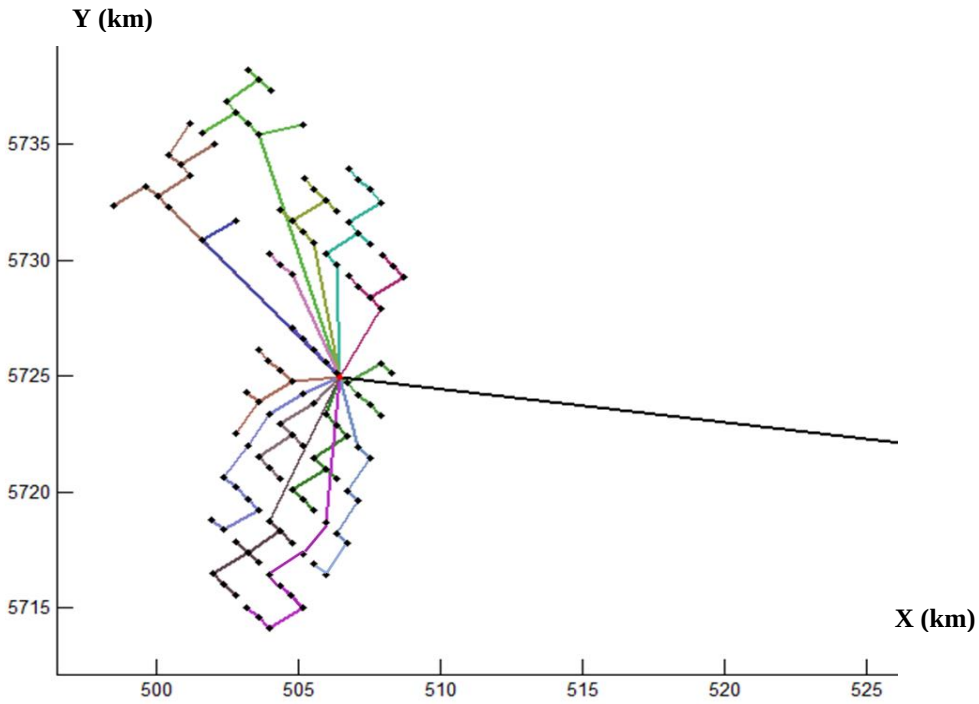	**1/ Full AC** 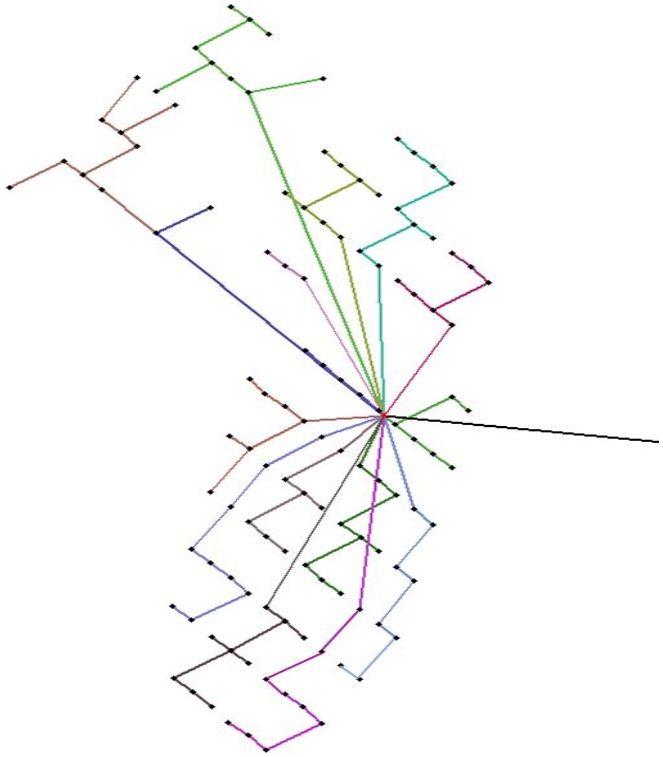

	2/ AC/HVDC 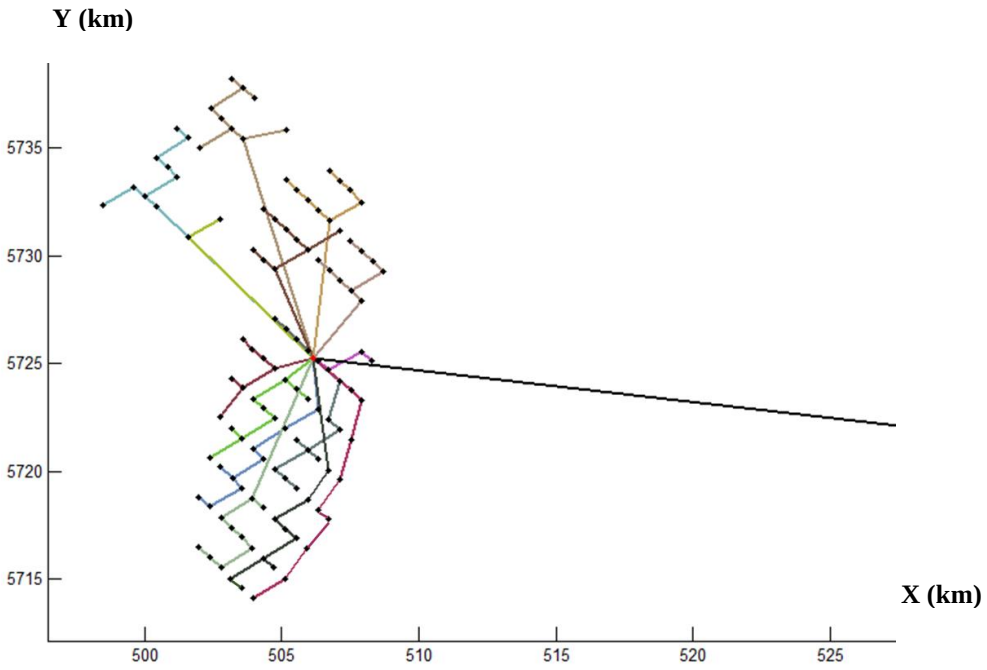 	**2/ AC/HVDC** 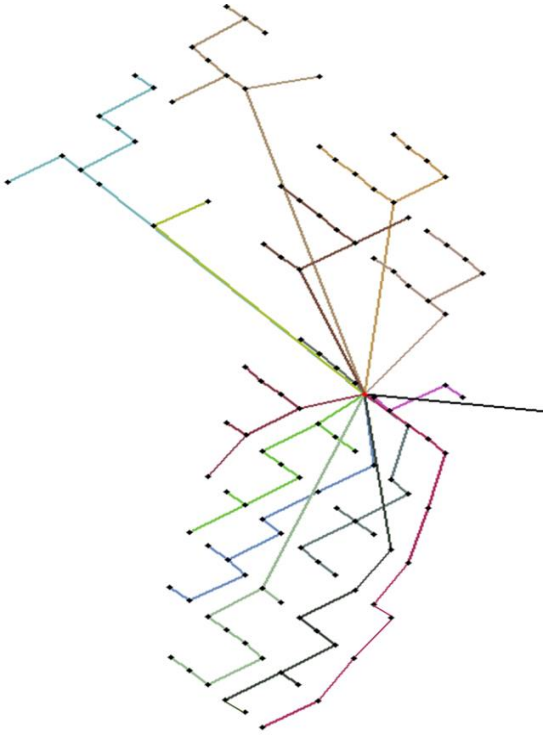

	3/ Full DC 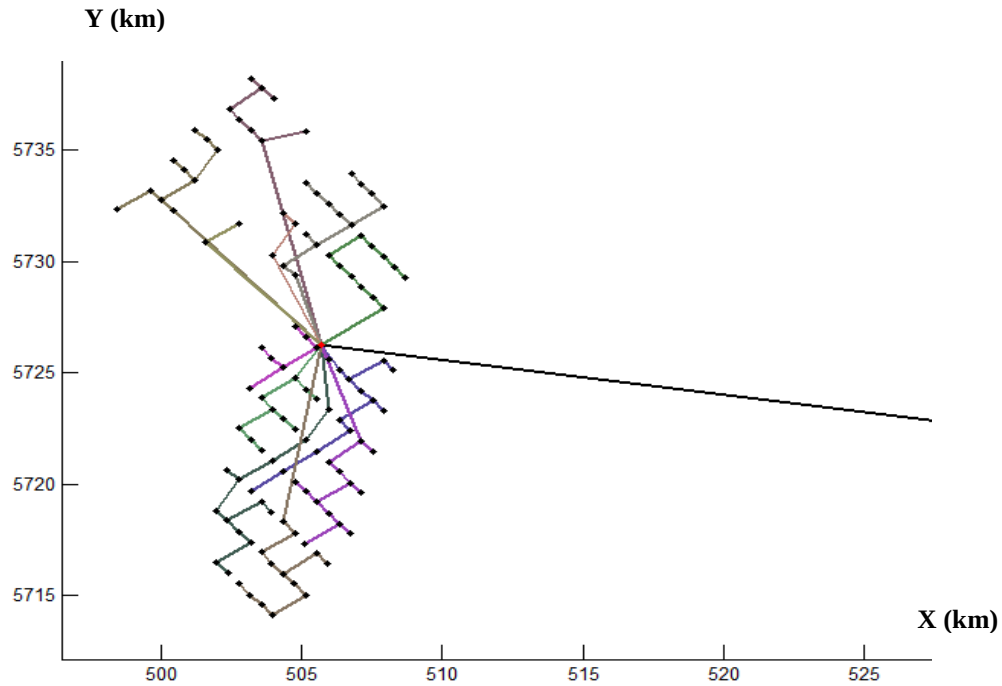	**3/ Full DC** 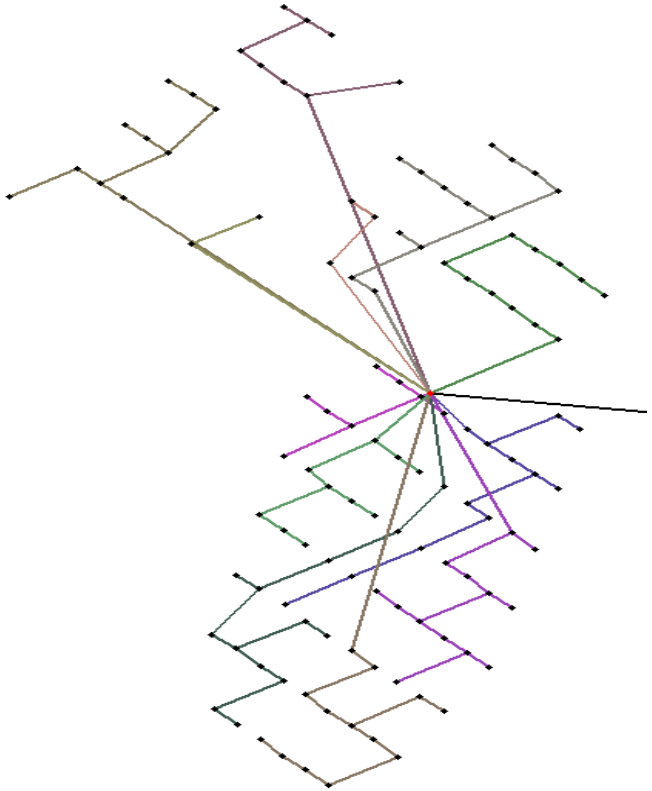

150 km	**1/ Full AC** 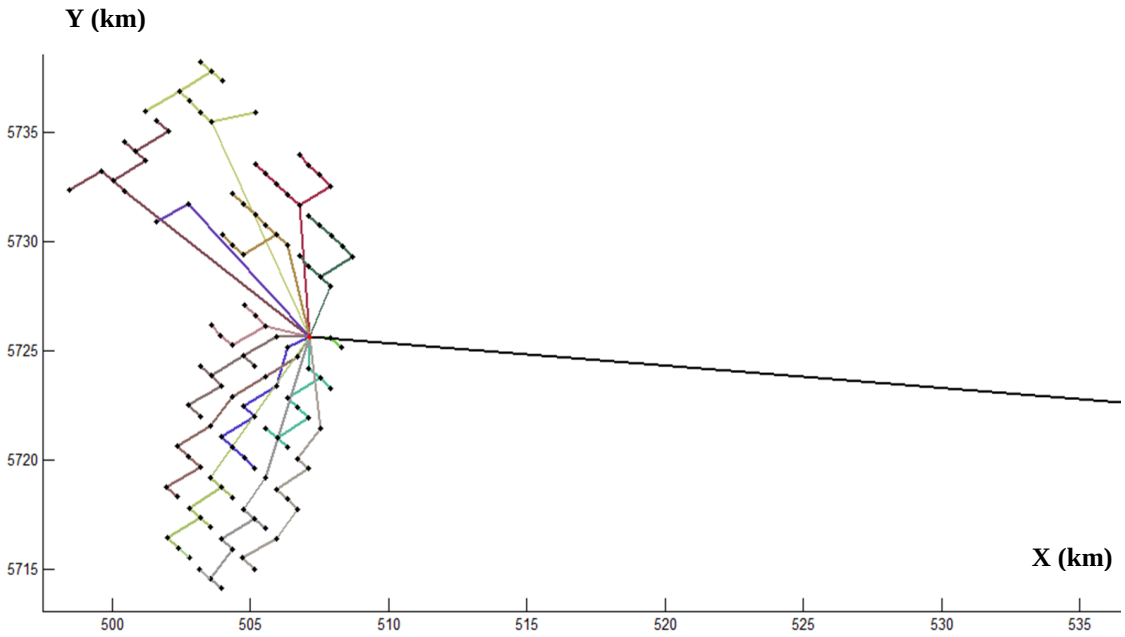	**1/ Full AC** 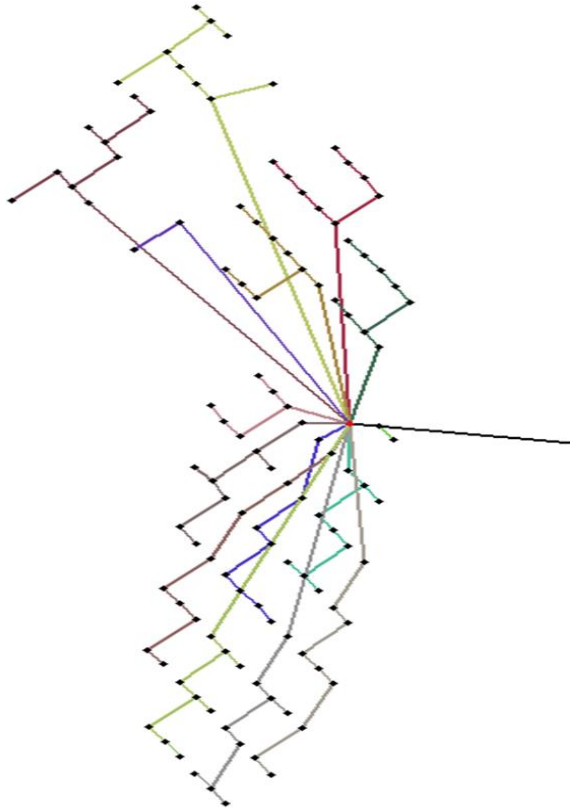

2/ AC/HVDC

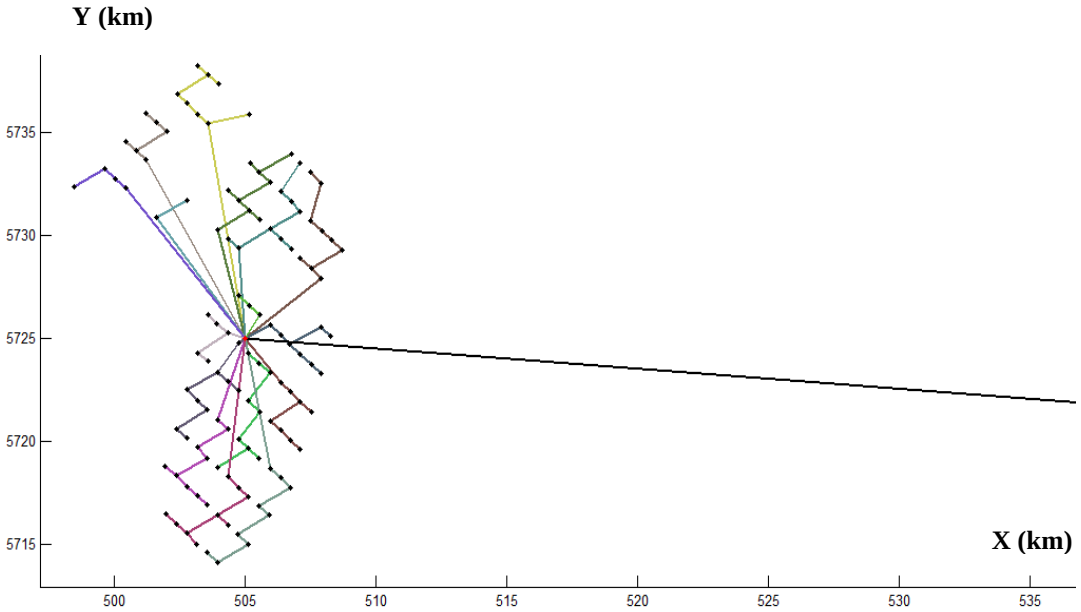

2/ AC/HVDC

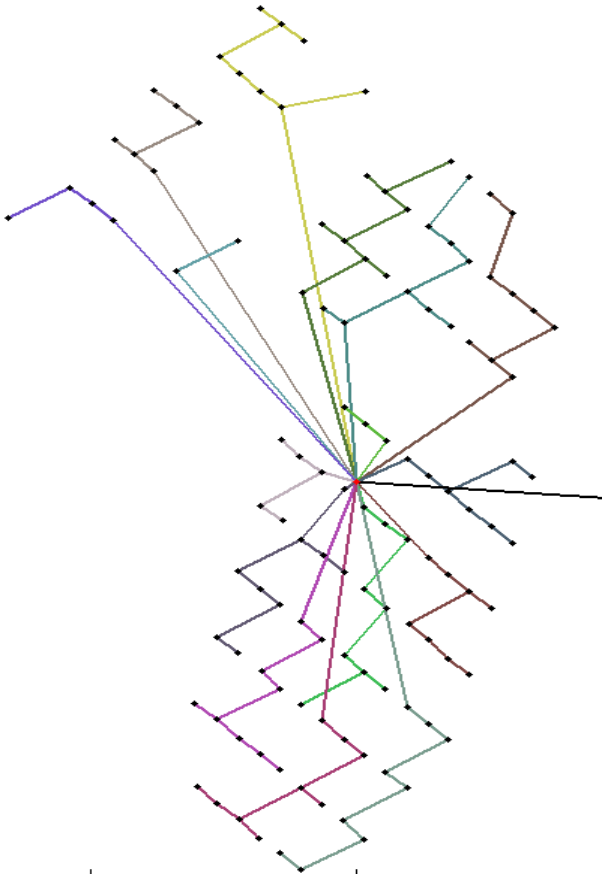

3/ Full DC

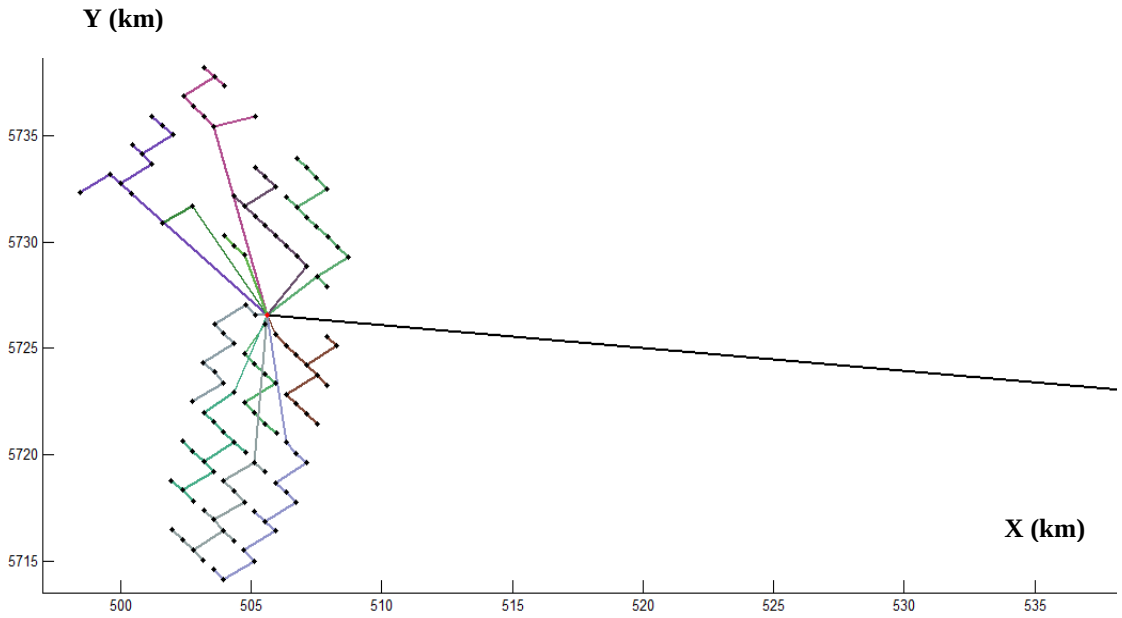

3/ Full DC

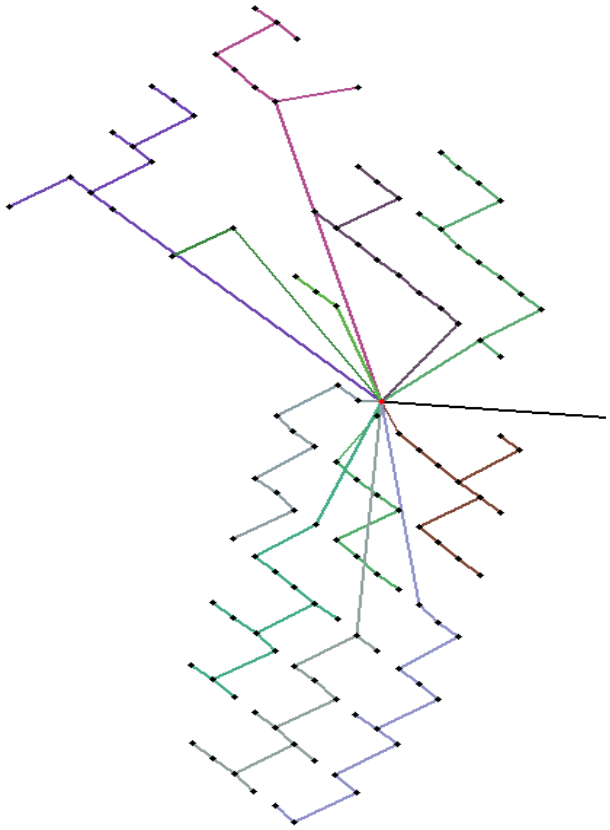

200 km	**1/ Full AC** 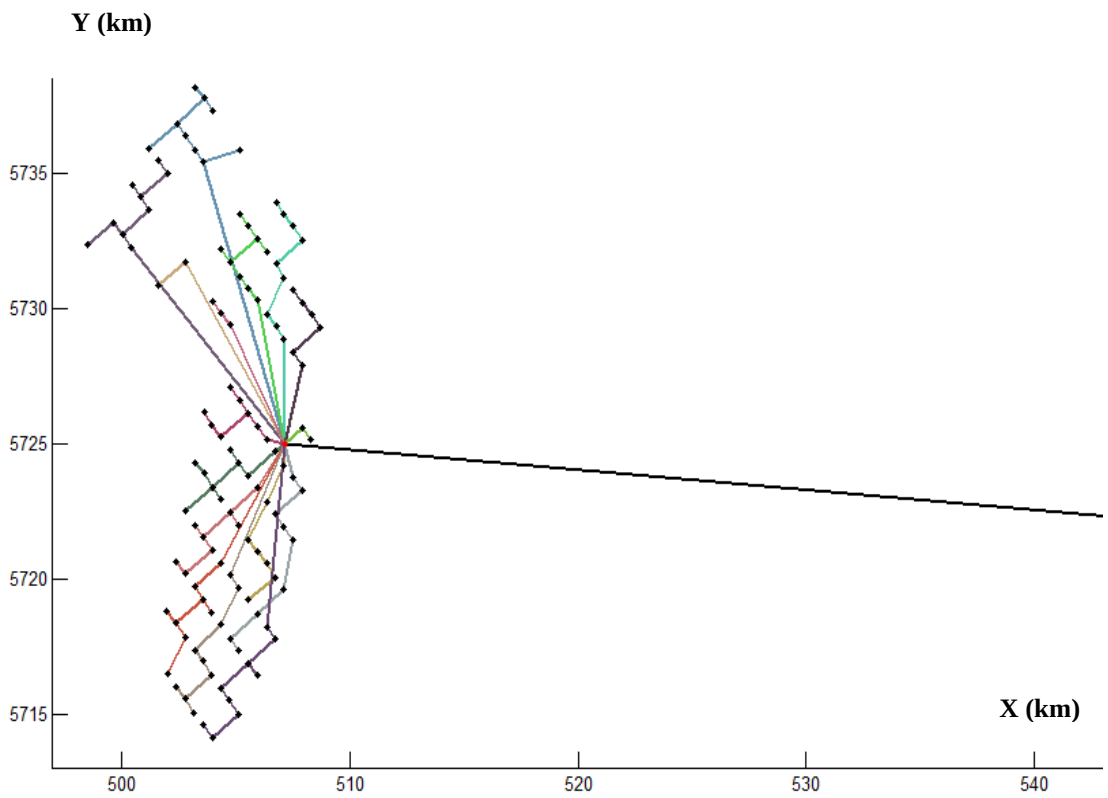	**1/ Full AC** 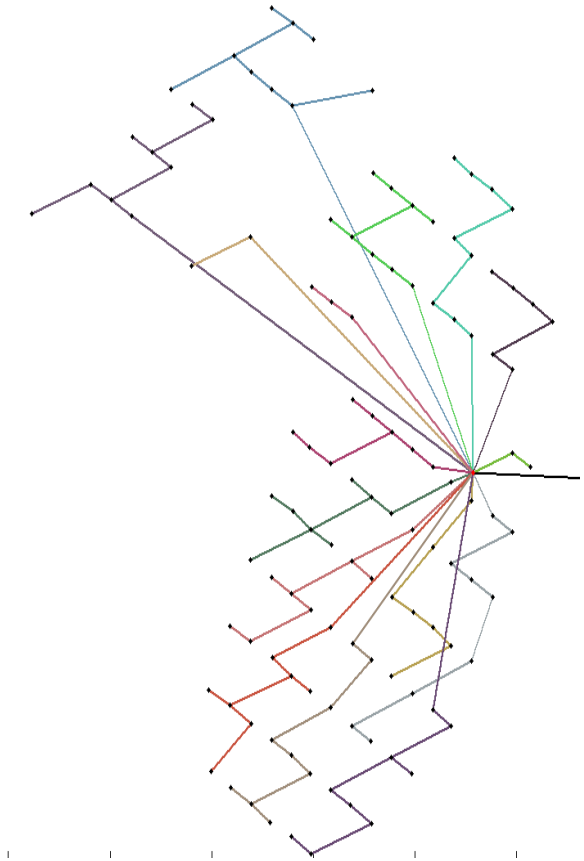

2/ AC/HVDC

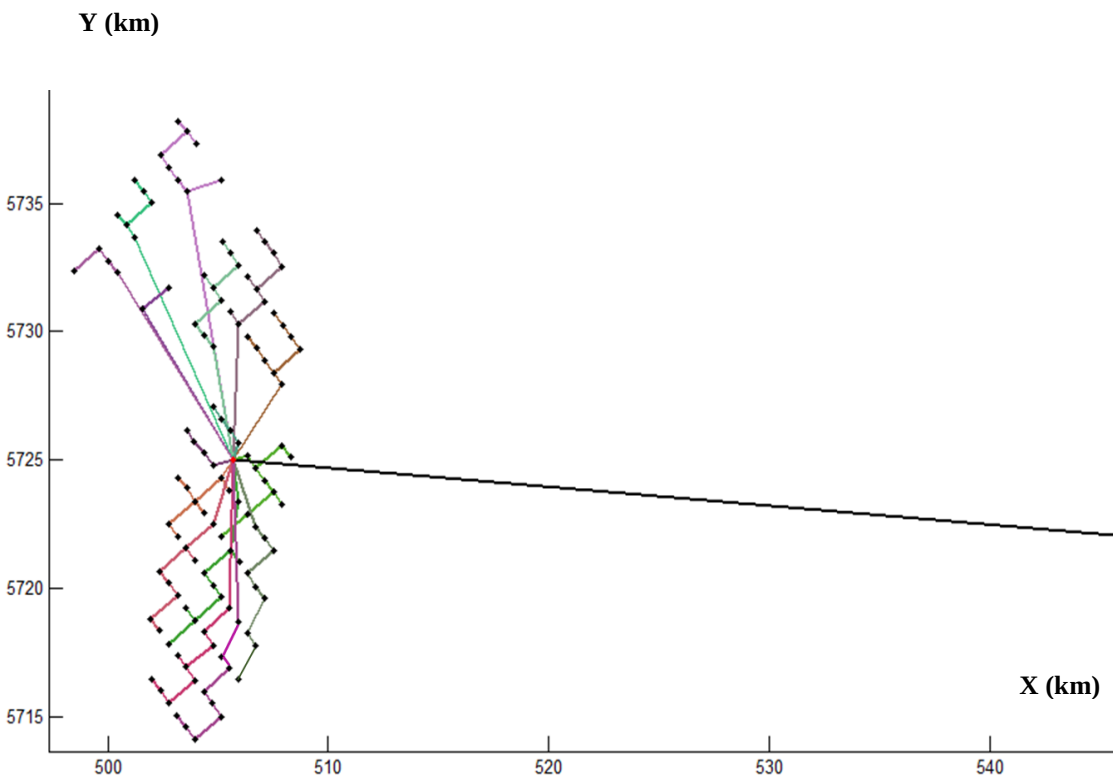

2/ AC/HVDC

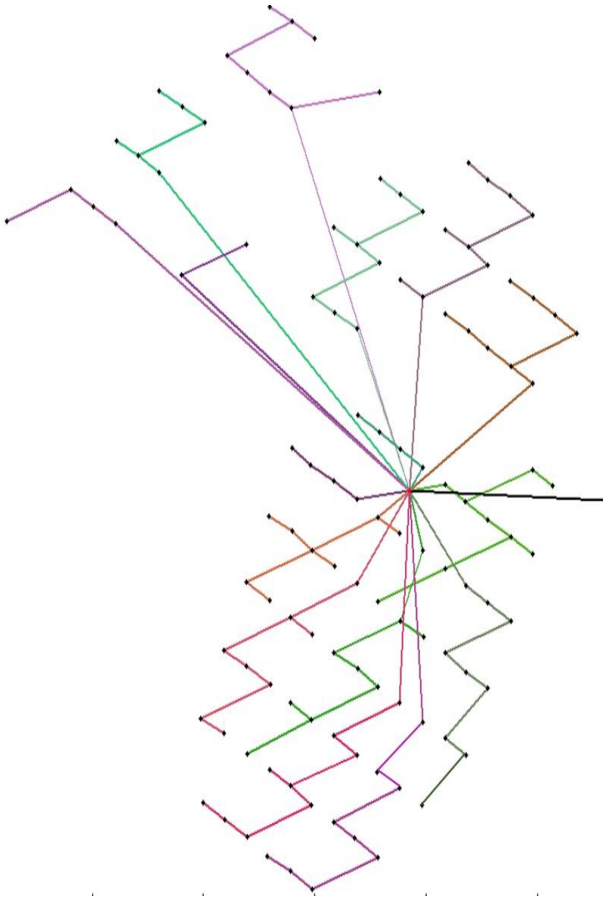

3/ Full DC

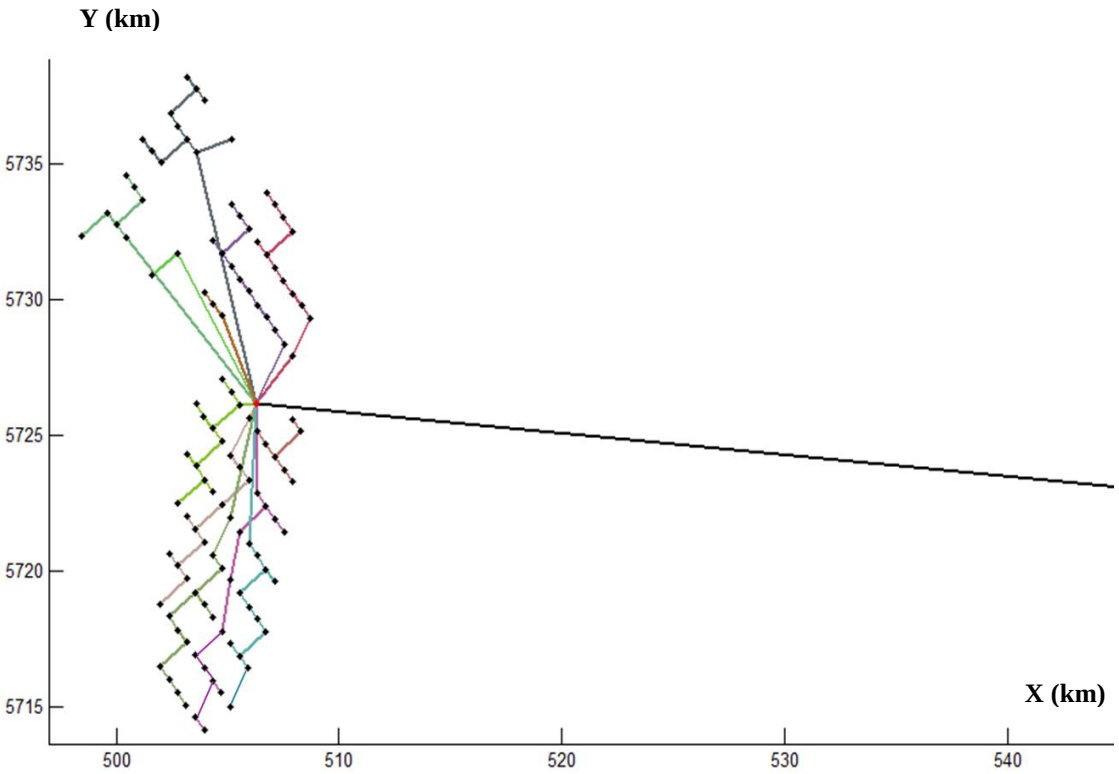

3/ Full DC

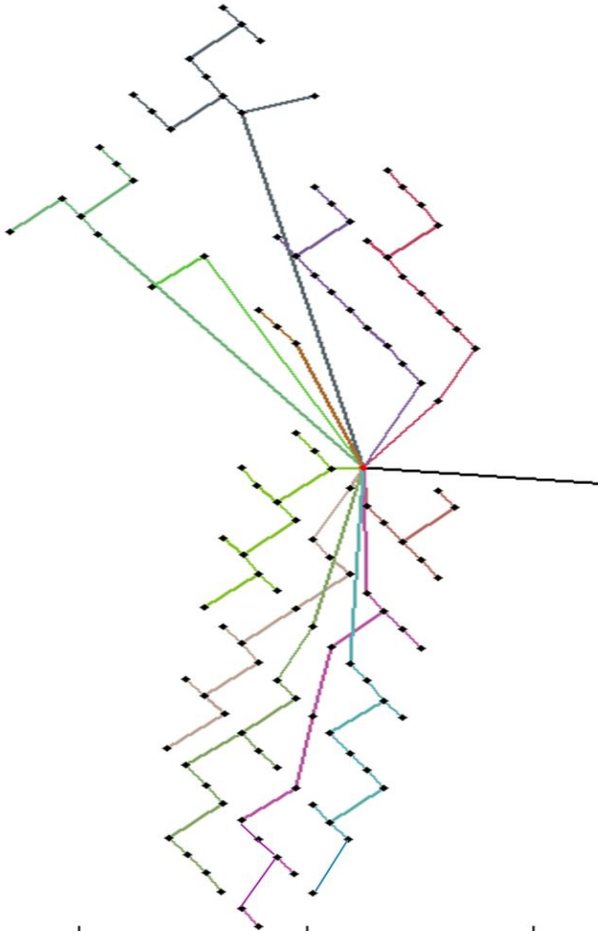

Table 3-11 presents the components cost for the three topologies for different distances. In fact, for all distances, there are components cost that are independent of the connection technology, such as the turbines and the foundations cost with a total of 1311.06 M€, the AC substation cost 66.57 M€ and the DC one that is more expensive by 85% (123.16 M€) and converters cost with 198.32 M€ (we suppose that AC/DC, DC/AC and DC/DC converters cost are the same). The results show that the MVDC and HVDC cables are less expensive than MVAC and HVAC cables even though they transmit the same power. In general, the DC switchgears cost are more important than the AC switchgears cost (example: 1.8 M€ compared to 1.0095 M€ for MV switchgears) but here we notice that the total cost of the HVAC switchgears is 0.92 M€ compared to 0.84 M€ for HVDC switchgears. Indeed, the additional cost is due to the fact that 3 parallel HVAC cables were used for the HV connection to the terrestrial network. For a distance 50 km, the cost of the converters is 14 times more expensive than the cost of the compensation equipment. The total CAPEX for respectively full AC, AC/HVDC and full DC architectures is 1774,96 M€, 1881,77 M€ and 1844,32 M€. One can conclude that for a distance 50 km the most economic topology is full AC connected wind farm. For 100 km, the compensation equipment cost evolves from 13.62 M€ for 50 km to 15.25 M€ for 100 km, this is explained by the Q_{comp} variation. Here, the HVAC cables present almost the triple price of the HVDC cables, the installation of three parallel HVAC cables for a transmission distance 100 km is the cause of this price increase. Consequently, the evaluated CAPEX respectively for full AC, AC/HVDC and full DC topologies is 1988.11 M€, 1953.73 M€ and 1924.74 M€. The most economic technology for a distance 100 km is full DC connected wind farm. For 150 km, according to the table data, the cost of the HVAC cables continues to rise to 607.75 M€. However, the HVDC cables cost is just 217.55 M€ for mixed AC/HVDC and 216.90 M€ for full DC. The CAPEX obtained for the three cases is respectively 2182. 17 M€, 2027.65 M€ and 1986,30 M€. The full DC topology is still the most economical of all topologies. Finally, and for 200 km, the data table below presents a peak in the HVAC cables cost with 804.46 M€, it even exceeds the foundations cost. One can conclude that for such a huge transmission distance 200 km, the full AC topology presents important cost so we can say that this technology is not advantageous compared to mixed and full DC architectures. The CAPEX evaluated for the three topologies is respectively 2383.91 M€, 2097.716 M€ and 2058.81 M€. The full DC connected wind farm is the most economical topology. Figures 3-16, 3-17, 3-18, 3-19 present histograms related to component cost for the three topologies for different transmission distances (50 km, 100 km, 150 km and 200 km).

Table 3-11 The Components cost for the three topologies for different distances

	50 km			**100 km**			**150 km**			**200 km**		
	Full AC	AC/HVDC	Full DC	Full AC	AC/HVDC	Full DC	Full AC	AC/HVDC	Full DC	Full AC	AC/HVDC	Full DC
MV cables (M€)	171,29	172,23	128,93	170,12	168,079	132,79	169,02	170,98	124,88	172,25	172,42	128,77
HV cables (M€)	197,4	70,49	70,87	413,78	146,6	147,43	607,75	217,55	216,9	804,46	286,17	285,52
Transformers (M€)	9,34	4,67	9,34	9,34	4,67	9,34	9,34	4,67	9,34	9,34	4,67	9,34
Substations (M€)	66,57	123,16	123,16	66,57	123,16	123,16	66,57	123,16	123,16	66,57	123,16	123,16
MV switchgears (M€)	1,0095	1,0095	1,8	1,076	1,0095	1,8	1,0095	1,076	1,8	1,076	1,076	1,8
HV switchgears (M€)	0,92	0,84	0,84	0,92	0,84	0,84	0,924	0,84	0,84	0,924	0,84	0,84
Compensation (M€)	13,62	-	-	15,25	-	-	16,5	-	-	18,23	-	-
Converters (M€)	-	198,32	198,32	-	198,32	198,32	-	198,32	198,32	-	198,32	198,32
Turbines (M€)	569,61	569,61	569,61	569,61	569,61	569,61	569,61	569,61	569,61	569,61	569,61	569,61
Foundations (M€)	741,45	741,45	741,45	741,45	741,45	741,45	741,45	741,45	741,45	741,45	741,45	741,45
CAPEX (M€)	**1771,2095**	**1881,7795**	**1844,32**	**1988,116**	**1953,7385**	**1924,74**	**2182.17**	**2027,65**	**1986,3**	**2383,91**	**2097,71**	**2058,81**

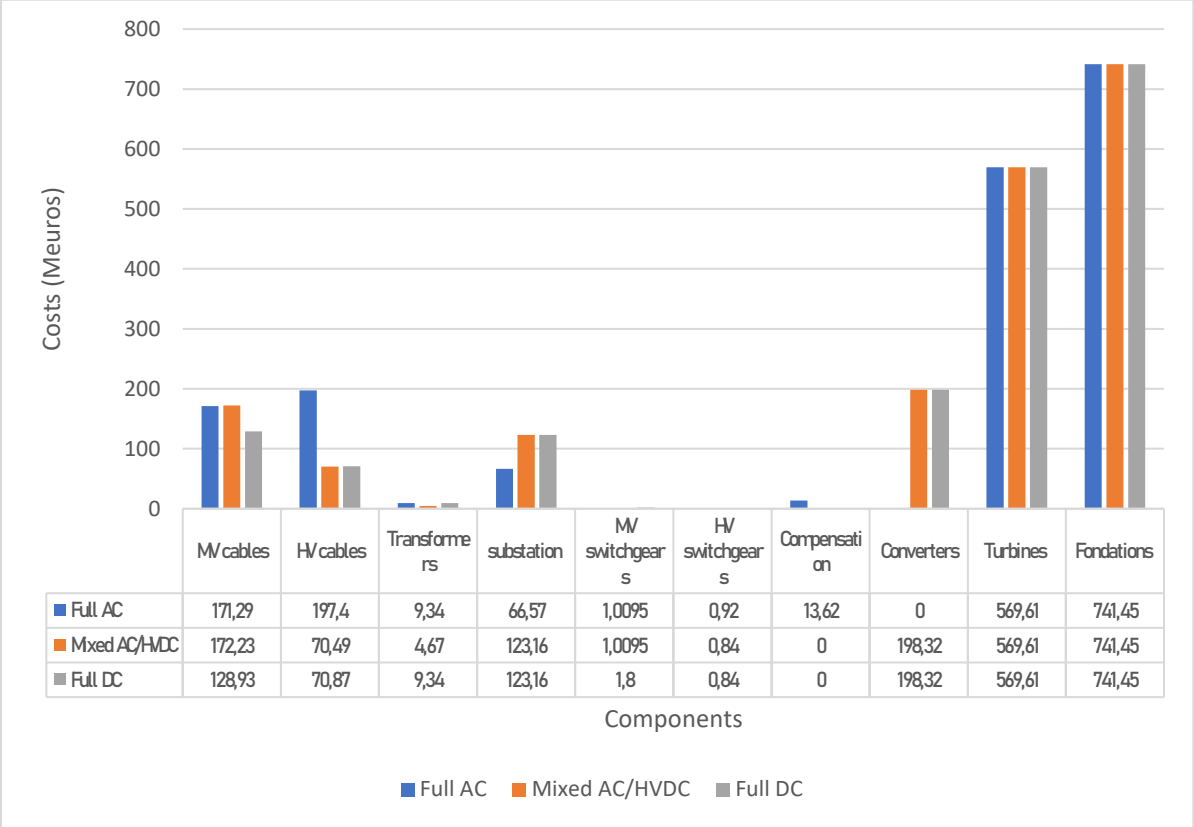

Figure 3-16 Component costs for different topologies for 50 km

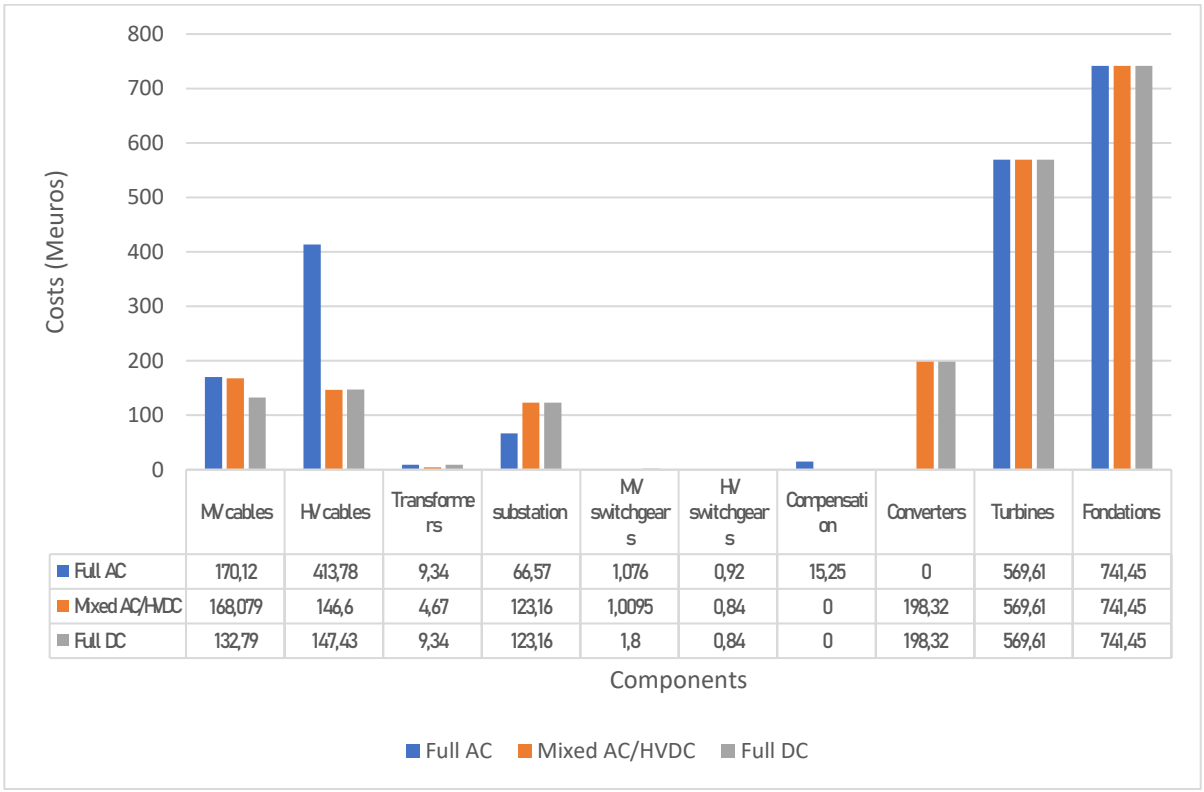

Figure 3-17 Component costs for different topologies for 100 km

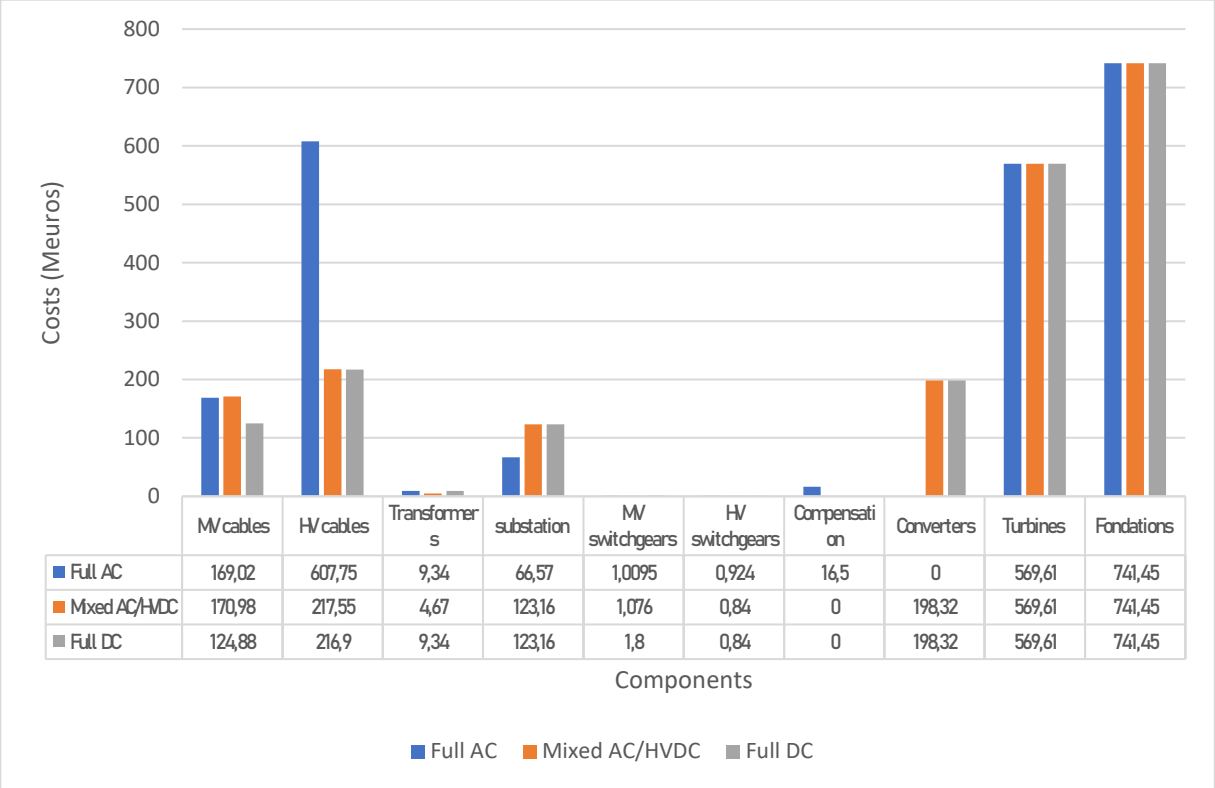

Figure 3-18 Component costs for different topologies for 150 km

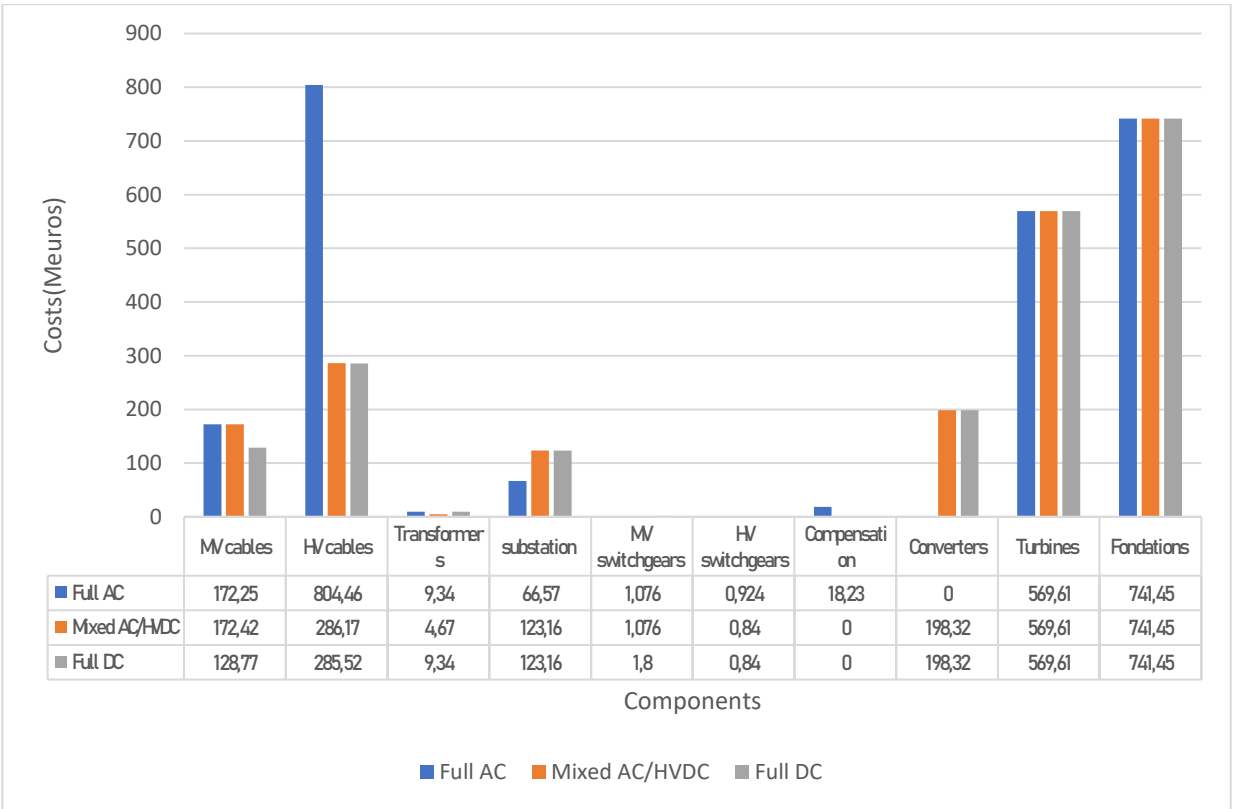

Figure 3-19 Component costs for different topologies for 200 km

3.3 Determination of the break-even distance

In this part, the comparison of losses of the different topologies is discussed. For all distances, we notice that converters losses present the most part of the overall losses with more than 60 % of the total losses whereas the MV losses are the lowest since the turbines are disposed next to each other so there is no important distance where the power can be lost. HV losses increase according to the transmission distance for the three topologies. Indeed, and for the full AC connected wind farm, HV losses evolve from 7.67 MW for 50 km to 29.32 MW for 200 km (increase of 29.32 MW for an additional 150 km). This is explained by the fact that for important transmission distance, the HVAC losses are high since the reactive losses are also important. However, the evolution of HVDC losses are less significant since they noted 0.7 MW for 50 km and 2.79 MW for 200 km (increase of 2.09 MW for an additional 150 km for AC/HVDC architecture). This is explained by the fact that DC cables present lower ohmic losses with the characteristics of higher cross-sections and lower electric resistances. For higher distances, HVDC transmission system presents less losses than HVAC system since ohmic losses continue to grow over the distance, whereas the converter losses remain the same.

If we compare both topologies AC/HVDC and full DC, we notice that the full DC presents less MV losses because the connection is made with MVDC cables which present obviously less losses than MVAC cables (only resistive losses). In contrast, the full DC technology have more converters losses since it contains DC/DC converters where its losses are calculated by the sum of the losses of the two DC/AC and AC/DC converters. This hypothesis may increase the total losses of the full DC connected topology. So, if it is assumed that the losses in a DC/DC converter are the same as in an AC/DC converter, the total converters losses would decrease and then full DC topologies would be more interesting than mixed AC/DC topologies for any transmission distance.

To conclude, the HVAC is the most advantageous transmission system for short distances while the HVDC system is the best one for long distances.

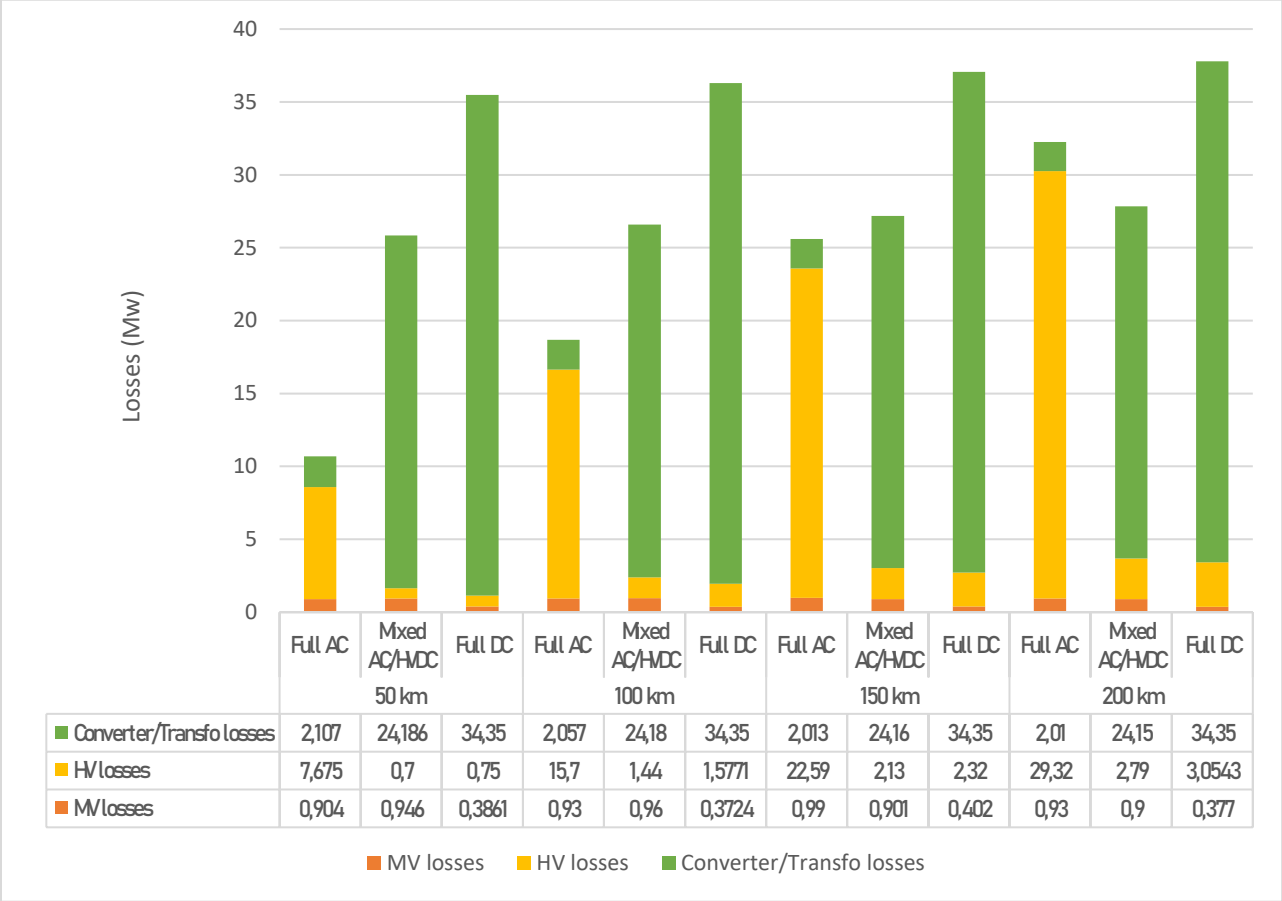

	Full AC	Mixed AC/HVDC	Full DC	Full AC	Mixed AC/HVDC	Full DC	Full AC	Mixed AC/HVDC	Full DC	Full AC	Mixed AC/HVDC	Full DC
	50 km			100 km			150 km			200 km		
Converter/Transfo losses	2,107	24,186	34,35	2,057	24,18	34,35	2,013	24,16	34,35	2,01	24,15	34,35
HV losses	7,675	0,7	0,75	15,7	1,44	1,5771	22,59	2,13	2,32	29,32	2,79	3,0543
MV losses	0,904	0,946	0,3861	0,93	0,96	0,3724	0,99	0,901	0,402	0,93	0,9	0,377

Figure 3-20 Different topologies losses according to transmission distance

The table below presents the total losses for the three topologies for different distances with and without wake effect calculation. The losses without wake effect are the sum of the different losses (MV losses, HV losses and converters/transfo losses) mentioned in figure 3-20.

Table 3-12 Total losses calculation with and without wake effect

	Total losses without wake effect (MW)			Total losses with wake effect (MW)		
	Full AC	Mixed AC/HVDC	Full DC	Full AC (+26 %)	Mixed AC/HVDC (+6%)	Full DC (+4%)
50 km	10.686	25.832	35.4861	13.46	27.38	36.90
100 km	18.687	26.58	36.2995	23.54	28.17	37.75
150 km	25.593	27.191	37.072	32.25	28.82	38.55
200 km	32.26	27.84	37.7813	40.65	29.51	39.29

Figure 3-21 exposes the break-even distance related to total losses for different topologies. The mixed AC/HVDC architecture presents less losses than all the others from a distance of 140 km from the coasts. Besides, the full DC is more interesting than the full AC from a distance of 190 km. On the other hand, full AC is still the best topology for distances of up to 140 km.

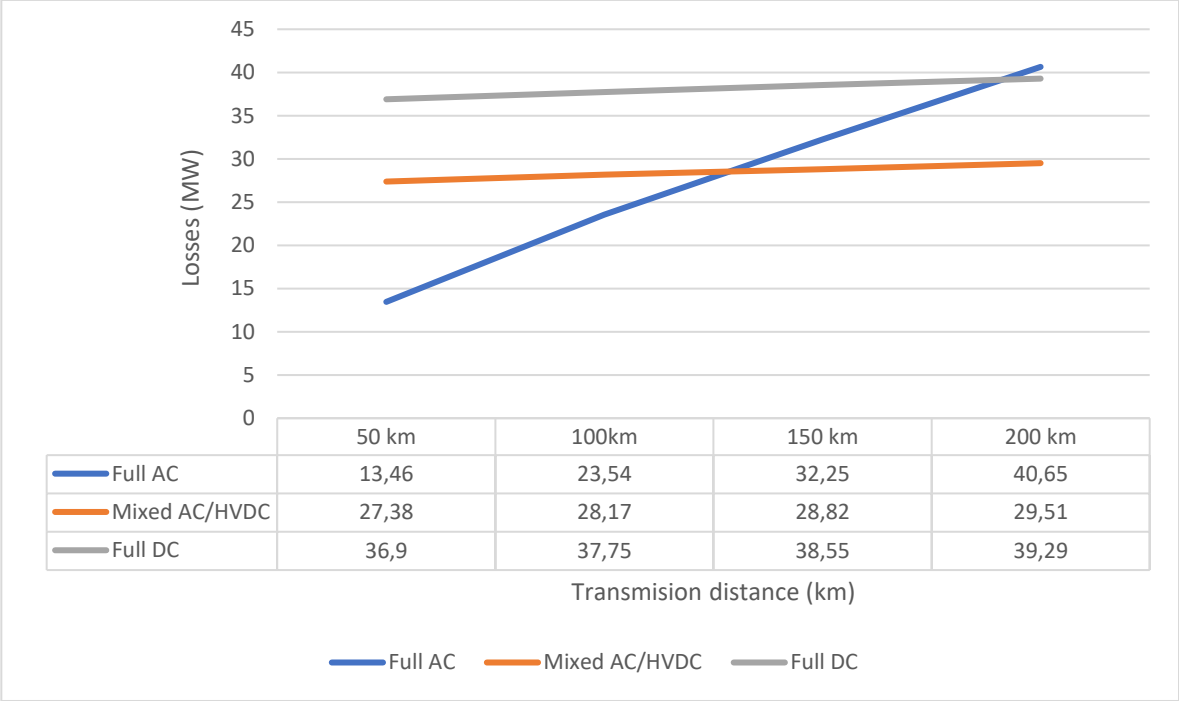

	50 km	100km	150 km	200 km
Full AC	13,46	23,54	32,25	40,65
Mixed AC/HVDC	27,38	28,17	28,82	29,51
Full DC	36,9	37,75	38,55	39,29

Figure 3-21 Losses evolution for different topologies according transmission distance

Figure 3-22 presents the LCOE evolution according the transmission distance for the three topologies. Like mentioned below, full AC topology has the least LCOE for distances between 50 km and 120 km. From a distance of 120 km the HVDC technology becomes more interesting. Here, the LCOE obtained takes into account the wake effect calculation.

As the distance rises, costs and losses of HVAC transmission technology overcomes the costs and losses of the HVDC system. The distance at which the break-even point occurs depends on many factors such as the rated power of the wind farm and the voltage level of both transmission technologies.

Furthermore, the expected cost and loss reductions in converters would definitively reduce the HVDC transmission technology cost. So, it is obvious that HVDC would become more competitive at even shorter distances since the most of the cost and losses come from converters.

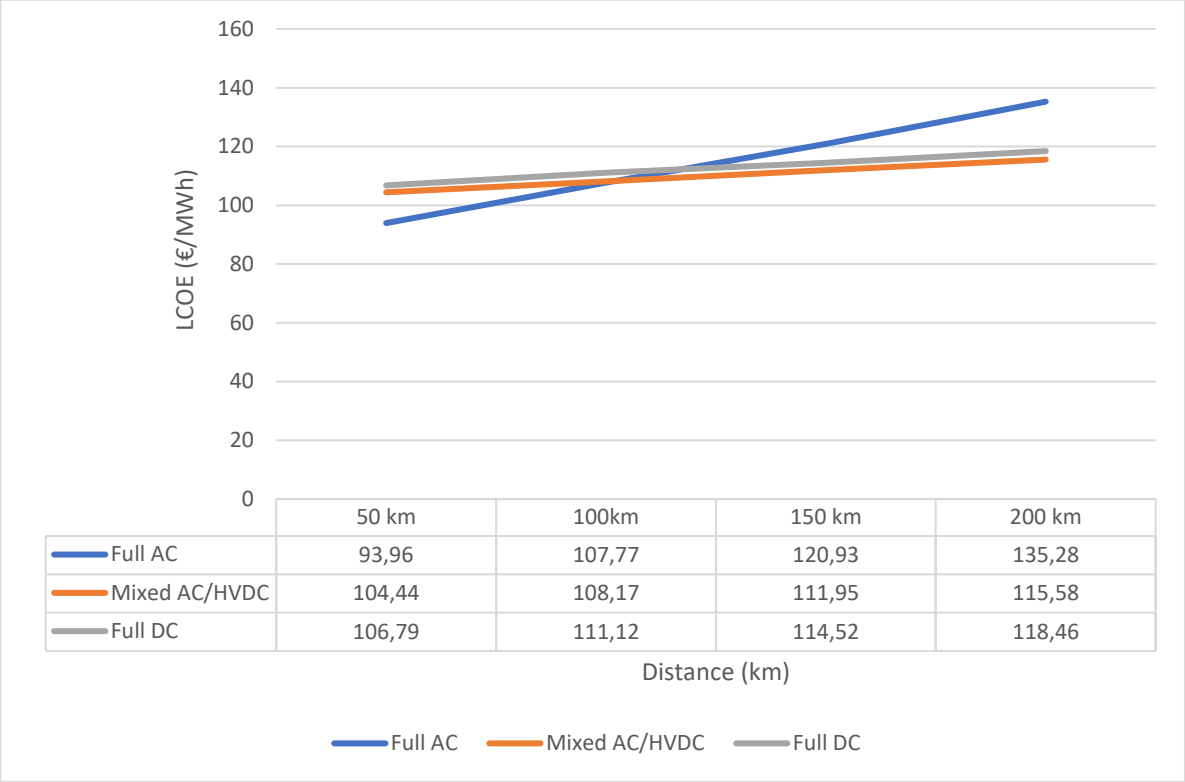

	50 km	100km	150 km	200 km
Full AC	93,96	107,77	120,93	135,28
Mixed AC/HVDC	104,44	108,17	111,95	115,58
Full DC	106,79	111,12	114,52	118,46

Figure 3-22 LCOE for different topologies according transmission distance

4 Multi-objective optimization

The multi objective optimization offers the possibility to minimize or to maximize more than one objective function. We can obtain several solutions with different values for each of the criteria that determine the best tradeoff between competing objectives. Nevertheless, the mono-objective optimization determines only one optimal solution for objective function that may be different from one optimization to another (multiple local optimums). The multi-objective optimization explores all the objective space by forming the Pareto front of the problem that represents all the solutions proposed for the two criteria.

The emphasis is done on the study of the trade-off between LCOE and AED. In fact, figure 3-23 shows the Pareto front of the three different topologies for a distance 50 km. We can see that the solution space is more explored with this multi-objective optimization approach. For a distance 50 km, the LCOE values of the AC optimized layouts are between 76.50 €/MWh and 99.60 €/MWh whereas the values obtained for AC/DC topologies reached the peak with a variation between 77.94 €/MWh and 149.24 €/MWh. Furthermore, full DC architectures have a LCOE variation between 85.10 €/MWh and 99.76 €/MWh. The high values of LCOE prices related to mixed AC/HVDC topologies are explained by their important CAPEX values for the distance 50

km (see table 3-11 where the CAPEX of AC/DC topology is the highest with 1881.77 M€ for 50 km). On the other hand, the AC layouts present the best AED values with the boundaries 316.07 MW and 324.62 MW. Nevertheless, mixed AC/DC and full DC connected wind farms transmit lower energy that vary respectively between [302.93, 309.76] MW and [297.03, 299.85] MW. Indeed, the HVDC transmission technology for a distance 50 km has significant power losses due to converter losses, in the opposite of HVAC system that present lower losses for such a distance (see figure 3-21).

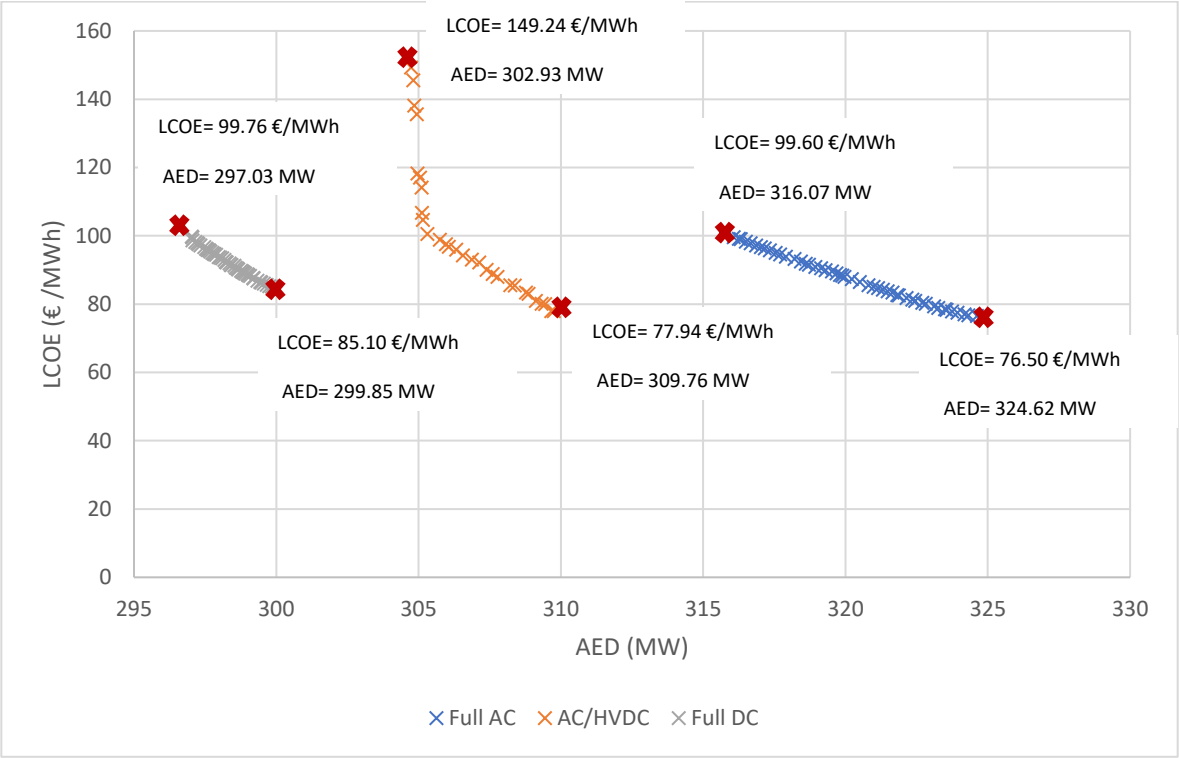

Figure 3-23 Multi-objective optimization (LCOE, AED) for different topologies for 50 km

The same multi-objective optimization approach is done for the distance 200 km. The two extremities of the distances 50 and 200 km have been purposely chosen to show the evolution of multi-objective optimization. The Pareto front of the different architectures is exposed in the figure below. For 200 km, full AC connected wind farms are the most expensive ones since they present highest LCOE due to their important value of CAPEX. The LCOE solutions variation is between 106.10 €/MWh and 139.44 €/MWh. On the other hand, full DC topologies present the lowest LCOE values (range= [94.51, 110.47] €/MWh) due to their lowest CAPEX (see table 3-11 for 200 km). Concerning the AED, the mixed AC/DC topology is in first position transmitting between [302.62, 307.52] MW followed by the AC layouts with values between [296.17, 302.85] MW. However, since DC architectures have important losses due to the significant losses of

DC/DC converters, the AED cannot exceed 296.91 MW (see figure 3-21). Hence, the compromise is as follows: if we want to have a low architecture cost, we choose full DC topology knowing that we transmit less energy. On the other hand, if we want to transmit the maximum of energy while increasing the LCOE, we choose the mixed connection AC/HVDC.

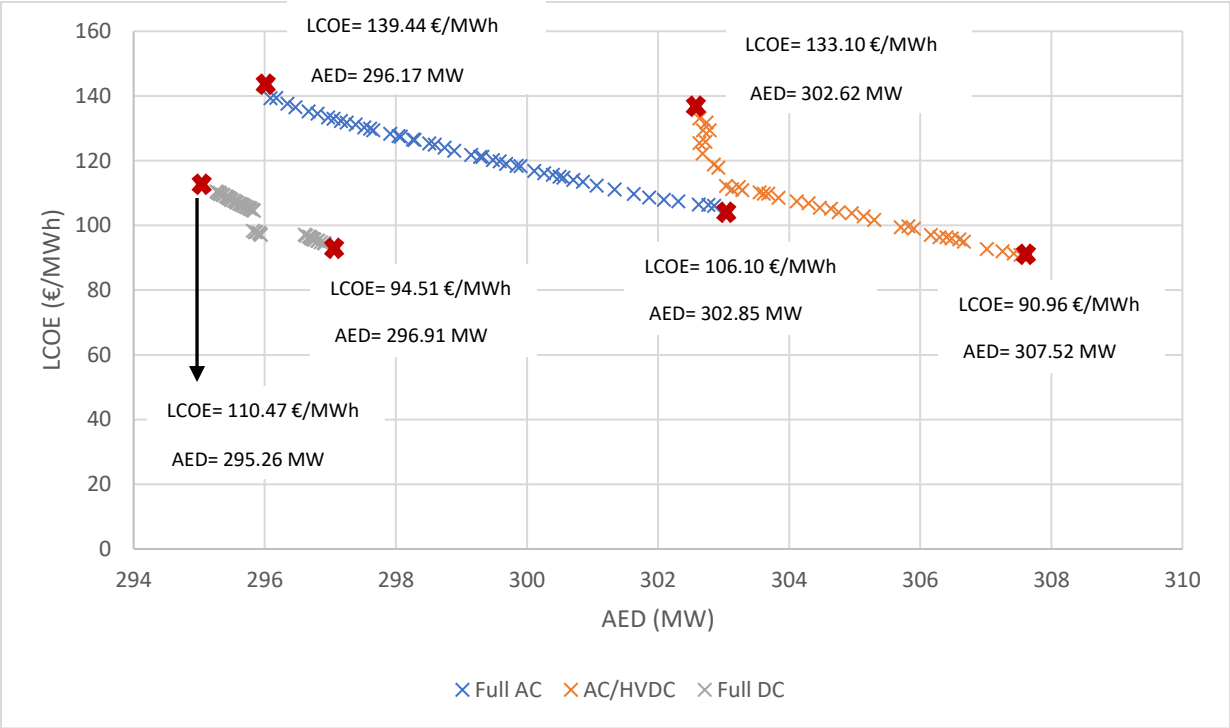

Figure 3-24 Multi-objective optimization (LCOE, AED) for different topologies for 200 km

5 Conclusion

In this chapter, we are interested in the study of three different electrical connection topologies. Our optimization framework is based on the LCOE calculation value. The optimization approach is validated on a real park case which is the Borssele I and II. In fact, the optimized topology presents lower LCOE with different electrical connection between wind turbines that means that with a different disposition of the MV collection network, we can optimize the cost and even the losses of the total topology. Then, a study was carried out for the wake effect impact for the three different topologies while considering the transmission distance variation. Since the losses of the topologies are not the same due to the different components used for each topology, the wake effect impact varies. Then, its percentage related to losses, AEP, and AED is determined depending on the distance variation. Since the ultimate goal is to determine the break-even distance for the three topologies (Full AC, mixed AC/DC and full DC), a comparison based on CAPEX, total losses and LCOE value is detailed. Thus, the results show that from a distance of

120 km the HVDC technology becomes more efficient than the HVAC one since the LCOE is lower.

The studied case of Borssele park has successfully test the economic and the electrical models shown in chapter 2, with the validation of the optimization algorithm effectiveness. Actually, the optimization for designing wind farms based only on one economic function such as LCOE, INVEST or AED, cannot allow to decide if that the park is really the optimal one or not. That's why wind farm designers should inspect different performances using several economic functions at the same time. This can be realized with the multi-objective optimization that links several proposed solutions optimizing more than one criterion, so the trade-off between the criteria is determined and it's up to the designers to decide which criteria to favor according to the park study.

Bibliography

[1] Online info: https://www.power-technology.com/projects/borssele-iii-iv-offshore-wind-farm/, ‘’Borssele Offshore Wind Farm‘’, © Copyright 2020 Verdict Media Limited.

[2] Netherlands Enterprise Agency, ‘’Borssele wind farm zone project & site description’’, Ministry of Economic Affairs, Tech. Rep. 2, Aug. 2015.

[3] Online info: https://offshorewind.rvo.nl/data-borssele, ‘’Data Borssele‘’, commissioned by the Ministry of Economic Affairs and Climate Policy.

[4] General Electric Haliade 150-6MW, https://en.wind-turbine-models.com/turbines/1446-general-electric-haliade-150-6mw

[5] B. Associates, ‘’Offshore wind cost reduction pathways Technology work stream‘’, prepared for The Crown Estate, 2012.

[6] M. D. Esteban et al., “Why offshore wind energy?” Renewable Energy, vol. 36, 2011.

[7] Eindwerk, Gilles daelemans, ‘’VSC HVDC in meshed networks’’, Master in electrical engineering, KU Leuven, 2008.

[8] A. Gerken, P. Heinrich, M. Richter, F. Peter, L. Krampe, and J. Hobohm, ‘’Cost Reduction Potentials of Offshore Wind Power in Germany’’, Prognos and Fichtner for the german offshore wind energy fundation and partners, 2013.

[9] Adwen, EDP Renewable, Eneco Energie, E.ON Climate Renewables, GE Renewable Energy, Iberdrola Renovables, MHI Vestas Offshore Wind, RWE Innogy, Siemens Wind Powe, Statoil, Vattenfall, ‘’Offshore wind cost reduction statement: Offshore wind can reduce costs to below €80’’, 2016.

Conclusions and perspectives

General conclusion

The development of large offshore wind farms is becoming a serious concern in the coming years due the production and installation expansion of offshore wind energy in the worldwide. In this thesis work, we have studied the optimization of the electrical architectures with different distribution and transmission networks AC and DC. In fact, with the deployment of the wind farm with important powers and far away coasts, searching a solution to minimize losses and costs remains a necessity and not an option.

The objective of this thesis is to develop an optimization design approach which serves as a decision-support tool for designing offshore wind farm electrical networks. The full AC connected wind farms are the first solutions proposed for electrical connection to onshore grid. This thesis work has integrated DC solutions both distribution and transmission networks. In fact, two architectures: the mixed AC/HVDC and the full DC are considered in order to study them and compare them with standard AC topologies.

In **Chapter 1**, a state of the art of offshore wind farms was successfully developed on several aspects relative to the current trends of global and especially European market of developing offshore wind farms. Indeed, an analyze was done for the different existing offshore wind topologies in AC, DC and mixed AC/DC. Thus, a preliminary comparison of the structures was shown and the difference between HVDC and HVAC was discussed. Besides, a state of the art of optimization approaches was presented. Consequently, a hybrid optimization approach using genetic and Prim algorithm is proposed. To assess the electrical performance of a given architecture concept, the proposed optimization algorithm aims to minimize the LCOE.

Chapter 2 was dedicated to show the electrical and economical models for an offshore wind farm. These models were applied as variables for the optimization algorithm. In fact, for each component, two analytical models are associated, (electrical and economical), the electrical one is exploited to evaluate the total losses of the electrical architecture under study. However, the economical one allows the calculation of the total investment cost CAPEX. Furthermore, the methods for designing the optimization framework were highlighted. In fact, the load flow calculations for different electrical architectures were shown through the library MatAC/DC. Only the DC load flow algorithm was developed since the library cannot model a total DC network. Thus, the load flow calculations were validated. Besides, for the integration of wake effect calculation, a state of the art of different wake models was presented. The choice was made on Katic Jensen model because it is the simplest and the fastest to implement. The algorithms

used to solve the optimization problem are GA and Prim, the two are complementary since the GA determines the turbine and the substations clusters and the prim's algorithm completes the connection between the turbines and the nearest substation as well as the connection between the DP and the nearest substation. Finally, the coupling between the load flow calculation taking into account wake effect and the optimization framework was detailed.

Finally, in **chapter 3**, the optimization framework was tested and validated on a real offshore wind farm Borssele I and II. So, a comparison between the performances of the real and the optimized topologies was shown. The validation was made by comparing the LCOE values. Indeed, the optimized one has presented lower LCOE thanks to a new connection of the MV collection network (different clustering so different cable characteristics).

Then, the wake model was integrated in both topologies (real and optimized Borssele park) in order to evaluate its impact. To develop more the study impact of wake effect, Katic Jensen model was integrated in the optimization of the three different electrical topologies full AC, mixed AC/DC and full DC. Since the losses of the topologies are not the same due to the different components used for each topology, the wake effect impact varies, and it can change with different transmission distances. In fact, the percentage of losses with wake effect are fixed to 26 % for AC topologies, whereas the mixed AC/DC and full DC ones have respectively 6 % and 4 % as wake effect impact percentages. The AEP doesn't change with distance variation, it remains the same for all electrical architectures since it depends only on wind turbines disposition (distance between turbines). For DC layouts, there is a little losses variation according to distance. This is explained by the fact that most of converter losses come from constant losses (independent of the current) so the current variation caused by the wake effect does not have much impact on total converter losses. So, as a conclusion, we can say that the wake effect has not so much impact on DC layouts as it impacts AC topologies.

Furthermore, a comparison based on CAPEX, total losses and LCOE value was detailed for the three topologies (Full AC, mixed AC/DC and full DC) in order to determine the break-even distance. Thus, the results show that from a distance of 120 km the HVDC technology becomes more efficient than the HVAC one since the LCOE is lower. So, we can say that we developed a technical-economic analysis tool to select the power transmission systems for offshore wind farms.

Finally, the multi-objective wind farm optimization problem was investigated. In fact, the optimization based only on one economic function such as LCOE, INVEST or AED, cannot

allow to decide the whole effectiveness of the park. It's really imperative to asses several aspects in the same time. This approach is done with the multi-objective optimization. In the example shown in chapter 3, two criteria were studied LCOE and AED for the three different topologies. The trade-off obtained for 50 km shows that AC topologies are the best solutions because they present the lowest LCOE values with the highest AED. However, for longer distance (200 km), a discussion was held: the lowest architecture cost with the transmission of less energy was full DC solutions, and the topology that transmits the maximum of energy while increasing the LCOE was the mixed AC/HVDC wind farms.

Perspectives

Although the work presented here has integrated a complete vision of optimization of offshore wind farms design with different electrical networks AC and DC, there are several studies that can be done in future work to complete the decision support framework:

- Reliability study which is an important criterion to take into account in addition to investment costs and power losses for designing the electrical system of an offshore wind farm. This study will allow to estimate in the long term the availability of the park that's mean the continuity of producing power. The reliability should be done for the three different topologies to complete the total scope of the comparison. Furthermore, the reliability study provides results that can be used to identify critical points in the power system. A better knowledge of these weak points during the design phase facilitates decision making for additional investment. This reduces the system interruption rate and maintenance costs over the operating life of the system.
- Sensitivity study related to economical models (CAPEX models) of the different components of the wind farm. The parametric sensitivity analysis allows to take into account the variation of components cost that generates a variation in final results such as LCOE value. Besides, the variation of the economic factors such as N: the lifetime of the park and the discount rate r can have influence on final results.
- The multi-objective study can show the trade-off between two or more criteria, it's a tool that allows the complete exploration of the proposed solutions. This approach must be taken into consideration and deserves to be further developed for the development of a complete optimization tool.
- The analytical Katic Jensen wake model can underestimate or overestimate the wake effect impact since it has a top hat velocity wake profile. However, it is not the accurate

representation of the wake effect profile. So, we should improve the wake model by using other models such as Gaussian model which has presented better results than the Jensen one.

- The integration of meshed networks either in AC or DC in the optimization framework. For AC/DC case, it allows to study the potential exchange between AC and DC networks for the stability system thanks to the active and reactive powers control in VSC HVDC converters.
- Taking into account the power changes along the transmission line, it means studying the voltage drops in cables.
- The integration of multi-terminal VSC HVDC in meshed networks and the study of its dynamic performance. Besides, the losses in multi-terminal VSC HVDC system can be investigated.

Appendixes

Appendix 1 HVDC configurations

There are two main configurations of HVDC connections: monopolar and bipolar.

Monopolar interconnectors consist of one high-voltage cable and the return path is made by the ground impedance that can cause corrosion on metallic objects (figure 1 (a)). However, it can be made through a low-voltage metal conductor (figure 1 (b)), this technic is recommended because the interference caused by the grounding electrodes are important and can induce environmental problems like the production of chemical elements such as chlorine in the sea. Nevertheless, a metallic return path increases the installation cost as well as the losses.

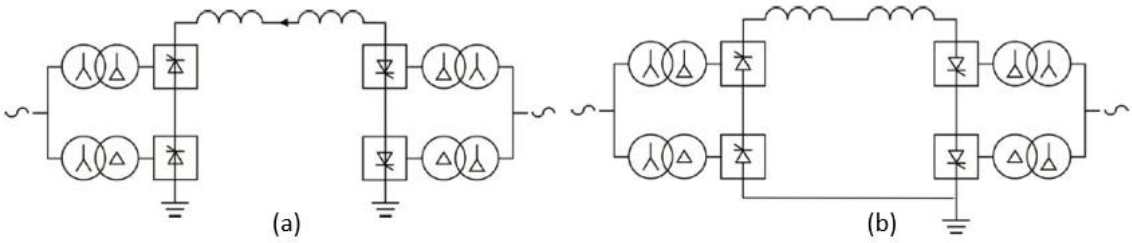

Figure 3. Monopolar HVDC connection with ground return (Alstom,2010), (b): Monopolar HVDC connection with metallic return cable (Alstom,2010)

The bipolar connection (figure 2) consists of a positive and a negative pole with a neutral point grounded. During operation, there is no return current in the ground so there are no corrosion problems. If one of the poles has a failure, the other one can operate with monopolar configuration linked to the ground as the return path.

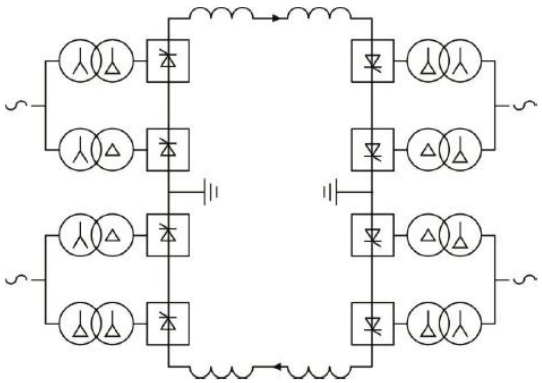

Figure 2. Bipolar HVDC configuration

A Multi-terminal connection (figure 3) is made as soon as there are more than two connection points on the HVDC line. Actually, there are only two multi-terminal HVDC configuration in

the world: the first is a three terminals line between Italy-Corsica-Sardinia and the second one is between Quebec-New England (five terminals).

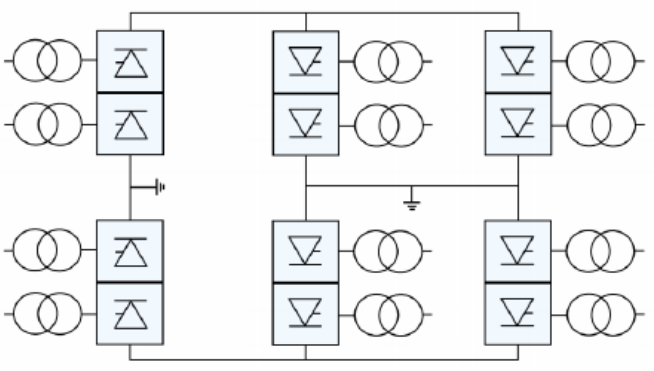

Figure 3. Multi-terminal HVDC configuration

Appendix 2 Cables characteristics

	MVAC		HVAC			MVDC			HVDC			
Rated Voltage (kV)	66 kV		220 kV			+/ - 80 kV			+/ - 320 kV			
Section (mm^2)	240	630	500	800	1000	240	400	630	240	630	1200	2000
Rated Power (MW)	54.9	81.7	250	295	330	92.16	120.64	160.16	446	797	1147	1540
Rated current (A)	480	715	655	775	866	576	754	1001	697	1246	1791	2406
R à 20 °C (mΩ/km)	85	41.4	39.1	24	21	75.40	47	28.30	75	27.3	15.1	9
C (nF/km)	220	320	140	170	190	-	-	-	-	-	-	-
L (mH/km)	0.38	0.33	0.43	0.4	0.39	-	-	-	-	-	-	-

Appendix 3 MMC modeling

The converter structure consists of identical sub-modules cascaded together instead of being connected in series. There are 6 arms in a three-phase MMC converter and N sub-modules in each arm. A sub-module is composed of several simple low-voltage power electronic components. The simplified configuration of the three-phase MMC and the submodule typology are shown in Figure 1.

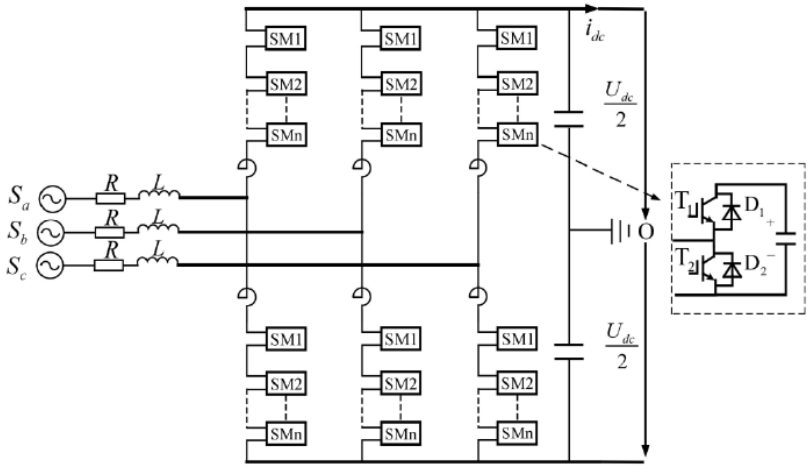

Figure 1. Simplified configuration of the MMC for wind turbine application

1/ MMC modeling

The equivalent circuit of sending-end of the MMC-HVDC transmission system is shown in the following figure. The equations are expressed in the reference a b c.

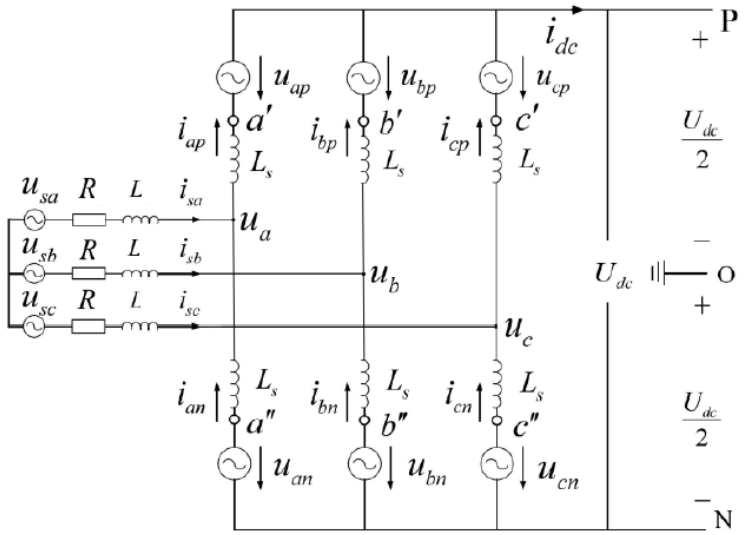

Figure 2. The equivalent circuit of the MMC-HVDC system

Considering that

$$U_{dc}= u_{ip}+u_{in} \text{ so } u_{i'o}=u_{i''o} \quad (1)$$

This means that the electric potential of a', b' and c' is equal respectively to a", b", c".

The MMC model in the reference a b c for a three-phase system is presented by the equation below.

$$\begin{cases} R\, i_{sa}+\left(L+\frac{L_S}{2}\right)\frac{di_{sa}}{dt}=u_{sa}-u_a \\ R\, i_{sb}+\left(L+\frac{L_S}{2}\right)\frac{di_{sb}}{dt}=u_{sb}-u_b \\ R\, i_{sc}+\left(L+\frac{L_S}{2}\right)\frac{di_{sc}}{dt}=u_{sc}-u_c \end{cases} \quad (2)$$

The voltage and current in phase a can be defined as:

$$u_a=U_m \sin(wt) \quad (3)$$
$$i_a=I_m \sin(wt-\varphi)$$

Then, the voltages and currents in one arm can be expressed by the following equations:

$$u_{ap}=\frac{1}{2}U_{dc}-u_a=\frac{1}{2}U_{dc}(1-m.\sin(wt)) \quad (4)$$

$$u_{an}=\frac{1}{2}U_{dc}+u_a=\frac{1}{2}U_{dc}(1+m.\sin(wt)) \quad (5)$$

$$i_{ap}=\frac{1}{3}I_{dc}+\frac{1}{2}i_a=\frac{1}{3}I_{dc}(1+k.\sin(wt-\varphi)) \quad (6)$$

$$i_{an}=\frac{1}{3}I_{dc}-\frac{1}{2}i_a=\frac{1}{3}I_{dc}(1-k.\sin(wt-\varphi)) \quad (7)$$

Where m is the voltage modulation index that can vary between 0.77 and 0.86 to guarantee a good operation margin between the maximum and the minimum fundamental AC output phase to neutral voltages. In general, the reactive power variation in a VSC converter is provided by the variation between the upper and the lower converter voltage limit, these limits are given by the modulation index. k is the current modulation index that links between the AC and the DC currents. m and k are expressed respectively by the following equations.

$$m=\frac{U_m}{\frac{U_{dc}}{2}} \quad (8)$$

$$k=\frac{\frac{I_m}{2}}{\frac{I_{dc}}{3}} \quad (9)$$

Therefore, the output voltage U_{dc} of the MMC and the voltage modulation index can be used to express the AC voltage.

$$u_a = \frac{1}{2} m\, U_{dc} \sin(wt) \tag{10}$$

Assuming that the converter losses are neglected compared to the transmission power, the law of energy conservation requires that the power in AC side and DC side must be equal.

$$3U_a I_a \cos\varphi = U_{dc} I_{dc} \tag{11}$$

Where U_a is the RMS AC voltage, I_a the RMS AC current and cos φ is the power factor in phase a. Both currents I_a and I_{dc} are primordial for converter power losses calculation.

2/ Modeling of power losses in MMC

The power losses of an overall VSC HVDC station consists of the losses of its different components. The main contributor to total losses is the valve losses that are engendered by IGBTs. These losses can be divided into conduction losses and switching losses.

2.1/ Conduction losses of the MMC

For conduction losses, the studies are based on the curve between the IGBT collector-emitter voltage V_{CE} and the DC collector current I_C to approximate the voltage characteristics of diodes and IGBTs.

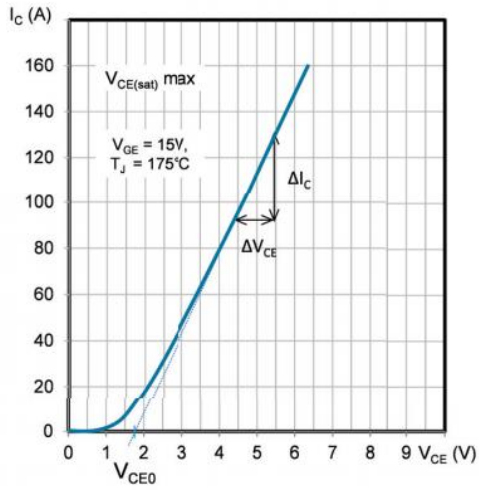

Figure 2-25 IGBT forward voltage

Therefore, after the approximation, the voltage equations (12) and (13) of IGBTs V_T and diodes V_D are defined.

$$V_D(t) = V_{D0} + R_D(T_j) i_D(t) \tag{12}$$

$$V_T(t)=V_{T0}+R_T(T_j)i_T(t) \tag{13}$$

Where V_{X0} and R_X are threshold voltage and forward conduction resistance of semiconductors, and both of them are related to the junction temperature T_j, which can be determined by the linear interpolation method described in equation (14).

$$\propto_{Tj}=(\propto_{Th}-\propto_{T1})\frac{T_j-T_1}{T_h-T_1}+\propto_{T1} \tag{14}$$

Where T_1=25°C and T_h=125°C .

Therefore, the values of V_{X0} and R_X for a certain junction temperature T_j are determined by the equations below.

$$V_{D0}(T_j)=(V_{D0}(T_h)-V_{D0}(T_1))\frac{T_j-T_1}{T_h-T_1}+V_{D0}(T_1) \tag{15}$$

$$V_{T0}(T_j)=(V_{T0}(T_h)-V_{T0}(T_1))\frac{T_j-T_1}{T_h-T_1}+V_{T0}(T_1) \tag{16}$$

$$R_D(T_j)=(R_D(T_h)-R_D(T_1))\frac{T_j-T_1}{T_h-T_1}+R_D(T_1) \tag{17}$$

$$R_T(T_j)=(R_T(T_h)-R_T(T_1))\frac{T_j-T_1}{T_h-T_1}+R_T(T_1) \tag{18}$$

The conduction losses P_{con} can be expressed by the arm current I and the junction temperature with the following equation.

$$P_{con\_x}=\frac{1}{T_0}\int_0^{T_0}V_x(t)\,I_x(t)\tau_x(t)dt \tag{19}$$

With

$$P_{con}=P_{con\_D}+P_{con\_T} \tag{20}$$

Where T_0 is the duty cycle, and τ_x is the pulse function, when semiconductors turn on, τ_x =1 and τ_x =0 otherwise.

The current of the upper and lower arms based on the DC current I_{dc} and the maximum AC current I_{arm} are defined as $I_{i1}(t)$ and $I_{i2}(t)$ (i=a,b,c), which can be expressed as follows:

$$I_{i1}(t)=\frac{1}{3}I_{dc}+\frac{1}{2}I_{arm}\sin(wt-\varphi) \tag{21}$$

$$I_{i2}(t)=\frac{1}{3}I_{dc}-\frac{1}{2}I_{arm}\sin(wt-\varphi) \tag{22}$$

Each submodule in the MMC contains four semiconductor devices, however, only one of them is conducting at a given duration. Depending on the direction of current flow, as well as the conducting mode (on state or bypassed state) of the submodule, the conducting semiconductor device is determined in the table below.

Table 1. Current flowing in semiconductor devices

State / Current direction	Positive	Negative
On-state	D1	T1
By-passed	T2	D2

Considering the current flowing in semiconductors in the above table, the pulse functions of each device in the submodule i ($1 \le i \le N$) can be expressed with the equation (23).

$$\begin{aligned} \tau_{D1} &= \frac{1}{2}(1+m \sin(wt-\varphi+i\lambda) \\ \tau_{D2} &= \frac{1}{2}(1-m \sin(wt-\varphi+i\lambda) \\ \tau_{T1} &= \frac{1}{2}(1+m \sin(wt-\varphi+i\lambda) \\ \tau_{T2} &= \frac{1}{2}(1-m \sin(wt-\varphi+i\lambda) \end{aligned} \tag{23}$$

Where λ is the carrier phase-shift angle and m is the modulation index.

Therefore, the conduction losses in a single submodule in phase a can are expressed by equation (24).

$$\begin{aligned} P_{con\_T1} &= \frac{1}{T_0}\int_{Ia1(t)<0} |I_a(t)|\left(V_{T0}+R_T\left(T_j\right)|I_a(t)|\right)\frac{1}{2}(1+m.\sin(wt-\varphi+i\lambda)dt \\ P_{con\_T2} &= \frac{1}{T_0}\int_{Ia1(t)>0} |I_a(t)|\left(V_{T0}+R_T\left(T_j\right)|I_a(t)|\right)\frac{1}{2}(1-m.\sin(wt-\varphi+i\lambda)dt \\ P_{con\_D1} &= \frac{1}{T_0}\int_{Ia1(t)<0} |I_a(t)|\left(V_{D0}+R_D\left(T_j\right)|I_a(t)|\right)\frac{1}{2}(1+m.\sin(wt-\varphi+i\lambda)dt \\ P_{con\_D2} &= \frac{1}{T_0}\int_{Ia1(t)>0} |I_a(t)|\left(V_{D0}+R_D\left(T_j\right)|I_a(t)|\right)\frac{1}{2}(1-m.\sin(wt-\varphi+i\lambda)dt \end{aligned} \tag{24}$$

2.2/ Switching losses of the MMC

Once the IGBT turns on or off, an energy is lost in the device, which is the switching energy loss. In fact, the turn-on of an IGBT is always accompanied by the turn-off of a diode in the path. The diode turn-off results also an energy loss. The turn-on, the turn-off energies of the IGBT, as well as the "recovery" energy of the diode, are respectively E_{on}, E_{off} and E_{rec}. Therefore, the switching losses of a semiconductor in the MMC converter are defined as follows.

$$P_{sw}(t)=\frac{1}{T_0}\sum_{j=1}^{M}\int_{t\in Ts}\frac{E\,(I(t))}{T_s}dt \tag{25}$$

Where T_s is the switching cycle and M is the switching times or recovery times of a device in a duty cycle T_0, E is the power loss of a device generated in a switching process, which can be E_{sw} and E_{rec}. The power losses of IGBT E_{sw} is the sum of E_{on} and E_{off} generated in a switching process can be expressed with equation (26).

$$E_{sw}(t)=\alpha+\beta I(t)+\gamma I^2(t) \tag{26}$$

Where α, β and γ are the fit coefficients to the power losses of switching devices.

Considering the influence of T_j, the above equation can be modified by adding a modification coefficient $\rho_i(T_j)$ (i=1,2,3 for turn-on and turn-off energy as well as recovery energy) in the constant driver resistance. Equation (26) presents the new E_{off}, E_{on} and E_{rec} considering $\rho_i(T_j)$.

$$\begin{aligned}E_{off}(t)&=(\alpha_1+\beta_1 I_T(t)+\gamma_1 I^2{}_T(t))\rho_1\\ E_{on}(t)&=(\alpha_2+\beta_2 I_T(t)+\gamma_2 I^2{}_T(t))\rho_2\\ E_{rec}(t)&=(\alpha_3+\beta_3 I_D(t)+\gamma_3 I^2{}_D(t))\rho_3\end{aligned} \tag{27}$$

With

$$\begin{aligned}\rho_1(T_j)&=\frac{1}{E_{off}(125)}\left[\frac{(E_{off}(125)-E_{off}(25))(T_j-25)}{100}+E_{off}(25)\right]\\ \rho_2(T_j)&=\frac{1}{E_{on}(125)}\left[\frac{(E_{on}(125)-E_{on}(25))(T_j-25)}{100}+E_{on}(25)\right]\\ \rho_3(T_j)&=\frac{1}{E_{rec}(125)}\left[\frac{(E_{rec}(125)-E_{rec}(25))(T_j-25)}{100}+E_{rec}(25)\right]\end{aligned} \tag{28}$$

The impact of the withstanding voltage V_{dc} of the device is also necessary to take into consideration by comparing it with the withstanding voltage under reference conditions V_{dcnom}. Thus, the switching losses of the IGBTs and diodes in a submodule can be expressed by the following equations.

$$
\begin{aligned}
P_{sw\_T1}(t)&=\rho_T(T_j)k_T(R_g)\frac{V_{dc}}{V_{dcnom}}f_0 f_s\int_{ia<0}\left[\alpha_T+\beta_T I\,(t)+\gamma_T I^2(t)\right]dt\\
P_{sw\_T2}(t)&=\rho_T(T_j)k_T(R_g)\frac{V_{dc}}{V_{dcnom}}f_0 f_s\int_{ia>0}\left[\alpha_T+\beta_T I\,(t)+\gamma_T I^2(t)\right]dt\\
P_{rec\_D1}(t)&=\rho_D(T_j)k_D(R_g)\frac{V_{dc}}{V_{dcnom}}f_0 f_s\int_{ia>0}\left[\alpha_D+\beta_D I\,(t)+\gamma_D I^2(t)\right]dt\\
P_{rec\_D2}(t)&=\rho_D(T_j)k_D(R_g)\frac{V_{dc}}{V_{dcnom}}f_0 f_s\int_{ia<0}\left[\alpha_D+\beta_D I\,(t)+\gamma_D I^2(t)\right]dt
\end{aligned}
\tag{29}
$$

Where, f_s is the switching frequency and $k(R_g)$ is the coefficient of driver resistance that is defined by the equation below.

$$k(R_g)=\frac{E_{sw}(R_g)}{E_{sw}(R_{gN})} \tag{30}$$

Where R_{gN} is the normal drive resistance in E-I curve of the device's datasheet.

Therefore, the power losses in one submodule are shown in equation (31).

$$P_{SM}=P1_{con\_T1}+P_{con\_T2}+P_{con\_D1}+P_{con\_D2}+P_{sw\_T1}+P_{sw\_T2}+P_{rec\_D1}+P_{rec\_D2} \tag{31}$$

In final, the total losses of the MMC converter are defined in equation (32).

$$P_{MMC}=\sum_{1}^{6N}P_{SM} \tag{32}$$

Appendix 4 Newton-Raphson method

The load flow calculation method in Mat AC/DC is based on the Newton-Raphson approach which is characterized by its rapid convergence efficiency compared to other methods (Gauss Seidel method). This algorithm is based on Taylor's law, the general form of Taylor's equation with neglecting high order items, is expressed below:

$$x^{(k+1)} = x^{(k)} - \frac{f(x^{(k)})}{f'(x^{(k)})} \tag{1}$$

Then the mismatch equations of n variables before the first iteration can be written as follow:

$$\begin{bmatrix} f_1(x_1^{(0)}, x_2^{(0)}, \ldots, x_n^{(0)}) \\ f_2(x_1^{(0)}, x_2^{(0)}, \ldots, x_n^{(0)}) \\ \vdots \\ f_n(x_1^{(0)}, x_2^{(0)}, \ldots, x_n^{(0)}) \end{bmatrix} = \begin{bmatrix} \frac{\partial f_1}{\partial x_1}(0) & \frac{\partial f_1}{\partial x_2}(0) \ldots & \frac{\partial f_1}{\partial x_n}(0) \\ \frac{\partial f_2}{\partial x_1}(0) & \frac{\partial f_2}{\partial x_2}(0) \ldots & \frac{\partial f_2}{\partial x_n}(0) \\ & \vdots & \\ \frac{\partial f_n}{\partial x_1}(0) & \frac{\partial f_n}{\partial x_2}(0) \ldots & \frac{\partial f_n}{\partial x_n}(0) \end{bmatrix} \begin{bmatrix} \Delta x_1^{(0)} \\ \Delta x_2^{(0)} \\ \vdots \\ \Delta x_n^{(0)} \end{bmatrix} \tag{2}$$

The equation (3) is used to update the new variables, the differential matrix is called Jacobian matrix.

$$x_i^{(1)} = x_i^{(0)} + \Delta x_i^{(0)} \quad (i=1,2, \ldots, n) \tag{3}$$

We consider that m is the number of PQ nodes and there is only one slack bus so the number of PV nodes is n-m-1. The active and reactive powers at node i are expressed by the following equations:

$$P_i = V_i \sum_{j=1}^{n} V_j (G_{ij} \cos \delta_{ij} + B_{ij} \sin \delta_{ij}) \tag{4}$$

$$Q_i = V_i \sum_{j=1}^{n} V_j (G_{ij} \sin \delta_{ij} - B_{ij} \cos \delta_{ij}) \tag{5}$$

Where i and j are the index of electrical system nodes, G_{ij} is the conductance of the nodal admittance matrix, B_{ij} is the susceptance of the nodal admittance matrix, V_i is the voltage of the ith node and δ_{ij} is the difference of the voltage angles between nodes i and j.

For PQ and PV nodes, the mismatch equations in polar coordinates form are as below:

$$-\Delta P_i = \sum_{j=1}^{n-1} \frac{\partial \Delta P_i}{\partial \Delta \delta_j} \Delta \delta_j + \sum_{j=1}^{n-1} \frac{\partial \Delta P_i}{\partial \Delta V_j} \Delta V_j \quad (6)$$

$$-\Delta Q_i = \sum_{j=1}^{m} \frac{\partial \Delta Q_i}{\partial \Delta \delta_j} \Delta \delta_j + \sum_{j=1}^{m} \frac{\partial \Delta Q_i}{\partial \Delta V_j} \Delta V_j \quad (7)$$

So, the overall calculating steps are:

Step 1: form the Nodal admittance matrix $Y_{ij} = G_{ij} + j\, B_{ij}$

Step 2: set the initial voltage V_i (0), δ_i (0), the iteration time k=0.

Step 3: bring in the approximation of each bus voltage to the mismatch equations and obtain the mismatch physical quantity ΔW_i (k).

Step 4: if not converged, calculate each element of Jacobian matrix using the approximating bus voltage.

Step 5: solve the mismatch equations, and obtain V_i (k), δ_i (k).

Step 6: renew each bus voltage, k=k+1, return to step 3 until converged condition is satisfied.

Step 7: calculate the power of slack bus and line power losses.

Appendix 5 Matpower/Mat AC/DC

Matpower manual

1/ AC bus matrix

Table B-1: Bus Data (`mpc.bus`)

name	column	description
`BUS_I`	1	bus number (positive integer)
`BUS_TYPE`	2	bus type (1 = PQ, 2 = PV, 3 = ref, 4 = isolated)
`PD`	3	real power demand (MW)
`QD`	4	reactive power demand (MVAr)
`GS`	5	shunt conductance (MW demanded at $V = 1.0$ p.u.)
`BS`	6	shunt susceptance (MVAr injected at $V = 1.0$ p.u.)
`BUS_AREA`	7	area number (positive integer)
`VM`	8	voltage magnitude (p.u.)
`VA`	9	voltage angle (degrees)
`BASE_KV`	10	base voltage (kV)
`ZONE`	11	loss zone (positive integer)
`VMAX`	12	maximum voltage magnitude (p.u.)
`VMIN`	13	minimum voltage magnitude (p.u.)
`LAM_P`†	14	Lagrange multiplier on real power mismatch (u/MW)
`LAM_Q`†	15	Lagrange multiplier on reactive power mismatch (u/MVAr)
`MU_VMAX`†	16	Kuhn-Tucker multiplier on upper voltage limit (u/p.u.)
`MU_VMIN`†	17	Kuhn-Tucker multiplier on lower voltage limit (u/p.u.)

2/ Generator matrix

Table B-2: Generator Data (`mpc.gen`)

name	column	description
`GEN_BUS`	1	bus number
`PG`	2	real power output (MW)
`QG`	3	reactive power output (MVAr)
`QMAX`	4	maximum reactive power output (MVAr)
`QMIN`	5	minimum reactive power output (MVAr)
`VG`‡	6	voltage magnitude setpoint (p.u.)
`MBASE`	7	total MVA base of machine, defaults to `baseMVA`
`GEN_STATUS`	8	machine status, > 0 = machine in-service; ≤ 0 = machine out-of-service
`PMAX`	9	maximum real power output (MW)
`PMIN`	10	minimum real power output (MW)
`PC1`*	11	lower real power output of PQ capability curve (MW)
`PC2`*	12	upper real power output of PQ capability curve (MW)
`QC1MIN`*	13	minimum reactive power output at `PC1` (MVAr)
`QC1MAX`*	14	maximum reactive power output at `PC1` (MVAr)
`QC2MIN`*	15	minimum reactive power output at `PC2` (MVAr)
`QC2MAX`*	16	maximum reactive power output at `PC2` (MVAr)
`RAMP_AGC`*	17	ramp rate for load following/AGC (MW/min)
`RAMP_10`*	18	ramp rate for 10 minute reserves (MW)
`RAMP_30`*	19	ramp rate for 30 minute reserves (MW)
`RAMP_Q`*	20	ramp rate for reactive power (2 sec timescale) (MVAr/min)
`APF`*	21	area participation factor
`MU_PMAX`†	22	Kuhn-Tucker multiplier on upper P_g limit (u/MW)
`MU_PMIN`†	23	Kuhn-Tucker multiplier on lower P_g limit (u/MW)
`MU_QMAX`†	24	Kuhn-Tucker multiplier on upper Q_g limit (u/MVAr)
`MU_QMIN`†	25	Kuhn-Tucker multiplier on lower Q_g limit (u/MVAr)

3/ AC branch matrix

Table B-3: Branch Data (`mpc.branch`)

name	column	description
`F_BUS`	1	"from" bus number
`T_BUS`	2	"to" bus number
`BR_R`	3	resistance (p.u.)
`BR_X`	4	reactance (p.u.)
`BR_B`	5	total line charging susceptance (p.u.)
`RATE_A`*	6	MVA rating A (long term rating), set to 0 for unlimited
`RATE_B`*	7	MVA rating B (short term rating), set to 0 for unlimited
`RATE_C`*	8	MVA rating C (emergency rating), set to 0 for unlimited
`TAP`	9	transformer off nominal turns ratio, if non-zero (taps at "from" bus, impedance at "to" bus, i.e. if $r = x = b = 0$, $tap = \frac{\lvert V_f \rvert}{\lvert V_t \rvert}$; $tap = 0$ used to indicate transmission line rather than transformer, i.e. mathematically equivalent to transformer with $tap = 1$)
`SHIFT`	10	transformer phase shift angle (degrees), positive ⇒ delay
`BR_STATUS`	11	initial branch status, 1 = in-service, 0 = out-of-service
`ANGMIN`†	12	minimum angle difference, $\theta_f - \theta_t$ (degrees)
`ANGMAX`†	13	maximum angle difference, $\theta_f - \theta_t$ (degrees)
`PF`‡	14	real power injected at "from" bus end (MW)
`QF`‡	15	reactive power injected at "from" bus end (MVAr)
`PT`‡	16	real power injected at "to" bus end (MW)
`QT`‡	17	reactive power injected at "to" bus end (MVAr)
`MU_SF`§	18	Kuhn-Tucker multiplier on MVA limit at "from" bus (u/MVA)
`MU_ST`§	19	Kuhn-Tucker multiplier on MVA limit at "to" bus (u/MVA)
`MU_ANGMIN`§	20	Kuhn-Tucker multiplier lower angle difference limit (u/degree)
`MU_ANGMAX`§	21	Kuhn-Tucker multiplier upper angle difference limit (u/degree)

Mat AC/DC manual

1/ DC bus matrix

Table 1: busdc data format

Index	NAME	Description
1	BUSDC_I	DC bus number
2	BUSAC_I	Corresponding AC bus number
		Note: Index BUSAC_I = 0 indicates no AC bus connection
3	GRIDDC	DC grid to which the DC bus is connected
4	PDC	P_{dc}, power withdrawn from the DC grid (MW)
5	VDC	U_{dc}, DC voltage (p.u.)
6	BASE_KVDC	base DC voltage (kV)
7	VDCMAX	maximum DC voltage (p.u.)
8	VDCMIN	minimum DC voltage (p.u.)
9	CDC	C_{dc}, DC bus capacitor size (p.u.) (not used in power flow)

2/ DC converter matrix

Table 2: convdc data format

Index	NAME	Description
Converter buses, control parameters and AC system data		
1	CONV_BUS	converter bus number (DC bus numbering)
2	CONVTYPE_DC	DC bus type (1 = constant power, 2 = DC slack, 3 = DC droop)
3	CONVTYPE_AC	AC bus type (1 = PQ, 2 = PV)
4	PCONV	P_s, active power injected in the AC grid (MW)

Table 2: convdc data format (continued)

Index	NAME	Description
5	QCONV	Q_s, reactive power injected in the AC grid (MVAr)
6	VCONV	U^{ref}, target voltage of converter connected AC bus (p.u.)
Impedance values		
7	RTF	R_{tf}, transformer resistance (p.u.)
8	XTF	X_{tf}, transformer reactance (p.u.)
9	BF	B_f, filter susceptance (p.u.)
10	RCONV	R_c, phase reactor resistance (p.u.)
11	XCONV	X_c, phase reactor reactance (p.u.)
12	BASEKVC	converter AC base voltage (kV)
13	VCMAX	$U_{c,max}$, maximum converter voltage magnitude (p.u.)
14	VCMIN	$U_{c,min}$, minimum converter voltage magnitude (p.u.)
15	ICMAX	I_{max}, maximum converter current (p.u.)
16	CONVSTATUS	converter status (1 = on, 0 = off)
Converter loss data		
17	LOSSA	a, constant loss coefficient (MW)
18	LOSSB	b, linear loss coefficient (kV)
19	LOSSCR	c_{rec}, rectifier quadratic loss coefficient (Ω)
20	LOSSCI	c_{inv}, inverter quadratic loss coefficient (Ω)
DC voltage droop constants (optional)		
21	DROOP	k, DC voltage droop (MW/p.u)
22	PDCSET	$P_{dc,set}$, voltage droop power set-point (MW)
23	VDCSET	$U_{dc,set}$, voltage droop voltage set-point (p.u.)
24	DVDCSET	$\Delta U_{dc,set}$ voltage droop deadband (p.u.) (optional)

Table 3: convdc named constants

Index	NAME	Description
CONVTYPE_DC constants		
3	DCDROOP	DC voltage droop
2	DCSLACK	DC slack bus
1	DCNOSLACK	constant active power bus
CONVTYPE_AC constants		
2	PVC	constant voltage converter control
1	PQC	constant reactive power converter control

3/ DC branch matrix

Table 4: busdc data format

Index	NAME	Description
1	F_BUSDC	i, from bus number
2	T_BUSDC	j, to bus number
3	BRDC_R	$R_{dc_{ij}}$, resistance (p.u.)
4	BRDC_L	$L_{dc_{ij}}$, inductance (p.u./s) (not used in power flow)
5	BRDC_C	$C_{dc_{ij}}$, total line charging capacity (p.u.*s) (not used in power flow)
6	RATEDC_A	rateA, MVA rating A (long term rating, not used)
7	RATEDC_B	rateB, MVA rating B (short term rating, not used)
8	RATEDC_C	rateC, MVA rating C (emergency rating, not used)
9	BRDC_STATUS	initial branch status, (1 - in service, 0 - out of service)
Columns typically added after the power flow		
10	PFDC	$P_{dc_{ij}}$, real power injected at "from" bus end (MW)
11	PTDC	$P_{dc_{ji}}$, real power injected at "to" bus end (MW)

DOCTORAT BRETAGNE LOIRE MATHSTIC

UNIVERSITÉ DE NANTES

Titre : Optimisation des architectures électriques des parcs éoliens offshore avec différents réseaux de distribution et de transmission AC et DC

Mots clés : ferme éolienne, architecture, dimensionnement, optimisation, réseau de distribution, réseau de transmission, HVDC, HVAC

Résumé : Dans le cadre du développement de l'installation des parcs éoliens offshore dans le monde entier, le travail de cette thèse s'attache à créer une plateforme d'optimisation des différentes architectures des fermes éoliennes offshore. En effet, commençant par les parcs totalement raccordés en AC, on a proposé l'intégration du réseau HVDC pour le transport, ensuite la technologie de raccordement totalement en DC s'est imposée. La nécessité de l'intégration du transport HVDC vient avec l'implantation des turbines à une grande distance des côtes dans le but de réduire les pertes tout en long de la distance de transmission. Au-delà de la modélisation des éléments électriques et de leur influence sur les différentes architectures, l'objectif ici est de prendre aussi en considération les aspects économiques liés au coût des turbines et de leurs fondations, des convertisseurs (AC/DC et DC/DC), des transformateurs, des sous stations offshores (AC ou DC) et des câbles sous-marins.

L'ensemble des éléments feront l'objet de modélisations et seront intégrés à une plateforme d'optimisation technico-économique qui a comme but la minimisation du LCOE (le coût global actualisé durant la période d'exploitation du parc). Pour des conditions plus réalistes, le calcul de l'effet de sillage entre les turbines est intégré dans l'algorithme d'optimisation. Les résultats principaux de cette thèse portent sur la comparaison entre les différentes technologies de raccordement en tenant compte de plusieurs aspects tels que la distance de transmission et la capacité totale de production du parc afin de définir les architectures les plus pertinentes. Cette plateforme d'optimisation présente un outil d'aide à la décision pour les industriels pour choisir la meilleure technologie durant la phase d'étude préliminaire.

Title : Optimization of electrical architectures of offshore wind farms with different distribution and transmission networks AC and DC

Keywords : offshore windfarm, topology, sizing, optimization, distribution network, transmission network, HVDC, HVAC

Abstract : With the development of offshore wind farms installations around the world, the work of this thesis focuses on creating an optimization platform of the different architectures of offshore wind farms. Indeed, starting with full AC-connected farms, the integration of the HVDC grid for transmission network is proposed, then the full DC connection topology is imposed. The need of HVDC transport integration comes with the location of the turbines at a great distance from the coast in order to reduce losses along the transmission distance.
Beyond the modeling of the electrical elements and their influence on the different architectures, the objective here is also to take into account the economic aspects related to the cost of turbines and their foundations, converters (AC/DC and DC/DC), transformers, offshore substations (AC or DC) and submarine cables.

All the elements will be modelled and integrated into a technical and economic optimization platform which aims to minimize the LCOE (the Levelized Cost Of Energy). For more realistic conditions, the wake effect calculation between the turbines is integrated in the optimization framework.
The main results of this thesis concern the comparison between the different connection technologies taking into account several aspects such as the transmission distance and the total production capacity of the park in order to define the most relevant architectures. This optimization platform presents a decision support tool for industrialists to choose the best technology during the preliminary study phase.